8-12-2016

Synthetic Development of Cyanine Dyes and Investigation of Their Interaction with Duplex DNA

Cory Holder
cholder1@gsu.edu

SYNTHETIC DEVELOPMENT OF CYANINE DYES AND INVESTIGATION OF THEIR INTERACTION WITH DUPLEX DNA

by

CORY HOLDER

Under the Direction of Maged M. Henary, Ph.D.

ABSTRACT

This thesis outlines two projects that examine interactions between DNA and cyanine dyes: 1) Investigation of monomethine cyanine dye through the synthesis and optical characteristics with a goal to synthetically manipulate these systems to develop a fluorescent biological probe. Several asymmetric and one symmetrical monomethine cyanine dyes were synthetically prepared and their optical properties versus structural changes were explored. Representative dyes were selected for spectroscopically investigating DNA binding to enhance existing probe designs. 2) Early stage development of a non-metalated photosensitizer for photodynamic therapy (PDT) by screening experimentally derived cleavage activities of a number of polymethine cyanine dyes with various adjoining heterocycles. Structural characteristics of these dyes which promoted cleavage in the dark were identified and eliminated to allow for more selective photo-induced cleavage to enhance the candidacy of these compounds as photosensitizing agents. All compounds were purified through recrystallization or column chromatography and were characterized via ^{1}H and ^{13}C nuclear magnetic resonance (NMR). Compounds from the first chapter were further characterized using mass spectrometry.

INDEX WORDS: polymethine cyanine, synthesis, spectroscopy, DNA, *in silico*

SYNTHETIC DEVELOPMENT OF CYANINE DYES AND INVESTIGATION OF THEIR INTERACTION WITH DUPLEX DNA

by

CORY HOLDER

A Thesis Submitted in Partial Fulfillment of the Requirements for the Degree of

Master of Science

in the College of Arts and Sciences

Georgia State University

2016

SYNTHETIC DEVELOPMENT OF CYANINE DYES AND INVESTIGATION OF THEIR INTERACTION WITH DUPLEX DNA

by

CORY HOLDER

Committee Chair: Maged M. Henary

Committee: Donald Hamelberg

Peng George Wang

Electronic Version Approved:

Office of Graduate Studies

College of Arts and Sciences

Georgia State University

August 2016

DEDICATION

I would like to dedicate this thesis to my family, without their support and encouragement I would not have been able to succeed. I would also like to dedicate this thesis to Olivia Clark, my best friend, thank you for being by my side through the highs and the lows.

ACKNOWLEDGEMENTS

I would like to thank my principal investigator Dr. Maged Henary for providing me with lab space, equipment and chemicals to complete the work presented in this thesis. I would like to acknowledge my committee members Dr. Maged Henary, Dr. Donald Hamelberg, and Dr. George Wang for taking time to read my thesis and for providing thoughtful feedback. I would also like to acknowledge Dr. Kathryn B. Grant and her research group, specifically Ziyi and Katie, for providing valuable insight to my projects and for keeping a positive attitude throughout our collaboration. Additionally, I would like to thank Dr. Gabor Patonay and his group members, Andrew, Eman, Kyle, and Walid, for several fruitful conversations that helped me design my experiments. I would also like to thank to my group members, Andy, Eduardo, Matt, Tyler, and Vincent. I would like to especially thank Kaitlyn Kiernan, Matt Laramie and Tyler Dost for helping me edit my thesis. I would like to thank the Georgia State University Department of Chemistry staff, especially Kedayne King, for helping me throughout my time at GSU. Lastly I would like to thank very special teachers I had throughout my education: Aunt Gena, Mrs. Propp, Dr. Martin, and Dr. Jenkins. Thank you all for helping me complete this stage of life.

TABLE OF CONTENTS

LIST OF TABLES

LIST OF FIGURES

LIST OF SCHEMES

1 INTRODUCTION

In 1856 C. G. Williams was attempting to develop a drug for treating malaria when he mistakenly synthesized a “magnificent blue colored” product by reacting the quinoline from cinchonine with amyl iodide and ammonia; he called this new class of dyes “cyanines”.[1] Around the same time von Babo was looking at decomposition products of cinchonine and produced a “very pretty blue” compound, which he named “irisin”, by treating quinoline with methyl sulfate and caustic potash.[2,3] This newly developed class of dyes was particularly interesting to investigators due to the brightness they exhibited and their ability to impart light sensitivity to silver halide emulsions in a spectral region where silver halide is normally not sensitive.[4-10] Since then, these dyes have been widely used in industry for photography and laser printing.[11] More recently, scientist have found biological and biomedical applications for this class of dyes such as fluorescent probes for tagging biomolecules, bone, cartilage, or organs.[12-15]

Imaging agents and stains have proven extremely useful in the fields of medicinal chemistry and chemical biology. These compounds allow for less invasive and more precise methods of diagnosis and treatment as well as providing insight into understanding currently unknown biological processes. Medicine is currently heading in the direction where patients will undergo more personalized and specialized treatments.[16] Imaging agents are being used more often in medicine as a major tool for these specialized treatments, specifically by targeting certain biomolecules. [16] The targeting biomolecules with imaging agents provides surgeons and scientist the ability to monitor changes in patients and, with photodynamic therapy, means to achieve highly localized treatment, minimizing side effects.[19] One of the most common biomolecules for targeting is DNA. Generally, DNA is a very useful target in medicine as it is involved with almost every change that living organisms undergo, both good and bad. Specifically, it is a primary target

for treating cancers because mutations of DNA are the cause of cancer. As of mid-2016, a majority of cancer patients undergo treatment with drugs which rely on DNA interaction to give off their therapeutic effects.[16-19]

This thesis covers two major projects covering the synthesis of mono-, tri-, and pentamethine cyanine dyes containing various heterocycles and investigation of different biomedical applications by utilizing their interaction with DNA. Chapter 1 [15] and 2 present the synthesis and optical properties of monomethine cyanine dyes and investigates their unique ability to exhibit up to 700-fold increase in fluorescence intensity upon binding to duplex DNA. The final chapter, Chapter 3, discusses the early stage development of tri- and pentamethine cyanine dyes as a photosensitizer for PDT. Several compounds were synthesized and screened for duplex DNA cleavage activity to determine the optimal structural features for a non-metalated photosensitizing agent.

2 CHAPTER 1: BENZ[C,D]INDOLIUM-CONTAINING MONOMETHINE CYANINE DYES: SYNTHESIS AND PHOTOPHYSICAL PROPERTIES

This chapter was adapted from the following publication: Soriano, E.[‡]; **Holder, C.**[‡]; Levitz, A.; Henary, M.; Benz[*c,d*]indolium-containing Monomethine Cyanine Dyes: Synthesis and Photophysical Properties. *Molecules* **2016**, 21, 23. *Invited manuscript.* This article belongs to the Special Issue Design and Synthesis of Novel Conjugated and Non Conjugated Small Molecules. [‡]Co-First authors. My contributions to the manuscript consisted of the synthetic, *in silico* and spectroscopic experiments, analysis, figure and manuscript preparation and frequent discussions concerning the project.

2.1 Introduction

Polymethine dyes represent a class of organic molecules with absorption bands that cover a broad spectral range (430-1100 nm) larger than any other class of dye system [1]. Cyanine dyes consist of two terminal aza-heterocycles connected via an electron deficient polymethine bridge that allows for a push/pull system between the two heterocycles. The delocalization of electrons across this bridge causes them to exhibit long wavelength absorption. In addition to the variable length of the conjugated system between the heterocycles, the heterocycles themselves can be altered which allows chemists to create dyes that possess ideal photophysical properties, such as high molar extinction coefficients ($>10^5$ M^{-1} cm^{-1}), tunable fluorescence intensities, and narrow absorption bands. Due to the diversity in function associated with this class of chromophore, an extensive number of cyanine dyes have been synthesized and developed for numerous applications in photographic processes and more recently as fluorescent probes for bio-molecular labeling and imaging [1-9].

As cyanine dyes have been shown to be highly modifiable for desirable properties such as solubility, permeability, and binding, these modifications can also cause changes in the dye's photophysical properties. Recently, the interpretation of the fluorogenic behavior of the monomethine cyanine dyes from in silico studies has been successfully used to design new fluorescent molecular rotors as viscosity sensors [10]. Two asymmetric dyes shown in Figure 1, thiazole orange (TO) and oxazole yellow (YO), are well known imaging probes in the biological sciences due to their enhanced photophysical properties which have been attributed to restricted torsional motion of the dye in the excited state upon binding to target a macromolecule (i.e. nucleic acid structure, protein) [11-14]. TO absorbs and fluoresces at 501 nm and 525 nm, respectively, while YO absorbs and fluoresces at 491 nm and 509 nm, respectively [15]. The dimers of these compounds are also known imaging probes and shown in Figure 1. YOYO absorbs and fluoresces at 450 nm [16] and 510 nm, respectively, while TOTO absorbs and fluoresces at 513 and 530 nm, respectively [17, 18]. Nonetheless, there is a lack of understanding of how the structure interplays with the optical performance (i.e. extinction coefficient and fluorescence)—especially for those monomethine cyanines with red-shifted wavelengths [9, 19-21]. Thus, it is important to understand how varying substituents and heterocycles would affect the optical properties of each dye.

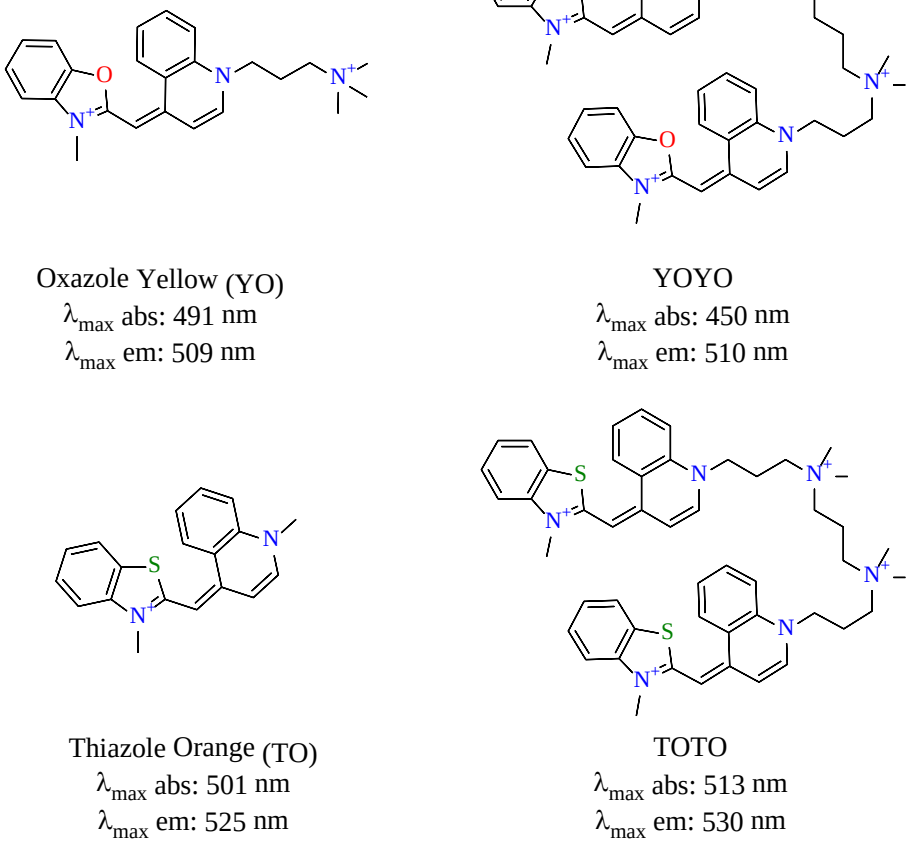

Figure 1 Commercially available monomethine cyanine dyes

Imaging of macromolecules such as DNA by staining with fluorescent compounds is of great interest; therefore, expanding the options of available probes is vital to several areas of research spanning from medical diagnostics to genomics [22-38]. The synthesis of low cost, easy to manipulate systems for fast analysis is required [8]. Fluorescent detection has rapidly become one of the most widely used techniques due to its sensitivity and noninvasiveness [39]. Ethidium bromide has commonly been used for the detection of DNA, however it has mutagenic effects and poses other environmental concerns [40-42]. On the other hand, cyanine dyes are sensitive, safe and highly modifiable.

Recently, our group has synthesized a series of benz[*c,d*]indol-1-ium-containing monomethine cyanines with separate adjoining heterocyclic moieties which were found to directly influence the optical properties of the dye system [20]. In this report seven additional red-shifted monomethine cyanine dyes were synthesized and the structural influence on their fluorogenic properties was investigated by comparing the optical characteristics, examining the change in chemical shifts of methine proton and carbon NMR spectra, determining the energy profile through in silico approaches, as well as demonstrating that the dyes can be employed as DNA binding agents. The ability to use the theoretical calculations of optical properties for fluorophores, such as monomethine dyes could be useful for the development of the viscosity detection methods or bioimaging agents with desirable optical profiles.

2.2 Results and Discussion

2.2.1 Synthesis

Toward gaining better understanding of the relationship between various heterocyclic substitutions and changes in optical properties we began to rationally design and investigate the effect of altering the heterocyclic substitution on the photophysical characteristics of the dye systems. Two sets of monomethine cyanines were explored without altering the benz[*c,d*]indole heterocycle half of the dye. The first set possessing different heterocycles including 2-methylbenzothiazole, 2-methylbenzoxazole, 3,3-dimethylbenz[*e*]indole or 2-methylquinoline, respectively, and the second set containing the same 3,3-dimethylindole heterocycle but with different substituents, one electron donating and one electron withdrawing, on the 5 position of the heterocyclic ring system.

The asymmetric red-shifted monomethine cyanine dyes were synthesized as shown in Scheme 1. The synthesis began with the alkylation of benz[*c*,*d*]indol-2(1H)-one **1** by reflux with iodobutane in acetonitrile. The alkylated amide **2** was then converted to the thioketone **3** under reflux with phosphorous pentasulfide in pyridine. The thioketone **3** was methylated to a thioether with iodomethane creating the key precursor, quaternary ammonium salt **4**, which was used as one heterocycle. The second heterocycle was synthesized beginning with a Fischer indole synthesis by refluxing 4-substituted phenylhydrazine hydrochlorides **7** and 3-methyl-2-butanone in glacial acetic acid. The synthesized heterocyclic derivatives **8**, 2-methylbenzothiazole, 2-methylbenzoxazole, 2,3,3-trimethylbenz[*e*]indole, and 2-methylquinoline were alkylated, respectively, with various alkyl halides in acetonitrile to form quaternary ammonium salts **5a-d** and **9a-c** which acted as the second heterocycle for the final dyes. The two heterocycles were then connected by a condensation reaction in acetonitrile with a catalytic amount of triethylamine to afford final dyes **6a-d** and **10a-c**.

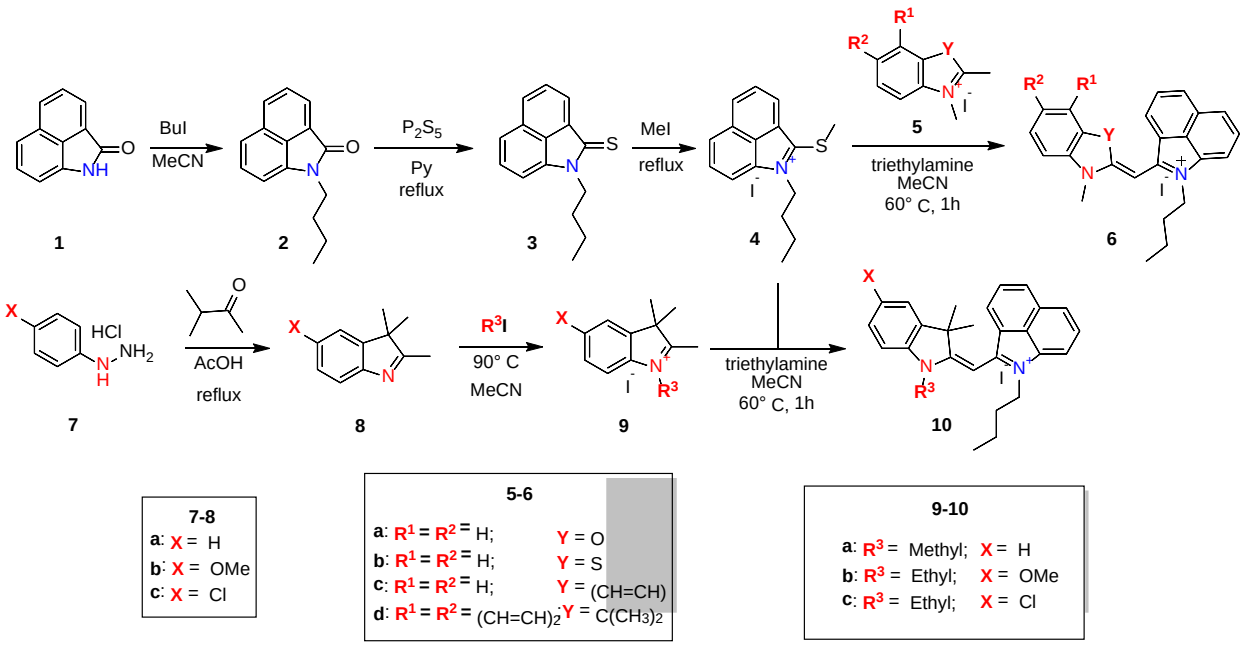

Scheme 1 Synthesis of Monomethine Dyes

The reaction begins with the deprotonation of the methyl group at the 2 position of the heterocycle. This activated methylene group of the various heterocyclic salts **5a-d** and **9a-c** displaces the methyl sulfide moiety of **4** and results in the formation of the asymmetrical monomethine dyes **6a-d** and **10a-c**. After isolation, the dyes were characterized by HRMS, ^{1}H and ^{13}C NMR and their photophysical properties were investigated.

2.2.2 Optical Properties

Optical properties are shown in Table 1. Absorption for each dye was recorded in methanol and 9/1 glycerol/methanol solution. Many monomethine cyanines display multiple bands which are attributed to different vibrionic bands of the same electronic transition [16]. Because the compounds did not fluoresce in methanol due the ability to freely rotate around the methine bridge in free flowing solvent, emission was recorded in a more viscous solvent, 9/1 glycerol/methanol solution. Representative UV-Vis spectra are shown in Figure 2. A symmetrical monomethine dye containing two benzothiazole heterocycles has a λ_{max} of 430 nm in ethanol [43]. It has been shown by Brooker et al. that if the nitrogen containing heterocycles are not identical, or if the relative stabilities of the two resonance forms are different, the absorption would not be at the midpoint [44]. The substitution of one of these heterocycles with benz[*c*,*d*]indole shifts the λ_{max} over 100 nm to 555 nm as seen in **6b**. This was accounted for by the further conjugated electron deficient system in the benz[*c*,*d*]indole heterocycle [1, 20, 45, 46]. The conjugated system has more electronegativity due to the oxygen atom in **6a** causing a blue shift of the λ_{max} to 498 nm [11, 47]. While the compounds containing 3,3-dimethylindole have similar absorption maxima to the benzothiazole compounds, the addition of an extra benzene ring as seen in **6d** red shifts the λ_{max} to 585 nm due to the increased conjugation through the heterocycle. All of the dyes displayed molar extinction coefficients in the range of 24,000-38,000 $M^{-1}cm^{-1}$. The dye with a methoxy substituted

indole heterocycle **10b** showed the lowest molar absorptivity at 24,800 $M^{-1}cm^{-1}$ due to the electron donating nature of the methoxy group introducing electron density back into the system [47, 48]. Aggregation was ruled out by measuring absorption of **6b** as a representative compound at various concentrations (5-25 μM) and the results were presented in the apppendix. Solvatochromic studies were performed on dye **6b** in five different solvents (ethanol, dimethyl formamide, dichloromethane, acetonitrile, and aqueous tris buffer). Less than 5 nm change in λ_{max} was observed. Such a small shift suggests that the electronic distribution of the ground state dye is virtually unaffected by the solvent polarity [47].

Table 1 Spectral Characteristics of Dyes **6a–d** and **10a-c**.

Dye	λ_{abs} (nm) [a]	λ_{abs} (nm) [b]	$\lambda_{emission}$ (nm) [b]	Stokes Shift (nm) [b]	ε (M^{-1} cm^{-1}) [a]
6a	498	505	570	65	37600
6b	555	563	609	46	32300
6c	585	587	609	22	36500
6d	553	557	625	68	25300
10a	537	552	657	105	33300
10b	563	569	606	37	24800
10c	552	571	662	91	30100

[a] methanol [b] methanol/glycerol 9/1 (*v*/*v*).

It has been reported that the fluorescence of these compounds cannot be observed in methanol alone because of a high nonradiative rate of return of the excited molecule as previously reported with many monomethine cyanines [20, 49-51]. However, when a viscous solution is used, the free rotation around the methine bridge is restricted and a fluorescence signal is observed as shown in Figure 2. Methanol (10%) was used in order to solubilize the compounds in the highly viscous glycerol. Fluorescence maxima ranged from 570 nm to 662 nm, almost reaching the near-

infrared region. The benzoxazole containing dye **6a** had the highest fluorescence intensity followed by benzothiazole containing dye **6b**. The quinoline containing dye **6c** had the least fluorescence intensity due to alternative relaxation pathways [52]. The largest Stokes shift, greater than 100 nm, was observed for the dye with an indole based heterocycle, 10a. Since the emission intensity was so low the Stokes shift reported could be slightly skewed due to low signal to noise. However, this finding is in agreement with red-shifted compounds previously synthesized by our group [20]. Large Stokes shift are ideal for imaging applications as the excitation light is farther from the fluorescence signal of the compound [39, 53].

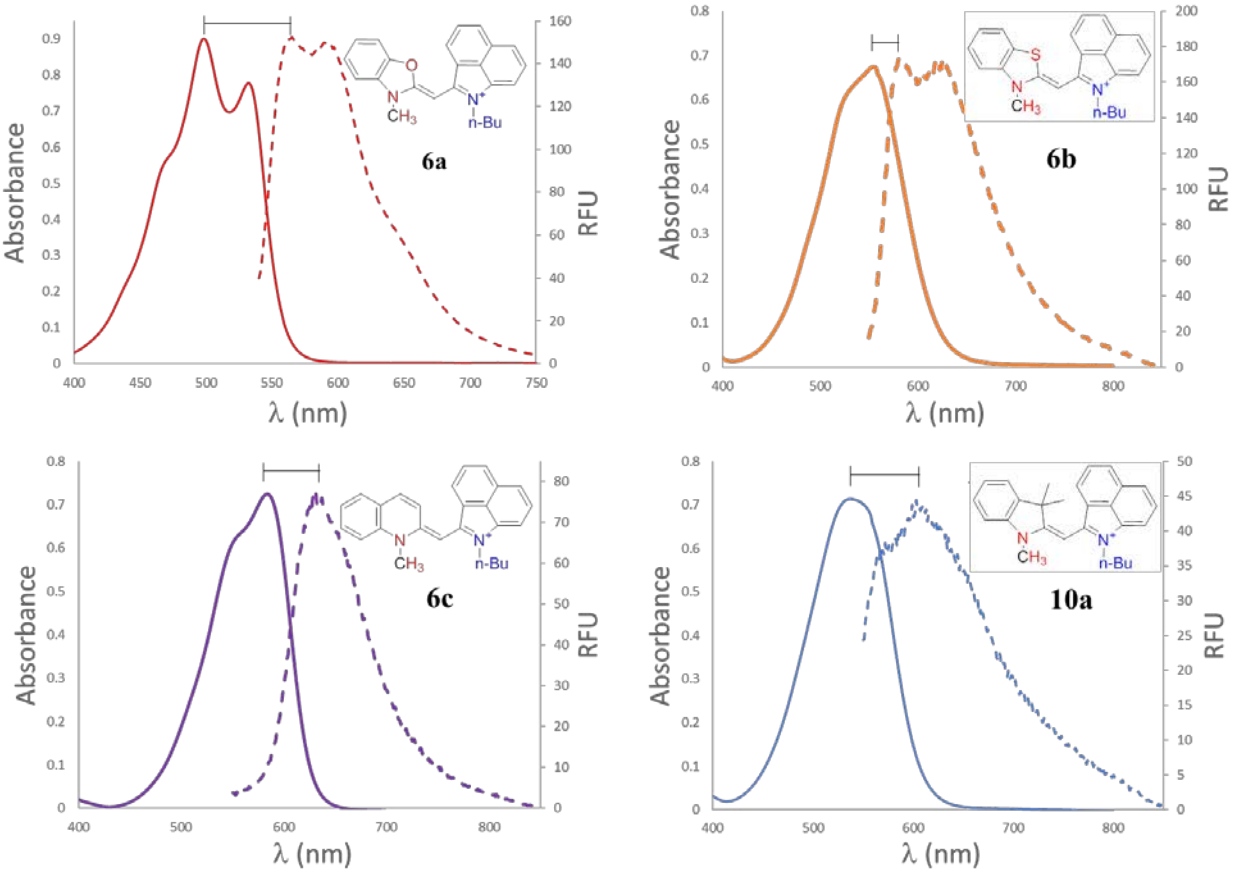

Figure 2 Absorbance (solid lines) and emission (dashed lines) in methanol/glycerol 9/1 spectra at 20 μM

2.2.3 Computational Evaluations

The electronic spectra of the monomethine dyes were investigated to help elucidate the trends described above in the optical properties. As shown by the calculations in Figure 3, over the series of dyes when the geometry is planar both the HOMO and LUMO orbitals are spread evenly throughout the dye. When the dyes are twisted out of plane the HOMO orbitals are localized around the more conjugated system benz[*c,d*]indole heterocycle. The energy transitions in cyanine dyes have been shown to be a dominant π–π* transition [11, 21], but if the dye assumes a twisted geometry the orbitals are not delocalized throughout the dye, as shown in Figure 3, and the system is not conjugated or planar [54].

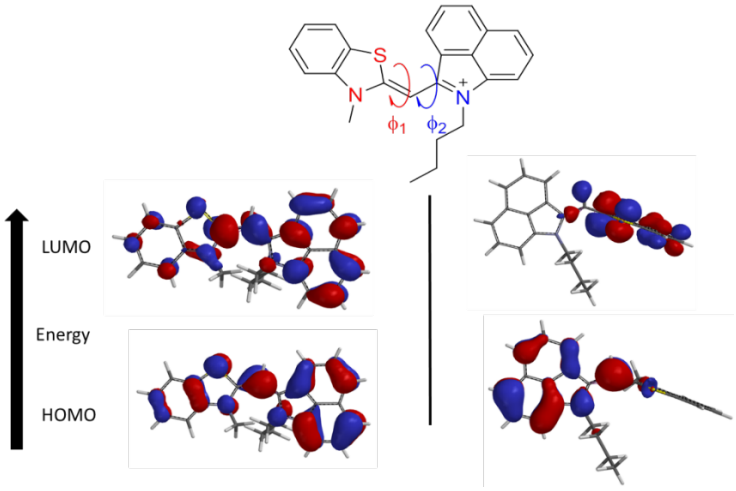

Figure 3 Frontier molecular orbitals of **6a** constrained in planar (left) and twisted (right) configurations

The geometry was constrained to keep the molecule planar to observe trends in the HOMO–LUMO gaps for comparing with excitation energies. As shown in Figure 4, the energy gap between HOMO and LUMO of compound **6d** containing a benz[*e*]indole heterocycle is the lowest among the series of dyes at 2.06 eV. This finding is corroborated by the bathochromic absorbance maximum of the benz[*e*]indole compared to the Fischer indole, benzothiazole, and

benzoxazole heterocycles which led to further delocalizing of the electrons and therefore stabilizing the orbitals.

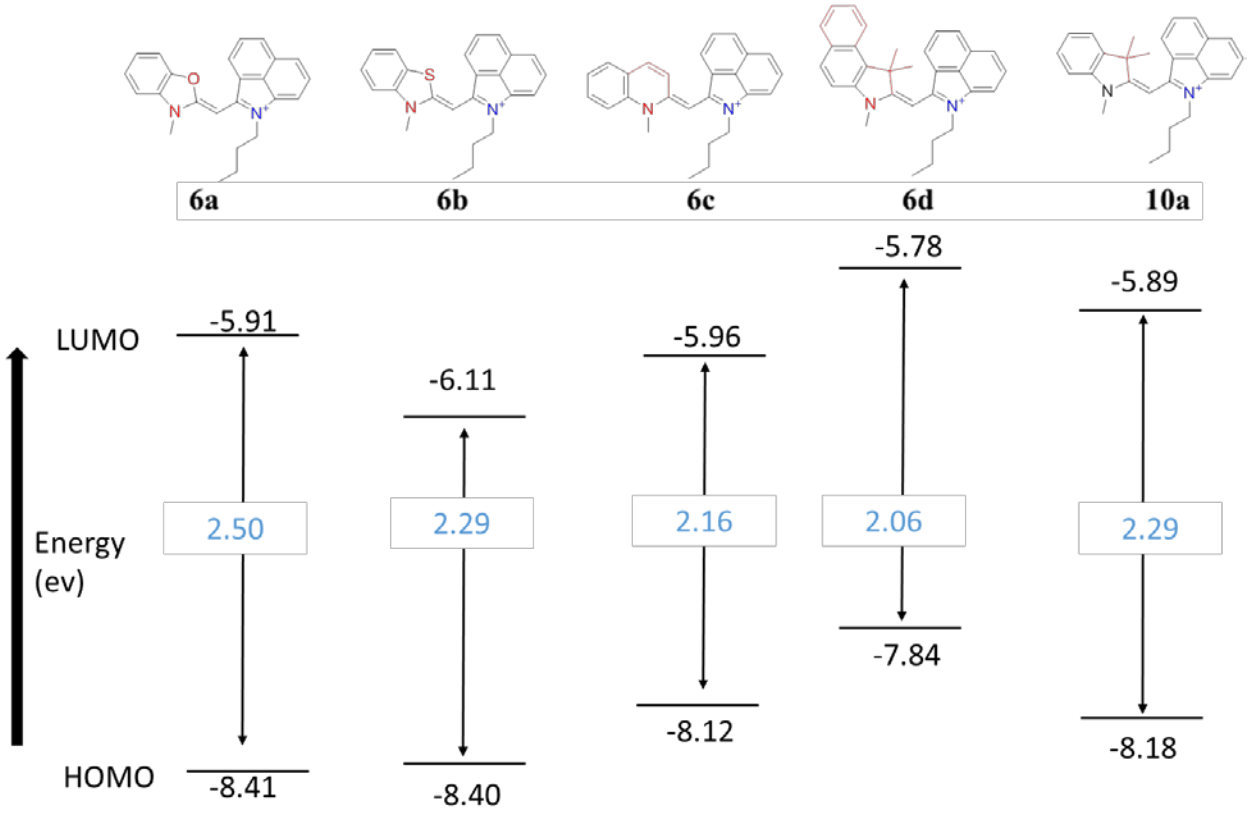

Figure 4 HOMO and LUMO orbital analysis of differing heterocycles in the monomethine system; energies (black), HOMO-LUMO gaps (blue)

The benzoxazole heterocycle in dye **6a** influenced the conjugated system shown by shifting the absorbance maximum to the blue. This dye **6a** shows the highest energy gap likely due to both the lone pair of electrons and electronegativity of the oxygen atom similar to dye **6b** with a sulfur containing benzothiazole heterocycle that had the second highest energy gap. Dye **10a** containing a 3,3-dimethylindole heterocycle had the same energy gap as **6b** with the benzothiazole heterocycle, but had higher energy.

The theoretical absorption λ_{max} values are plotted along with the experimental data as shown in Figure 5. Time-dependent density functional theory (TD-DFT) has been shown to work well for large conjugated molecules because the orbitals are obtained by solving the Kohn-Sham equation involving exchange and correlation (XC) terms [55]. Although a discrepancy gap is observed between the theoretical and experimental results, the observed trends in absorbance wavelength are almost the same with the calculated absorbance wavelength giving slightly blue-shifted values [47].

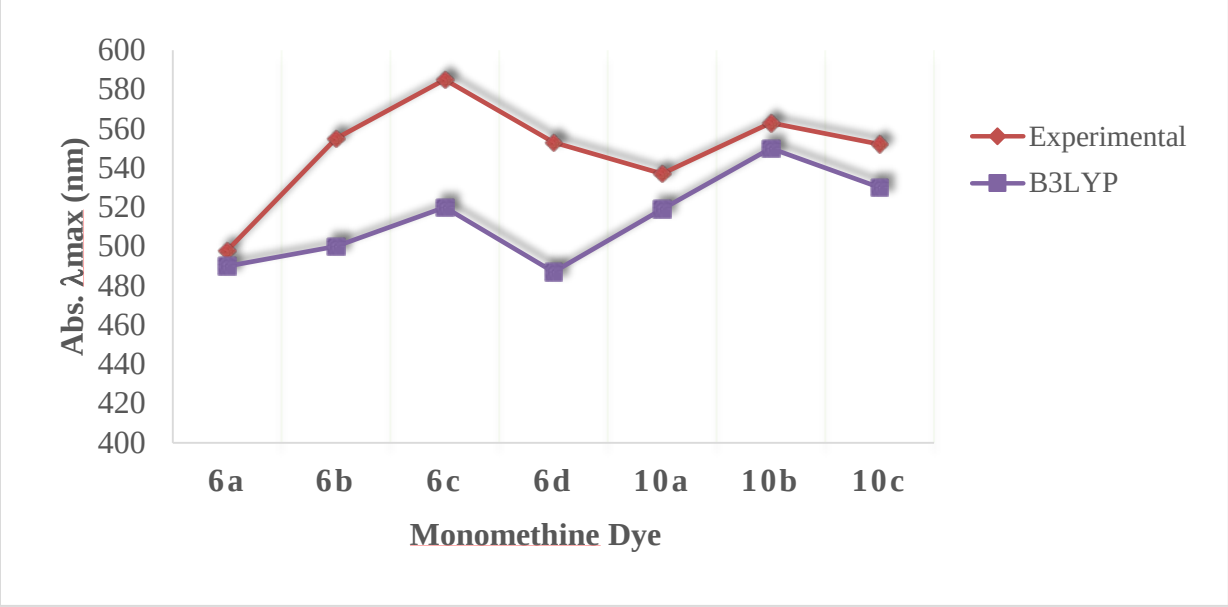

Figure 5 Experimental and Calculated λ_{max} values

Table 2 λ_{max}, NMR shifts, and computational charges of monomethine cyanine dyes.

	Heterocycle Included in Monomethine Dye	λ_{abs} (nm) exp.	λ_{abs} (nm) calc.	Charge of Methine Carbon	Methine ^{13}C Shift (ppm)	Methine ^{1}H Shift (ppm)	N-CH_3 ^{1}H Shift (ppm)
6a	benzoxazole	498	490	−0.535	75.51	6.15	4.05
6b	benzothiazole	555	500	−0.421	87.40	6.47	4.16
6c	quinoline	585	520	−0.526	93.65	6.35	4.37

6d	benz(*e*)indole	553	487	−0.284	94.10	6.43	3.60
10a	dimethylindole	542	519	−0.328	82.78	6.30	3.47
	Substitution at the 5-position of heterocycle **10a**						
10a	H	542	519	−0.328	82.78	6.31	-
10b	OMe	563	550	−0.316	83.44	6.23	-
10c	Cl	552	530	−0.344	83.81	6.29	-

Calculated values obtained via TD-DFT in vacuum, NMR run in DMSO-d_6 at 25 °C.

As shown in Figure 6 and Table 2, the observed change of the chemical shift of the methine-proton is most likely due to altering the electron density from the surrounding atoms. Taking into account that the overall charges and the length of the conjugated system are similar in all of these compounds, the molecular electrostatic potential (MEP) maps shown in Figure 6 do not present sharp contrasting features. However, the subtle differences in molecular structure of the compounds are clearly reflected. The negative (red and yellow) and the positive (blue) regions represent the distribution of the electrostatic potential in the molecule. Oxygen is more electronegative then sulfur, and therefore increases the delocalization of electrons through the dye corresponding to a λ_{max} shift from 555 nm (**6b**) to 498 nm (**6a**) and a shift of methine-proton from 6.47 (**6b**) to 6.15 ppm (**6a**). Sulfur is only slightly more electronegative than carbon causing a smaller methine-proton shift from 6.47 (**6b**) to 6.30 ppm (**10a**) and corresponding to a similar shift in λ_{max} from 555 nm (**6b**) to 542 (**10a**). An increase in conjugation leads to bathochromic shift of the absorbance maxima from 542 in **10a** to 553 in 6d with the extra benzene ring. Furthermore, the benz[*e*]indole heterocycle in **6d** also corresponds the largest shift of the methine-proton at 6.43 ppm due to the lack of the electron density around the methine chain and increased conjugation in the heterocycle.

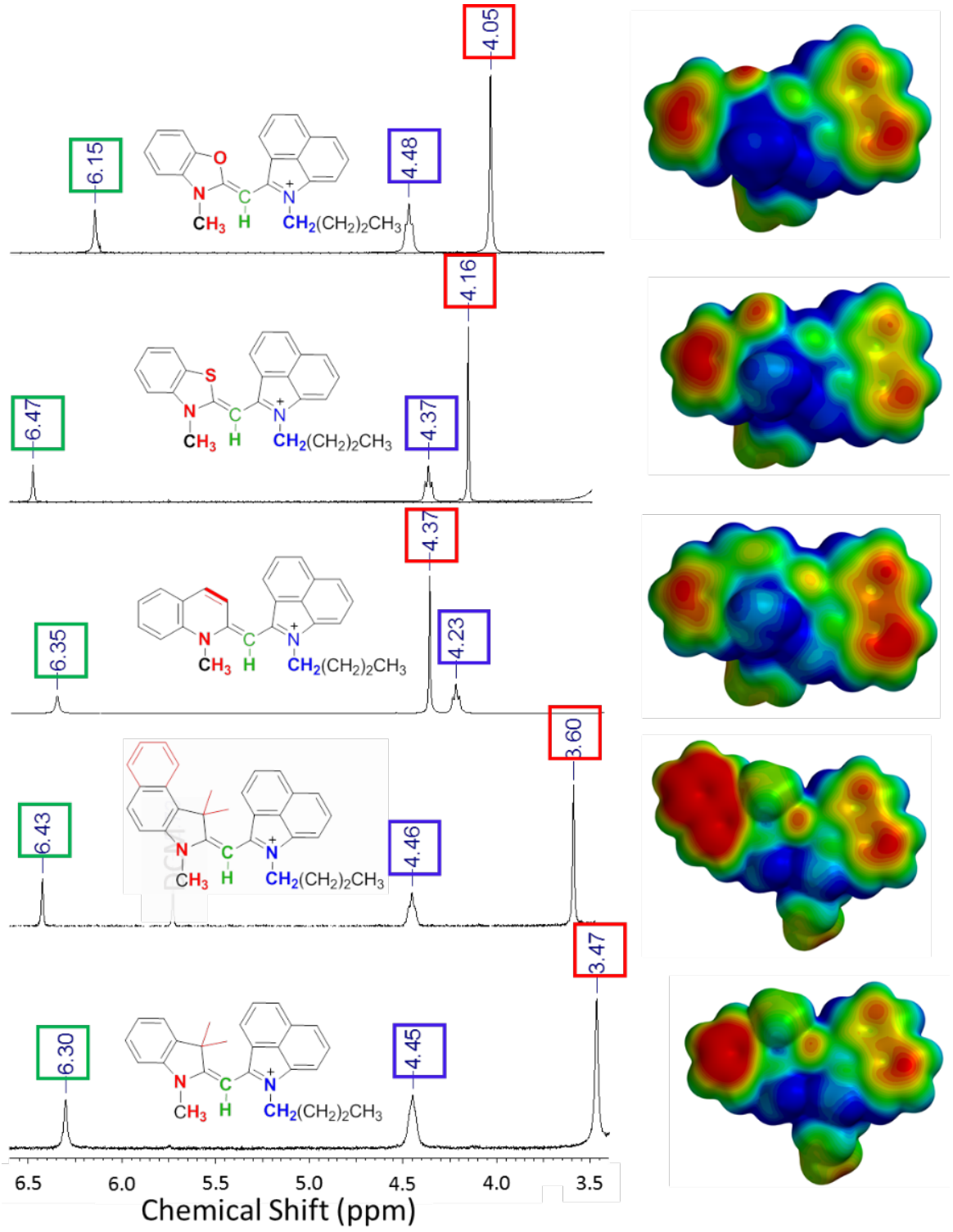

Figure 6 ^{1}H NMR shift of methine proton in DMSO-d6 at 25 ^{o}C, Calculated EMP (right)

2.2.4 DNA Binding

It has been reported that a combination of a crescent shape complements the helical DNA minor groove, hydrogen bond donors and acceptors on the side of the molecule facing the DNA, a cationic center to enhance electrostatic interactions with negatively charged phosphate groups, and hydrophobic character from an extended fused heterocyclic structure allows for optimization of the compound for DNA minor groove interactions [56-59]. Dye **6b**, which is crescent shaped and has an overall hydrophobic structure, includes a sulfur on the side suggested by computational data to be facing the DNA (Figure 7) and contains delocalized positive charge throughout the polymethine chain; therefore, it was selected for DNA binding as a representative example of the series.

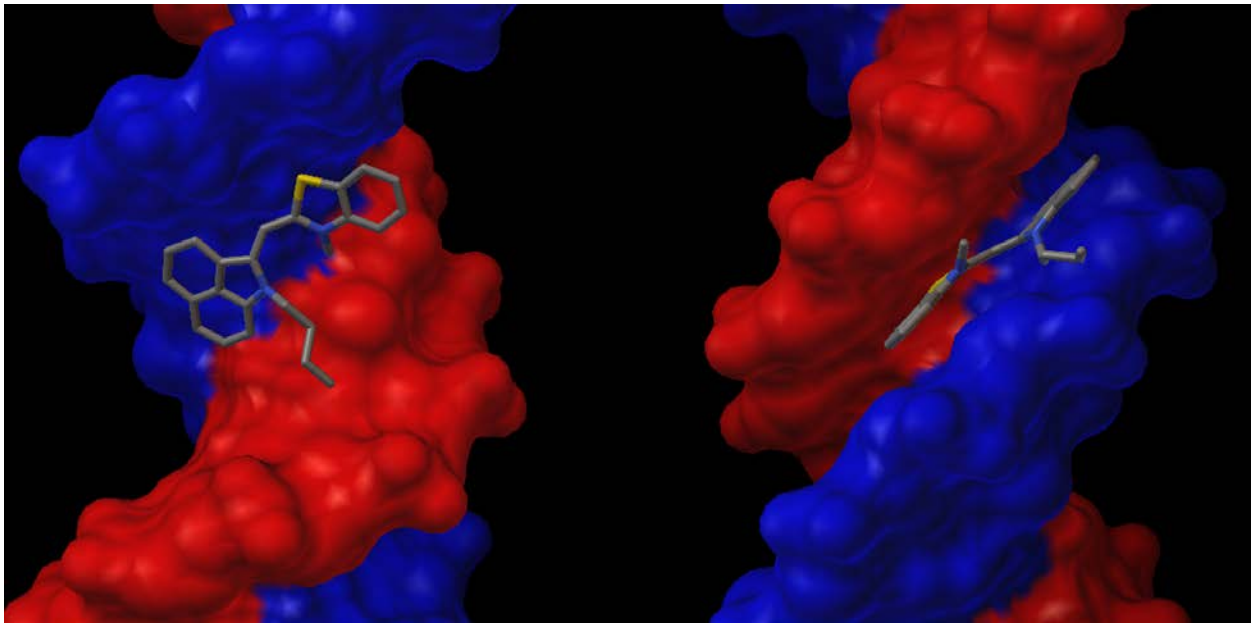

Figure 7 Dye **6b** with fixed torsion angles and planar geometry suggested to bind to the major (left) and minor (right) grooves of dsDNA by computational studies

As presented in Figure 8, the fluorescence spectrum of **6b** in Tris-HCl buffer exhibits a particularly weak fluorescence spectrum with 2 local maxima at 565 nm and 630 nm. The 565 nm

band is red shifted to 582 nm when ct-DNA is added and an increase in fluorescence is observed. Similar to the previously described enhancement in glycerol, a viscous solvent, this enhancement is also attributable to the fact that on excitation the inability to freely rotate around the methine bond due to binding does not allow for non-radiative deactivation of the ground state causing the dye to fluoresce. Using a double reciprocal plot, the binding constant, K_b, of **6b** was determined to be 1.0×10^4 M^{-1} which is on par with similar monomethine cyanine dyes [8].

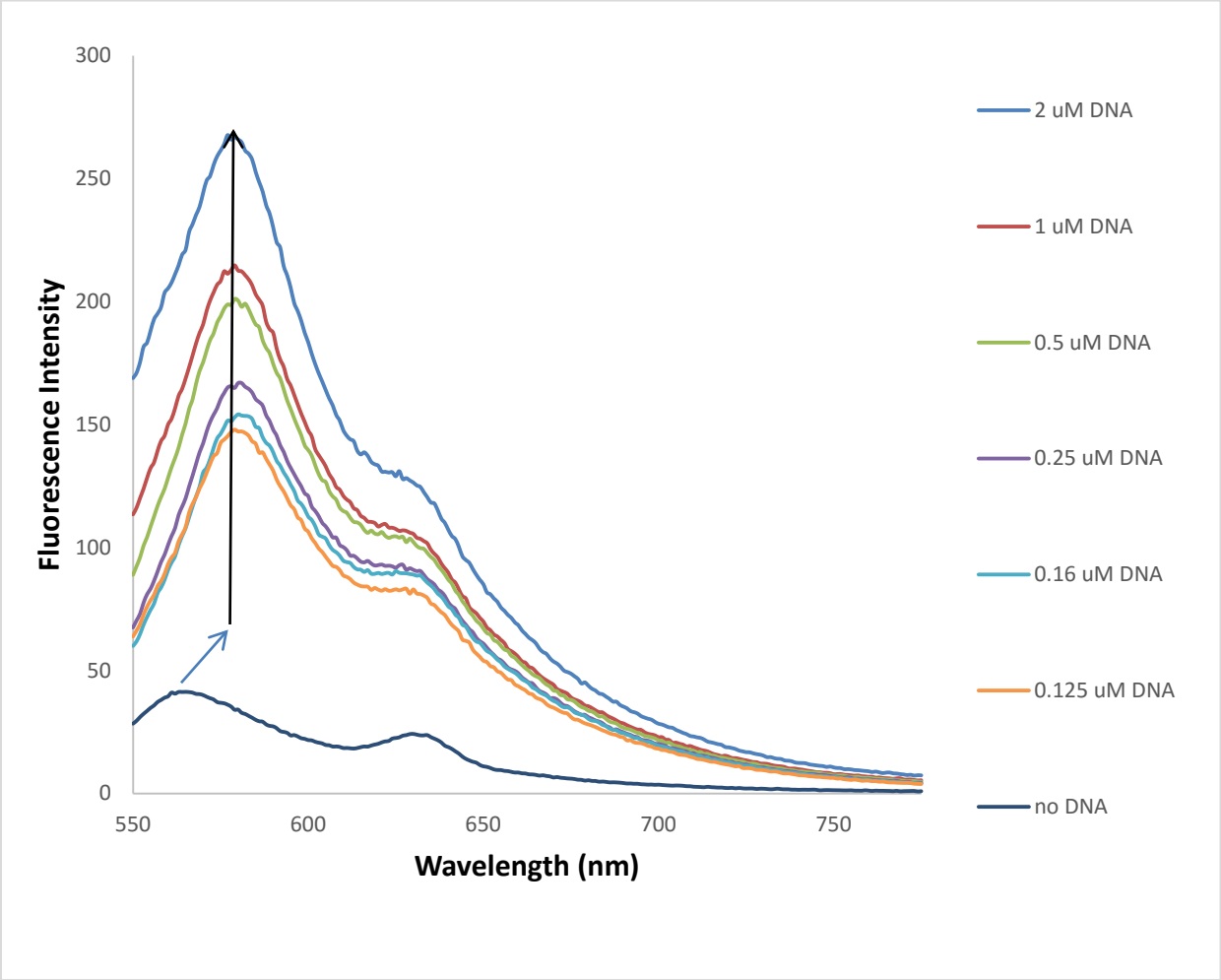

Figure 8 Emission spectra of dye **6b** (10 μM) in Tris-HCl buffer with and without ct-DNA (excitation wavelength 520 nm)

Although dye **6b** is structurally similar to TO (Figure 1), a known intercalating agent, it is intriguing to investigate interactions at the molecular level. Therefore, computational studies were

conducted to get better insight on the mode of binding for these red shifted monomethines. The 264D (a dodecamer d(CGCAAATTTGCG)$_2$) was chosen from the Protein Data Bank as a representative model for dsDNA binding. Molecular docking was then performed on **6b** using Autodock (Figure 7). As it turns out, docking was achieved in both the minor and major grooves. Our computational data indicates higher propensity to bind in the minor groove based on relative scoring. Surprisingly, **6b** did not display intercalation based on these computational studies. This could be due to the bulkiness of the benz[*c,d*]indole heterocycle. Further studies such as electrophoresis unwinding assays or crystallography can be conducted in the future to more accurately define the binding modes of these compounds.

2.3 Experimental

2.3.1 General Information

All chemicals and solvents were of American Chemical Society grade or HPLC purity and were used as received. HPLC grade methanol and glycerol were purchased from Sigma-Aldrich (Saint Louis, MO). All other chemicals were purchased from Fisher Scientific (Pittsburgh, PA, USA) or Acros Organics. The reactions were followed using silica gel 60 F254 thin layer chromatography plates (Merck EMD Millipore, Darmstadt, Germany). The ^{1}H NMR and ^{13}C NMR spectra were obtained using high quality Kontes NMR tubes (Kimble Chase, Vineland, NJ) rated to 500 MHz and were recorded on a Bruker Avance (400 MHz) spectrometer DMSO-d_6 or CD_3Cl-d_3. High-resolution accurate mass spectra (HRMS) were obtained at the Georgia State University Mass Spectrometry Facility using a Waters Q-TOF micro (ESI-Q-TOF) mass spectrometer. HPLC data was obtained using a Waters 2487 dual detector wavelength absorption detector with wavelengths set at 260 and 600 nm. The column used in LC was a Waters Delta-Pak 5 µM 100Å

3.9×150 mm reversed phase C18 column, with a flow rate of 1mL/min employing a 5-100% acetonitrile/water/0.1% formic acid gradient. All compounds tested were > 95% pure. Infrared spectra (FT-IR) were obtained using a PerkinElmer Spectrum 100 spectrometer (appendix). UV-Vis/NIR absorption spectra were recorded on a Varian Cary 50 spectrophotometer interfaced with Cary WinUV Scan Application v3.00 using VWR disposable polystyrene cuvettes with a 1 cm pathlength. Laser Induced Fluorescence (LIF) emission spectra were acquired using Shimadzu RF-5301 Spectroflurophotometer (Shimadzu Corporation Analytical Instruments Division, Duisburg, F. R. Germany) interfaced to a PC with RF-5301PC software using Sigma-Aldrich disposable polystyrene fluorimeter cuvettes with a 1 cm pathlength. All spectral measurements were recorded at room temperature. The data analysis and calculations were carried out using Microsoft Excel (Microsoft Corporation, Redmond, Wa).

2.3.2 Synthesis

2.3.2.1 General Synthetic Procedure for the indolium salts 4 and 9a-c

Thioether **4** was previously synthesized by our group and others [20, 60].

The substituted indoles **8** were synthesized as previously reported by our group and others [20, 61]. Each individual compound **8** was dissolved in acetonitrile and alkyl halide was added. The reaction mixture was then refluxed for 12 h. Thin layer chromatography (TLC) was used to monitor the reaction progress using a mixture of 4/1 dichloromethane/hexanes. Upon cooling to room temperature, the quaternary ammonium salts **9a-c** were precipitated in diethyl ether and collected by vacuum filtration [36, 62].

2.3.2.2 General Synthesis of the monomethine dyes

Thioether **4** and each quaternary ammonium salt **5a-d** and **9a-c**, respectively, were dissolved in acetonitrile and a catalytic amount of triethlyamine was added to the solution. The reaction mixture was refluxed at 60 °C for 1 h and monitored by UV-Vis. Upon cooling to room temperature, the corresponding dyes **6a-d** and **10a-c** were precipitated by adding diethyl ether. The solid was collected by vacuum filtration and triethyl ammonium salts were removed by washing with deionized water. The final dyes were purified via precipitation from methanol with diethyl ether.

A monomethine cyanine dye, 1-butyl-2-[(3-methyl-1,3-benzoxazol-2(3H)-ylidene)methyl]benzo[*c,d*]indolium iodide (**6a**); Yield 0.43 g, 69%; mp >260 °C; ^{1}H NMR (400 MHz, DMSO-d_6): δ ppm 0.95 (t, J = 7.1 Hz, 3 H), 1.44-1.49 (m, 2 H), 1.82-1.85 (m, 2 H), 4.04 (s, 3 H), 4.48 (t, *J* = 7.3 Hz, 2 H), 6.14 (s, 1 H), 7.55 - 7.67 (m, 3 H), 7.73 (t, *J* = 8.6 Hz, 1 H), 7.82 - 7.89 (m, 2 H), 8.04 (t, *J* = 7.3 Hz, 1 H), 8.15 (d, *J* = 7.1 Hz, 1 H), 8.39 (d, *J* = 7.6 Hz, 1 H), 9.17 (d, *J* = 7.6 Hz, 1 H); ^{13}C NMR (100 MHz, DMSO-d_6): δ ppm 14.3, 20.1, 30.2, 32.0, 75.5, 110.1, 112.3, 112.6, 126.6, 127.2, 129.7, 129.7, 130.3, 130.4, 131.8, 132.9, 141.1, 146.8, 155.6, 162.0; HRMS (ESI): Calcd for $C_{24}H_{23}N_{2O}$+ m/z 355.1805, obsd m/z 355.1791.

A monomethine cyanine dye, 1-butyl-2-[(3-methyl-1,3-benzothiazol-2(3H)-ylidene)methyl]benzo[*c,d*]indolium iodide (**6b**); Yield 0.37 g, 57%; mp 249-251 °C; ^{1}H NMR (400 MHz, DMSO-d_6): δ ppm 0.96 (t, *J* = 7.3 Hz, 3 H), 1.43-1.49 (m, 2 H), 1.75 - 1.92 (m, 2 H), 4.16 (s, 3 H), 4.37 (t, *J* = 7.2 Hz, 2 H), 6.47 (s, 1 H), 7.55 (d, *J* = 7.3 Hz, 1 H), 7.59 - 7.72 (m, 2 H), 7.74 - 7.81 (m, 2 H), 7.89 (t, *J* = 7.8 Hz, 1 H), 8.04 (d, *J* = 8.3 Hz, 1 H), 8.20 (d, *J* = 7.8 Hz, 1 H), 8.32 (d, *J* = 8.1 Hz, 1 H), 9.25 (d, *J* =7 .6 Hz, 1 H); ^{13}C NMR (100 MHz, DMSO-d_6): δ ppm 13.8,

19.7, 29.7, 35.4, 43.4, 87.0, 109.0, 115.0, 122.0, 123.6, 124.7, 126.8, 128.8, 129.2, 129.6, 129.7, 132.3, 141.0, 141.2, 154.0, 165.9; HRMS (ESI): Calcd for $C_{24}H_{23}N_2S^+$ m/z 371.1576, obsd m/z 371.1566.

A monomethine cyanine dye, 1-butyl-2-[(1-methylquinolin-2(1H)-ylidene)methyl] benzo[*c,d*]indolium iodide (**6c**); Yield 0.44 g, 69%; mp 225-227 °C; ^{1}H NMR (400 MHz, DMSO-d_6): δ ppm 0.95 (t, *J* = 7.2 Hz, 3 H), 1.40 - 1.54 (m, 2 H), 1.79-1.85 (m, 2 H), 4.25 (t, *J* = 7.3 Hz, 2 H), 4.37 (s, 3 H), 6.35 (s, 1 H), 7.31 (d, *J* = 7.3 Hz, 1 H), 7.55 - 7.62 (m, 2 H), 7.65 (t, *J* = 7.7 Hz, 1 H), 7.82 (t, *J* = 7.4 Hz, 1 H), 8.07 (t, *J* = 7.7 Hz, 1 H), 8.12 (d, *J* = 8.1 Hz, 1 H), 8.21 (d, *J* = 7.8 Hz, 1 H), 8.35 (d, *J* = 8.1 Hz, 2 H), 8.58 - 8.71 (m, 2 H); ^{13}C NMR (100 MHz, DMSO-d_6): δ ppm 13.9, 19.7, 29.7, 42.9, 93.6, 106.4, 118.4, 120.0, 123.7, 127.5, 128.9, 129.5, 129.7, 130.4, 133.9, 141.2, 152.1, 157.0; HRMS (ESI): Calcd for $C_{26}H_{25}N_2^+$ m/z 365.2012, obsd m/z 365.1999.

A monomethine cyanine dye, 1-butyl-2-[(1,1,3-trimethyl-1,3-dihydro-2H-benzo[*e*]indol-2-ylidene)methyl]benzo[*c,d*]indolium iodide (**6d**); Yield 0.52 g, 72%; mp 190-192 °C; ^{1}H NMR (400 MHz, DMSO-*d*6): δ ppm 0.95 (t, *J* = 7.3 Hz, 3 H), 1.45 (q, *J* = 7.3 Hz, 2 H), 1.80 - 1.97 (m, 8 H), 3.60 (s, 3 H) 4.46 (t, *J* = 7.3 Hz, 2 H), 6.43 (s, 1 H), 7.60 (t, *J* = 7.5 Hz, 1 H), 7.67 - 7.78 (m, 3 H), 7.81 (d, *J* = 7.3 Hz, 1 H), 7.84 - 7.93 (m, 3 H), 8.14 (d, *J* = 8.0 Hz, 1 H), 8.21 (d, *J* = 8.7 Hz, 1 H), 8.35 (d, *J* = 8.2 Hz, 2 H); ^{13}C NMR (100 MHz, DMSO-d_6): δ ppm 13.7, 19.7, 25.2, 29.8, 43.8, 53.2, 54.9, 82.9, 110.4, 113.1, 122.9, 123.0, 124.1, 125.8, 127.7, 128.0, 128.6, 129.3, 129.6, 129.8, 130.0, 130.2, 130.3, 132.1, 132.3, 133.6, 140.8, 141.3, 156.5, 181.1; HRMS (ESI): Calcd for $C_{31}H_{31}N_2^+$ m/z 431.2482, obsd m/z 431.2469.

A monomethine cyanine dye, 1-butyl-2-[(1,1,3-trimethyl-1,3-dihydro-1H-indol-2-ylidene)methyl]benzo[*c,d*]indolium iodide (**10a**); Yield 0.42 g, 63%; mp 238-240 °C; ^{1}H NMR

(400 MHz, DMSO-d_6): δ ppm 0.95 (t, *J* = 7.08 Hz, 3 H), 1.42-1.47 (m, 2 H), 1.65 (s, 6 H), 1.85-1.88 (m, 2 H), 3.47 (s, 3 H), 4.46 (t, *J* = 7.0 Hz, 2 H), 6.31 (s, 1 H), 7.44 (t, *J* = 7.3 Hz, 1 H), 7.51 - 7.63 (m, 2 H), 7.69 - 7.85 (m, 4 H), 7.88 - 7.96 (m, 2 H), 8.38 (d, *J* = 8.0 Hz, 1 H); ^{13}C NMR (100 MHz, DMSO-d_6): δ ppm 13.6, 19.6, 25.6, 29.7, 43.8, 45.7, 51.4, 82.9, 110.9, 113.3, 122.7, 123.2, 123.9, 126.4, 128.6, 129.1, 129.1, 129.5, 130.0, 130.2, 132.5, 140.1, 140.6, 143.9, 156.9, 179.5; HRMS (ESI): Calcd for $C_{27}H_{29}N_2$+ m/z 381.2325, obsd m/z 381.2313.

A monomethine cyanine dye, 1-butyl-2-[(3-ethyl-5-methoxy-1,1-dimethyl-1,3-dihydro-1H-indol-2-ylidene)methyl]benzo[*c,d*] indolium iodide (**10b**); Yield 0.65 g, 90%; mp 187-189 °C; ^{1}H NMR (400 MHz, DMSO-d_6): δ ppm 0.92 (t, *J* = 7.2 Hz, 3 H), 1.14 (t, *J* = 6.7 Hz, 3 H), 1.37-1.43 (m, 2 H), 1.61 (s, 6 H), 1.79-1.83 (m, 2 H), 3.85 (s, 3 H), 4.20 (q, *J* = 6.3 Hz, 2 H), 4.39 (t, *J* = 6.1 Hz, 2 H), 6.23 (s, 1 H), 7.10 (d, *J* = 9.9 Hz, 1 H), 7.40 (s, 1 H), 7.58 - 7.67 (m, 2 H), 7.70 (t, *J* = 7.9 Hz, 1 H), 7.77 - 7.87 (m, 2 H), 7.87 - 7.94 (m, 1 H), 7.91 (d, *J* = 7.5 Hz, 1 H), 8.30 (d, *J* = 8.0 Hz, 2 H); ^{13}C NMR (100 MHz, DMSO-d_6): δ ppm 13.3, 13.7, 19.5, 25.1, 29.7, 43.4, 45.6, 51.9, 56.0, 83.4, 109.5, 109.9, 113.8, 115.3, 122.4, 124.1, 127.3, 129.4, 129.5, 129.9, 130.1, 132.1, 134.8, 140.9, 142.8, 154.9, 158.9, 179.4; HRMS (ESI): Calcd for $C_{29}H_{33}N_2O$+ m/z 425.2587, obsd m/z 425.2576.

A monomethine cyanine dye, 1-butyl-2-[(5-chloro-3-ethyl-1,1-dimethyl-1,3-dihydro-1H-indol-2-ylidene)methyl]benzo[*c,d*] indolium iodide (**10c**); Yield 0.25 g, 34%; mp 152-154 °C; ^{1}H NMR (400 MHz, DMSO-d_6): δ ppm 0.91 (t, *J* = 7.2 Hz, 3 H), 1.08 (t, *J* = 6.7 Hz, 3 H), 1.37-1.43 (m, 2 H), 1.63 (s, 6 H), 1.81-1.84 (m, 2 H), 4.16 (q, *J* = 6.7 Hz, 2 H), 4.47 (t, *J* = 6.3 Hz, 2 H), 6.29 (s, 1 H), 7.59 (d, *J* = 8.7 Hz, 1 H), 7.67 (d, *J* = 8.7 Hz, 1 H), 7.71 - 7.81 (m, 2 H), 7.85 - 7.95 (m, 3 H), 8.10 (d, *J* = 7.3 Hz, 1 H), 8.39 (d, *J* = 8.2 Hz, 1 H); ^{13}C NMR (100 MHz, DMSO-d_6): δ ppm

13.0, 13.7, 19.4, 25.4, 29.9, 43.8, 45.7, 51.5, 83.8, 111.8, 115.5, 123.5, 123.7, 123.9, 128.4, 128.9, 129.2, 129.6, 130.1, 130.6, 133.2, 140.5, 140.8, 142.7, 156.8, 179.1; HRMS (ESI): Calcd for $C_{28}H_{30}N_2Cl+$ m/z 429.2092, obsd m/z 429.2083.

2.3.3 Stock Solutions for Optical Measurements

Stock solutions were prepared by weighing the solid of each individual compound on a 5-digit analytical balance and adding solvent via class A volumetric pipette to make a 1.0 mM solution. The vials were vortexed for 20 s and then sonicated for 5 min to ensure complete dissolution. When not in use, the stock solutions were stored in a dark at 4 °C. For emission spectra in methanol/glycerol solutions the concentrations were prepared *via* the dilution of the stock solution in methanol followed by the addition of the appropriate volume of glycerol to achieve the desired concentrations.

2.3.4 Method of Determining Absorbance and Fluorescence

Stock solutions were used to prepare five dilutions of dyes with concentrations ranging from 5-25 μM using a class A volumetric pipette in order to maintain absorption between 0.1 and 1.0. The dye solutions were diluted ten-fold for fluorescence in order to minimize inner filter effect. The absorption spectra of each sample were measured in duplicate from 400 to 750 nm. Aggregation of **6b** was ruled out by measuring absorption at different concentrations. Dye **6b** was tested for solvatochromic changes in absorption by dissolving the dye in five different solvents (ethanol, dimethyl formamide, dichloromethane, acetonitrile, and aqueous tris buffer) to observe any change in λ_{max}. The emission spectra of each sample were measured in duplicate with a 530 nm excitation wavelength and slit widths of 5 nm for both excitation and emission. Emission spectra were corrected automatically by our developed method file used for reading the spectrofluorometer.

2.3.5 Computational methods

The structure of each compound was first optimized using the TD-DFT method with the hybrid exchange-correlation functional, B3LYP/6-31G* basis set using SPARTAN '14 (Irvine, CA) [63]. The torsional angles from the quaternary nitrogen to the α-carbon on the alternate heterocycle were restricted to 0° to get the calculated absorbance values, LUMO and HOMO orbitals, and electrostatic potential maps. The calculated LUMO and HOMO orbitals were obtained using a restricted hybrid HF-DFT SCF calculation performed with B3LYP/6-31G* basis set. The electrostatic potential maps were investigated for the optimized structures at HF/6-31G*. DNA docking studies were achieved using AutoDockTools 1.5.6 (La Jolla, CA, USA). Results of DNA docking study with dye 6b under constraints were obtained by making all bonds within the dye to be non-rotatable and planar [64, 65]. Polar and aromatic hydrogens were added to the DNA using GROMACS package [66] using GROMOS 53A6 force field [67] and Gasteiger Marsili charges [68]. A 78 × 70 × 64 grid box with a resolution of 0.375 Å was created encompassing the entire DNA using module AutoGrid 4.0. Dye **6b** was then added and simulations were performed using Genetic Algorithm (GA).

2.3.6 DNA Binding Studies

A stock solution of **6b** (1×10^{-4} M) and ct-DNA type 1 (7.5×10^{-3} M) were prepared in ethanol and Tris-HCl buffer solution, respectively. Fluorescence titration with ct-DNA concentrations (0-200 mM) were made by mixing 35 μL **6b** solution with Tris-HCl buffer solution with and without ct-DNA to a total volume of 3500 μL in a fluorescence cuvette to make working solutions of 10 μM **6b**. Fluorescence spectra were measured in duplicate with excitation at 520 nm and slit widths of 10 nm for both excitation and emission.

2.4 Conclusion

A series of 7 monomethine cyanines were synthesized in good yield with red-shifted absorbance properties in comparison to previously synthesized monomethine cyanine dyes. Although the benz[*c*,*d*]indolium containing monomethine cyanine dyes in this report are non-fluorescent in free flowing solvent, when the dyes are in a viscous environment their fluorescence becomes observable due to the restricted ability to rotate around the methine bridge. Computational methods outlined above were shown to be useful as a predictive tool for determining their optical properties. Dye **6b** was chosen as a representative example for DNA binding studies and was shown to bind DNA with an observable increase in fluorescence. Computational studies suggest it is binding the minor groove. Utilizing the described techniques these dyes could be developed as potential biological probes. Future studies will investigate how the different heterocycles and substituents affect binding to biological targets.

2.5 REFERENCES for INTRODUCTION

1. Williams, C.H.G.,*Trans. R. Soc. Edinburgh* **1856**, 21, 377
2. Von Babo, *Prakt. Chem.* **1857**, 72, 73
3. Von Babo, *Chem. Zentr.* **1858**, 218
4. Hoogewerff, S., Van Dorp, W.A., *Brit. Chem. Abstracts* **1883**, 89
5. Bloch, O., Hamer, F.M., *Phot. J.* **1928**, 68, 21
6. Bloch, O., Hamer, F.M., *Chem. Zentr.* **1928**, 1, 874
7. Bloch, O., Hamer, F.M., *Brit. Chem. Abstracts* **1928**, B, 285
8. Doja, M.Q., *Chem. Rev*., **1932**, 11 (3), 273–321
9. The Theory of the Photographic Process. By C. E. Kenneth MEES. 1124 pp. New York: The Macmillan Company, **1944**
10. Paddy, J.F, *Trans. Faraday Soc*., **1964**, 60, 1325-1334
11. Mishra, A., Behera, P.K., Mishra, B.K., Behera, G.B., *Chem. Rev*. **2000**, 100, 1973−2011
12. Hyun, H., Owens, E. A., Wada, H., Levitz, A., Park, G., Park, M. H., Frangioni, J. V., Henary, M. and Choi, H. S. (**2015**), Cartilage-Specific Near-Infrared Fluorophores for Biomedical Imaging. *Angew. Chem. Int. Ed*., 54: 8648–8652.
13. Choi, H.S., Gibbs, S.L., Lee, J.H.*et al.*, *Nat. Biotech.* **2013**, 31, 148–153
14. H. Hyun, M. H. Park, E. A. Owens, H. Wada, M. Henary, H. J. M. Handgraaf, A. L. Vahrmeijer, J. V. Frangioni, H. S. Choi, *Nat. Med.* **2015**, 21, 192–197
15. Soriano, E., Holder, C., Levitz, A., Henary, M., *Molecules* **2016**, 21 (1), 23
16. Weissleder R, Pittet MJ. *Nature* **2008**, 452, 580–589.
17. Chen, J. Stubbe, J., *Nat. Rev. Cancer*, **2005**, 5, 102–112

18. Johnstone, T.C., Park,G.Y., Lippard, S.J, *Anticancer Res*., **2014**, 34, 471–476

19. Li, Z. Grant, K.B., *RSC Adv*., **2016**, 6, 24617-24634

2.6 REFERENCES for Chapter 1

1. Mishra, A.; Behera, R.K.; Behera, P.K.; Mishra, B.K.; Behera, G.B. Cyanines during the 1990s: A Review. *Chem. Rev*. **2000**, 100, 1973–2012.

2. Pisoni, D.S.; Todeschini, L.; Borges, A.C.A.; Petzhold, C.L.; Rodembusch, F.S.; Campo, L.F. Symmetrical and Asymmetrical Cyanine Dyes. Synthesis, Spectral Properties, and BSA Association Study. *J. Org. Chem*. **2014**, 79, 5511–5520.

3. Wada, H.; Hyun, H.; Vargas, C.; Gravier, J.; Park, G.; Gioux, S.; Frangioni, J.V.; Henary, M.; Choi, H.S. Pancreas-Targeted NIR Fluorophores for Dual-Channel Image-Guided Abdominal Surgery. *Theranostics* **2015**, 5, 1–11.

4. Hyun, H.; Wada, H.; Bao, K.; Gravier, J.; Yadav, Y.; Laramie, M.; Henary, M.; Frangioni, J.V.; Choi, H.S. Phosphonated Near-Infrared Fluorophores for Biomedical Imaging of Bone. *Angew. Chem. Int. Ed. Engl*. **2014**, 53, 10668–10672.

5. Hyun, H.; Owens, E.A.; Wada, H.; Levitz, A.; Park, G.; Park, M.H.; Frangioni, J.V.; Henary, M.; Choi, H.S. Cartilage-Specific Near-Infrared Fluorophores for Biomedical Imaging. *Angew. Chem. Int. Ed. Engl*. **2015**, 54, 8648–8652

6. Njiojob, C.N.; Owens, E.A.; Narayana, L.; Hyun, H.; Choi, H.S.; Henary, M. Tailored Near-Infrared Contrast Agents for Image Guided Surgery. *J. Med. Chem*. **2015**, 58, 2845–2854.

7. Hyun, H.; Park, M.H.; Owens, E.A.; Wada, H.; Henary, M.; Handgraaf, H.J.M.; Vahrmeijer, A.L.; Frangioni, J.V.; Choi, H.S. Structure-inherent targeting of near-infrared fluorophores for parathyroid and thyroid gland imaging. *Nat. Med*. **2015**, 21, 192–197.

8. El-Shishtawy, R.M.; Asiri, A.M.; Basaif, S.A.; Rashad Sobahi, T. Synthesis of a new beta-naphthothiazole monomethine cyanine dye for the detection of DNA in aqueous solution. *Spectrochim. Acta A* **2010**, 75, 1605–1609.

9. Henary, M.; Levitz, A. Synthesis and applications of unsymmetrical carbocyanine dyes.*Dyes Pigment*. **2013**, 99, 1107–1116.

10. Silva, G.L.; Ediz, V.; Yaron, D.; Armitage, B.A. Experimental and Computational Investigation of Unsymmetrical Cyanine Dyes: Understanding Torsionally Responsive Fluorogenic Dyes. *J. Am. Chem. Soc*. **2007**, 129, 5710–5718.

11. Cao, J.; Wu, T.; Hu, C.; Liu, T.; Sun, W.; Fan, J.; Peng, X. The nature of the different environmental sensitivity of symmetrical and unsymmetrical cyanine dyes: An experimental and theoretical study. *Phys. Chem. Chem. Phys*. **2012**, 14, 13702–13708.

12. Deligeorgiev, T.G.; Gadjev, N.I.; Drexhage, K.-H.; Sabnis, R.W. Preparation of intercalating dye thiazole orange and derivatives. *Dyes Pigments* **1995**, 29, 315–322.

13. Thompson, M. Synthesis, Photophysical Effects, and DNA Targeting Properties of Oxazole Yellow-Peptide Bioconjugates. *Bioconjugate Chem*. **2006**, 17, 507–513.

14. Dähne, S.; Resch-Genger, U.; Wolfbeis, O.S. Near-Infrared Dyes for High Technology Applications; Daehne, S., Resch-Genger, U., Wolfbeis, O.S., Eds.; Kluwer: Dordrecht, The Netherland; Boston, MA, USA, **1998**.

15. Nygren, J.; Svanvik, N.; Kubista, M. The interactions between the fluorescent dye thiazole orange and DNA. *Biopolymers* **1998**, 46, 39–51.

16. Joseph, M.J.; Taylor, J.C.; McGown, L.B.; Pitner, B.; Linn, C.P. Spectroscopic studies of YO and YOYO fluorescent dyes in a thrombin-binding DNA ligand. *Biospectroscopy* **1996**, 2, 173–183.

17. Kabatc, J. Multicationic monomethine dyes as sensitizers in two- and three-component photoinitiating systems for multiacrylate monomers. *J. Photochem. Photobiol. A* **2010**, 214, 74–85.

18. Hirons, G.T.; Fawcett, J.J.; Crissman, H.A. Toto and Yoyo—New Very Bright Fluorochromes for DNA Content Analyses by Flow-Cytometry. *Cytometry* **1994**, 15, 129–140.

19. Dietzek, B.; Brüggemann, B.; Persson, P.; Yartsev, A. On the excited-state multi-dimensionality in cyanines. *Chem. Phys. Lett*. **2008**, 455, 13–19.

20. Soriano, E.; Outler, L.; Owens, E.A.; Henary, M. Synthesis of Asymmetric Monomethine Cyanine Dyes with Red-Shifted Optical Properties. *J. Heterocycl. Chem.* **2015**, 52, 180–184.

21. Upadhyayula, S.; Nunez, V.; Espinoza, E.M.; Larsen, J.M.; Bao, D.D.; Shi, D.W.; Mac, J.T.; Anvari, B.; Vullev, V.I. Photoinduced dynamics of a cyanine dye: Parallel pathways of non-radiative deactivation involving multiple excited-state twisted transients. *Chem. Sci.***2015**, 6, 2237–2251.

22. Sameiro, M.; Goncalves, T. Fluorescent Labeling of Biomolecules with Organic Probes.*Chem. Rev.* **2009**, 109, 190–212.

23. Lavis, L.D.; Raines, R.T. Bright ideas for chemical biology. *ACS Chem. Biol*. **2008**, 3, 142–155.

24. Mann, S. Life as a nanoscale phenomenon. *Angew. Chem. Int. Ed. Engl*. **2008**, 47, 5306–5320.

25. Resch-Genger, U.; Grabolle, M.; Cavaliere-Jaricot, S.; Nitschke, R.; Nann, T. Quantum dots versus organic dyes as fluorescent labels. *Nat. Methods* **2008**, 5, 763–775.

26. Chen, A.K.; Cheng, Z.; Behlke, M.A.; Tsourkas, A. Assessing the sensitivity of commercially available fluorophores to the intracellular environment. *Anal. Chem*. **2008**,80, 7437–7444.

27. Simeonov, A.; Jadhav, A.; Thomas, C.J.; Wang, Y.; Huang, R.; Southall, N.T.; Shinn, P.; Smith, J.; Austin, C.P.; Auld, D.S.; Inglese, J. Fluorescence spectroscopic profiling of compound libraries. *J. Med. Chem*. **2008**, 51, 2363–2371.

28. Longmire, M.R.; Ogawa, M.; Hama, Y.; Kosaka, N.; Regino, C.A.; Choyke, P.L.; Kobayashi, H. Determination of optimal rhodamine fluorophore for in vivo optical imaging. *Bioconjugate Chem.* **2008**, 19, 1735–1742.

29. Johnsson, N.; Johnsson, K. Chemical tools for biomolecular imaging. *ACS Chem. Biol.***2007**, 2, 31–38.

30. Marti, A.A.; Jockusch, S.; Stevens, N.; Ju, J.; Turro, N.J. Fluorescent hybridization probes for sensitive and selective DNA and RNA detection. *Acc. Chem. Res*. **2007**, 40, 402–409.

31. Willis, R.C. Portraits of life, one molecule at a time. *Anal. Chem*. **2007**, 79, 1785–1788.

32. Hama, Y.; Urano, Y.; Koyama, Y.; Bernardo, M.; Choyke, P.L.; Kobayashi, H. A comparison of the emission efficiency of four common green fluorescence dyes after internalization into cancer cells. *Bioconjugate Chem*. **2006**, 17, 1426–1431.

33. Yuste, R. Fluorescence microscopy today. Nat. Methods **2005**, 2, 902–904.

34. Lichtman, J.W.; Fraser, S.E. The neuronal naturalist: Watching neurons in their native habitat. *Nat. Neurosci*. **2001**, 4, 1215–1220.

35. Selvin, P.R. The renaissance of fluorescence resonance energy transfer. *Nat. Struct. Biol.***2000**, 7, 730–734.

36. Hu, H.; Owens, E.A.; Su, H.; Yan, L.; Levitz, A.; Zhao, X.; Henary, M.; Zheng, Y.G. Exploration of Cyanine Compounds as Selective Inhibitors of Protein Arginine Methyltransferases: Synthesis and Biological Evaluation. *J. Med. Chem.* **2015**, 58, 1228–1243.

37. Nanjunda, R.; Owens, E.; Mickelson, L.; Dost, T.; Stroeva, E.; Huynh, H.; Germann, M.; Henary, M.; Wilson, W. Selective G-Quadruplex DNA Recognition by a New Class of Designed Cyanines. *Molecules* **2013**, 18, 13588–13607.

38. Mapp, C.T.; Owens, E.A.; Henary, M.; Grant, K.B. Oxidative cleavage of DNA by pentamethine carbocyanine dyes irradiated with long-wavelength visible light. *Bioorganic Med. Chem. Lett.* **2014**, 24, 214–219.

39. Lakowicz, J.R. Principles of Fluorescence Spectroscopy, 3rd ed.; Springer: New York, NY, USA, **2006**.

40. Kantor, G.J.; Hull, D.R. An effect of ultraviolet light on RNA and protein synthesis in nondividing human diploid fibroblasts. *Biophys. J.* **1979**, 27, 359–370.

41. Cerutti, P.A. Prooxidant states and tumor promotion. *Science* **1985**, 227, 375–381.

42. Marks, R. An overview of skin cancers. Incidence and causation. *Cancer* **1995**, 75, 607–612.

43. Krasnaya, Z.A.; Tret'yakova, E.O.; Kachala, V.V.; Zlotin, S.G. Synthesis of conjugated polynitriles by the reactions of β-dimethylaminoacrolein aminal and 1-dimethylamino-1,3,3-trimethoxypropane with 2-dicyanomethylene-4,5,5-trimethyl-3-cyano-2,5-dihydrofuran. *Mendeleev Commun*. **2007**, 17, 349–351.

44. Brooker, L.G.S.; Keyes, G.H.; Williams, W.W. Color and Constitution. V.1 The Absorption of Unsymmetrical Cyanines. Resonance as a Basis for a Classification of Dyes. *J. Am. Chem. Soc*. **1942**, 64, 199–210.

45. Williams, C.G. XXVI.—Researches on Chinoline and its Homologues. *Earth Environ. Sci. Trans. R. Soc. Edinb.* **1857**, 21, 377–401.

46. Yarmoluk, S.M.; Kovalska, V.B.; Losytskyy, M.Y. Symmetric cyanine dyes for detecting nucleic acids. *Biotech. Histochem*. **2008**, 83, 131–145.

47. Levitz, A.; Ladani, S.T.; Hamelberg, D.; Henary, M. Synthesis and effect of heterocycle modification on the spectroscopic properties of a series of unsymmetrical trimethine cyanine dyes. *Dyes Pigments* **2014**, 105, 238–249.

48. Murphy, S.; Yang, X.Q.; Schuster, G.B. Cyanine Borate Salts That Form Penetrated Ion-Pairs in Benzene Solution—Synthesis, Properties, and Structure. *J. Org. Chem*. **1995**, 60, 2411–2422.

49. Deligeorgiev, T.G.; Zaneva, D.A.; Kim, S.H.; Sabnis, R.W. Preparation of monomethine cyanine dyes for nucleic acid detection. *Dyes Pigments* **1998**, 37, 205–211.

50. Timcheva, I.I.; Maximova, V.A.; Deligeorgiev, T.G.; Gadjev, N.I.; Sabnis, R.W.; Ivanov, I.G. Fluorescence spectral characteristics of novel asymmetric monomethine cyanine dyes in nucleic acid solutions. *FEBS Lett.* **1997**, 405, 141–144.

51. Oster, G.; Nishijima, Y. Fluorescence and Internal Rotation: Their Dependence on Viscosity of the Medium1. *J. Am. Chem. Soc.* **1956**, 78, 1581–1584.

52. Potts, K.T. Heteropentalenes, in Chemistry of Heterocyclic Compounds: Special Topics in Heterocyclic Chemistry; Weissberger, A., Taylor, E.C., Eds.; John Wiley & Sons, Inc.: Hoboken, NJ, USA, **1977**; Volume 30.

53. Escobedo, J.O.; Rusin, O.; Lim, S.; Strongin, R.M. NIR dyes for bioimaging applications.*Curr. Opin. Chem. Biol.* **2010**, 14, 64–70.

54. Kuhn, H. A Quantum-Mechanical Theory of Light Absorption of Organic Dyes and Similar Compounds. *J. Chem. Phys*. **1949**, 17, 1198–1212.

55. Bickelhaupt, F.M.; Baerends, E.J. Kohn-Sham Density Functional Theory: Predicting and Understanding Chemistry. Rev. *Comput. Chem*. **2000**, 15, 1–86.

56. Cantor, C.R.; Schimmel, P.R. Biophysical Chemistry; W.H. Freeman: San Francisco, CA, USA, **1980**.

57. Shaikh, S.A.; Ahmed, S.R.; Jayaram, B. A molecular thermodynamic view of DNA-drug interactions: A case study of 25 minor-groove binders. *Arch. Biochem. Biophys.* **2004**, 429, 81–99.

58. Chaires, J.B.; Ren, J.; Hamelberg, D.; Kumar, A.; Pandya, V.; Boykin, D.W.; Wilson, W.D. Structural selectivity of aromatic diamidines. *J. Med. Chem.* **2004**, 47, 5729–5742.

59. Fairley, T.A.; Tidwell, R.R.; Donkor, I.; Naiman, N.A.; Ohemeng, K.A.; Lombardy, R.J.; Bentley, J.A.; Cory, M. Structure, DNA minor groove binding, and base pair specificity of alkyl- and aryl-linked bis(amidinobenzimidazoles) and bis(amidinoindoles). *J. Med. Chem.* **1993**, 36, 1746–1753.

60. Sinha, S.H.; Owens, E.A.; Feng, Y.; Yang, Y.; Xie, Y.; Tu, Y.; Henary, M.; Zheng, Y.G. Synthesis and evaluation of carbocyanine dyes as PRMT inhibitors and imaging agents.*Eur. J. Med. Chem*. **2012**, 54, 647–659.

61. Nanjunda, R.; Owens, E.A.; Mickelson, L.; Alyabyev, S.; Kilpatrick, N.; Wang, S.; Henary, M.; Wilson, W.D. Halogenated pentamethine cyanine dyes exhibiting high fidelity for G-quadruplex DNA. *Bioorg. Med. Chem.* **2012**, 20, 7002–7011.

62. Narayanan, N.; Patonay, G. A New Method for the Synthesis of Heptamethine Cyanine Dyes: Synthesis of New Near-Infrared Fluorescent Labels. *J. Org. Chem*. **1995**, 60, 2391–2395.

63. Shao, Y.; Molnar, L.F.; Jung, Y.; Kussmann, J.; Ochsenfeld, C.; Brown, S.T.; Gilbert, A.T.B.; Slipchenko, L.V.; Levchenko, S.V.; O'Neill, D.P.; et al. Advances in methods and algorithms in a modern quantum chemistry program package. *Phys. Chem. Chem. Phys*.**2006**, 8, 3172–3191.

64. Morris, G.M.; Huey, R.; Lindstrom, W.; Sanner, M.F.; Belew, R.K.; Goodsell, D.S.; Olson, A.J. AutoDock4 and AutoDockTools4: Automated docking with selective receptor flexibility. *J. Comput. Chem*. **2009**, 30, 2785–2791.

65. Ricci, C.G.; Netz, P.A. Docking Studies on DNA-Ligand Interactions: Building and Application of a Protocol To Identify the Binding Mode. *J. Chem. Inf. Model.* **2009**, 49, 1925–1935.

66. Kulchin, Y.N.; Vitrik, O.B.; Kamenev, O.T.; Romashko, R.V. Vector Fields Reconstruction by Fiber Optic Measuring Network; SPIE: Bellingham, WA, USA; **2001**; pp. 100–108.

67. Oostenbrink, C.; Soares, T.; van der Vegt, N.A.; van Gunsteren, W. Validation of the 53A6 GROMOS force field. *Eur. Biophys. J.* **2005**, 34, 273–284.

68. Gasteiger, J.; Marsili, M. Iterative partial equalization of orbital electronegativity—A rapid access to atomic charges. *Tetrahedron* **1980**, 36, 3219–3228.

3 CHAPTER 2: SYNTHESIS AND CHARACTERIZATION OF MONOMETHINE CYANINE DYES AS FLUORESCENT DNA PROBES

This chapter includes my contribution to a follow-up manuscript to the previous chapter: Andrew Levitz[‡], **Cory Holder**[‡], Eduardo Soriano, and Maged Henary. "Synthesis and Characterization of Monomethine Cyanine Dyes as Fluorescent DNA Probes" *In preparation*.

[‡]Co-First Authors.

3.1 Introduction

As previously discussed in chapter 1, monomethine cyanine dyes possess a valuable characteristic of only displaying fluorescence when the rotation around the methine bridge is restricted. While there is still much to explore regarding what effect structure has on the photophysical properties, our lab has developed ways to redshift the monomethine scaffold by altering the terminal heterocycles. [1,2] Understanding how to redshift the monomethine cyanine dyes allows for the enhancement of existing molecular probes such as the ones shown above in Figure 1 by minimizing background absorption and fluorescence.

The objective of the project discussed in this chapter is to design and analyze monomethine cyanine dyes that can be used to explore the viability of this class of compounds as molecular probes, specifically for duplex DNA. Our group has previously demonstrated that monomethine cyanine dyes can be redshifted by including benz[*c,d*]indole heterocycle as a terminus[1] and as shown by several groups, the brightness of polymethine cyanine dyes can be increased by incorporating heterocycles such as benzoxazole and benzothiazole [3-5]

This project includes synthesizing benz[*c,d*]indole containing symmetric and asymmetric dyes conjugated to quinoline, benzothiazole, benzoxazole, dimethyl indole, benz[*e*]indole and benz[*c,d*]indole. These monomethine cyanine dyes were analyzed for their potential use as nucleic

acid probes via both computational and experimental methods. Computationally the physicochemical properties were explored by using Spartan '14. Experimentally, the optical profiles of the dyes were investigated using UV/Vis and fluorescence spectroscopy. In the previous chapter we demonstrated that monomethine dyes containing benzothiazole show almost 10-fold increase in fluorescence, when bound to DNA. The binding constant between ct-DNA fiber and each monomethine dye was determined by analyzing the fluorescence spectra of the dyes with and without DNA present. In this current chapter we have developed a new monomethine system containing benz[*c,d*]indole and benzoxazole as terminal heterocycles that exhibits a nearly 700-fold increase in fluorescence when bound to duplex DNA.

3.2 Results and Discussion

3.2.1 Monomethine Cyanine Dye Synthesis

Five asymmetric and one symmetrical red-shifted monomethine cyanine dyes were synthesized as shown in Scheme 2.

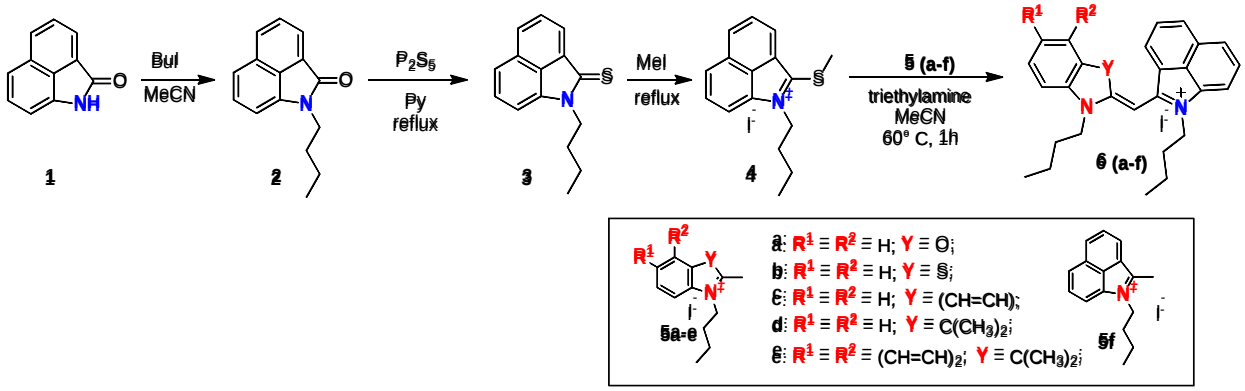

Scheme 2 Synthesis of monomethine cyanine dyes containing benz[c,d]indolium heterocycle.

The synthesis began with the alkylation of benz[*c,d*]indol-2(1H)-one **1** by reflux with iodobutane in acetonitrile. Alkylated amide **2** was then converted to the thione **3** under reflux with phosphorous pentasulfide in pyridine. The thioketone **3** was methylated to a thioether with

iodomethane creating the quaternary ammonium salt **4**, which was used as one of the terminal heterocycles. 2-methylbenzoxazole, 2-methylbenzothiazole, 2-methylquinoline, and 2,3,3-trimethylindole, were each alkylated respectively with iodobutane in a sealed tube at 100 °C for 24 h to afford salts **5a-d**. Compound **5f** was prepared from thioether **4** via the synthetic procedure developed by Ficken and Kendall. [6, 7] The two heterocycles were then condensed in acetonitrile with a catalytic amount of triethylamine to afford final dyes **6a-f**.

3.2.2 Optical properties

After the dyes were synthesized the optical properties were investigated via UV/Vis and fluorescence spectroscopy. Stock solutions were prepared by weighing the solid powder of each individual compound on a 5-digit analytical balance and adding solvent via class A volumetric pipette to make a 1.0 mM solution. The vials were vortexed for 20 s and then sonicated for 5 min to ensure complete dissolution. When not in use, the stock solutions were stored in a dark at 4 °C. Stock solutions were used to prepare five dilutions of dyes with concentrations ranging from 5-25 μM using a class A volumetric pipette in order to maintain absorption between 0.1 and 1.0. The dye solutions were diluted ten-fold for fluorescence in order to minimize inner filter effect. The absorption spectrum of each sample was measured in duplicate from 400 to 750 nm.

Table 3 Molar absorptivity of the monomethine dyes. Ethanol was used as the solvent for the experimental UV/Vis.

Dye	$E._{HOMO}$ *(eV)*	$E._{LUMO}$ *(eV)*	λ_{max} *(exp.)*	λ_{max} *(calc.)*	ε $(M^{-1}cm^{-1})$
6a	-8.31	-6.06	500	490	39,830
6b	-8.20	-5.60	560	505	30,700
6c	-7.99	-5.96	585	522	35,900
6d	-8.08	-5.87	559	530	25,209

The emission spectrum of each sample was measured in duplicate with a 530 nm excitation wavelength and slit widths of 5 nm for both excitation and emission. Emission spectra were corrected automatically by our developed method file used for reading the spectrofluorometer data output. The results of the UV/Vis experiment is shown above in Table 3. Molar absorptivity was calculated using the Beer-Lambert law and dye **6a** gave the largest attenuation coefficient (ε). Additionally the predicted HOMO/LUMO energy gaps correspond to the experimentally observed absorption max. This means that dye **6a** has the ability to absorb the most light, at a specific wavelength, compared to all other compounds tested in this study. Consequently dye **6a** is the best candidate for becoming a molecular probe.

3.2.3 Spectral Characterization

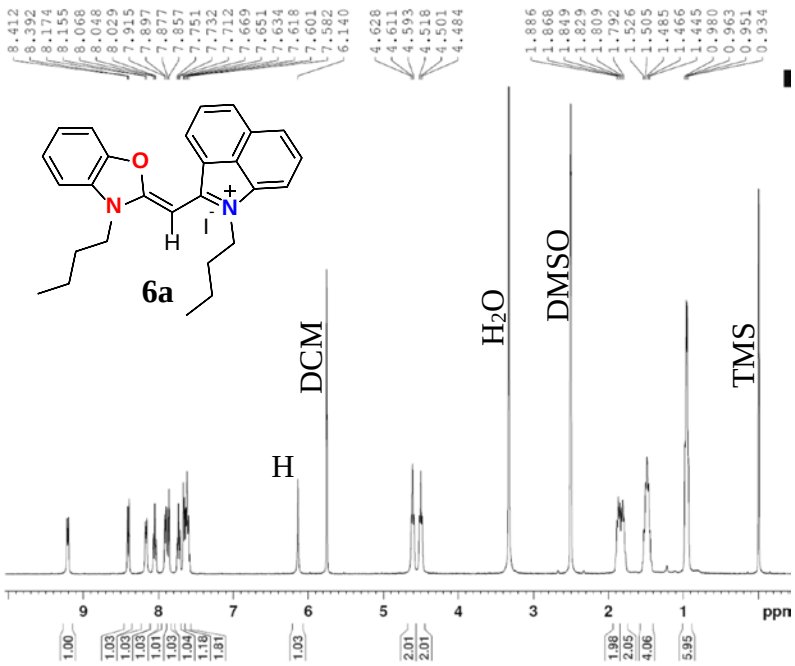

Figure 9 ^{1}H NMR of dye **6a** in DMSO-d_6

All dyes were analyzed via ^{1}H and ^{13}C NMR to verify purity of the dye. Dye **6a** was chosen as a representative example to discuss the ^{1}H and ^{13}C NMR characterization. As illustrated above,

in the representative ^{1}H NMR of dye **6a** which was taken shortly after a column with dichloromethane (DCM) and methanol. To assign ^{1}H NMR signals to the structure of the dye, it helps to visualize the compound in three parts: the two end terminals and the methine unit, as shown in Figure 9. Signals in the aromatic region from dye **6a** should integrate to eleven protons: four from the benzoxazole, one from the methine proton and six from the benz[*c,d*]indole. The easiest part to assign would be the methine singlet that theoretically should integrate to 1. This signal is found in the spectrum above with a chemical shift of 6.14 ppm. The singlet at 5.76 ppm corresponds to the known chemical shift of the protons in dichloromethane in DMSO-d_6. The benzoxazole heterocycle should produce two doublets and two triplets in the aromatic region with a total integration of 4 protons. Two doublets at 7.73 ppm and 7.88 ppm both share a *J* coupling constant of 8 Hz, similar to the triplets with a chemical shift of 8.05 ppm and 8.17 ppm with *J* coupling constants of 7.6 Hz and 8 Hz respectively. Although the *J* values of the two triplets are not identical they could still be from the same environment and the difference in the coupling constant could be attributed to machine error, if this is not the case then the last triplet is overlapping other peaks in one of the multiplets. The matching integration combined with similar coupling constants and correct splitting suggest these signals represent chemically similar environments that best align with the benzoxazole terminus of dye **6a**. By process of elimination, the remaining signals in the aromatic region can be assigned to the benz[*c,d*]indole end of dye **6a**. The multiplet ranging from 7.58 ppm to 7.67 integrates to four protons leaving only two unassigned aromatic protons which are found at 7.92 ppm and 9.22 ppm with both signals displaying a *J* coupling constant of 7.2 Hz.

Dye **6a** should have 8 signals in the aliphatic region of the ^{1}H NMR spectrum that integrate to 18 protons. The two end CH_3 groups are represented by the multiplet ranging from 0.93-0.99

ppm which integrates to 6 protons. The two multiplets at 1.44-1.52 ppm and 1.79-1.87 ppm must correspond to the four CH_2 groups positioned in the middle of the butyl chain. The methylene groups closest to the nitrogen of their respective heterocycles are represented by two triplets with chemical shifts of 4.50 ppm and 4.61 ppm each integrating to 2 protons. Based off of smaller *J* coupling constants, the signal at 4.50 ppm could be assigned to the benz[*c*,*d*]indole.

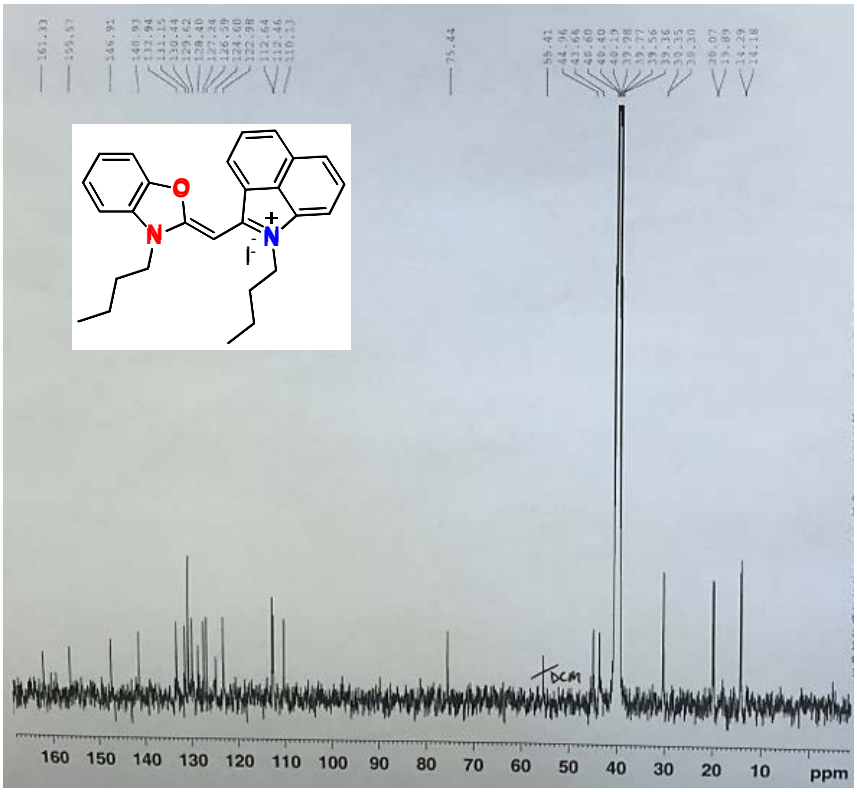

Figure 10 ^{13}C NMR of dye **6a** in DMSO-d_6

For dye **6a** there should be 27 unique signals in a ^{13}C NMR spectra. As shown in the spectra displayed in Figure 10, only 25 signals from dye **6a** were observed. All eight signals in the aliphatic region are present from 14.18 ppm to 44.96 ppm. The signature septet of DMSO is present along with DCM from the column. The signal at 75.44 ppm can be attributed to the methine carbon. 16 signals are present from 110.30-161.33 ppm representing the carbons in both heterocyclic rings.

Two signals were not present and it can be assumed that these signals belonged to quaternary aromatic carbons. These peaks could show with more scans.

3.2.4 Physicochemical Results

The monomethine dyes were then analyzed via Spartan ’14 version 1.14 to calculate their physicochemical properties. All of these dyes were modeled in 3-dimensions with a restricted dihedral angle to disallow rotation at the methine carbon. Their geometries were optimized using HF-DFT hybrid exchange-correlation functional and B3LYP/6-31G* basis set. The calculations were set up to predict the energy of the compounds at ground state and then the dyes were experimentally evaluated via UV/Vis spectroscopy. The experimentally derived results agreed with the trend of the computationally predicted energy gap of dye **6a**, which are shown below in Figure 11. HOMO/LUMO energy gaps of all dyes were calculated with Spartan ’14 and are shown in the appendix.

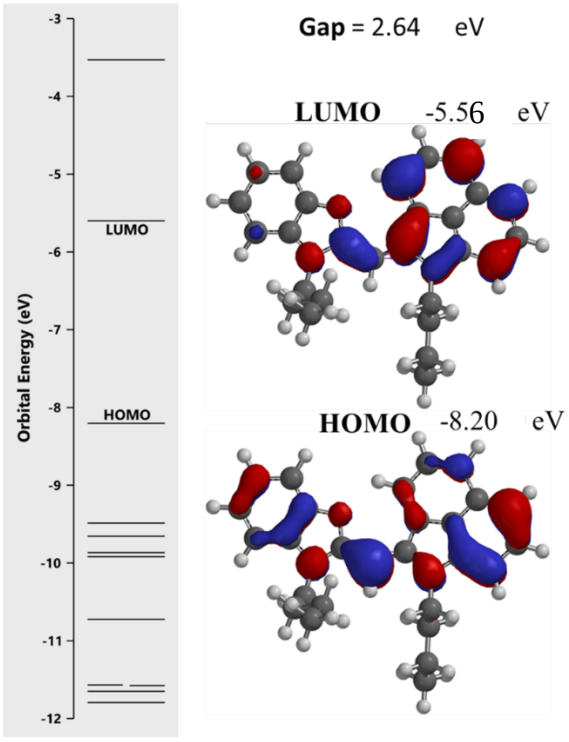

Figure 11. HOMO/LUMO diagrams of dye **6a** calculated in Spartan '14

The physicochemical properties were then compared to the binding constants (K_b) to try to find a trend with these calculated properties and their spectra, shown below in Table 4. From the data presented in Table 4 below, the only apparent trend seems to be the lower polarizability and Log (P), the higher the binding affinity is exhibited in these systems.

Table 4. Physicochemical properties via Spartan '14 compared to the experimentally determined binding constants and ^{1}H NMR chemical shifts.

	K_b (M^{-1})	***MW*** *(amu)*	***Log(P)***	***TPSA*** *($Å^2$)*	***Methine Proton*** *(ppm)*	***Dipole*** *(debye)*	***Polarizabililty***
6a	1.6×10^4	524.446	7.68	5.525	6.14	2.16	76.21
6b	1.1×10^4	540.508	8.25	0.978	6.46	3.66	76.79
6c	3.2×10^2	534.485	8.69	1.184	6.23	2.73	78.29
6d	2.9×10^{-8}	550.528	9.23	0.998	6.32	1.84	80.41
6e	NA	600.588	10.23	0.993	NA	3.14	84.57
6f	NA	558.507	9.01	1.212	NA	0.68	80.11

Next, fluorescence of all synthesized compounds shown in scheme 2 were tested in ethanol and it was observed that none of the dyes exhibited fluorescence emission in ethanol. It was shown by our lab that only when asymmetric monomethine cyanine's ability to rotate around the methine bridge is restricted is there emission of photons.[1] As was demonstrated previously in Chapter 1 that monomethine cyanine dyes can bind to duplex DNA and when bound they can absorb and then emit light. [2] This unique feature of "turn-on" fluorescence was utilized for determining binding constants between each dye and duplex DNA for each of the compounds. The experimental fluorescence data obtained suggests that compounds featuring the dimethyl group at the 3 position have lower binding constants compared to those without this feature. One explanation for this phenomenon could be attributed to the fact that the dimethyl groups are perpendicular to the plane of the flat rings of the heterocycles providing steric hindrance resulting in reduced binding affinity. Compound **6c** contains quinoline, which features multiple resonance

pathways that result in several non-radiative relaxation pathways. This can be very useful for different therapeutic applications but is not ideal for an optical probe.[8]

Of the dyes presented in this Scheme 2, the one containing benzoxazole heterocycle, **6a**, displayed the greatest increase in fluorescence when in the presence of duplex ct-DNA. This could be explained by the tendency of benzoxazole to decrease non-radiative deactivation due to fast intersystem crossing.[9] Additionally, the benzoxazole end of **6a** are much less likely to sterically hinder binding compared to that of **6d**. As shown in Figure 12 below, these two dyes do not display a dramatic increase in fluorescence upon exposure to duplex DNA.

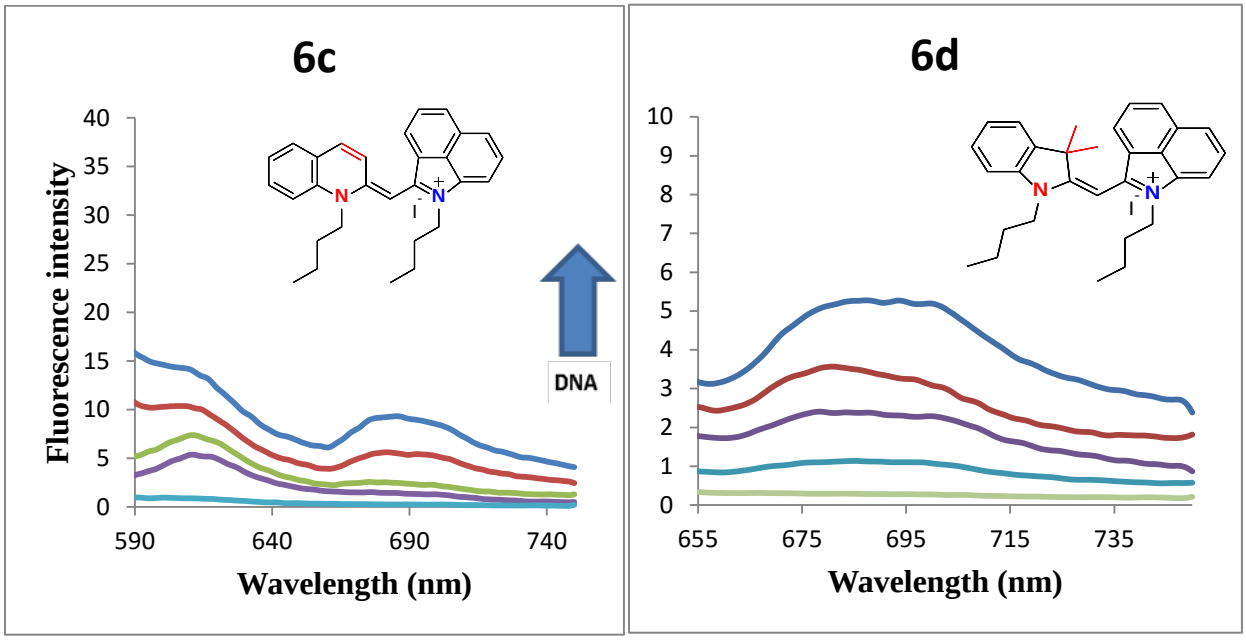

Figure 12. Representative fluorescence spectrum of Dye **6c** and **6d**, 10 uM, increasing from 0 to 20uM of duplex DNA.

As presented in Figure 13, the fluorescence spectrum of free dye **6a** in Tris-HCl buffer exhibits negligible fluorescence emission. When ct-DNA is added an increase in fluorescence is observed up to 700-fold. Similarly to the previously described enhancement in glycerol, a viscous solvent, this enhancement is also attributed to the fact that on excitation the inability to freely rotate

around the methine bond due to binding does not allow for non-radiative deactivation of the ground state causing the dye to emit photons. [1, 2]

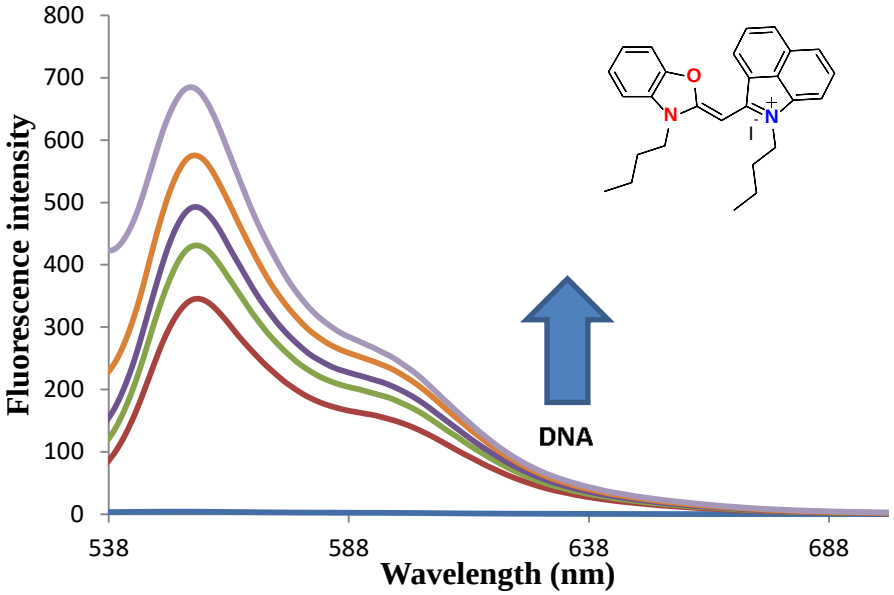

Figure 13. Representative fluorescence spectrum of Dye **6a**, 10 uM, increasing from 0 mM to 200 mM of duplex DNA.

Using a double reciprocal plot ,shown below in Figure 13, the binding constant, K_b, of **6a** was determined to be 1.6×10^4 M^{-1}, which is on par with similar monomethine cyanine dyes. [10] This was done by analyzing emission intensity of 10 uM of free dye and increasing concentration of ct-DNA, up to 200 mM, while the concentration of dye **6a** stayed the same.

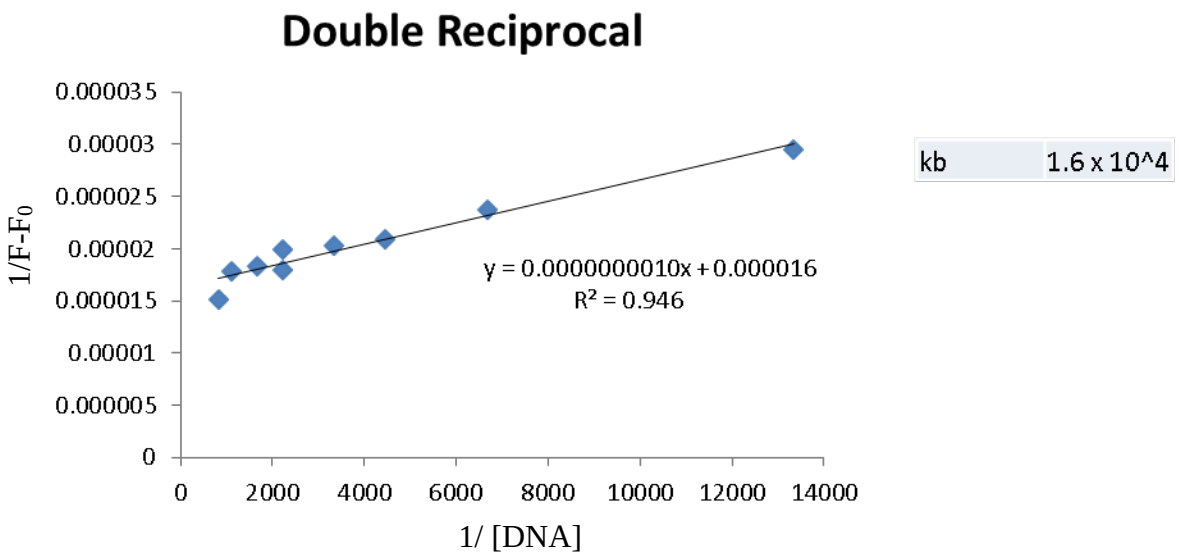

Figure 14 double reciprocal plot from multiple fluorescence trials of dye **6a** with increasing ct-DNA

Dye **6a** could be beneficial as a molecular probe due to its redshifted nature caused by the incorporation of benz[*c,d*]indole and by not including quinoline; quinolines are known to experience non-radiative return of decay. The closer the absorption and emission gets to the optical window (650-1200 nm) the less background absorption and fluorescence occurs from biomolecules. [11] Ideally in a biomolecular probe, more energy will be converted into photons instead of heat, making for easier detection and reduction of potential harm to surrounding areas.

3.3 Experimental

3.3.1 General Information

All chemicals and solvents were of American Chemical Society grade or HPLC purity and were used as received. HPLC grade methanol and glycerol were purchased from Sigma-Aldrich (Saint Louis, MO). All other chemicals were purchased from Fisher Scientific (Pittsburgh, PA, USA) or Acros Organics. The reactions were followed using silica gel 60 F254 thin layer

chromatography plates (Merck EMD Millipore, Darmstadt, Germany). The ^{1}H NMR and ^{13}C NMR spectra were obtained using high quality Kontes NMR tubes (Kimble Chase, Vineland, NJ) rated to 500 MHz and were recorded on a Bruker Avance (400 MHz) spectrometer DMSO-d_6 or CD_3Cl. UV-Vis/NIR absorption spectra were recorded on a Varian Cary 50 spectrophotometer interfaced with Cary WinUV Scan Application v3.00 using VWR disposable polystyrene cuvettes with a 1 cm pathlength. Laser Induced Fluorescence (LIF) emission spectra were acquired using Shimadzu RF-5301 Spectroflurophotometer (Shimadzu Corporation Analytical Instruments Division, Duisburg, F. R. Germany) interfaced to a PC with RF-5301PC software using Sigma-Aldrich disposable polystyrene fluorimeter cuvettes with a 1 cm pathlength. All spectral measurements were recorded at room temperature. The data analysis and calculations were carried out using Microsoft Excel (Microsoft Corporation, Redmond, Wa).

3.3.2 Synthesis

3.3.2.1 General Synthetic Procedure for the heterocyclic salts

Compound **4** was previously synthesized by our group and others. [1, 2, 12]

Each individual heterocycle was dissolved in acetonitrile and butyl iodide was added. The reaction mixture was then refluxed for 12 h. Thin layer chromatography (TLC) was used to monitor the reaction progress using a mixture of 4/1 dichloromethane/hexanes. Upon cooling to room temperature, the quaternary ammonium salts **5a-e** were precipitated in diethyl ether and collected by vacuum filtration.[13, 14] Salt **5f** was synthesized from the thioether, **4**, as described by our group and others.[6,7]

3.3.2.2 General Synthesis of the monomethine dyes

Compound **4** and each quaternary ammonium salt **5a-f** respectively, were dissolved in acetonitrile and a catalytic amount of triethlyamine was added to the solution. The reaction mixture was refluxed at 60 °C for 1 h and monitored by UV-Vis until completion. Upon cooling to room temperature, the corresponding dyes **6a-f** were precipitated by adding diethyl ether to the reaction flask. The solid was collected by vacuum filtration and triethyl ammonium salts were removed by washing with deionized water. The final dyes were purified via precipitation from methanol with diethyl ether or column chromatography DCM/MeOH (19/1).

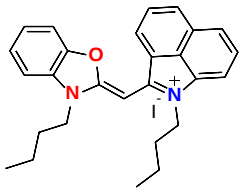

A monomethine cyanine dye**,** 1-butyl-2-((3-butylbenzo[*d*]oxazol-2(3H)-ylidene)methyl) benzo[*c,d*]indol-1-ium iodide (**6a**); (60%); ^{1}H NMR (400 MHz, DMSO-*d*6): δ ppm 0.96 (m, 6 H), 1.50 (m, 4 H), 1.83 (m, 4 H) 4.50 (t, *J* = 6.8 Hz, 2 H), 4.61 (t, *J* = 7.2 Hz, 2 H), 6.14 (s, 1 h), 7.62 (m, 4 H), 7.73 (t, *J* = 8 Hz, 1H) 7.88 (d, *J* = 8 Hz, 1H), 7.92 (d, *J* = 7.2 Hz, 1H) 8.05 (t, *J* = 7.6 Hz, 1H) 8.17 (d, *J* = 8 Hz, 1H) 9.22 (d, *J* = 7.2 Hz, 1H) ^{13}C NMR (100 MHz, DMSO-*d*6) δ ppm 14.18, 14.29, 19.89, 20.07, 30.30, 30.35, 43.66, 44.96, 75.44, 110.3, 112.46, 112.64, 122.98, 124.60, 126.59, 127.24, 128.40, 129.62, 130.44, 131.15, 132.94, 140.93, 146.91, 155.57, 161.33.

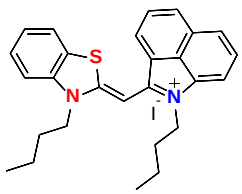

A monomethine cyanine dye, 1-butyl-2-((3-butylbenzo[*d*]thiazol-2(3H)-ylidene)methyl) benzo[*c*,*d*]indol-1-ium iodide, (**6b**); (65%); ^{1}H NMR (400 MHz, DMSO-*d*6): δ ppm 0.966 (m, 6 H), 1.53 (m, 4 H), 1.85 (m, 4 H) 4.40 (t, *J* = 7 Hz, 2 H), 4.76 (t, *J* = 7.6 Hz, 2 H), 6.46 (s, 1 h), 7.60 (m, 5 H), 7.90 (t, *J* = 7.6 Hz, 1 H) 8.08 (d, *J* = 8.4 Hz, 1 H), 8.35 (d, *J* = 8.0 Hz, 1 H) 9.34 (d, *J* = 7.2 Hz, 1 H) ^{13}C NMR (100 MHz, DMSO-*d*6) δ ppm 14.16, 14.25, 19.94, 20.16, 30.09, 30.21, 43.89, 47.76, 87.22, 109.68, 115.24, 122.59, 124.19, 124.89, 125.74, 127.04, 127.76, 128.29, 129.33, 129.71, 130.00, 132.84, 140.70, 141.35, 154.67, 164.96.

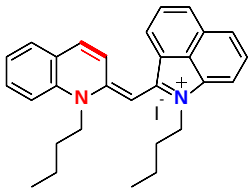

A monomethine cyanine dye, 1-butyl-2-((1-butylbenzo[cd]indol-2(1H)-ylidene)methyl) quinolin-1-ium iodide, (**6c**); (69%); ^{1}H NMR (400 MHz, DMSO-*d*6): δ ppm 0.98 (m, 6H), 1.48 (m, 2H), 1.59 (q, *J* = 7.2 Hz, 2H), 1.80 (m, 2H), 1.94 (m, 2H), 4.25 (t, *J* = 7.2 Hz, 2H), 4.88 (t, *J* = 7.2 Hz, 2H), 6.23 (s, 1H), 7.33 (m, 1H), 7.62 (m, 3H), 7.83 (t, *J* = 7.6 Hz, 1H), 8.10 (m, 2H), 8.23 (d, *J* = 8.0 Hz, 1H), 8.32 (d, *J* = 7.2 Hz, 1H), 8.39 (d, *J* = 8.0 Hz, 1H), 8.67 (m, 2H) 13C NMR (100 MHz, DMSO-*d*6) δ ppm 14.07, 14.25, 19.89, 20.23, 30.04, 30.12, 43.39, 51.12, 92.58, 106.88, 118.70, 120.54, 124.38, 125.07, 125.81, 127.73, 128.05, 129.42, 129.96, 130.31, 130.47, 130.31, 130.47, 130.91, 134.61, 139.24, 142.08, 142.52, 152.91, 156.47.

3.3.3 Stock Solutions for Optical Measurements

Stock solutions were prepared by weighing the solid of each individual compound on a 5-digit analytical balance and adding solvent via class A volumetric pipette to make a 1.0 mM solution. The amber vials were vortexed for 20 s and then sonicated for 5 min to ensure complete dissolution. When not in use, the stock solutions were stored in a dark at 4 °C.

3.3.4 Method of Determining Absorbance and Fluorescence

Stock solutions were used to prepare five dilutions of dyes with concentrations ranging from 5-25 μM using a class A volumetric pipette in order to maintain absorption between 0.1 and 1.0. The dye solutions were diluted ten-fold for fluorescence in order to minimize inner filter effect. The absorption spectra of each sample were measured in duplicate from 400 to 750 nm. The emission spectra of each sample were measured in duplicate with slit widths of 5 nm for both excitation and emission. Emission spectra were corrected automatically by our developed method file used for reading the spectrofluorometer output data.

3.3.5 Computational methods

The structure of each compound was first optimized using the TD-DFT method with the hybrid exchange-correlation functional, B3LYP/6-31G* basis set using Spartan '14 (Irvine, CA).[15] The torsional angles from the quaternary nitrogen to the α-carbon on the alternate heterocycle were restricted to 180° to get the calculated absorbance values, LUMO and HOMO orbitals, physicochemical properties and electrostatic potential maps. The calculated LUMO and HOMO orbitals were obtained using a restricted hybrid HF-DFT SCF calculation performed with B3LYP/6-31G* basis set. The electrostatic potential maps were investigated for the optimized structures at HF/6-31G*.

3.3.6 DNA Binding Studies

A stock solution of the dyes (1×10^{-4} M) and ct-DNA type 1 (7.5×10^{-3} M) were prepared in ethanol and Tris-HCl buffer solution, respectively. Fluorescence titration with ct-DNA concentrations (0-200 mM) were made by mixing 35 μL of respective dye solution with Tris-HCl buffer solution with and without ct-DNA to a total volume of 3500 μL in a fluorescence cuvette to

make working solutions of 10 μM of dye. Fluorescence spectra were measured in duplicate with excitation at 520 nm and slit widths of 10 nm for both excitation and emission.

3.4 Conclusion

A series of monomethine cyanines were synthesized in good yield with red-shifted absorbance properties in comparison to previously synthesized monomethine cyanine dyes. Although the benz[*c*,*d*]indolium containing monomethine cyanine dyes in this report are non-fluorescent in free flowing solvent, when the dyes are in an environment that can restrict their rotation around the methine bridge their fluorescence becomes observable. Computational methods outlined above were shown to be useful as a predictive tool for determining their optical properties, and maybe provided insight to what physicochemical properties would encourage binding to duplex DNA. All dyes were experimentally tested to determine their binding affinity to ct-DNA. Dye **6a** stood out as the best candidate as a starting point for building a new molecular probe due to it having relatively strong binding affinities and having the highest increase in fluorescence; up to 700-fold. Utilizing the described techniques these dyes could be developed as potential biological probes. Future studies will investigate how different substitutions on the heterocycles could increase binding affinities and increase optical activity to various biological targets.

3.5 REFERENCES for Chapter 2

1. Soriano, E.; Outler, L.; Owens, E.A.; Henary, M. Synthesis of Asymmetric Monomethine Cyanine Dyes with Red-Shifted Optical Properties. *J. Heterocycl. Chem. 2015, 52, 180–184.*

2. Soriano, E.; Holder, C.; Levitz, A.; Henary, M. Benz[c,d]indolium-containing Monomethine Cyanine Dyes: Synthesis and Photophysical Properties. *Molecules* **2016**, 21, 23.

3. Hirons, G. T., Fawcett, J. J. and Crissman, H. A. (**1994**), TOTO and YOYO: New very bright fluorochromes for DNA content analyses by flow cytometry. *Cytometry*, 15: 129–140.

4. B. Armitage *Top. Heterocycl. Chem.*, 14 (**2008**), p. 11

5. Benvin, A. L.; Creeger, Y.; Fisher, G. W.; Ballou, B.; Waggoner, A. S.; Armitage, B. A.; *J. Am. Chem. Soc.* **2007**, 129, 2025− 2034

6. Ficken, G. E.; Kendall, J. D.; *J. Chem. Soc*., **1960**, 1537-1541

7. Henary, M., Mojzych, M., Say, M. and Strekowski, L. ***(2009),*** Functionalization of benzo[c,d]indole system for the synthesis of visible and near-infrared dyes. *J. Heterocyclic Chem.*, 46: 84–87

8. M. Mac, T. Uchacz, M. Andrzejak, A. Danel, P. Szlachcic*;* Photophysical of some donor-acceptor 1H-pyrazolo[3,4-b]quinolines: radiative versus non-radiative electron transfer processes. *J Photochem Photobiol A Chem*, 187 (**2007**), pp. 78–86

9. Reiser, A., Leyshon, L.J., Saunders, D. Mijovic, M. V., Bright, A., Bogie, J., Fluorescence of aromatic benzoxazole derivatives. *J. Am. Chem. Soc*., **1972**, 94 (7), pp 2414–2421

10. El-Shishtawy, R.M.; Asiri, A.M.; Basaif, S.A.; Rashad Sobahi, T. Synthesis of a new beta-naphthothiazole monomethine cyanine dye for the detection of DNA in aqueous solution. *Spectrochim. Acta A* **2010**, 75, 1605–1609.

11. Smith, A. M., Mancini, M.C., Nie, S., Bioimaging; Second Window for *in* vivo imaging. Nature *Nanotechnology* **2009**, 4 (11) 710-711

12. Sinha, S.H.; Owens, E.A.; Feng, Y.; Yang, Y.; Xie, Y.; Tu, Y.; Henary, M.; Zheng, Y.G. Synthesis and evaluation of carbocyanine dyes as PRMT inhibitors and imaging agents. Eur. J. Med. Chem. **2012**, 54, 647–659.

13. Hu, H.; Owens, E.A.; Su, H.; Yan, L.; Levitz, A.; Zhao, X.; Henary, M.; Zheng, Y.G. Exploration of Cyanine Compounds as Selective Inhibitors of Protein Arginine Methyltransferases: Synthesis and Biological Evaluation. J. Med. Chem. **2015**, 58, 1228–1243.

14. Narayanan, N.; Patonay, G. A New Method for the Synthesis of Heptamethine Cyanine Dyes: Synthesis of New Near-Infrared Fluorescent Labels. J. Org. Chem. **1995**, 60, 2391–2395.

15. Shao, Y.; Molnar, L.F.; Jung, Y.; Kussmann, J.; Ochsenfeld, C.; Brown, S.T.; Gilbert, A.T.B.; Slipchenko, L.V.; Levchenko, S.V.; O'Neill, D.P.; et al. Advances in methods and algorithms in a modern quantum chemistry program package. Phys. Chem. Chem. Phys.**2006**, 8, 3172–3191.

4 CHAPTER 3: INVESTIGATION OF DNA CLEAVAGE BY POLYMETHINE CYANINE DYES

This chapter is my contribution to a manuscript in preparation in collaboration with Prof. Kathryn B. Grant and her research group: **Cory Holder**[‡], Ziyi Li[‡], Eduardo Soriano, Kaitlyn Kiernan, Kathryn B. Grant, and Maged Henary. "An Investigation of Autoxidation and DNA Cleavage by Polymethine Cyanine Dyes and Analogs in Aqueous Solutions" In preparation. [‡]Co-First Authors.

4.1 Introduction

As mentioned in the Introduction above, a majority of anti-cancer drugs rely on interactions with DNA to elicit their therapeutic effects. [1] Unfortunately, most anti-cancer agents kill cells whether they are healthy or not, resulting in major side effects for cancer patients. [2-4] Photodynamic therapy (PDT) can help minimize the number of healthy cells killed due to its ability to allow for high localization of treatment, ultimately reducing the harsh side effects from traditional anti-cancer treatments. PDT is a type of treatment which uses light to activate a photosensitizer which, in the case of this study, can release energy that promotes oxidative damage to DNA or other macromolecules in diseased cells. For these photosensitizers to be effective, they must promote damage to DNA only when irradiated with light in order to allow for highly localized treatment.[1]

Cyanine dyes have been shown to be great tools in medical applications such as bioimaging agents and as non-metalated photosensitizers for PDT.[1, 5-7] In 2014, Grant, Henary *et. al.* looked at the interaction between DNA and symmetrical pentamethine cyanine dyes containing

benz[*e*]indolium heterocycles.[6] They discovered that pentamethine cyanines containing a halogen substituted at the meso-position show increased cleavage activity of plasmid DNA.

In this report, both trimethine and pentamethine cyanine dyes containing phenanthridinium and quinolonium derivatives have been synthesized and purified for investigation of DNA cleavage with the goal of developing a photosensitizer for PDT. The structural features of these dyes which exhibited no cleavage in the dark (thermal cleavage) and high cleavage when excited with a specific wavelength (photo cleavage) were identified as necessary components for creating an optimized PDT agent. This was determined through several cleavage and stability assays of dye and DNA combinations which were performed by Dr. Grant's lab.

4.2 Experimental

4.2.1 Trimethine synthesis

A series of four trimethine phenanthridinium containing cyanine dyes, **6a-d**, were synthesized as shown below in Scheme 3. The amide, **1**, was formed by reacting 2-aminobiphenyl with acetic anhydride at 0 ^{o}C for 1 h. The product, **1**, was then precipitated with water and subsequently filtered and dried overnight. To develop the brominated phenanthridinium dyes the amide **1**, was brominated using HBr in acidic conditions to afford compound **2.** 6-methylphenanthridine and 2-bromo-6-methylphenanthidine, **3** and **4**, were synthesized by refluxing compound **1** or **2** in phosphoryl chloride ($POCl_3$) for 48 h. Then the solution was neutralized with NaOH and the product, either **3** or **4**, was extracted and concentrated. Four phenanthradinium iodide salts, **5a-d,** were made by alkylating compound **3** for **5a-b**, and **4** for **5c-d**, with their respective iodoalkanes for 24 h. The final dyes **6a-d** were then formed using 2 eq. of salts **5a-d** with 1.1 eq. triethoxymethane and a catalytic amount of triethylamine in acetic

anhydride for 1 h at 90 °C. The crude products were precipitated out using diethyl ether and purified using column chromatography with a gradient increase in polarity (DCM/MeOH).

In Scheme 3 below, phenanthridine was chosen as the heterocycle for synthesizing trimethine dyes to be tested for DNA cleavage. This heterocycle was selected because the extensive use of a similar structure, Ethidium Bromide, as a DNA probe.

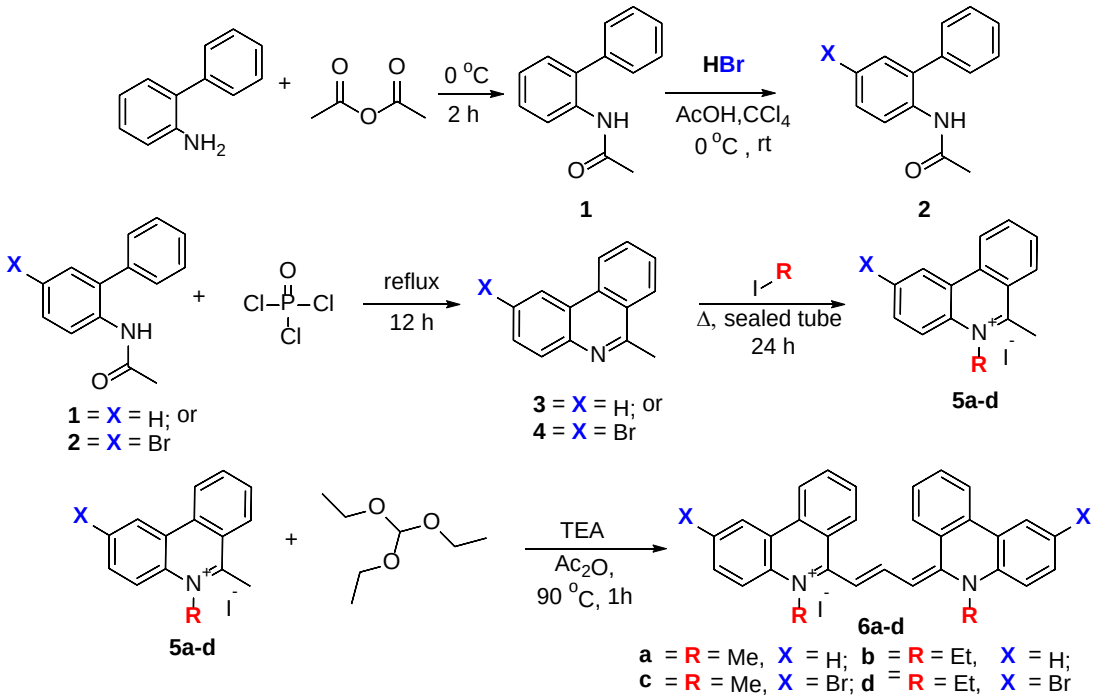

Scheme 3 Synthesis of trimethine cyanine dyes containing phenanthridinium heterocycle.

After synthesizing the phenanthridinium containing agents it was important to test different heterocycles. Quinoline was a good choice because it is readily available in most synthetic labs and has been used in cyanines since their discovery. First 4-methylquinoline PDT agents were designed because of the extended conjugation that this system provides. Compared to the 2-methylquinoline and 6-methylphenanthridine, 4-methylquinoline possesses one extra double bond between the nitrogens of the heterocycles which increase the λ_{abs} by around 100 nm. In Scheme 4 below, four trimethine cyanine dyes were synthesized from commercially available lepidine. Salts

7a-c were created by reacting the respective iodoalkanes with lepidine in a sealed tube for 24 h. The final dyes **8**, **9** and **10** were synthesized through condensation of 2 eq. of the salts **7a**, **7b** and **7c**, respectively with 1.1 eq. of triethoxymethane and a catalytic amount of triethlamine in acetic anhydride. Compound **11** was condensed from **7a** and 1,1,1-triethoxyethane with the same conditions described for **8-10**. The reactions were monitored by UV/Vis until completion. The final dyes, **8-11**, were precipitated with diethyl ether, recrystallized with methanol, and purified via column chromatography with a gradient solvent system of 0-7% MeOH in DCM.

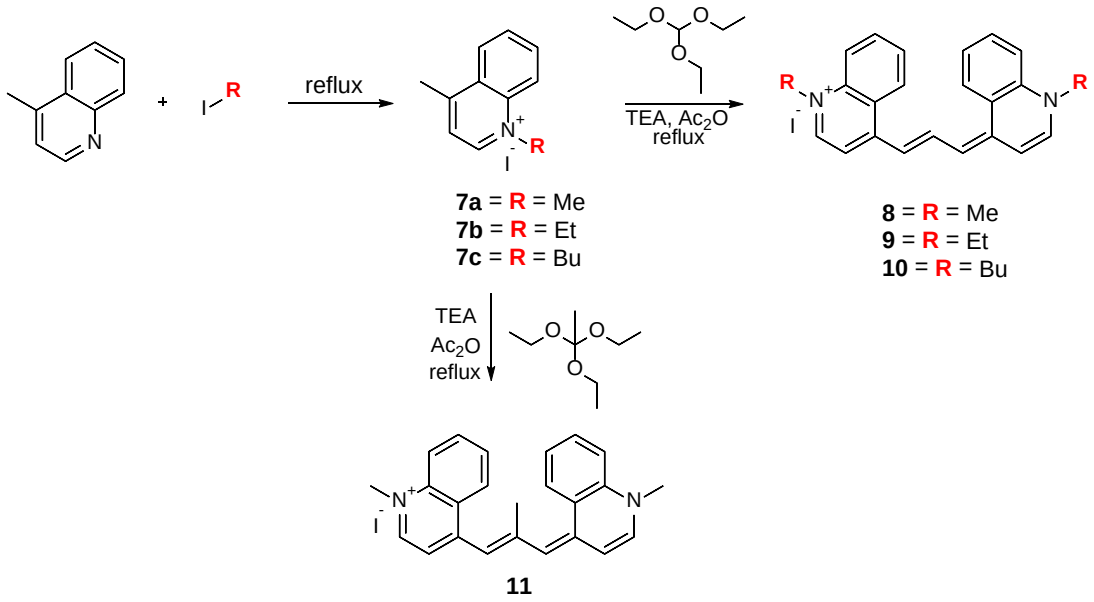

Scheme 4 Synthesis of trimethine cyanine dyes containing lepidine as the terminal heterocycle

The final set of trimethine cyanine dyes were synthesized from commercially available heterocycle, quinaldine. The salts **12 a-c** were created by reacting the respective iodoalkanes with quinaldine following an S_N2 pathway. The final dyes **13-15** were synthesized from 2 eq. of the quinaldine salts (**12 a-c**) and a catalytic amount of triethylamine and excess triethoxymethane and acetic anhydride for 30 min at 100 ^oC. This reaction was monitored via UV/Vis spectroscopy. The

final products were precipitated out using diethyl ether or ethyl acetate and purified using column chromatography.

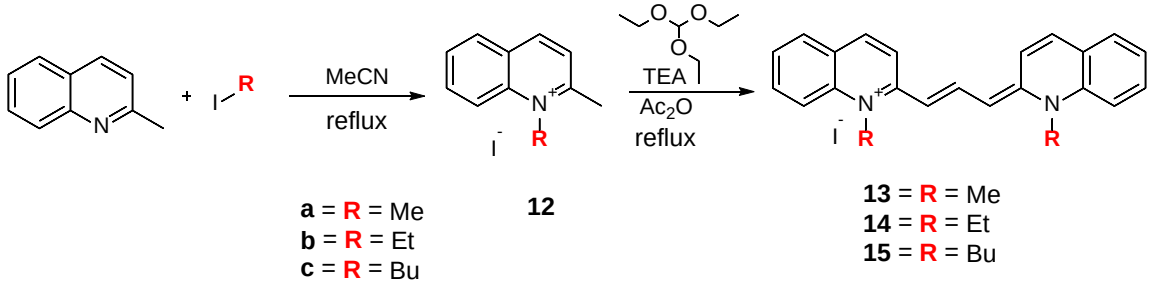

Scheme 5 Synthesis of trimethine cyanine dyes containing quinaldine heterocycle

4.2.2 DNA thermal Cleavage investigation.

All of the dyes shown in Schemes 3-5 and dozens of compounds synthesized by other members of our group were screened for the cleavage activity with duplex DNA. Theses cleavage assays were performed by Dr. Grant's Lab to analyze their cleavage activity in the dark because it is important to identify what structural features would promote this behavior as compounds that promote dark cleavage are also cytotoxic. To create a useful PDT agent the amount of dark cleavage must be reduced or eliminated. The dyes, shown in Figure 14 below, were screened for thermal cleavage activity by Ziyi Li in Dr. Kathy Grant's lab.

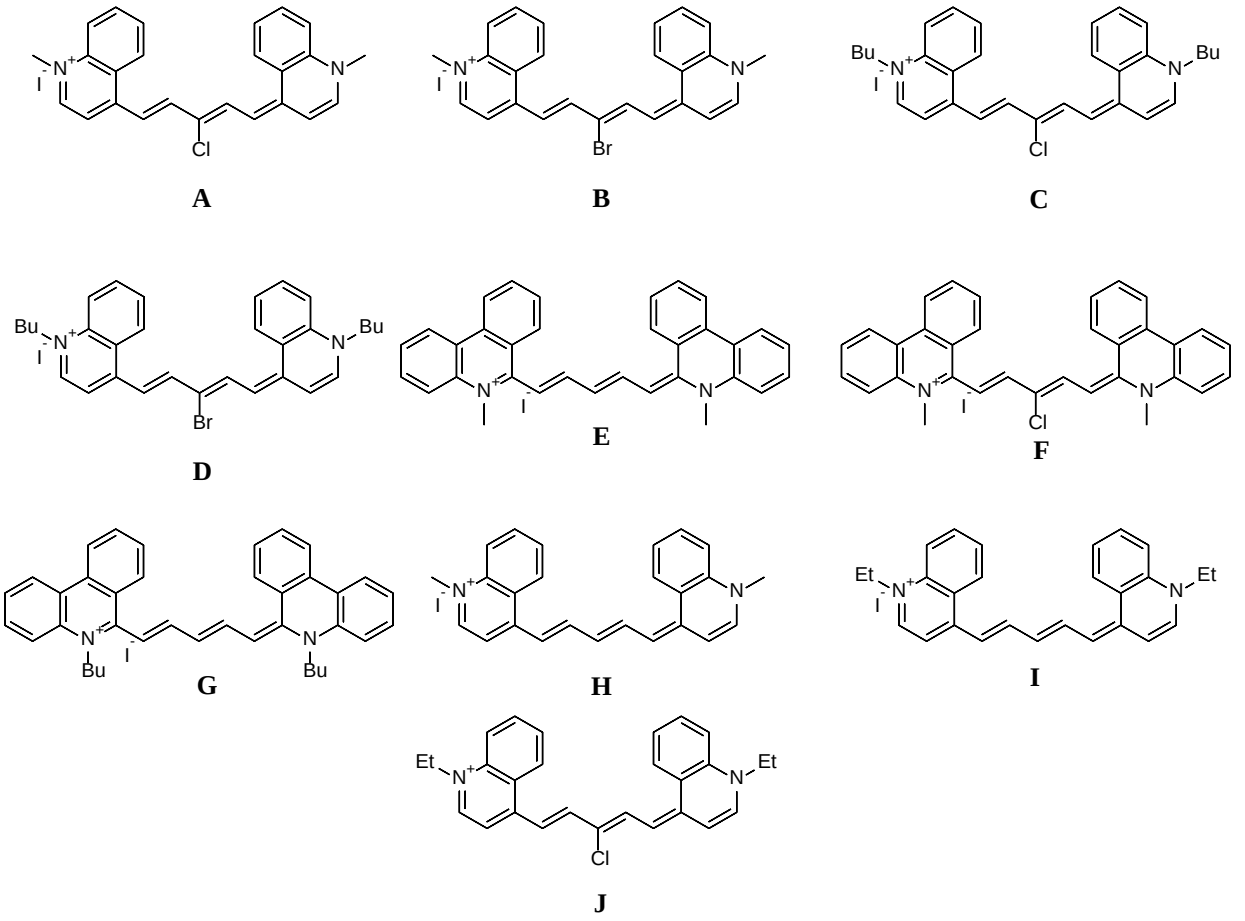

Figure 15 Polymethine cyanine dyes screened for thermal cleavage activity.

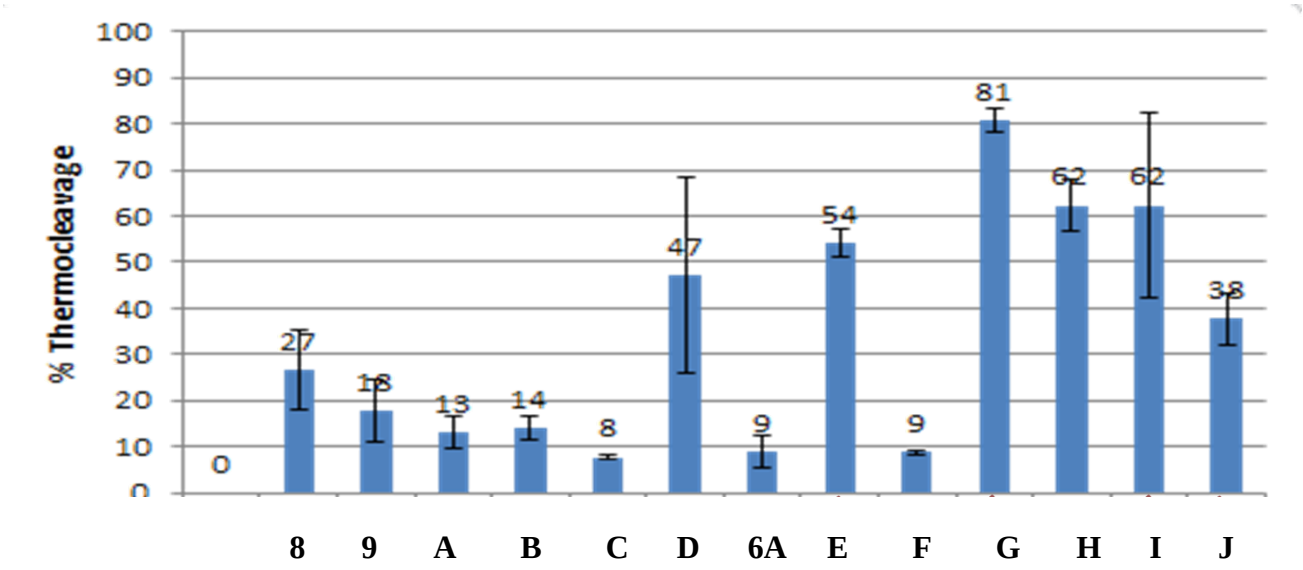

Figure 16 thermal cleavage assay of 25 uM polymethine cyanine dyes **6a, 8, 9** and the dyes **A-J** and 38 uM bp.

In this first generation of cleavage assays, several symmetric polymethine cyanine dyes were screened. As Shown in Figure 16, some of these dyes displayed great cleavage activity in the dark while others did not. From this experiment we started to notice structural features that seemed to promote cleavage activity with plasmid DNA. We are trying to create a photosensitizer that requires excitation at a long wavelength (>689 nm) thereby eliminating a majority of trimethine cyanine dyes, specifically those with quinaldinium. We have also observed that by substituting a halogen at the meso position we can minimize thermal cleavage activity induced by the dyes. In Figure 17 below, dye **E** displayed an alarming activity for thermal cleavage in the dark at physiological temperature. To rule out outside effects a control was performed that did not contain any dye. You can very clearly see that the control produced minimal nicked DNA and absolutely no linear DNA was observed. Dye **E** show a significant amount of cleavage producing a large amount of nicked plasmid and small amounts of linear. This indicates that phenanthridinium containing compounds would not make good candidates as photosensitizers. Preliminary data obtained showed quinaldinium containing trimethine dyes show very minimal thermal cleavage, however, they have absorption maxima below the desired wavelength (>689 nm). [1]

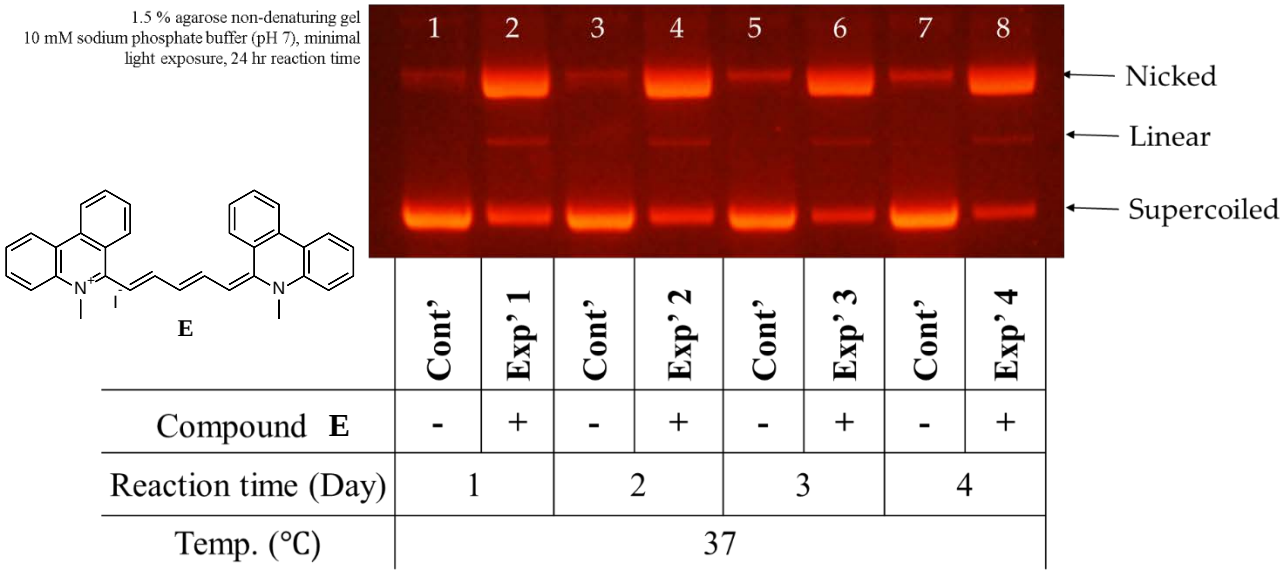

Figure 17. Thermal cleavage gel of 25 uM dye **E** and 38 uM bp.

It can be inferred that quinoline containing pentamethine cyanine dyes with halogens substituted at the meso position will make for the best photosensitizers for PDT. The next step of this project was to synthesize and purify asymmetric and symmetric quinaldinium dyes to test for photo induced cleavage.

4.2.3 Pentamethine Synthesis

Although the 4-methylquinoline provides extended conjugation it also seems to display more dark cleavage than 2-methylquinoline derivatives. Therefore, pentamethine cyanine dyes containing 2-methylquinoline were synthesized to increase their absorbance wavelength and test for their ability to promote photo-induced cleavage.

The brominated linker, **16-Br**, was created by gently heating mucobromic acid with aniline in dry ethanol until the starting material is consumed according to TLC.[6] The pentamethine quinaldinium cyanine dyes were synthesized by adding 2 eq. of the previously synthesized salt, **12**, to either linker **16-Br**, for dye **17**, or **16-H**, to produce dyes **18** and **19**. All three dyes were precipitated with diethyl ether and recrystallized from methanol. Column chromatography was not required for purification of these three dyes.

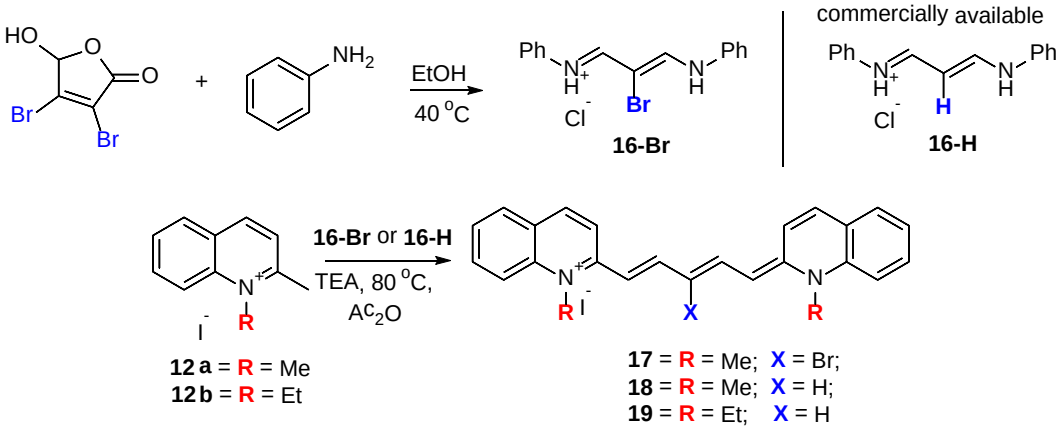

Scheme 6 synthesis of pentamethine cyanine dyes containing quinaldine heterocycle

Finally an asymmetric pentamethine cyanine dye was synthesized for comparison to the symmetrical quinaldinium pentamethine cyanine dyes. For the alternate heterocycle, 1,2,3,3-tetramethylindolium iodide was selected because it is a common component of the cyanine dye system and is cheap and readily available in our lab. 1,2,3,3-tetramethylindolium iodide was condensed in a 1:1 molar equivalent of (3-(phenylamino)allylidene)benzenaminium chloride in the presence of sodium acetate in a solution of acetic anhydride at room temperature for 15 min to afford the half-dye intermediate **20**. This intermediate was not isolated and was used *in situ* for synthesizing the final asymmetric agent **21**. By adding the heterocyclic salt **12a** to the intermediate **20** in the presence of a catalytic amount of triethylamine in acetic anhydride for 30 min at 80 ^{o}C. The dye was precipitated with ethyl acetate and purified via column chromatography (MeOH/DCM, 1/19) as described above.

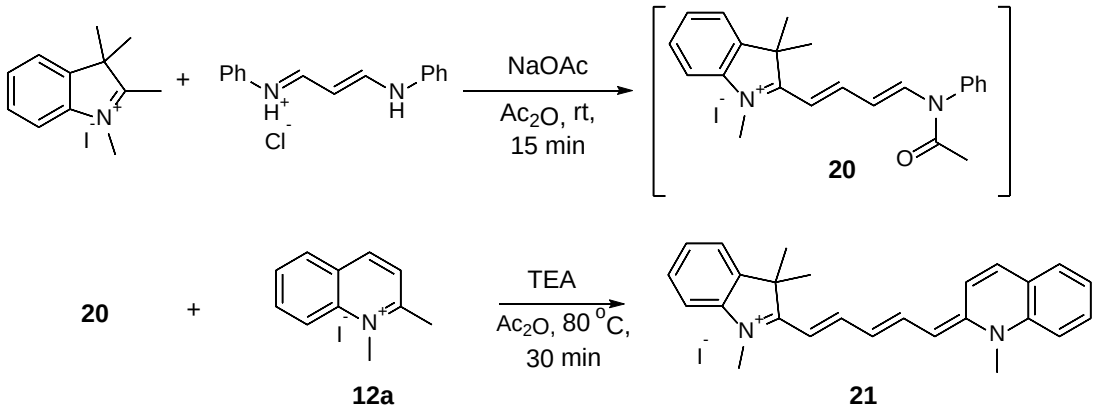

Scheme 7 Asymmetric pentamethine cyanine dye synthesis

4.2.4 DNA Photo Cleavage investigation.

The following cleavage studies were performed by Kaitlyn Kiernan from Dr. Kathy Grant's research group. All cleavage experiments were conducted with 25 μM dye concentrations.

Dyes **17**, **18**, and **21** were selected to screen for their photo-induced cleavage activity with plasmid DNA. Below in Figure 18, the three dyes were tested for cleavage with and without 700 nm light excitation. As expected, dye **17** showed the least amount of thermal cleavage and the highest amount of photo cleavage. This agrees with the trend established by the experiments conducted above in 4.2.2.

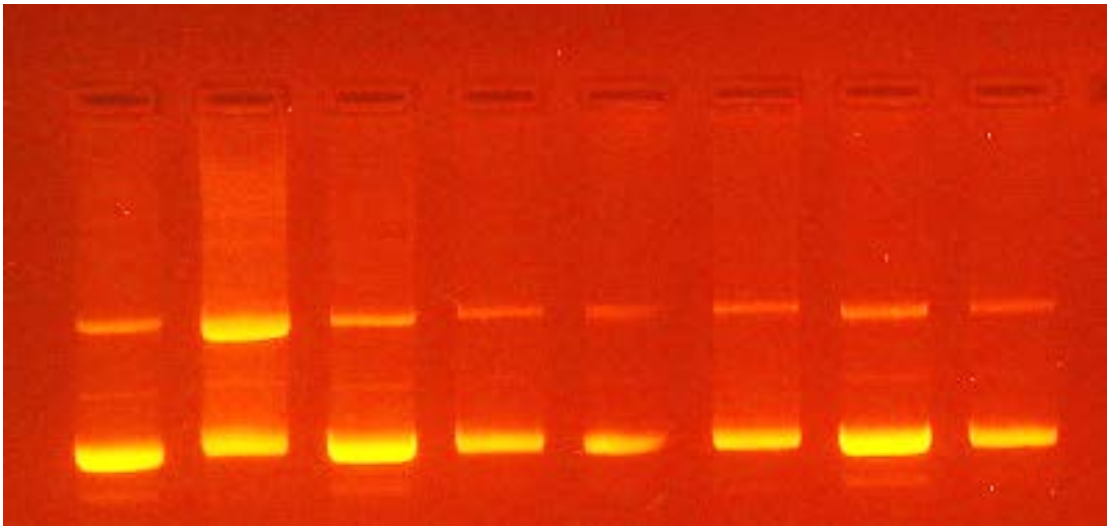

Plasmid	+	+	+	+	+	+	+	+
25 uM dye	-	**17**	**21**	**18**	-	**17**	**21**	**18**
700 nm light	-	+	+	+	+	-	-	-

Figure 18 photo and thermal cleavage of 38 uM bp DNA gel of 25 uM agents **17**, **18** and **21** at room temperature**.**

In Figure 19 below, these agents were tested further by monitoring their cleavage activity at low temperature and physiological temperature to rule out any cleavage not promoted a light source.

To test if the dyes would promote photo-induced cleavage in plasmid DNA at low temperature, the dyes were kept at 10 ºC and irradiated with a 700 nm light source, as shown in Figure 19 below.

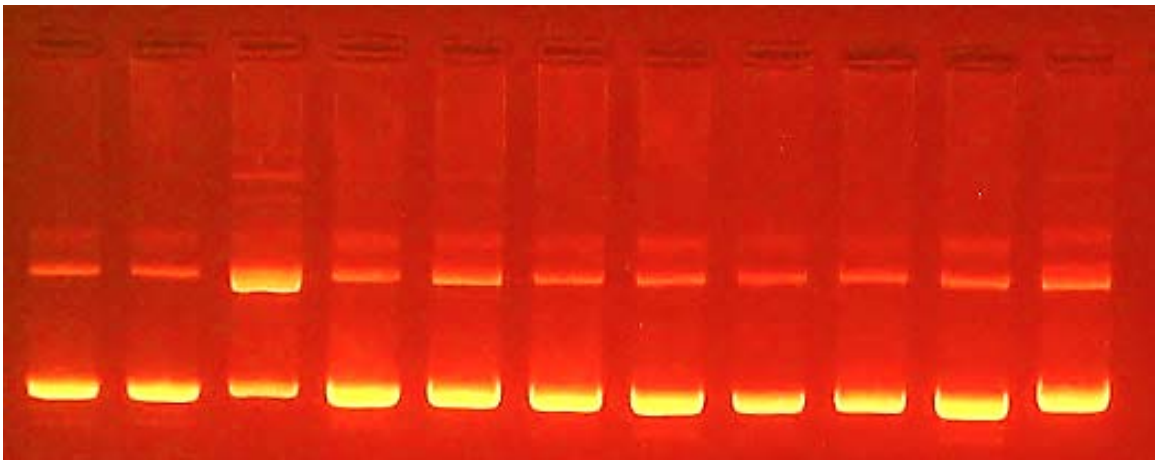

Lane	*1*	*2*	*3*	*4*	*5*	*6*	*7*	*8*	*9*	*10*	*11*
25 uM Dye	-	-	**17**	**21**	**18**	**17**	**21**	**18**	**17**	**21**	**18**
Plasmid	+	+	+	+	+	+	+	+	+	+	+
Light	+	-	+	+	+	-	-	-	-	-	-
Temp	10	10	10	10	10	10	10	10	37	37	37

Figure 19 photo and thermal cleavage 38 uM bp DNA gel of 25 uM of dyes **17**, **18** and **21**.

This was done for one hour. Dye **17** once again stood out for being the only candidate demonstrating photo-cleavage at low temperatures. Additionally, the dyes were investigated to determine if they would thermally cleave plasmid DNA at physiological temperature. All of the dyes performed well in this thermal study which was expected.

4.3 CONCLUSIONS

After synthesizing several polymethine cyanine dyes with various structural features and then screening them for their cleavage promotion with duplex DNA, we have

developed a SAR profile that could help future design of an effective cyanine photosensitizers for PDT. It was demonstrated that by extending the polymethine chain and incorporating halogens at the meso position, we can induce high photo cleavage of duplex DNA upon the excitation of the photosensitizers with low-energy light. Additionally, we have identified structural features that have the dangerous ability to promote cleavage of duplex DNA in the dark and cold such as phenanthridinium containing pentamethine cyanine dyes. By keeping the structural features that promote photo-induced cleavage, and eliminating those that promote "dark"-cleavage allowed for us to enhance the efficacy of these potential photosensitizers.

4.4 Experimental

All chemicals and solvents were of American Chemical Society grade or HPLC purity and were used as received. HPLC grade methanol and glycerol were purchased from Sigma-Aldrich (Saint Louis, MO). All other chemicals were purchased from Fisher Scientific (Pittsburgh, PA, USA) or Acros Organics. The reactions were followed using silica gel 60 F254 thin layer chromatography plates (Merck EMD Millipore, Darmstadt, Germany). The ^{1}H NMR and ^{13}C NMR spectra were obtained using high quality Kontes NMR tubes (Kimble Chase, Vineland, NJ) rated to 500 MHz and were recorded on a Bruker Avance (400 MHz) spectrometer DMSO-d_6 or CD_3Cl. UV-Vis/NIR absorption spectra were recorded on a Varian Cary 50 spectrophotometer interfaced with Cary WinUV Scan Application v3.00 using VWR disposable polystyrene cuvettes with a 1 cm pathlength. All spectral measurements were recorded at room temperature. The data analysis and calculations were carried out using Microsoft Excel (Microsoft Corporation, Redmond, Wa).

4.4.1 General Synthesis

4.4.1.1 Trimethine Cyanine Dyes

A mixture of the individual salts (2 eq.), triethylorthoformate or triethylorthoacetate (1 eq.), a catalytic amount of triethylamine and 4 mL of acetic anhydride was boiled for up to 1 h. The dye was suction filtered, washed with ethyl ether and dried.[8]

4.4.1.2 Pentamethine Cyanine Dyes

A mixture of individual salts (2 equivalents), either malonaldehyde bisphenylimine monohydrochloride, **16-H** or the brominated, **16-Br** analog (1 eq.) and triethylamine (3 eq.) were refluxed for 3 hrs in acetic anhydride and then cooled to room temperature. The crude compound was precipitated with diethyl ether or ethyl acetate from reaction mixture and was filtered and dried.[9]

4.4.2 NMR Analysis

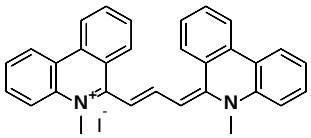

A trimethine cyanine dye, 5-methyl-6-((1E,3E)-3-(5-methylphenanthridin-6(5H)-ylidene) prop-1-en-1-yl)phenanthridin-5-ium iodide; (**6a**); (35%); ^{1}H NMR (400 MHz, DMSO-d_6) δ ppm 4.16 (s, 6 H), 7.20 (d, *J* = 13.14 Hz, 2 H), 7.56 (t, *J* = 7.45 Hz, 2 H), 7.77 (t, *J* = 8.00 Hz, 4 H), 7.87 (d, *J* = 8.59 Hz, 2 H), 7.94 (t, *J* = 7.10 Hz, 3 H), 8.45 (d, *J* = 8.34 Hz, 2 H), 8.58 (d, *J* = 7.83 Hz, 2 H), 8.64 (d, *J* = 8.34 Hz, 2 H) ^{13}C NMR (100 MHz, DMSO-*d*6) δ ppm 42.96, 108.43, 118.43, 122.44, 123.53, 123.95, 125.85, 126.80, 128.84, 129.60, 131.29, 132.04, 133.73, 138.31, 152.55, 155.60.

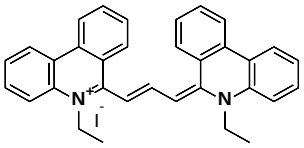

A trimethine cyanine dye, 5-ethyl-6-((E)-3-((E)-5-ethylphenanthridin-6(5H)-ylidene) prop-1-en-1-yl) phenanthridin-5-ium iodide; (**6b**) A dark green solid (35%) ^{1}H NMR (400 MHz, DMSO-d6) δ ppm 1.55 (t, *J* = 6.8 Hz, 6H), 4.65 (q, *J* = 6.8 Hz, 4H), 7.12 (d, *J* = 12.8 Hz, 2H) 7.56 (m, 2H), 7.76 (m, 5H), 7.95 (m, 4H) 8.35 (d, *J* = 8.0 Hz, 2H), 8.61 (t, *J* = 7.2 Hz, 4H) ^{13}C NMR (100 MHz, DMSO-*d*6) δ ppm 13.31, 45.86, 108.77, 117.77, 122.62, 123.32, 124.35, 125.65, 125.78, 129.25, 131.53, 131.62, 132.84, 134.00, 136.16, 155.38, 155.47.

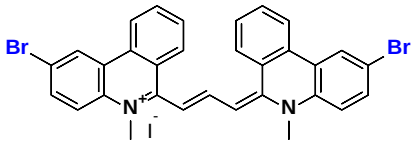

A trimethine cyanine dye, 2-bromo-6-((E)-3-((E)-2-bromo-5-methylphenanthridin-6(5H)-ylidene)prop-1-en-1-yl)-5-methylphenanthridin-5-ium iodide; (**6c**); A dark green solid (42%) ^{1}H NMR (400 MHz, DMSO-d6) δ ppm 4.16 (s, 6H), 7.25 (d, J = 12.0 Hz, 2H), 7.84 (m, 3H), 7.95 (m, 6H), 8.49 (d, J = 8.0 Hz, 2H) 8.76 (d, *J* = 8.0 Hz, 2H), 8.85 (m, 2H) ^{13}C NMR (100 MHz, DMSO-*d*6) δ ppm

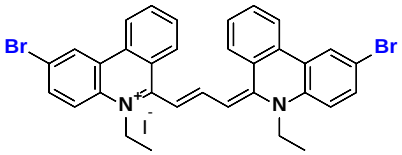

A trimethine cyanine dye, 2-bromo-6-((E)-3-((E)-2-bromo-5-ethylphenanthridin-6(5H)-ylidene)prop-1-en-1-yl)-5-ethylphenanthridin-5-ium iodide; (**6d**); A dark green solid (40%) ^{1}H NMR (400 MHz, DMSO-*d*6) δ ppm 1.52 (t, *J* = 6.4 Hz, 6H), 4.62 (m, 4H), 7.14 (d, *J* = 12.8 Hz, 2H), 7.77 (m, 3H), 7.92 (m, 6H), 8.33 (d, *J* = 8.0 Hz, 2H), 8.70 (d, *J* = 8.0 Hz, 2H), 8.82 (s, 2H)

^{13}C NMR (100 MHz, DMSO-*d*6) δ ppm 13.24, 46.11, 109.55, 118.53, 120.05, 123.83, 124.66, 126.13, 126.68, 129.93, 131.47, 131.73, 134.02, 134.14, 135.39, 155.41.

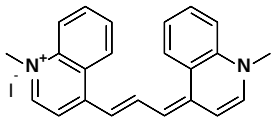

A trimethine cyanine dye, 1-methyl-4-((1E,3Z)-3-(1-methylquinolin-4(1H)-ylidene)prop-1-en-1-yl)quinolin-1-ium iodide; (**8**); A dark blue crystalline solid (31%) ^{1}H NMR (400 MHz, DMSO-*d*6) δ ppm 3.98 (s, 6H), 7.09 (d, *J* = 13.2 Hz, 2H), 7.61 (t, J = 7.6 Hz, 2H), 7.74 (d, *J* = 7.2 Hz, 2H), 7.82 (t, *J* = 8.4 Hz, 2H), 7.87 (d, *J* = 8.4 Hz, 2H), 8.10 (d, J = 7.2 Hz, 2H) 8.37 (d, *J* = 8.4 Hz, 2H), 8.66 (t, *J* = 12.8 Hz, 1H). ^{13}C NMR (100 MHz, DMSO-*d*6) δ ppm 41.85, 108.73, 110.74, 117.89, 124.39, 125.01, 126.41, 133.06, 139.41, 141.80, 142.86, 148.81.

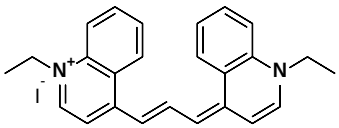

A trimethine cyanine dye, 1-ethyl-4-((1E,3Z)-3-(1-ethylquinolin-4(1H)-ylidene)prop-1-en-1-yl)quinolin-1-ium iodide; (**9**); A blue cyrystaline solid (34%) ^{1}H NMR (400 MHz, DMSO-*d*6) δ ppm 1.41 (t, *J* = 7.07 Hz, 6 H), 4.46 (q, *J* = 6.99 Hz, 4 H), 7.09 (d, J = 13.14 Hz, 2 H), 7.59 (t, J = 7.58 Hz, 2 H), 7.77 (d, J = 7.33 Hz, 2 H), 7.81 - 7.87 (m, 2 H), 7.89 - 7.93 (m, 2 H), 8.14 (d, *J* = 7.33 Hz, 2 H), 8.37 (d, J = 8.34 Hz, 2 H), 8.67 (t, J = 12.88 Hz, 1 H). ^{13}C NMR (100 MHz, DMSO-d6) δ ppm 14.98, 48.86, 109.23, 110.91, 117.66, 124.63, 125.37, 126.25, 133.12, 138.21, 140.80, 143.02, 148.80

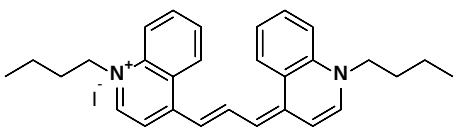

A trimethine cyanine dye, 1-butyl-4-((1E,3Z)-3-(1-butylquinolin-4(1H)-ylidene)prop-1-en-1-yl)quinolin-1-ium iodide. (**10**); A blue cyrstaline solid (29%) ^{1}H NMR (400 MHz, $CDCl_3$) δ ppm 0.99 (t, *J* = 7.33 Hz, 6 H), 1.41 - 1.52 (m, 4 H), 1.87 (t, *J* = 7.45 Hz, 4 H), 4.27 (t, *J* = 7.33 Hz, 4 H), 6.88 (d, *J* = 12.88 Hz, 2 H), 7.49 (t, *J* = 7.71 Hz, 2 H), 7.54 (d, *J* = 8.59 Hz, 2 H), 7.68 - 7.73 (m, 2 H), 7.93 (q, *J* = 7.49 Hz, 4 H), 8.26 (d, *J* = 8.34 Hz, 2 H), 8.59 (t, *J* = 12.68, 1 H)

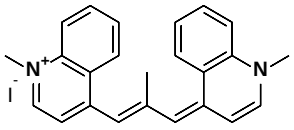

A trimethine cyanine dye, 1-methyl-4-((E)-2-methyl-3-((Z)-1-methylquinolin-4(1H)-ylidene)prop-1-en-1-yl)quinolin-1-ium iodide. (**11**); A blue cyrstaline solid (40%) ^{1}H NMR (400 MHz, DMSO-*d*6) δ ppm 2.47 (s, 3H), 4.41 (s, 6H), 6.63 (s, 2H), 7.93 (t, *J* = 7.6 Hz, 2H), 8.16 (t, *J* = 8.0 Hz, 2H), 8.32 (d, *J* = 8.8 Hz, 2H), 8.41 (d, *J* = 6.8 Hz, 2H), 8.74 (d, *J* = 8.4 Hz, 2H), 9.03 (d, *J* = 6.8 Hz, 2H). ^{13}C NMR (100 MHz, DMSO-*d*6) δ ppm 44.57, 66.19, 96.95, 116.88, 119.63, 125.65, 126.18, 128.93, 134.52, 138.77, 148.09, 151.57.

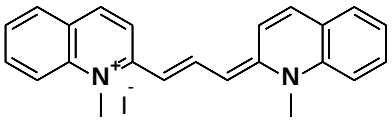

A trimethine cyanine dye, 1-methyl-2-((1E,3E)-3-(1-methylquinolin-2(1H)-ylidene)prop-1-en-1-yl)quinolin-1-ium iodide. (**13**); A dark blue crystalline solid (45%) ^{1}H NMR (400 MHz, DMSO-*d*6) δ ppm 3.92 (s, 6H), 6.54 (d, *J* = 12.8 Hz, 2H), 7.46 (t, *J* = 7.2 Hz, 2H), 7.75 (t, *J* = 7.6 Hz, 2H), 7.84 (d, *J* = 7.6 Hz, 2H), 7.90 (d, *J* = 8.8 Hz, 2H), 8.02 (d, *J* = 9.6 Hz, 2H) 8.30 (d, *J* = 9.6 Hz, 2H), 8.68 (t, *J* = 12.8 Hz, 1H). ^{13}C NMR (100 MHz, DMSO-*d*6) δ ppm 36.66, 106.69, 116.94, 120.36, 124.90, 125.30, 129.34, 132.69, 135.92, 140.10, 147.09, 153.50

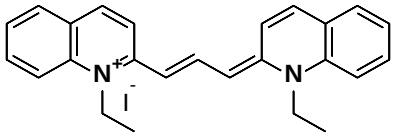

A trimethine cyanine dye, 1-ethyl-2-((1E,3E)-3-(1-ethylquinolin-2(1H)-ylidene)prop-1-en-1-yl)quinolin-1-ium iodide; (**14**); A blue cyrystaline solid (42%) ^{1}H NMR (400 MHz, DMSO-*d*6) δ ppm 1.44 (t, *J* = 6.8 Hz, 6 H), 4.47-4.49 (m, 4 H), 6.58 (d, *J* = 12.8 Hz, 2 H), 7.45 (t, *J* = 7.2 Hz, 2 H), 7.75 (t, *J* = 8.0 Hz, 2 H), 7.83 - 7.89 (m, 4 H), 8.00 (d, *J* = 9.2 Hz , 2 H), 8.30 (d, *J* = 9.6 Hz, 2 H), 8.70 (t, *J* = 12.8 Hz, 1 H). ^{13}C NMR (100 MHz, DMSO-*d*6) δ ppm 12.96, 43.33, 105.85, 116.51, 120.50, 125.13, 125.31, 129.57, 132.91, 136.00, 139.00, 147.92, 152.39.

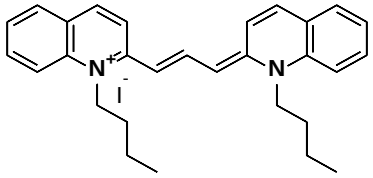

A trimethine cyanine dye, 1-butyl-2-((1E,3E)-3-(1-butylquinolin-2(1H)-ylidene)prop-1-en-1-yl)quinolin-1-ium iodide; (**15**); A blue cyrstaline solid (40%) ^{1}H NMR (400 MHz, $CDCl_3$) δ ppm 1.03 (t, *J* = 7.2 Hz, 6 H), 1.57 - 1.62 (m, 4 H), 1.79 (t, *J* = 7.2 Hz, 4 H), 4.44 (m, 4 H), 6.49 (d, *J* = 12.8 Hz, 2 H), 7.48 (t, *J* = 7.6 Hz, 2 H), 7.77 (t, *J* = 8.4 Hz, 2 H), 7.87 (t, *J* =8.0 , 4 H), 8.02 (d, *J* = 9.2 Hz, 2 H), 8.32 (d, *J* = 9.6 Hz, 2 H), 8.70 (t, *J* = 12.8, 1 H). ^{13}C NMR (100 MHz, DMSO-*d*6) δ ppm 14.15, 19.75, 29.36, 47.50, 105.86, 116.73, 120.53, 125.13, 125.41, 129.61, 132.95, 136.11, 139.23, 147.79, 152.66.

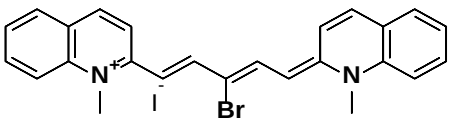

A pentamethine cyanine dye, 2-((1E,3Z)-3-bromo-5-((E)-1-methylquinolin-2(1H)-ylidene)penta-1,3-dien-1-yl)-1-methylquinolin-1-ium iodide; (**17**); A green powder (49%). ^{1}H

NMR (400 MHz, DMSO-*d*6) δ ppm 4.00 (s, 6H), 6.32 (d, *J* = 13.2 Hz, 2 H), 7.53 (t, *J* = 7.6 Hz, 2 H), 7.81 (t, *J* = 7.6 Hz, 2 H), 7.90-7.94 (m, 4H), 8.02 (d, *J* = 8.8 Hz, 2 H), 8.22 (d, *J* = 9.6 Hz, 2 H), 8.34 (d, *J* = 13.2 Hz, 2 H). ^{13}C NMR (100 MHz, DMSO-*d*6)

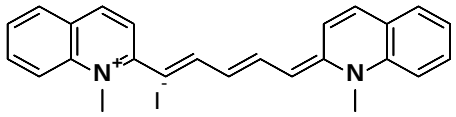

A pentamethine cyanine dye, 1-methyl-2-((1E,3E)-5-((E)-1-methylquinolin-2(1H)-ylidene)penta-1,3-dien-1-yl)quinolin-1-ium iodide; (**18**); A green powder (56%). ^{1}H NMR (400 MHz, DMSO-*d*6) δ ppm 3.88 (s, 6 H), 6.38 (d, *J* = 12.8 Hz, 2 H), 6.58 (t, *J* = 11.2 Hz, 1 H), 7.43 (m, 2 H), 7.71-7.74 (m, 2 H), 7.79-7.85 (m, 6 H), 7.97-8.04 (m, 4 H). ^{13}C NMR (100 MHz, DMSO-*d*6)

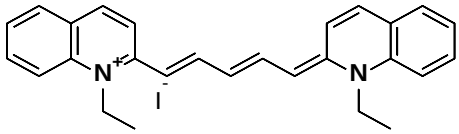

A pentamethine cyanine dye, 1-ethyl-2-((1E,3E)-5-((E)-1-ethylquinolin-2(1H)-ylidene)penta-1,3-dien-1-yl) quinolin -1-ium iodide. (**19**); A green powder (58%). ^{1}H NMR (400 MHz, DMSO-*d*6) δ ppm 1.38 (s, 6 H), 4.44 (m, 4 H), 6.34 (d, *J* = 13.2 Hz, 2 H), 6.48 (t, *J* = 12.0 Hz, 1 H), 7.42 (t, *J* = 6.4 Hz, 2 H), 7.71-7.86 (m, 6 H), 7.96-8.07 (m, 4 H). ^{13}C NMR (100 MHz, DMSO-*d*6) 12.76, 43.24,105.84, 116.43, 119.89, 125.15, 125.31, 129.57, 133.03, 136.18, 139.18, 150.29, 151.27.

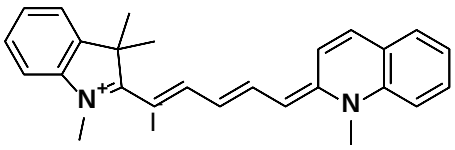

A pentamethine cyanine dye, 1,3,3-trimethyl-2-((1E,3E)-5-((E)-1-methylquinolin-2(1H)-ylidene)penta-1,3-dien-1-yl)-3H-indol-1-ium iodide; (**21**); A blue solid (41%). ^{1}H NMR (400 MHz, $CDCl_3$) δ ppm 1.62 (s, 3 H), 1.75 (s, 6 H), 4.22 (s, 3 H) 5.82 (d, *J* = 13.3 Hz, 1 H), 6.63 (t, *J* = 11.6 Hz, 2 H), 6.92 (d, *J* = 7.6 Hz, 1 H), 7.10 (t, *J* = 7.0 Hz, 1 H), 7.28-7.32 (m, 2 H), 7.50 (t, *J* = 7.4 Hz, 1 H) 7.76-7.82 (m, 2 H), 7.90 (d, *J* = 8.8 Hz, 1 H), 8.04 (m, 1 H) 8.16 (d, *J* = 8.8 Hz, 1 H), 8.44 (m, 2H). ^{13}C NMR (100 MHz, $CDCl_3$)

4.5 REFERENCES for Chapter 3

1. Li, Z., Grant, K.B., *RSC Adv*., **2016**, 6, 24617
2. Johnstone, T.C., Park,G.Y., Lippard, S.J, *Anticancer Res*., **2014**, 34, 471–476
3. Anticancer drug—friend or foe, *InTech*, Rijeka, **2014**
4. Joensuu, H., *Lancet Oncol*., **2008**, 9(3), 304.
5. Shemesh, C.S., Hardy, C.W., Yu, D.S., Fernandez, B., Zhang,H.,*Photodiagn. Photodyn. Ther*., **2014**, 11, 193–203
6. Mapp, C.T., Owens, E.A., Henary, M., Grant, K.B. *Bioorg. Med. Chem. Lett*., **2014**, 24, 214–219.
7. Nguyen, Q.T., Tsien, R.Y., *Nat. Rev. Cancer*, **2013**, 13, 653–662.
8. Sinha, S.H., Owens, E.A., Feng, Y., Yang, Y., Xie, Y., Tu, Y., Henary, M., Zheng, Y.G., *European Journal of Medicinal Chemistry* 54 (**2012**) 647-659
9. Nanjunda, R., Owens, E.A., Mickelson, L., Alyabyev, S., Kilpatric, N., Wang, S., Henary, M., Wilson, W.D., *Bioorganic & Medicinal Chemistry* 20 (**2012**) 7002–7011

APPENDICES

Appendix A: Monomethine Chapter I

Appendix A.1. **Compound 6a**

^{1}H NMR (400 MHz, DMSO-d6) 25 °C

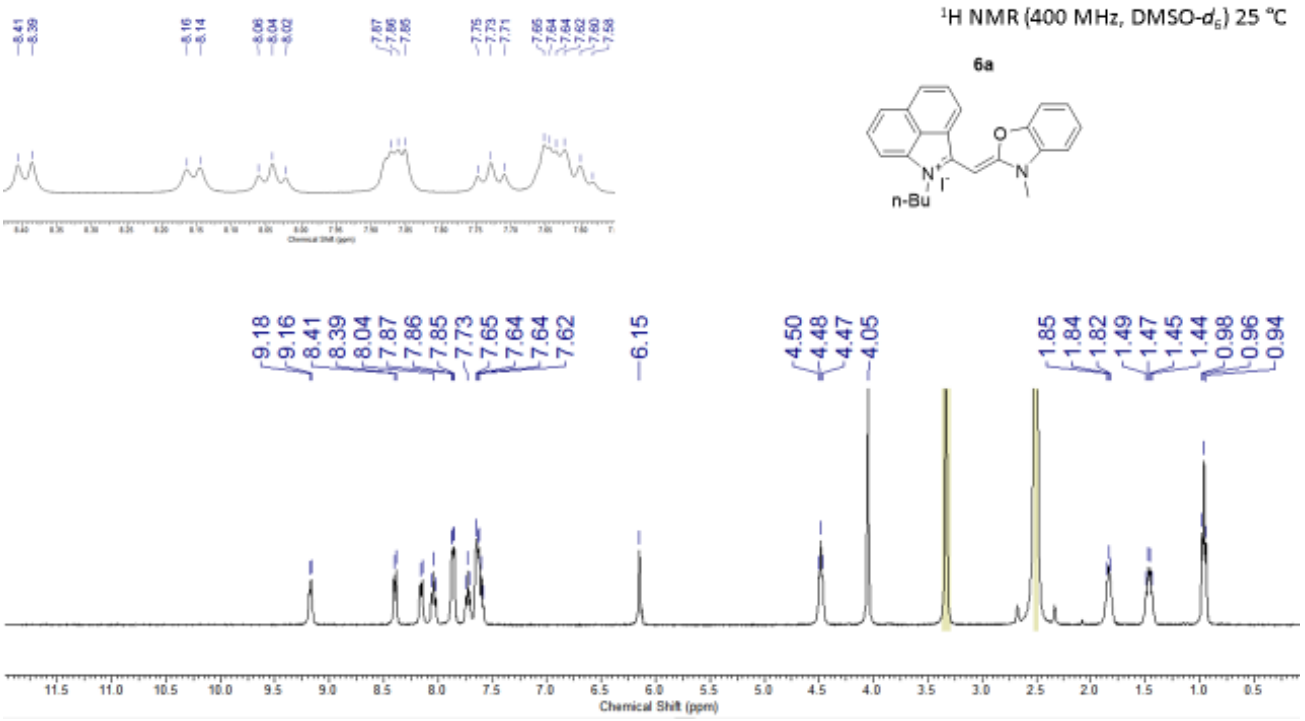

^{13}C NMR (100 MHz, DMSO-d6) 25 °C

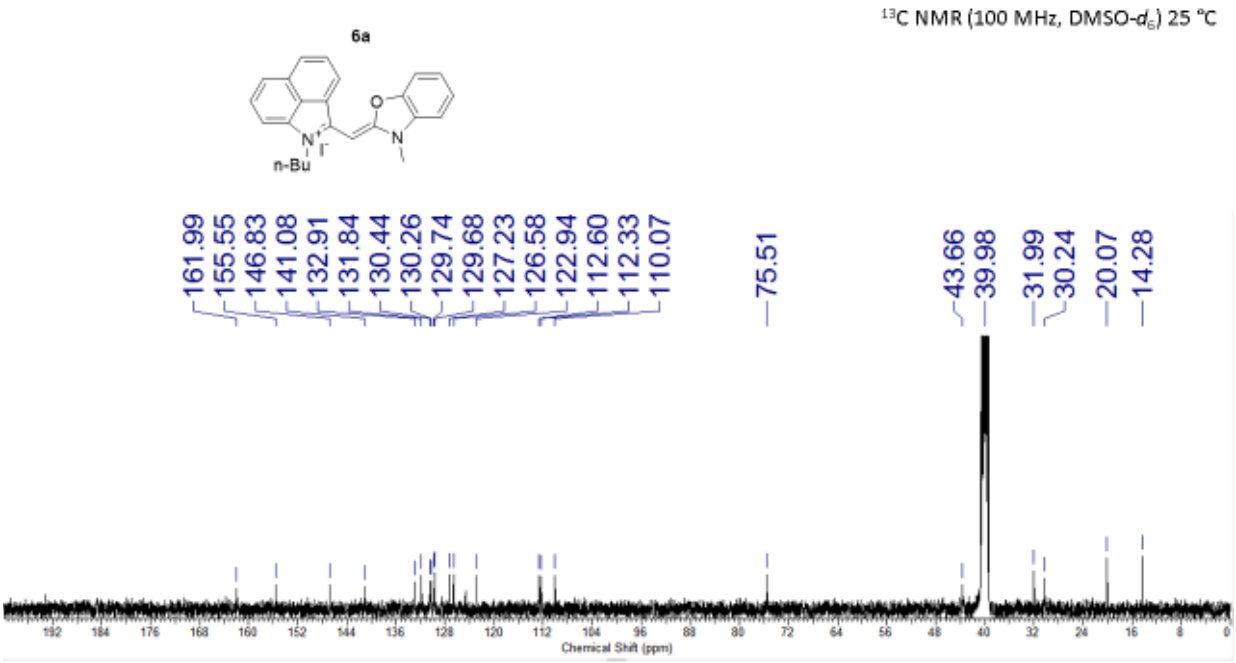

HRMS-ESI

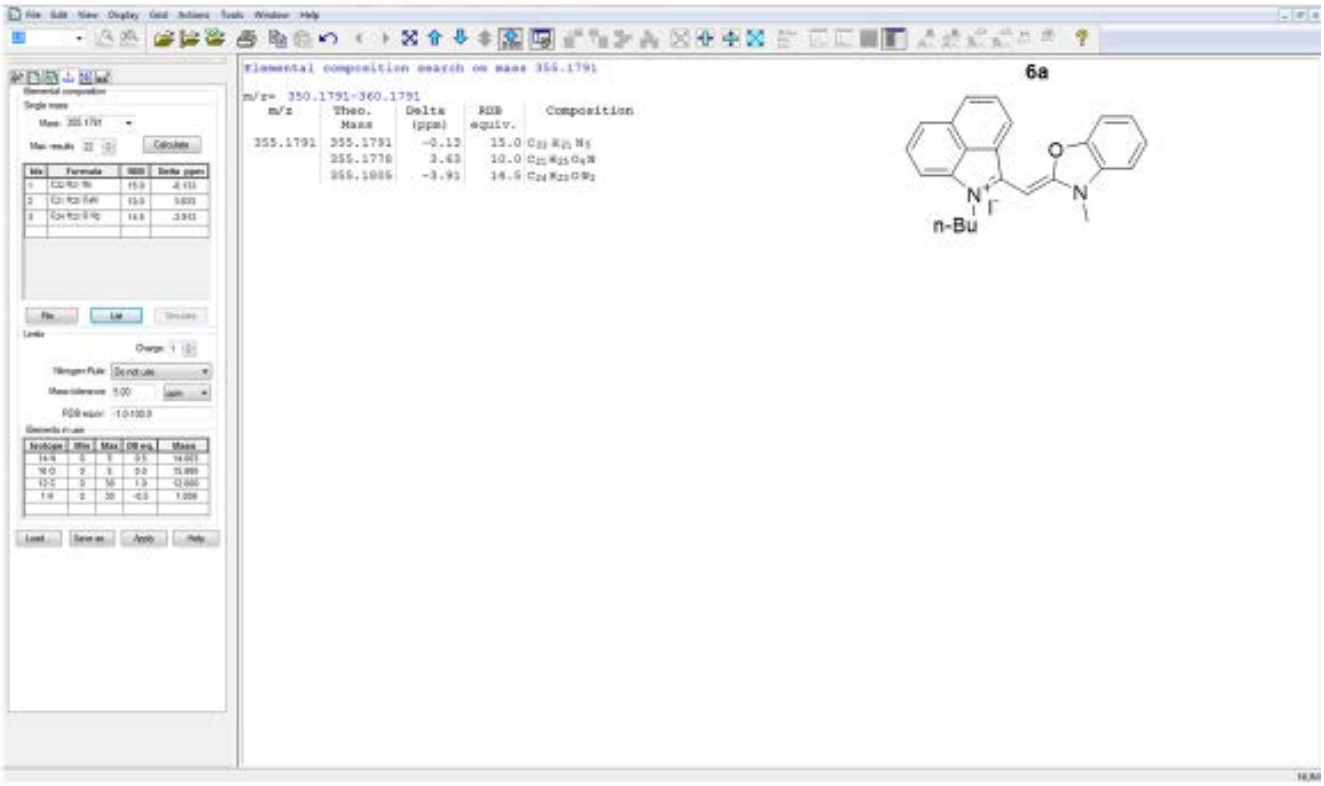

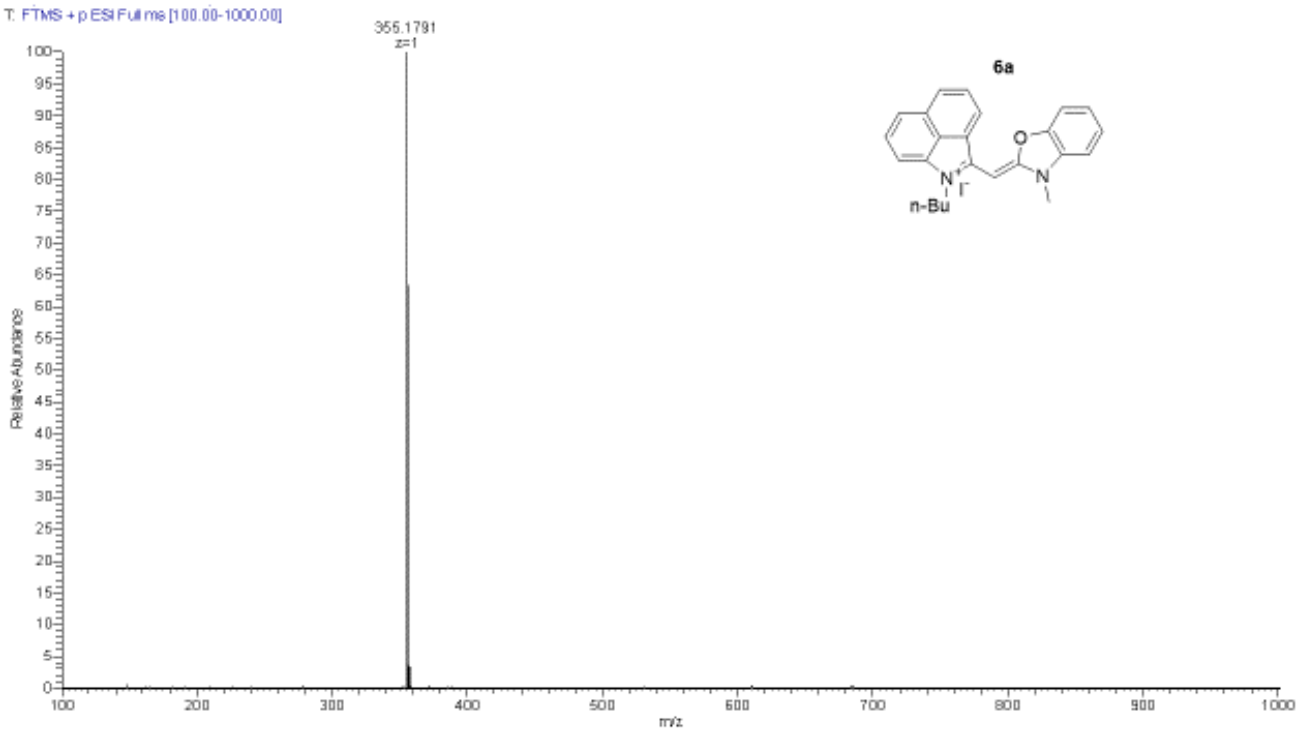

Infrared

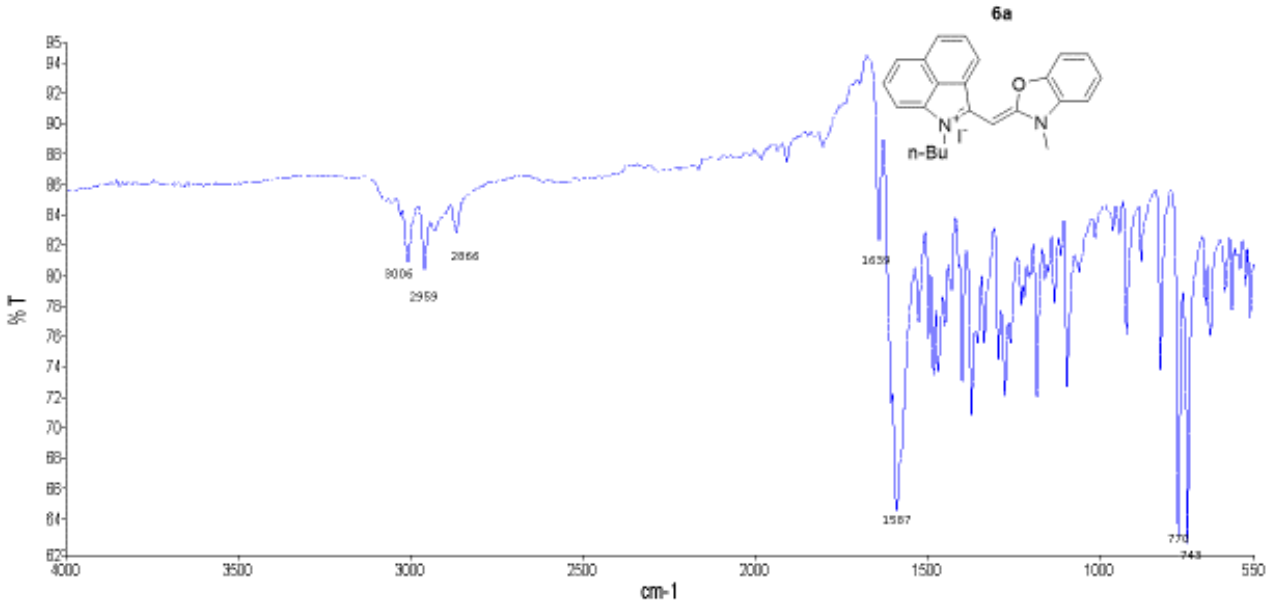

HPLC

HPLC data was obtained using a Waters 2487 dual detector wavelength absorption detector with wavelengths set at 260 and 600 nm. The column used in LC was a Waters Delta-Pak 5 µM 100Å 3.9×150 mm reversed phase C18 column, with a flow rate of 1mL/min employing a 5-100% acetonitrile/water/0.1% formic acid gradient.

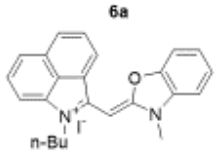

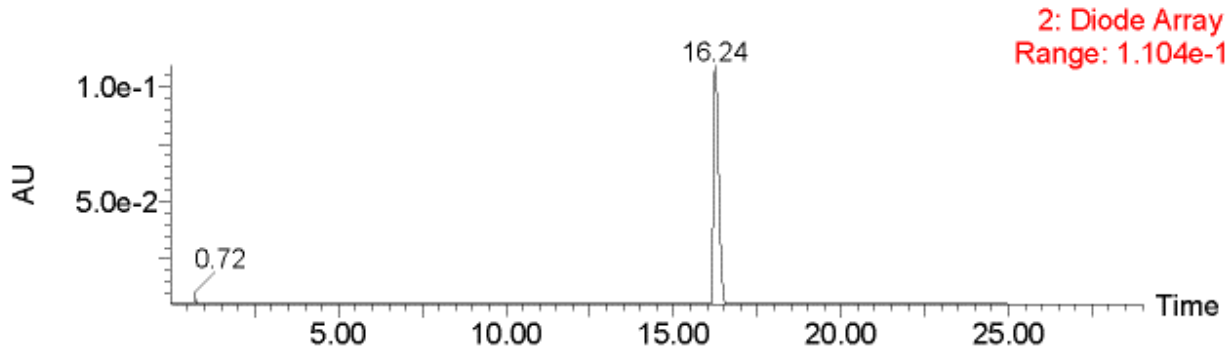

Appendix A.2. **Compound 6b**

^{1}H NMR (400 MHz, DMSO-d6) 25 °C

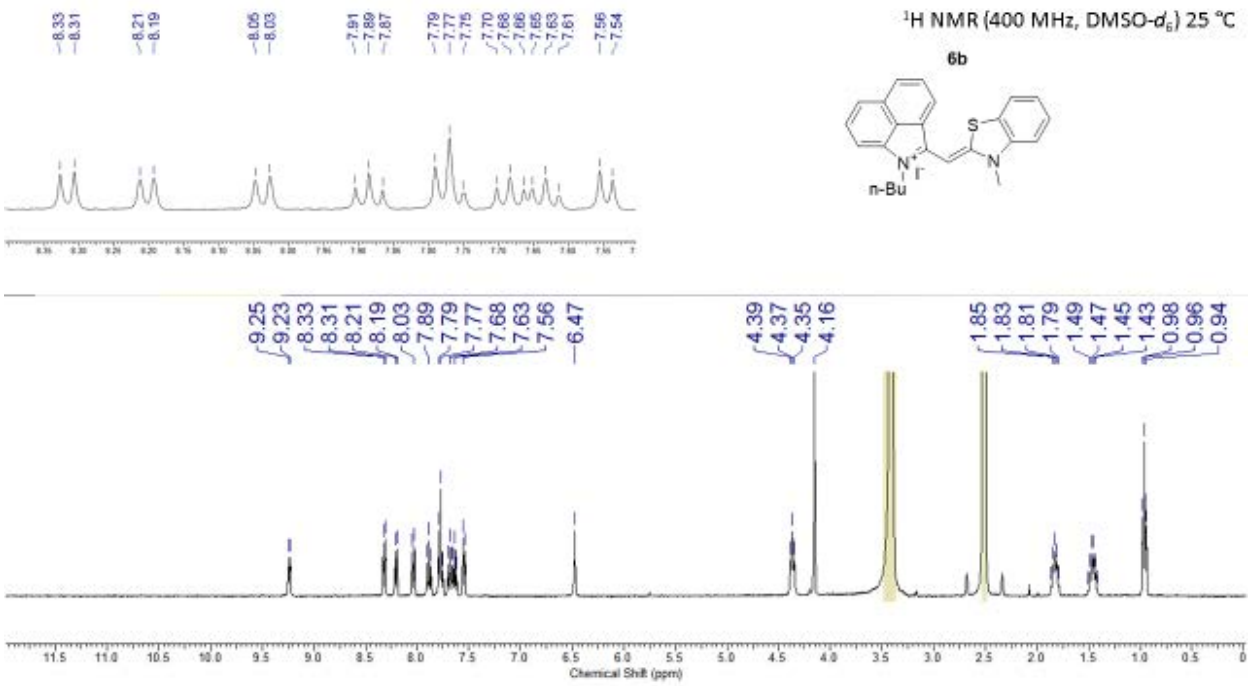

^{13}C NMR (100 MHz, DMSO-d6) 25 °C

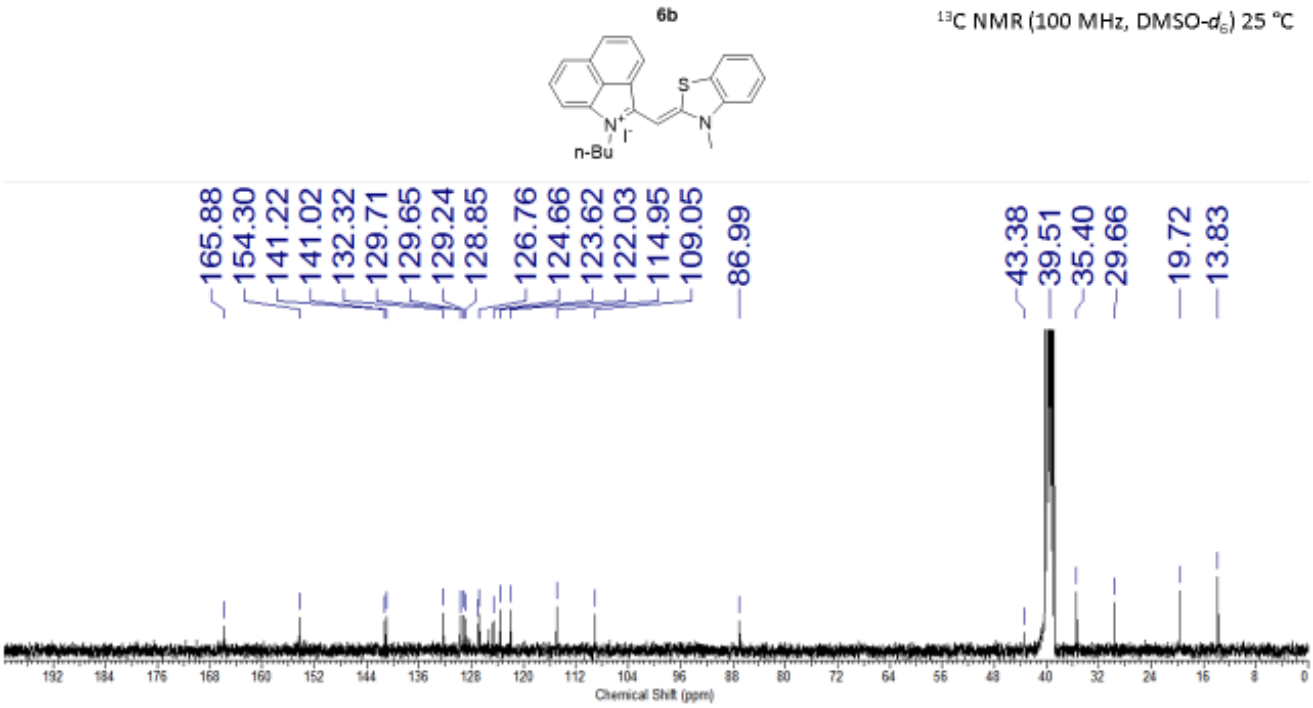

HRMS-ESI

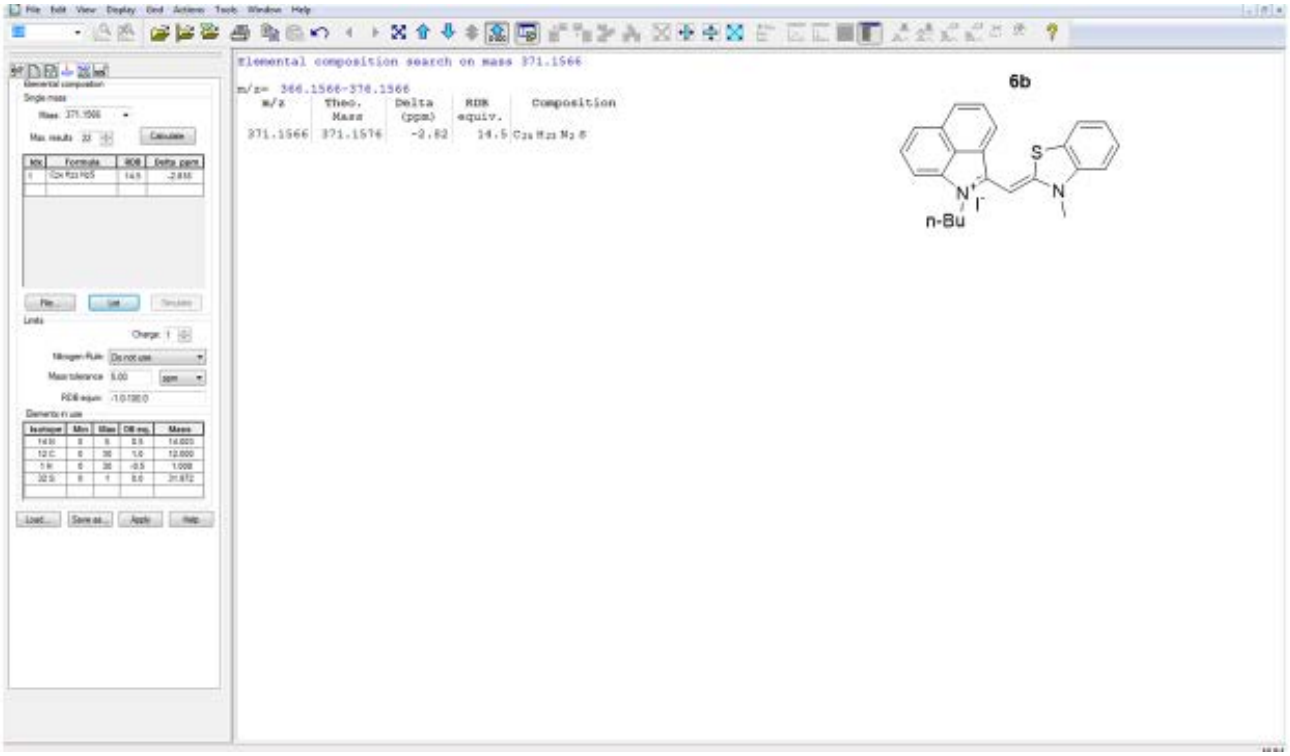
Elemental composition search on mass 371.1566
m/z= 366.1566-376.1566
m/z
Theo. Mass
Delta (ppm)
RDB equiv.
Composition
371.1566
371.1574
-2.82
14.5
C24 H22 N2 S
6b
n-Bu

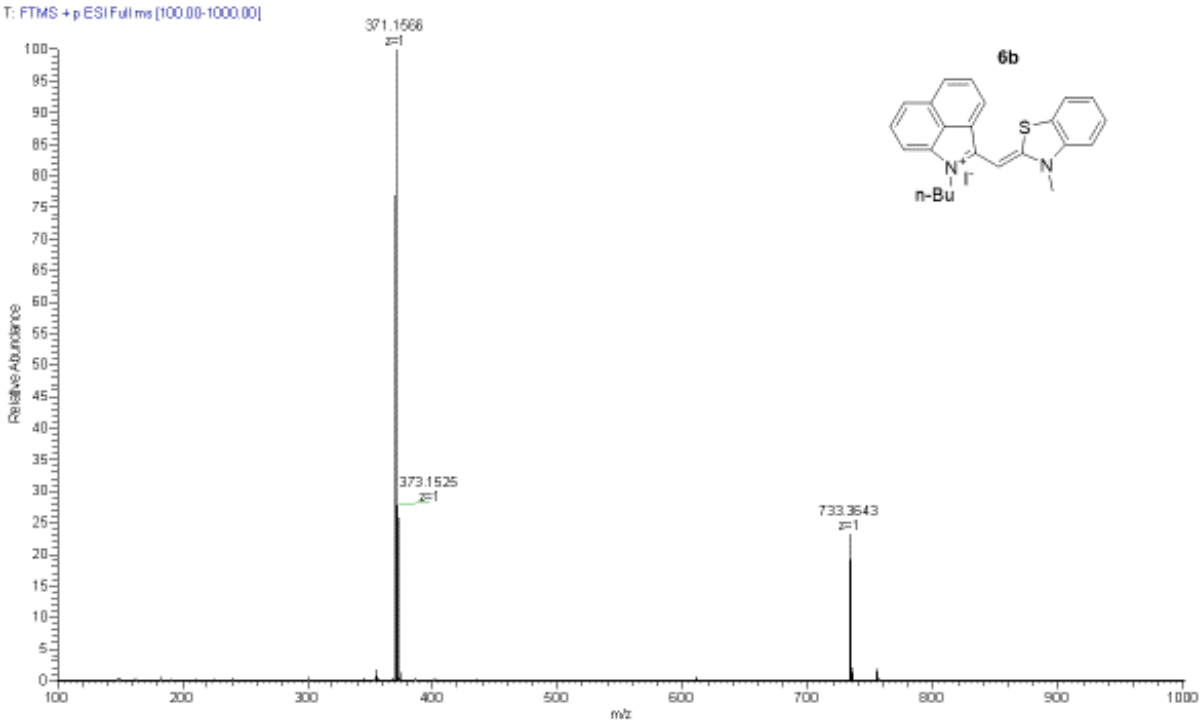
T: FTMS + p ESI Full ms [100.00-1000.00]
371.1566
z=1
373.1525
z=1
733.3643
z=1
6b
n-Bu
Relative Abundance
m/z

INFRARED

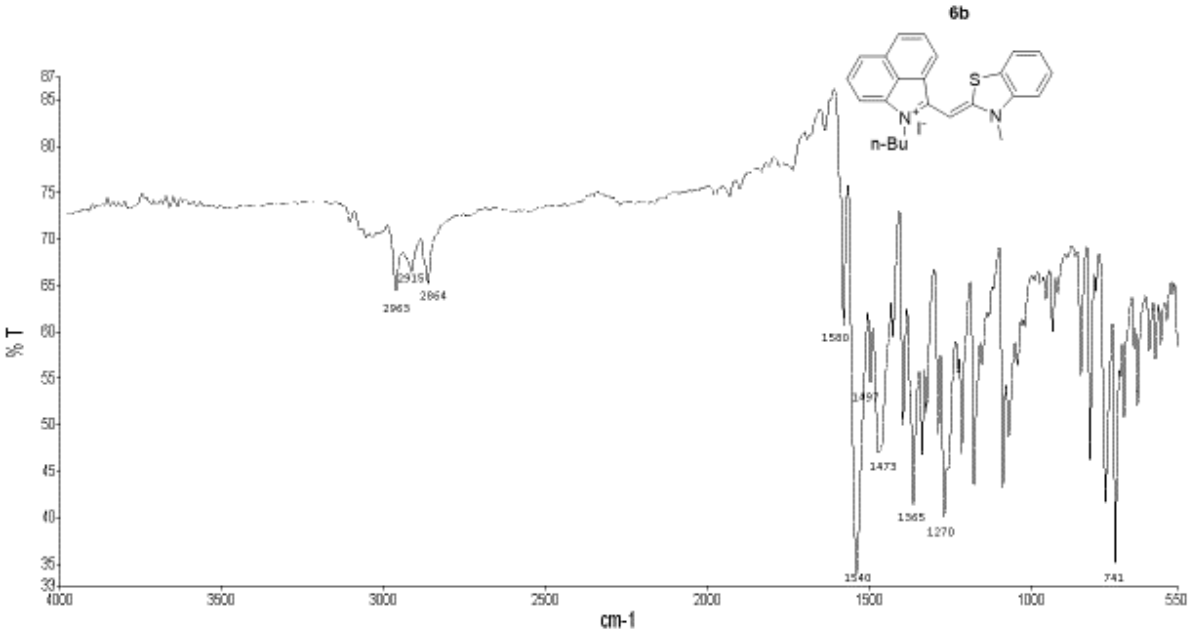

HPLC

HPLC data was obtained using a Waters 2487 dual detector wavelength absorption detector with wavelengths set at 260 and 600 nm. The column used in LC was a Waters Delta-Pak 5 µM 100Å 3.9×150 mm reversed phase C18 column, with a flow rate of 1mL/min employing a 5-100% acetonitrile/water/0.1% formic acid gradient.

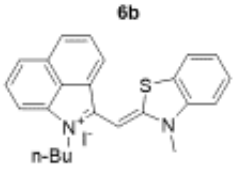

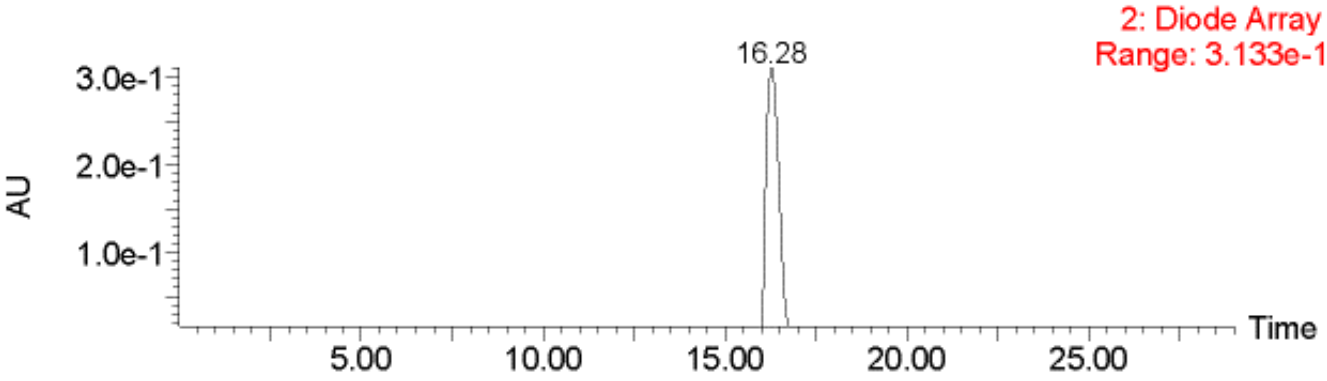

Aggregation

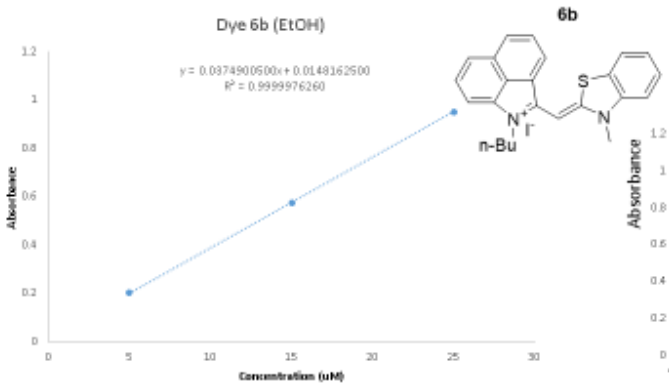

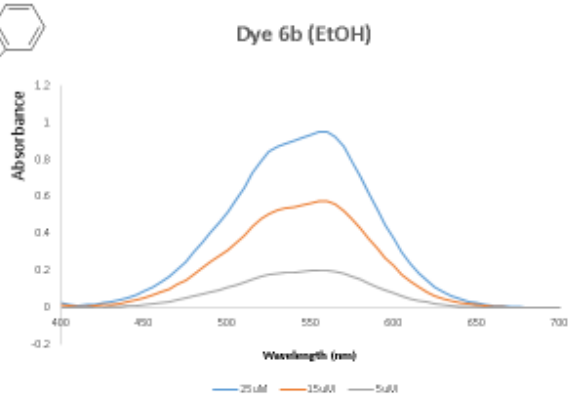

Aggregation of **6b** was ruled out by measuring absorption at different concentrations. The ratio between the absorption at 560 nm and 520 nm remains the same at high and low concentrations.

uM Dye 6b	560nm	520nm	ratio
25	0.952401	0.7903	1.205113248
15	0.5765	0.47902	1.20349881
5	0.2026	0.1675	1.209552239

Solvatochromism

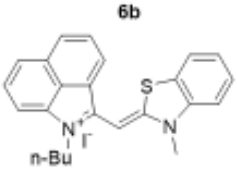

Dye **6b** was tested for solvatochromic changes in absorption by dissolving the dye **6b** in 5 different solvents (ethanol, dimethyl formamide, dichloromethane, acetonitrile, and aqueous tris buffer) to observe any change in λmax. Less than 5 nm change in λmax was observed. Such a small shift suggests that the distribution of the ground state dye is virtually unaffected by the solvent polarity.

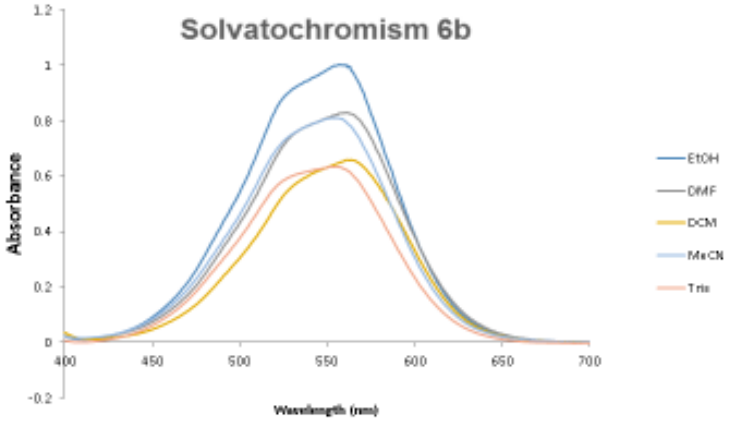

Appendix A.3. **Compound 6c**

^{1}H NMR (400 MHz, DMSO-d6) 25 °C

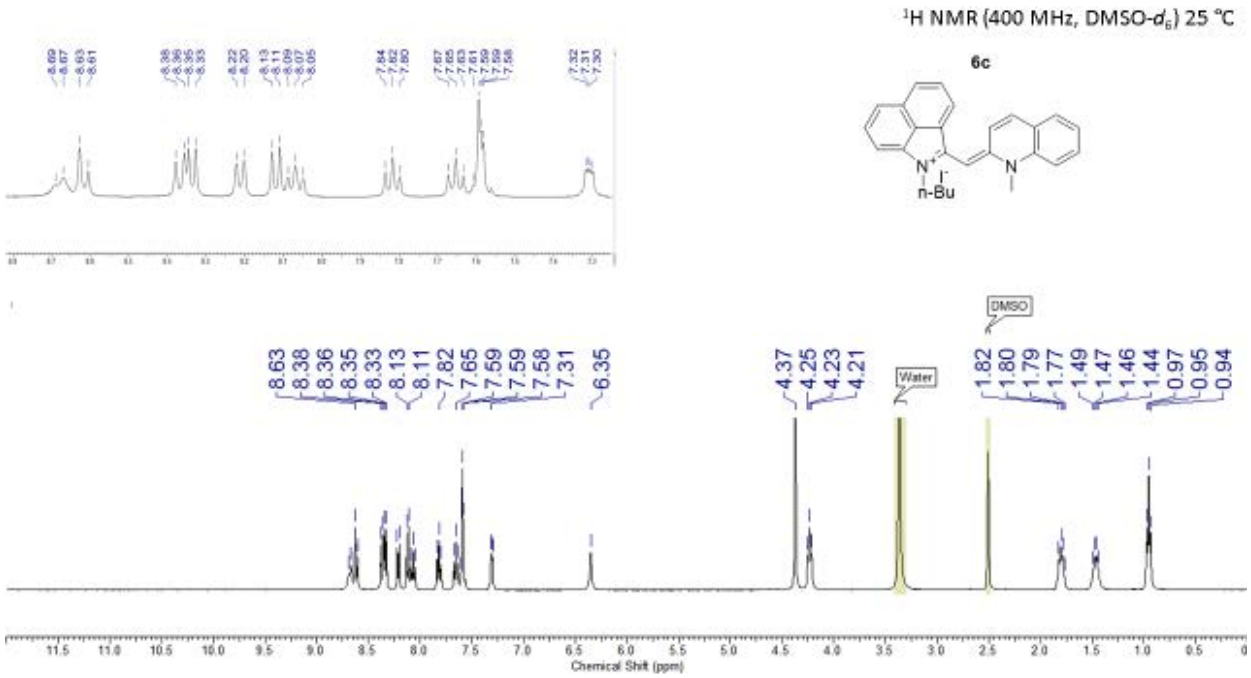

^{13}C NMR (100 MHz, DMSO-d6) 25 °C

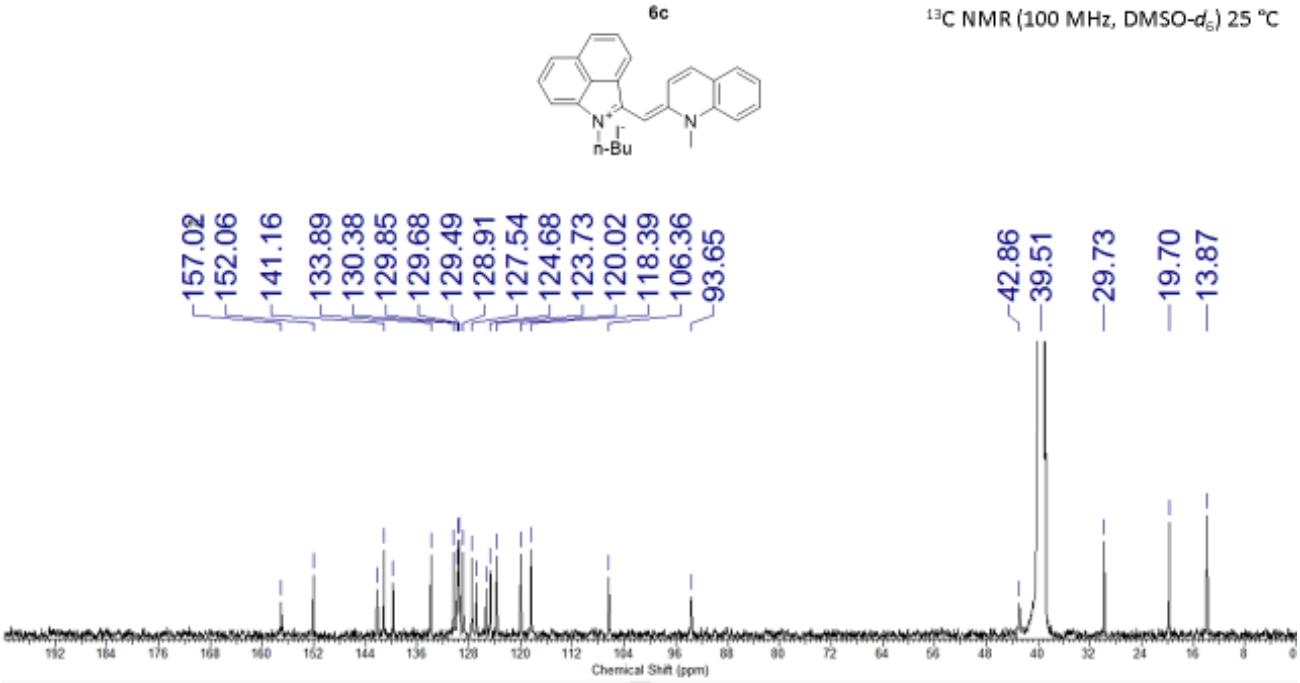

HRMS-ESI

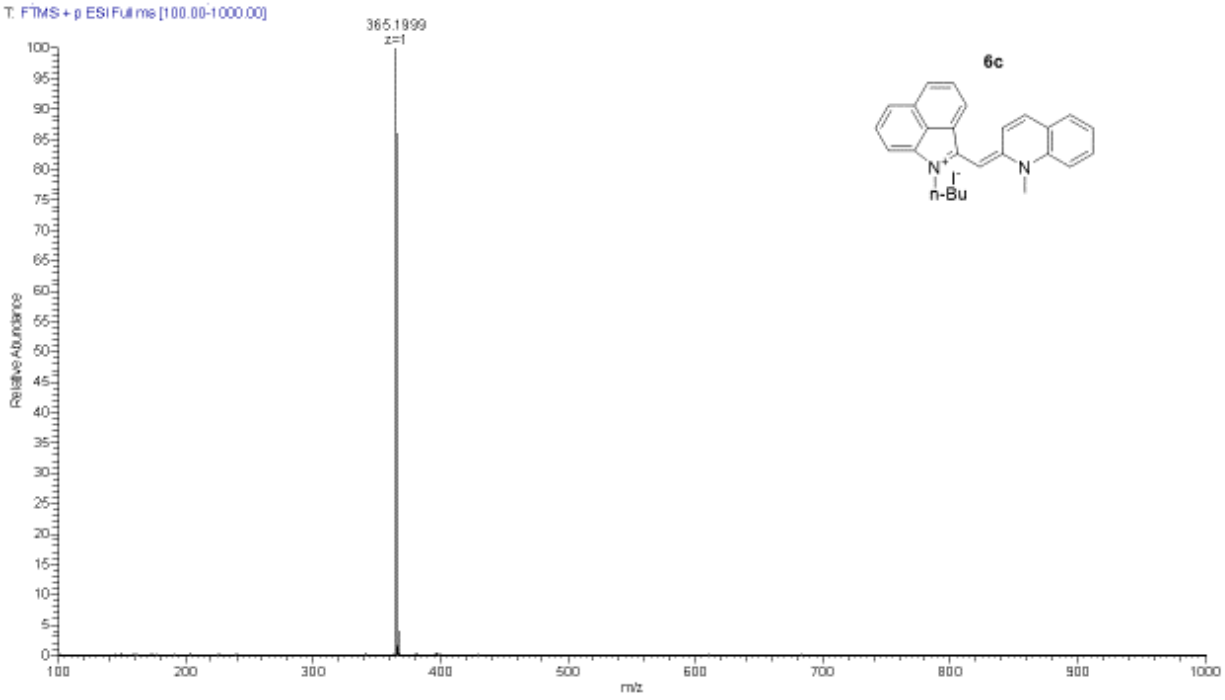
T: FTMS + p ESI Full ms [100.00-1000.00]
365.1999
z=1
6c
n-Bu
Relative Abundance
m/z

Appendix A.4. **Compound 6d**

^{1}H NMR (400 MHz, DMSO-d6) 25 °C

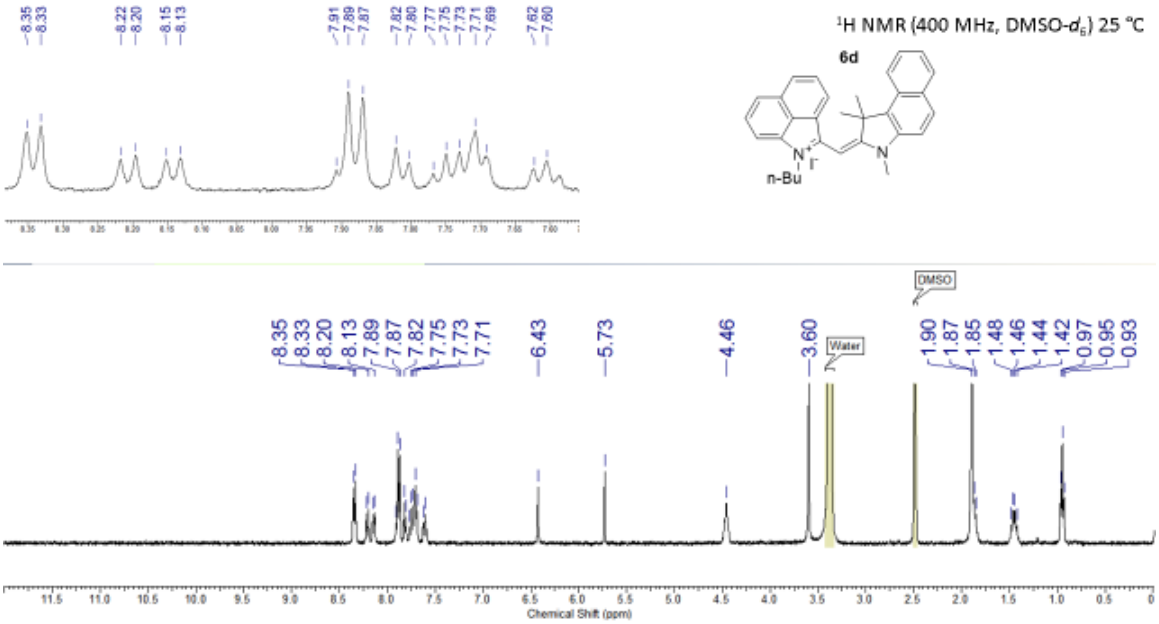

^{13}C NMR (100 MHz, DMSO-d6) 25 °C

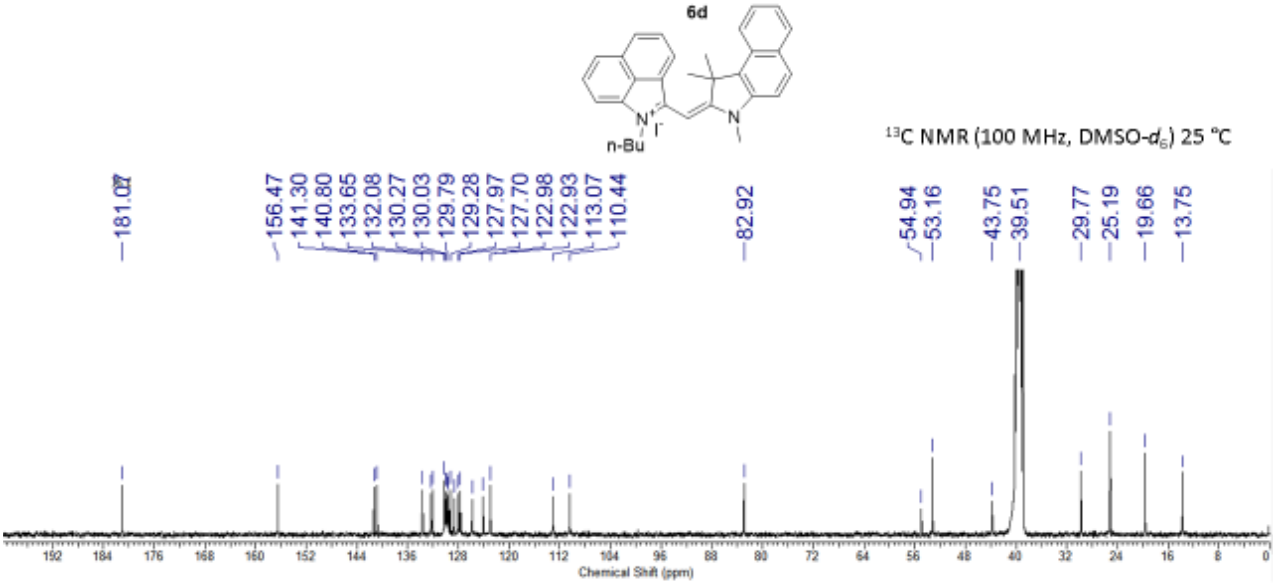

HRMS-ESI

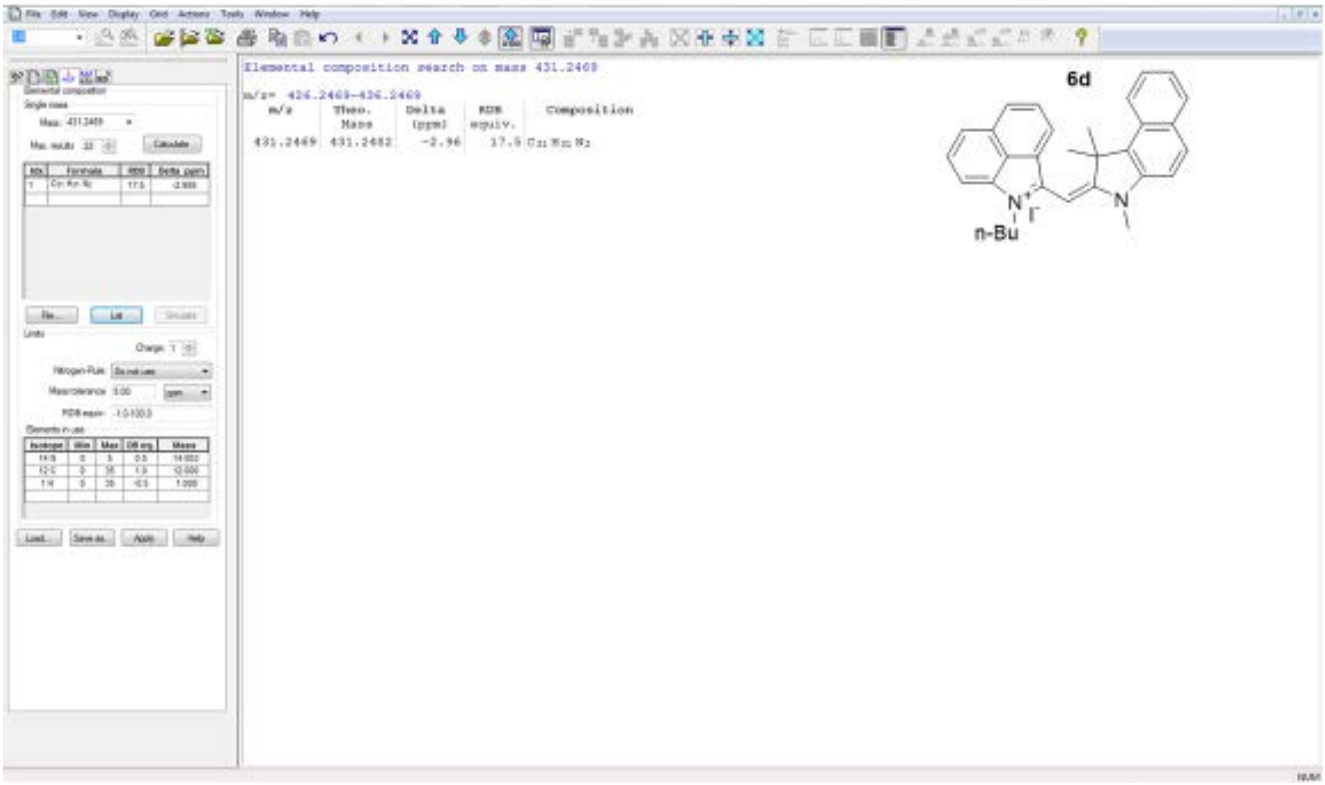
Elemental composition search on mass 431.2469
m/z= 426.2469-436.2469
m/z
Theo. Mass
Delta (ppm)
RDB equiv.
Composition
431.2469
431.2482
-2.96
17.5
6d
n-Bu

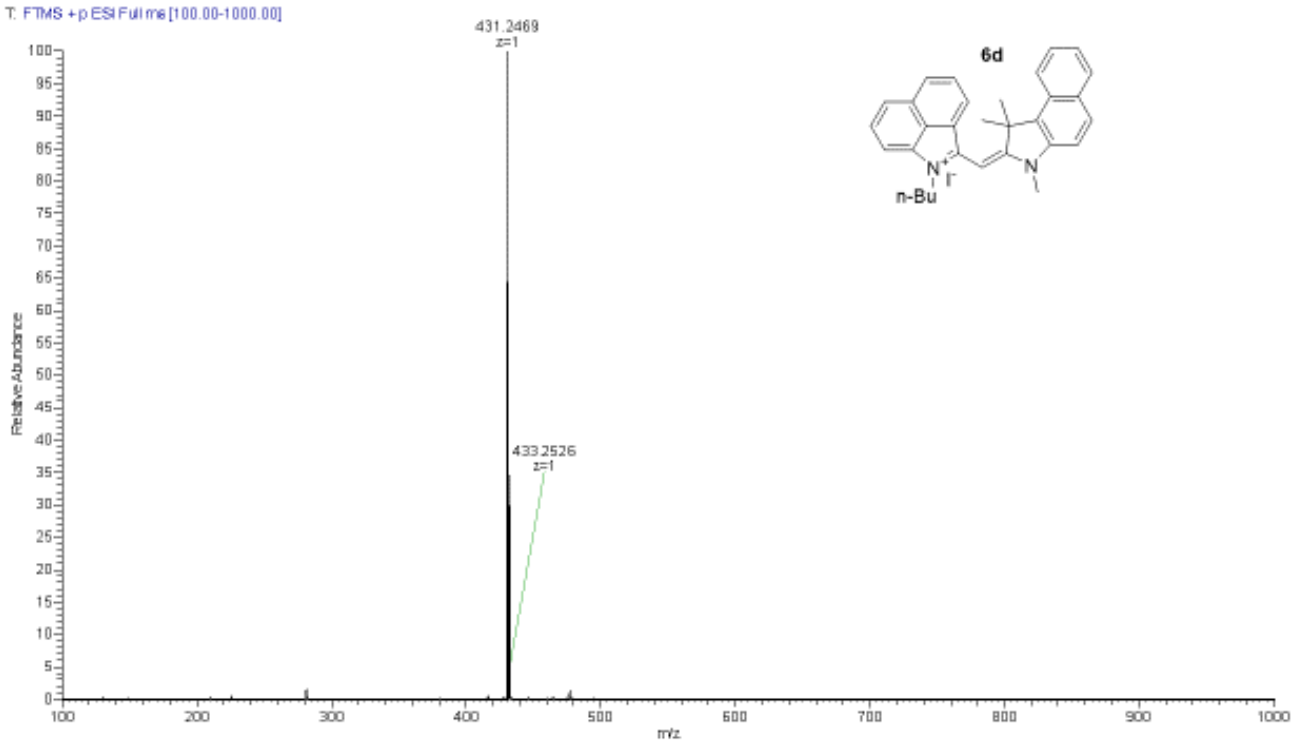
T: FTMS + p ESI Full ms [100.00-1000.00]
431.2469
z=1
433.2526
z=1
6d
n-Bu
Relative Abundance
m/z

HPLC

HPLC data was obtained using a Waters 2487 dual detector wavelength absorption detector with wavelengths set at 260 and 600 nm. The column used in LC was a Waters Delta-Pak 5 µM 100Å 3.9×150 mm reversed phase C18 column, with a flow rate of 1mL/min employing a 5-100% acetonitrile/water/0.1% formic acid gradient.

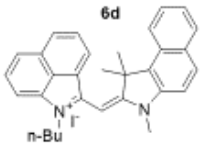

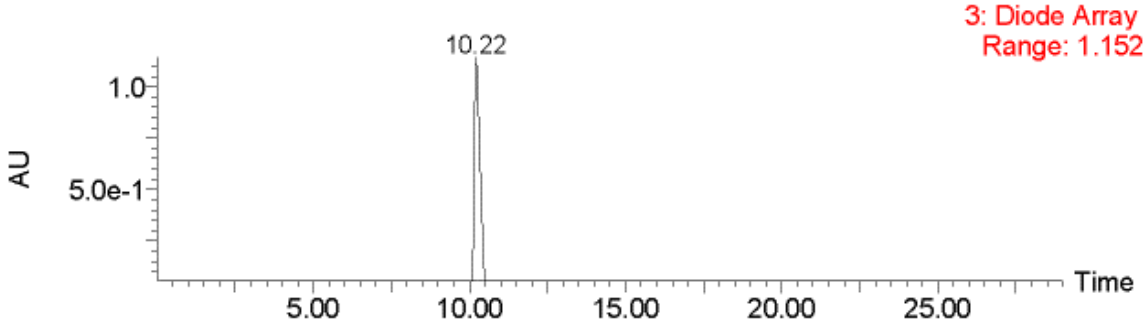

Appendix A.5. **Compound 10a**

^{1}H NMR (400 MHz, DMSO-d6) 25 °C

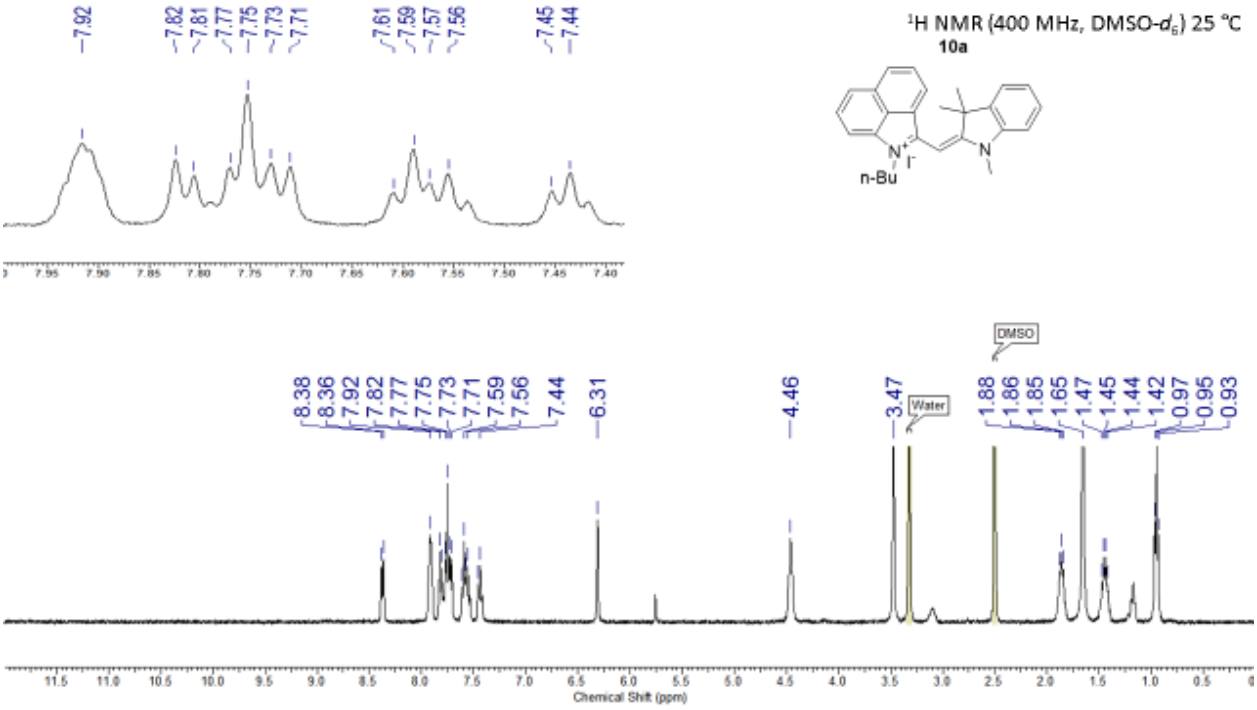

^{13}C NMR (100 MHz, DMSO-d6) 25 °C

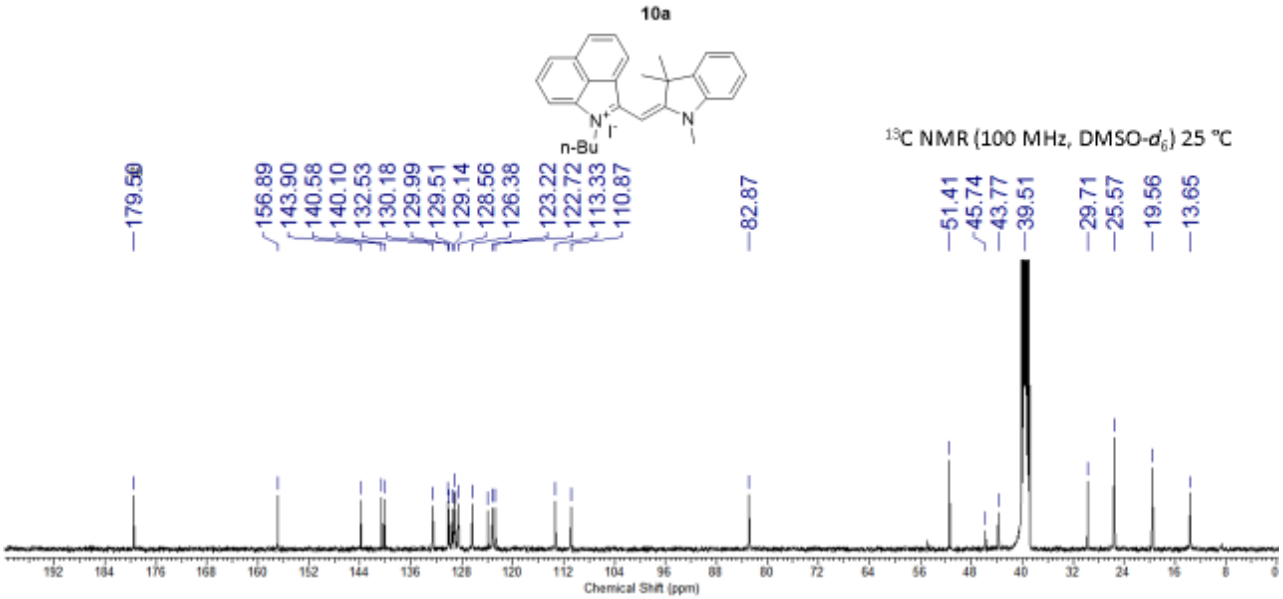

HRMS-ESI

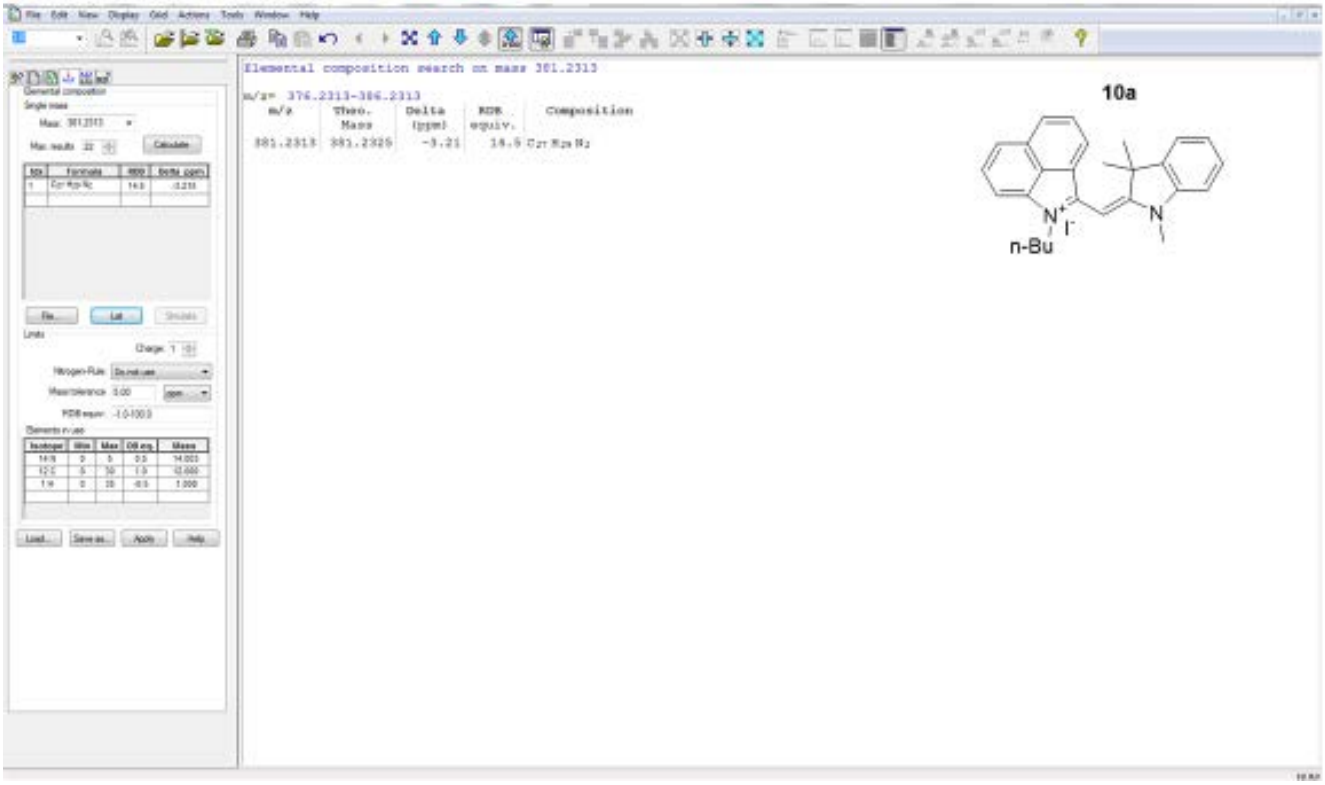
Elemental composition search on mass 381.2313
m/z= 376.2313-386.2313
m/z
Theo. Mass
Delta (ppm)
RDB equiv.
Composition
381.2313
381.2325
-3.21
16.5
10a
n-Bu

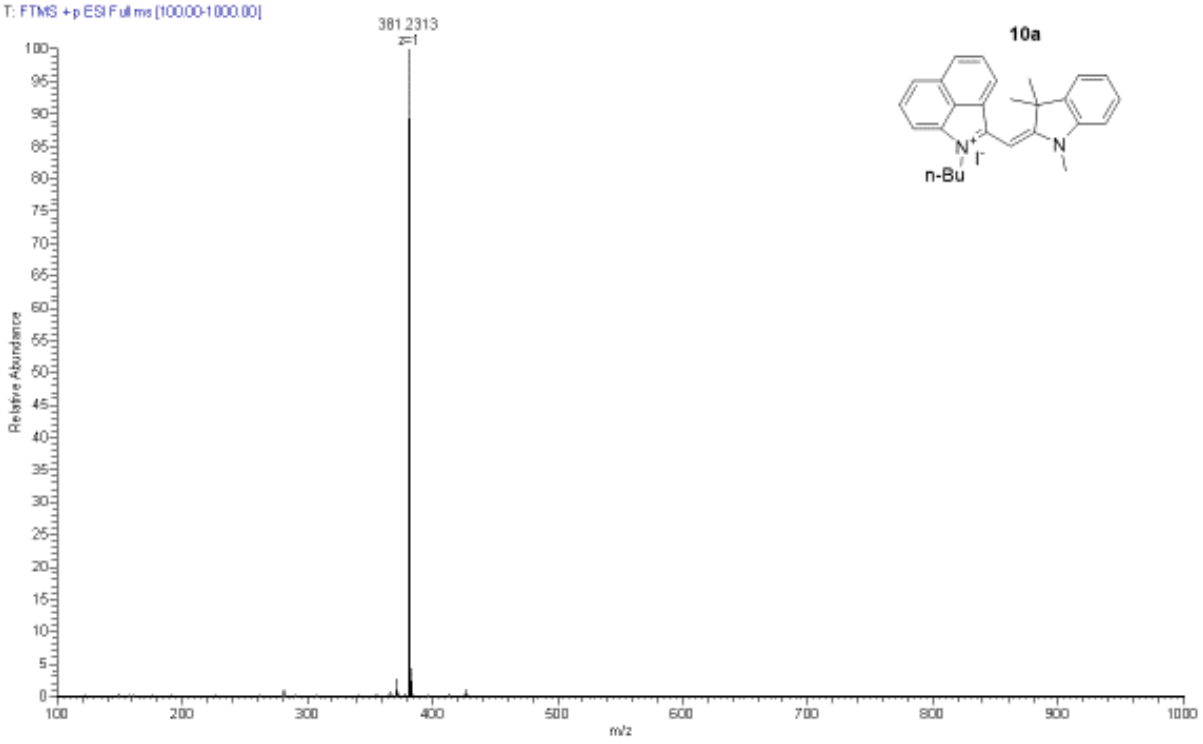
T: FTMS + p ESI Full ms [100.00-1000.00]
381.2313
z=1
10a
n-Bu
Relative Abundance
m/z

INFRARED

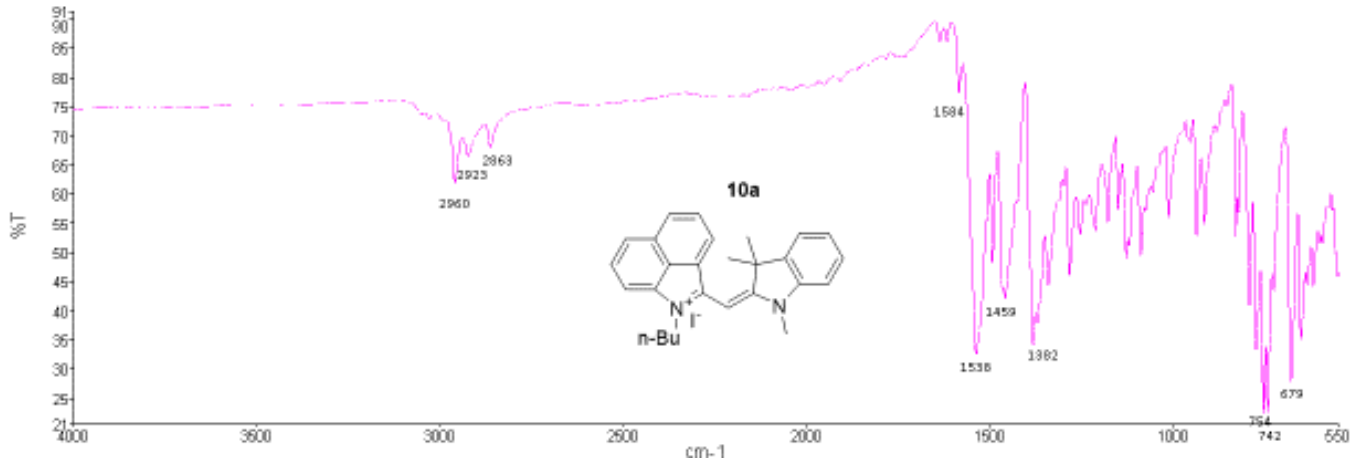

HPLC

HPLC data was obtained using a Waters 2487 dual detector wavelength absorption detector with wavelengths set at 260 and 600 nm. The column used in LC was a Waters Delta-Pak 5 µM 100Å 3.9×150 mm reversed phase C18 column, with a flow rate of 1mL/min employing a 5-100% acetonitrile/water/0.1% formic acid gradient.

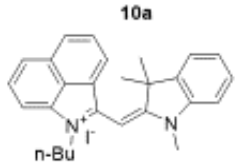

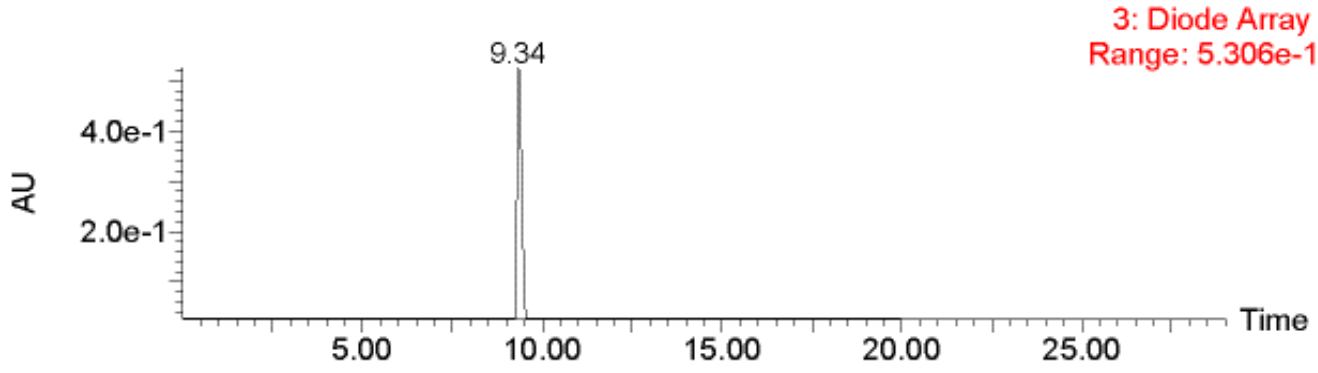

Appendix A.6. **Compound 10b**

^{1}H NMR (400 MHz, DMSO-d6) 25 °C

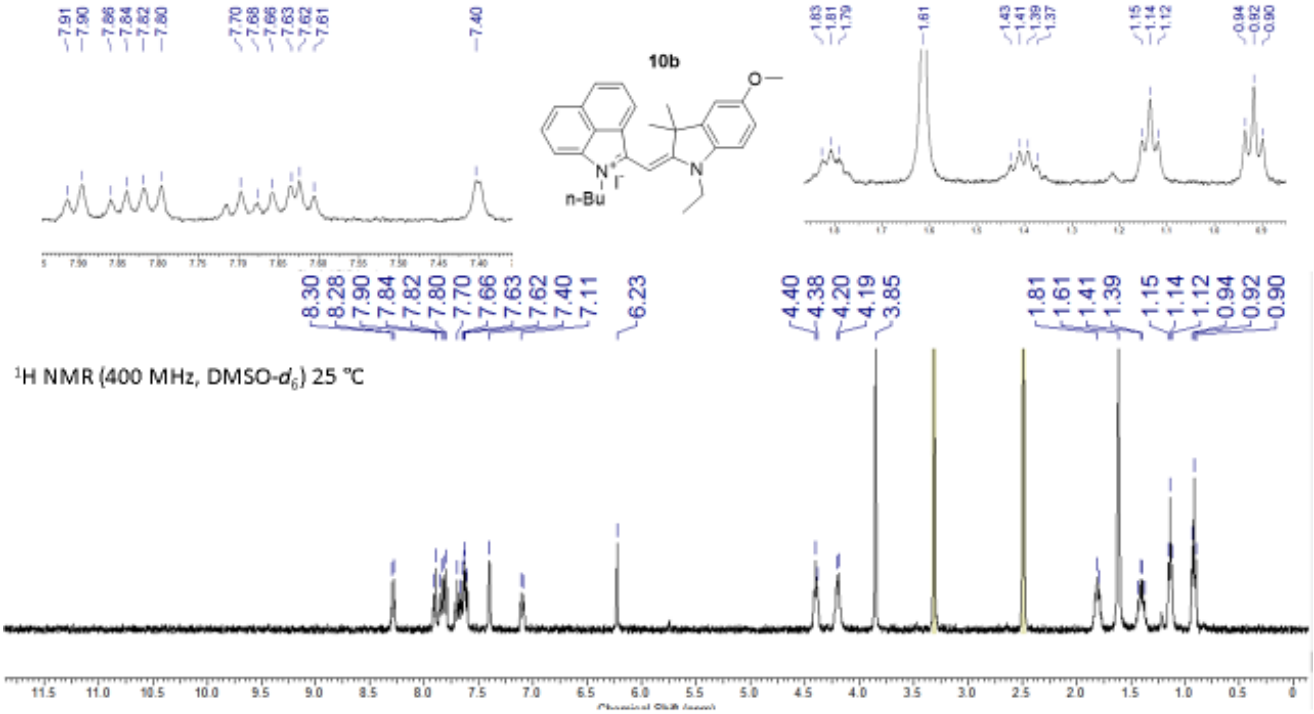

^{13}C NMR (100 MHz, DMSO-d6) 25 °C

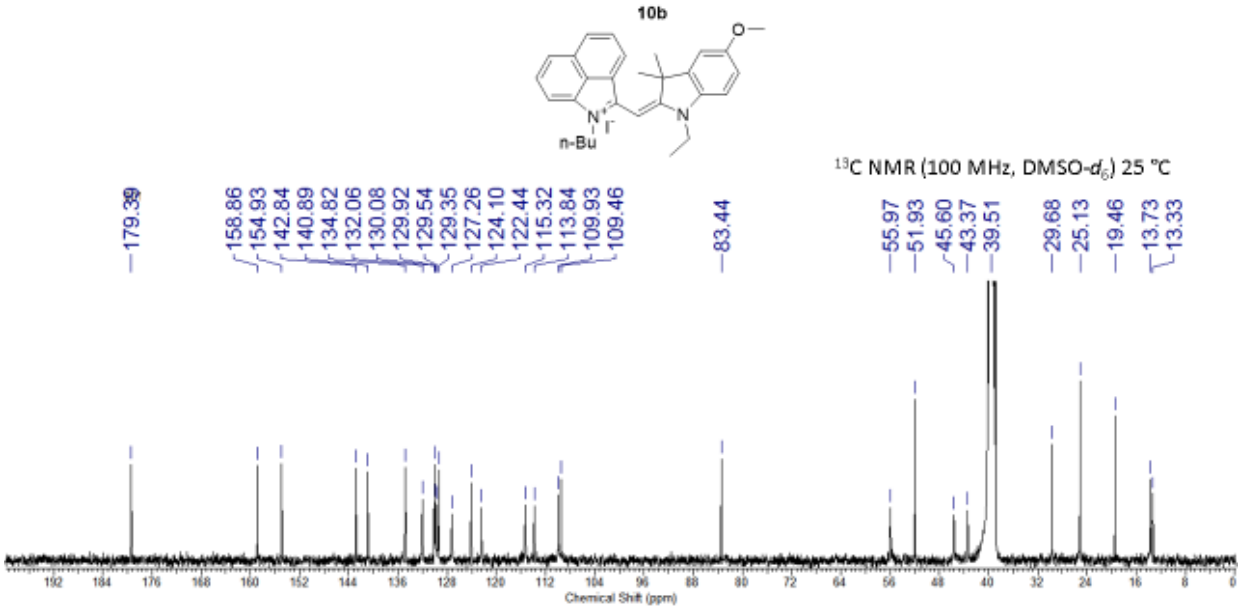

HRMS-ESI

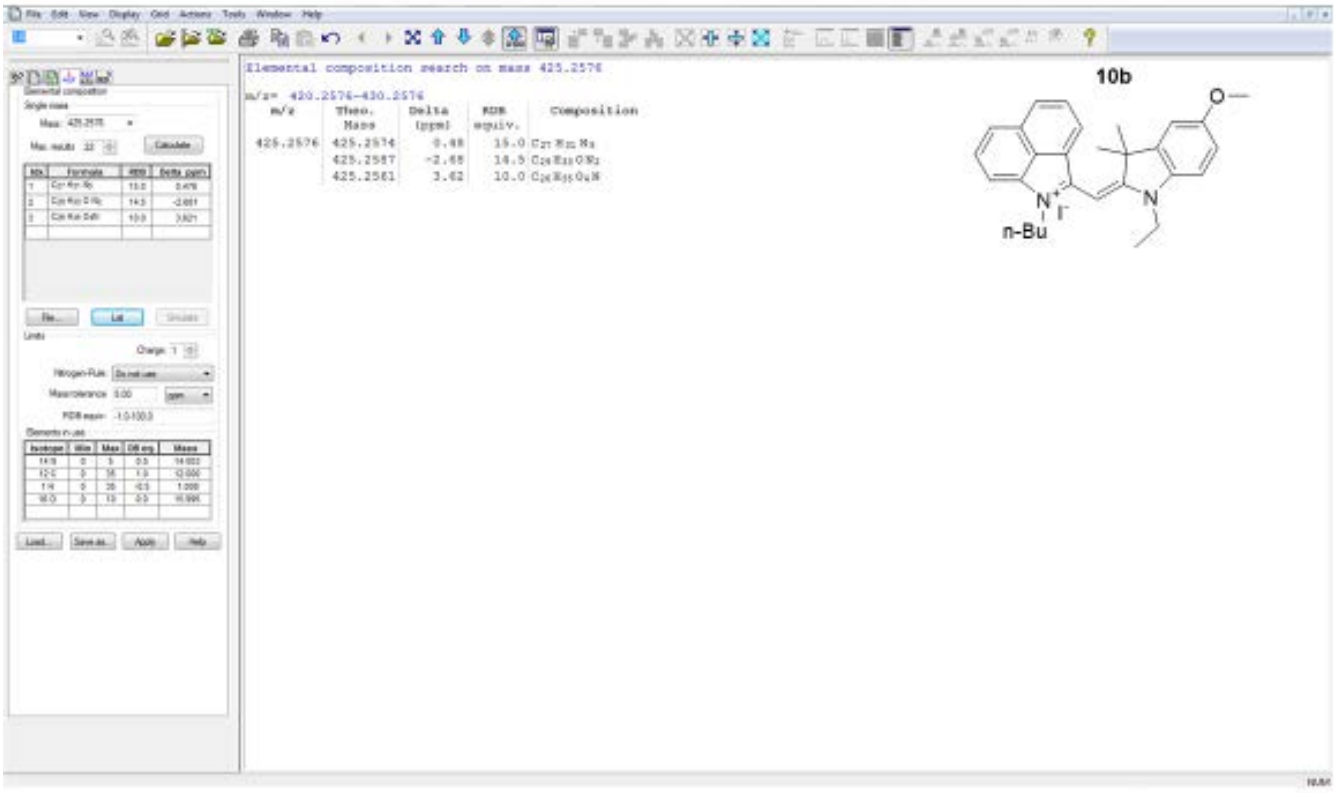
Elemental composition search on mass 425.2576
m/z= 420.2576-430.2576
m/z Theo. Mass Delta (ppm) RDB equiv. Composition
425.2576 425.2574 0.48 15.0 C27 H33 N2
425.2587 -2.65 14.5 C26 H33 O N2
425.2561 3.62 10.0 C26 H33 O4 N
10b
n-Bu

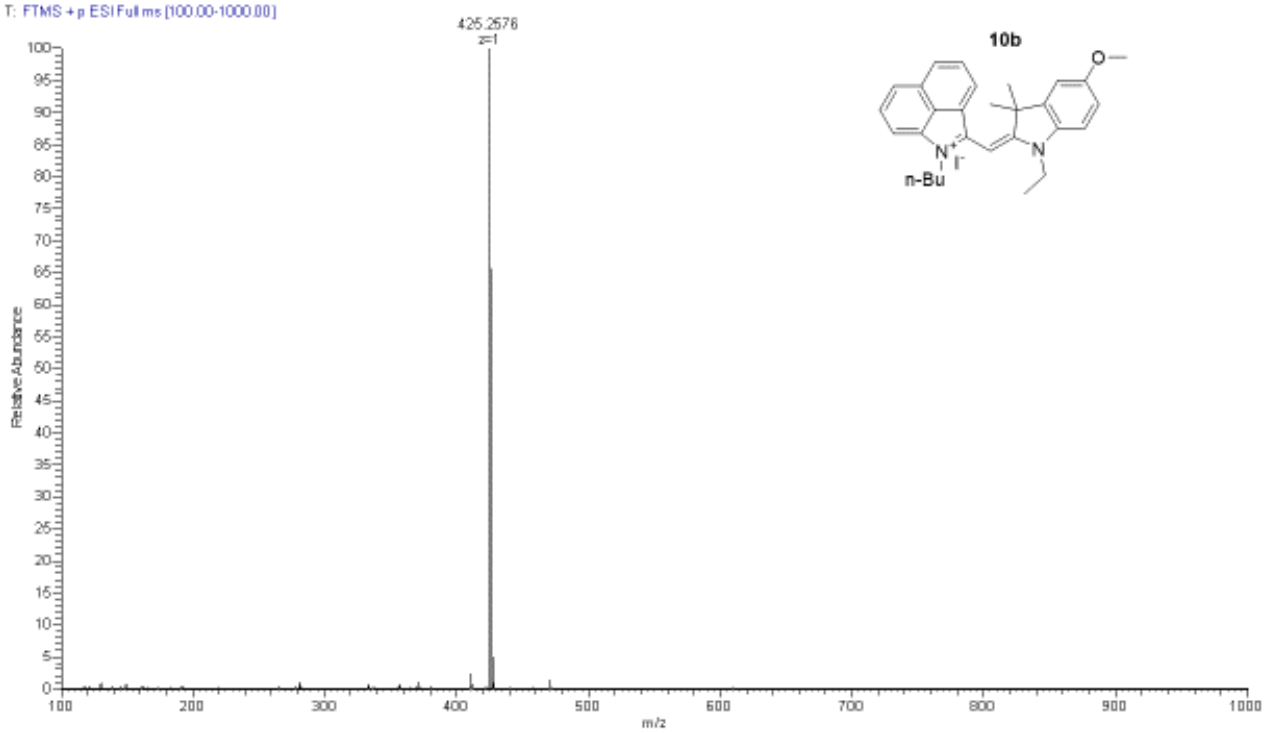
T: FTMS + p ESI Full ms [100.00-1000.00]
425.2576
z=1
10b
n-Bu
Relative Abundance
m/z

HPLC

HPLC data was obtained using a Waters 2487 dual detector wavelength absorption detector with wavelengths set at 260 and 600 nm. The column used in LC was a Waters Delta-Pak 5 µM 100Å 3.9×150 mm reversed phase C18 column, with a flow rate of 1mL/min employing a 5-100% acetonitrile/water/0.1% formic acid gradient.

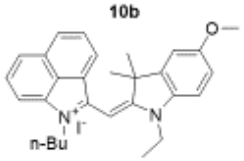

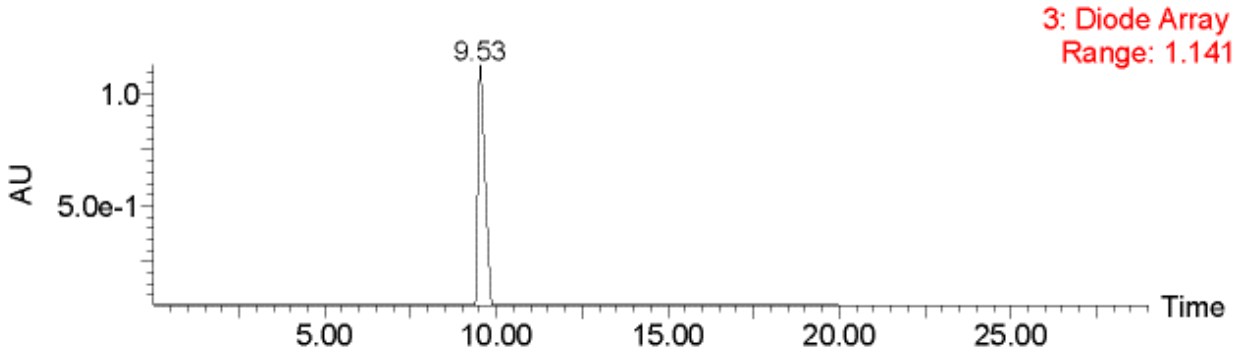

Appendix A.7. **Compound 10c**

^{1}H NMR (400 MHz, DMSO-d6) 25 °C

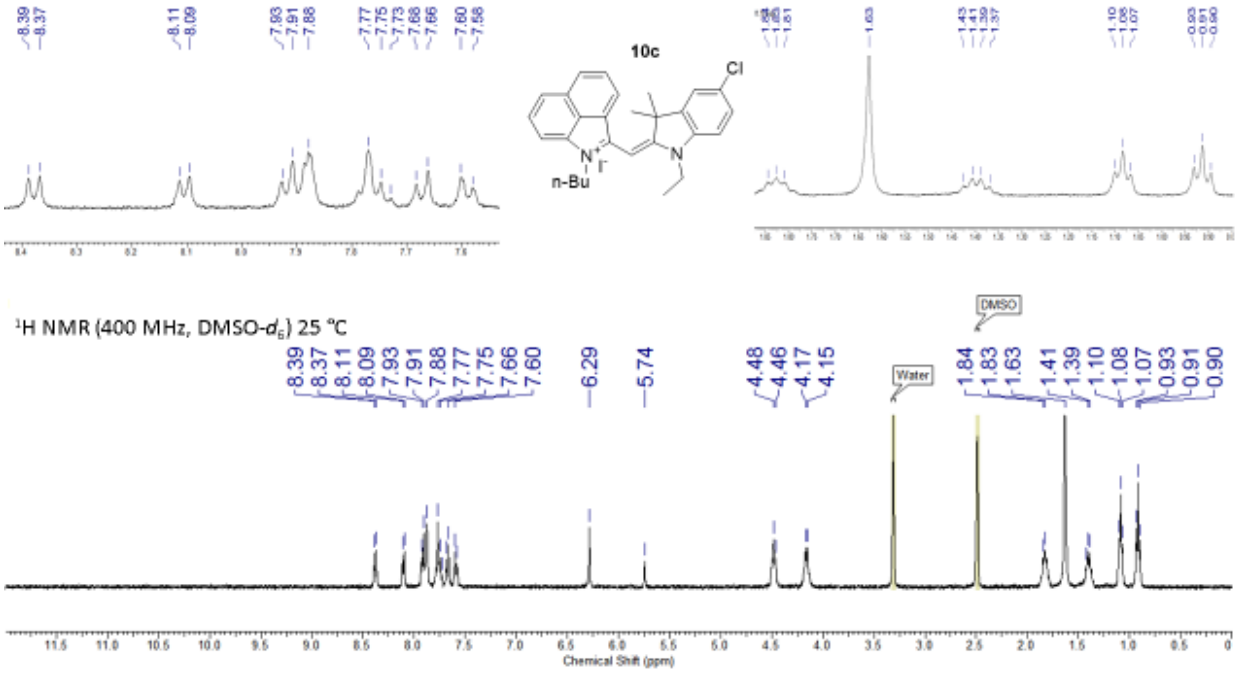

^{13}C NMR (100 MHz, DMSO-d6) 25 °C

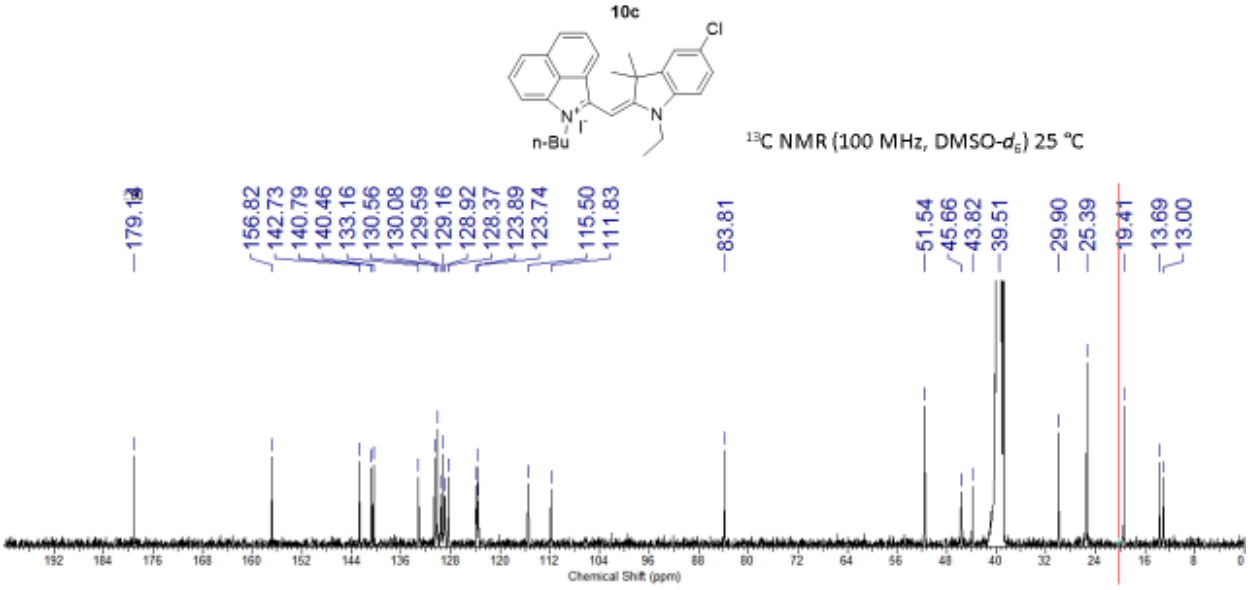

HRMS-ESI

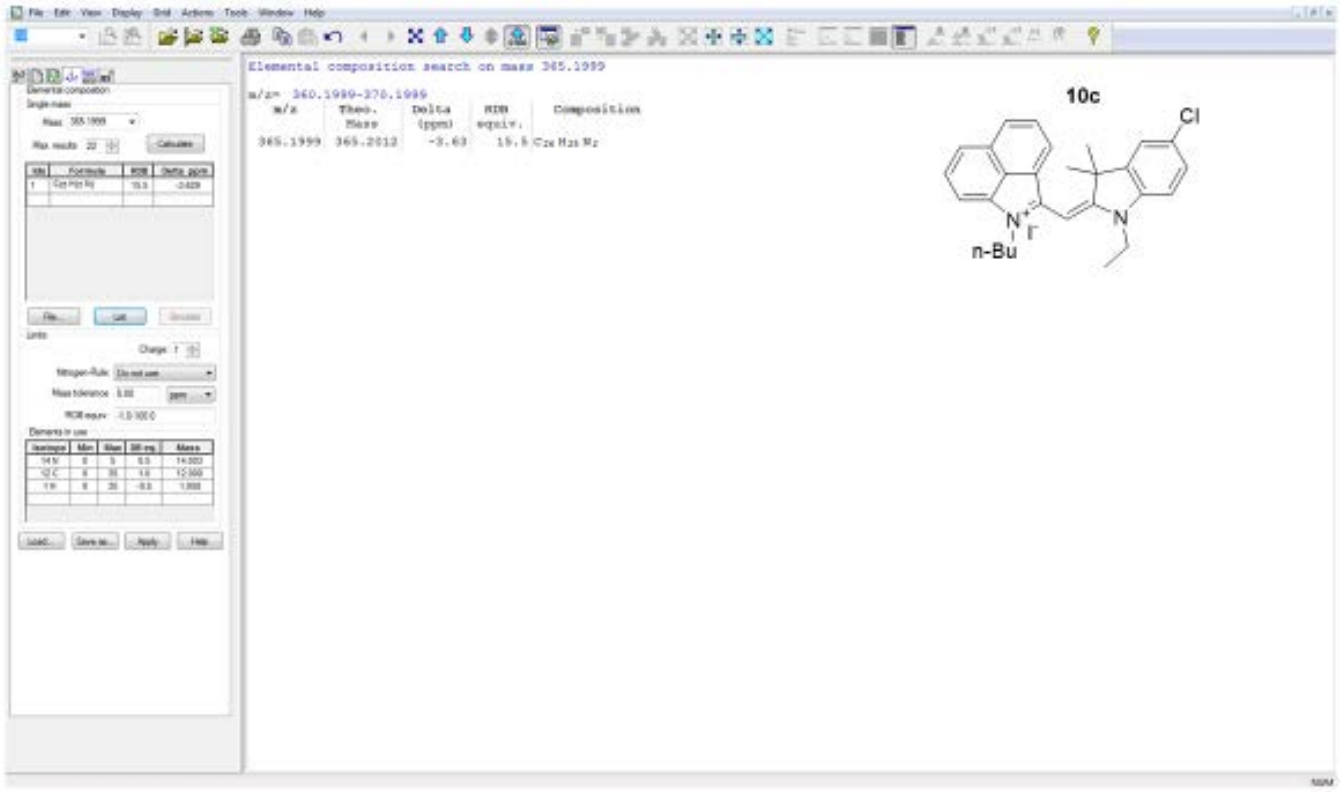
Elemental composition search on mass 365.1999
m/z= 360.1999-370.1999
m/z
Theo. Mass
Delta (ppm)
RDB equiv.
Composition
365.1999
365.2012
-3.63
15.5
C26 H29 N2
10c
Cl
N
n-Bu

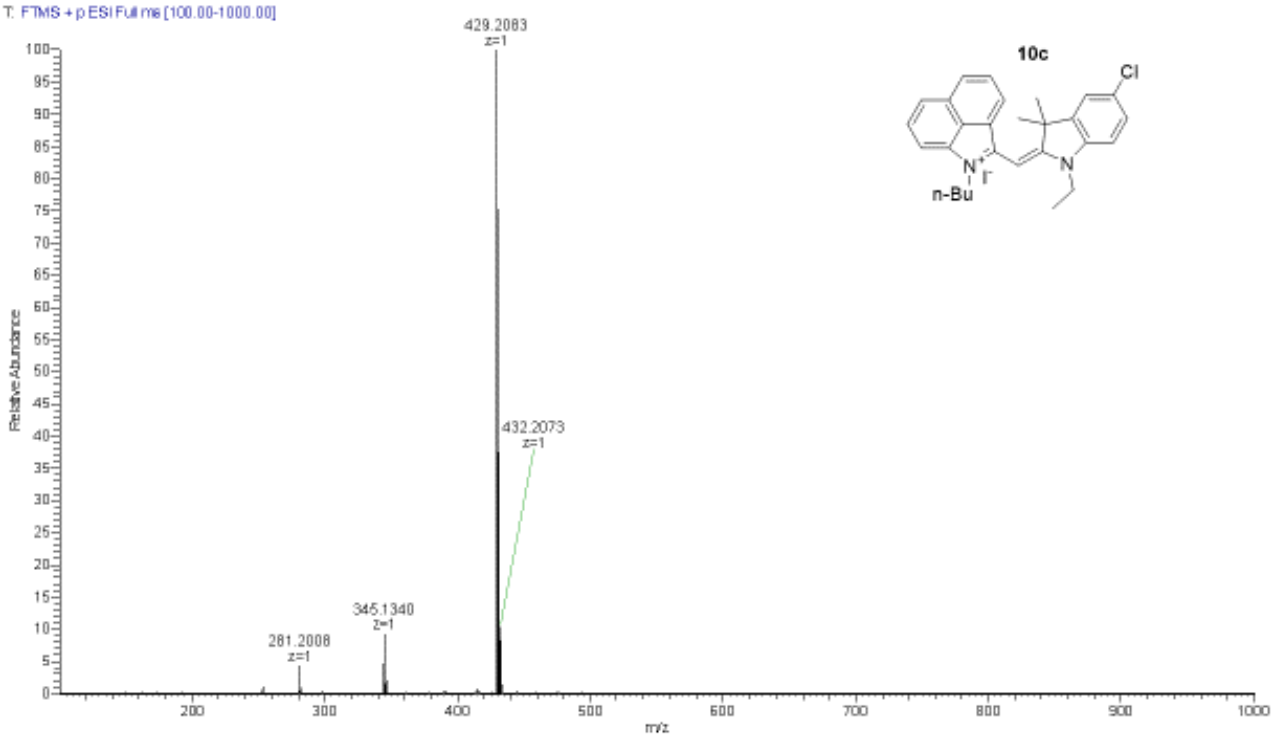
T: FTMS + p ESI Full ms [100.00-1000.00]
429.2083
z=1
432.2073
z=1
345.1340
z=1
281.2008
z=1
Relative Abundance
m/z
10c
Cl
N
n-Bu

HPLC

HPLC data was obtained using a Waters 2487 dual detector wavelength absorption detector with wavelengths set at 260 and 600 nm. The column used in LC was a Waters Delta-Pak 5 µM 100Å 3.9×150 mm reversed phase C18 column, with a flow rate of 1mL/min employing a 5-100% acetonitrile/water/0.1% formic acid gradient.

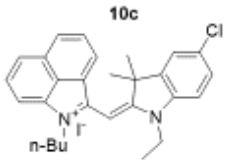

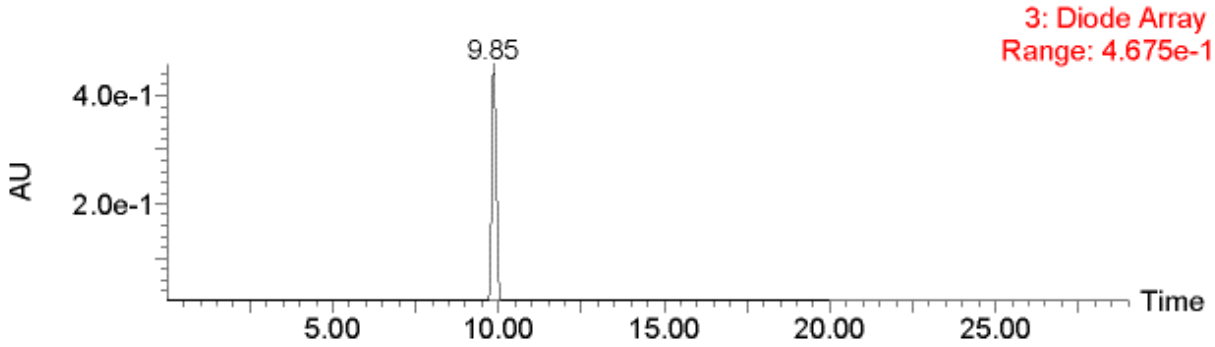

Appendix B Monomethine Chapter 2

Appendix B.1. **Compound 6a**

^{1}H NMR (400 MHz, DMSO-d6) 25 °C

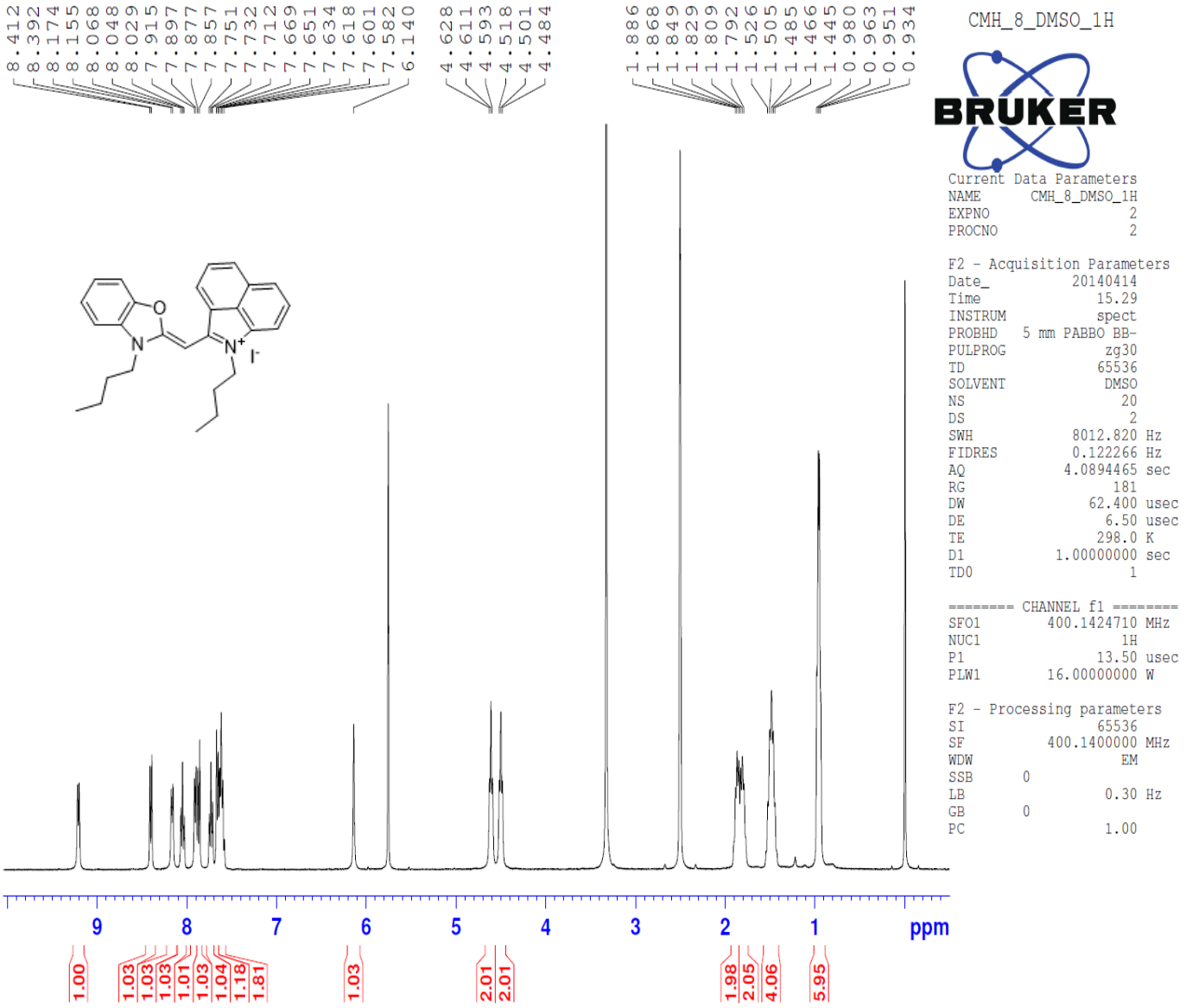

^{13}C NMR (100 MHz, DMSO-d6) 25 °C

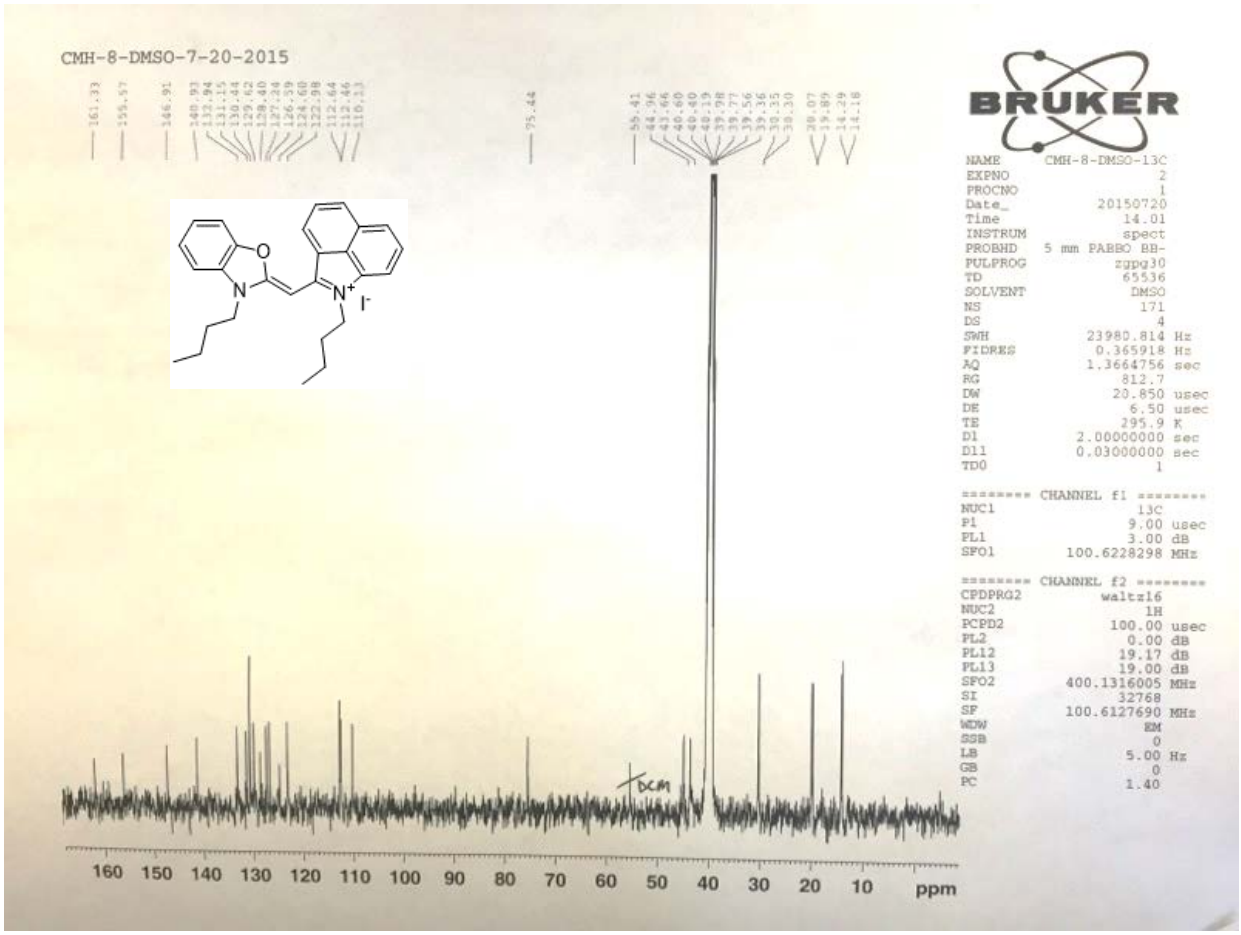

UV/Vis

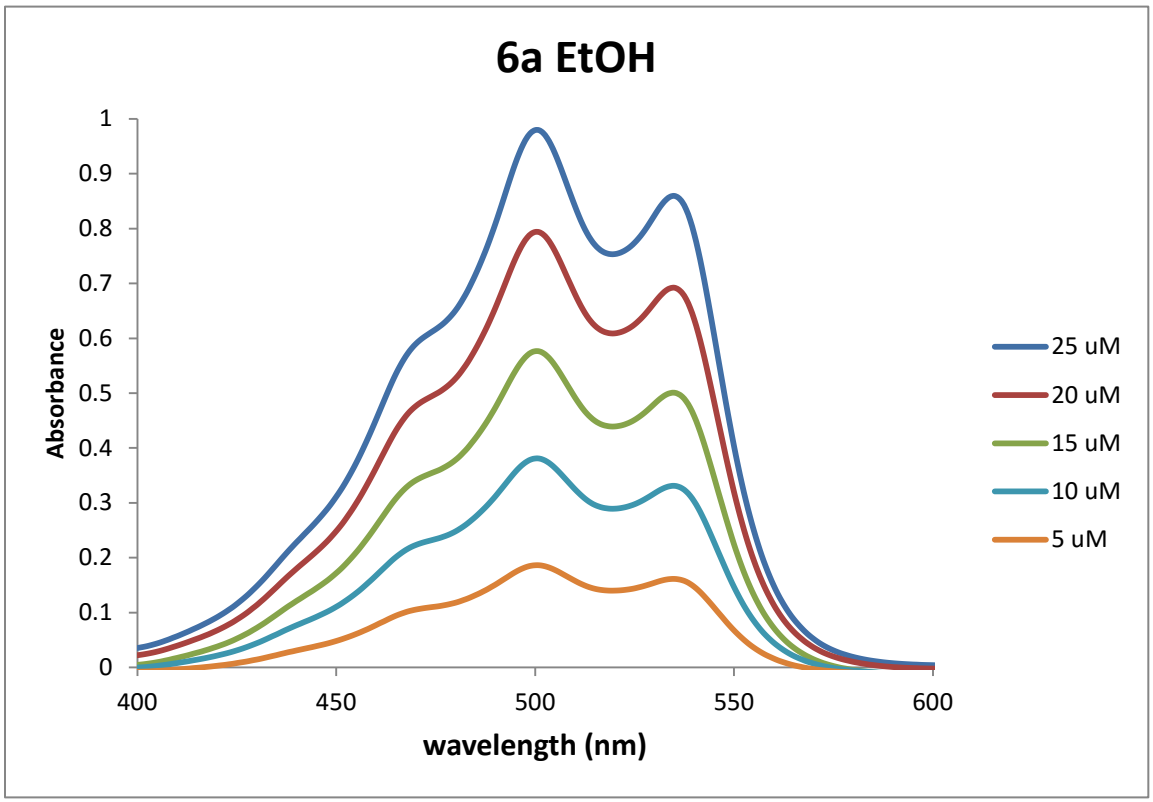
6a EtOH
Absorbance
wavelength (nm)
25 uM
20 uM
15 uM
10 uM
5 uM

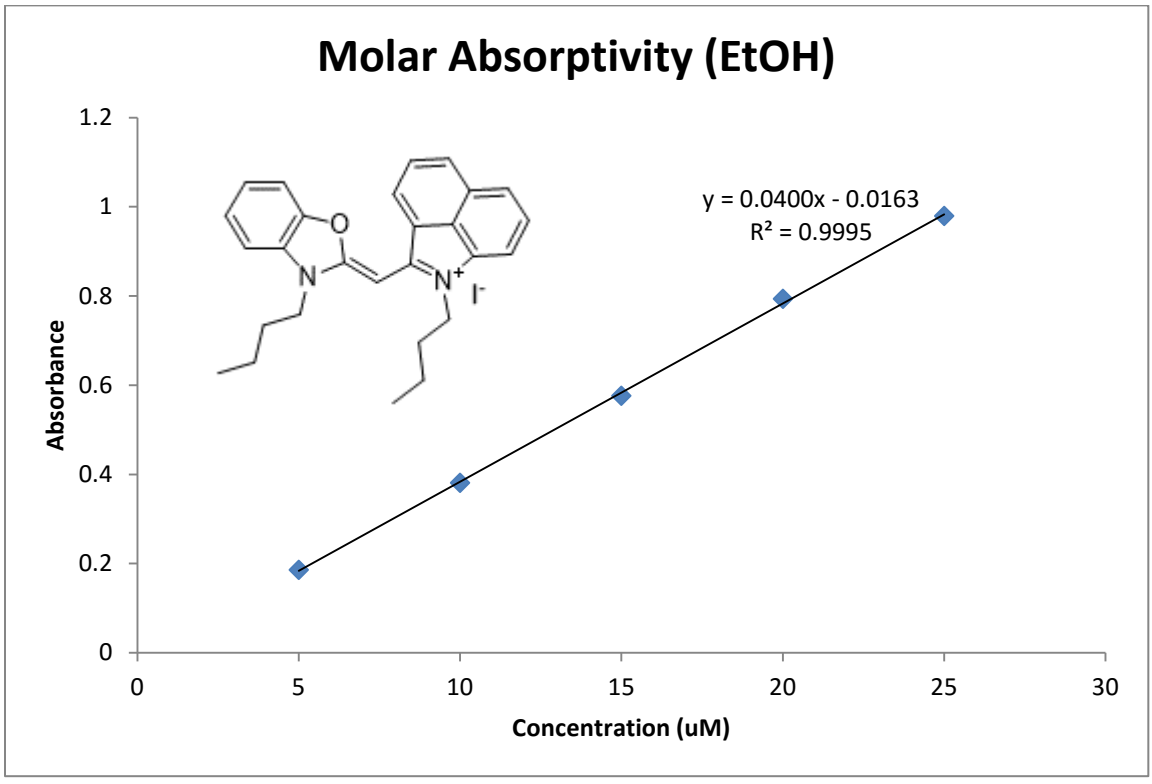
Molar Absorptivity (EtOH)
y = 0.0400x - 0.0163
R² = 0.9995
Absorbance
Concentration (uM)

DNA binding

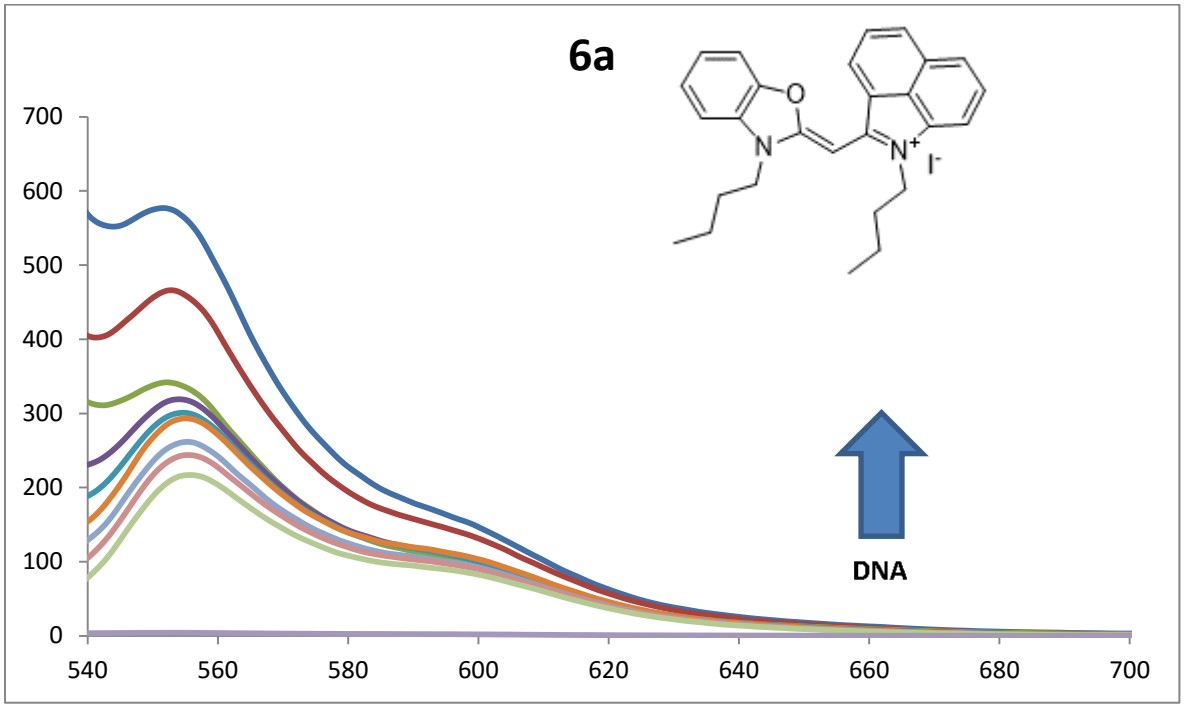
6a
700
600
500
400
300
200
100
0
540
560
580
600
620
640
660
680
700
DNA

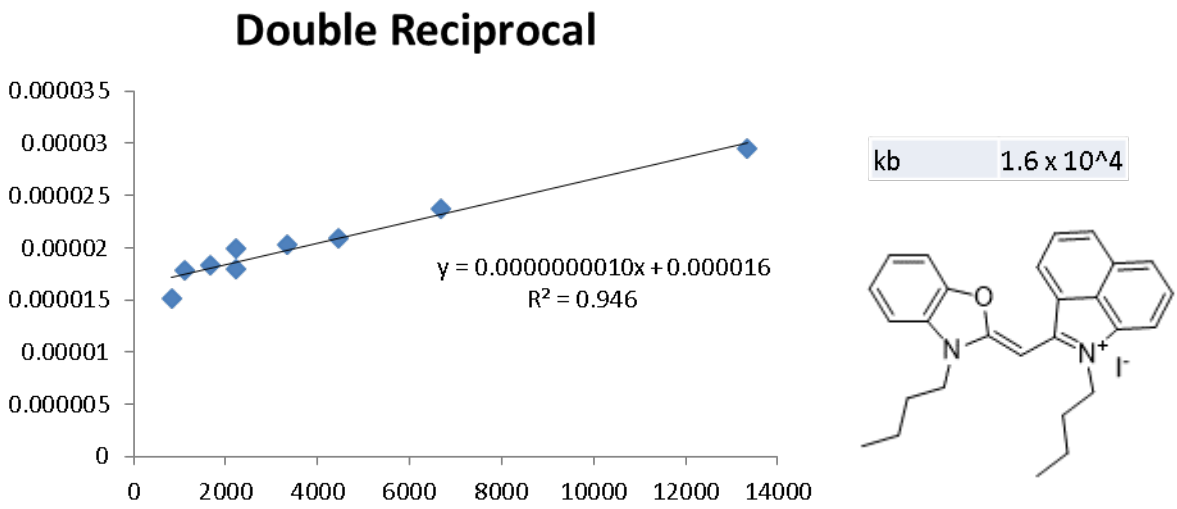
Double Reciprocal
0.000035
0.00003
0.000025
0.00002
0.000015
0.00001
0.000005
0
0
2000
4000
6000
8000
10000
12000
14000
y = 0.0000000010x + 0.000016
R² = 0.946
kb
1.6 x 10^4

Electropotential map [kJ/mol]

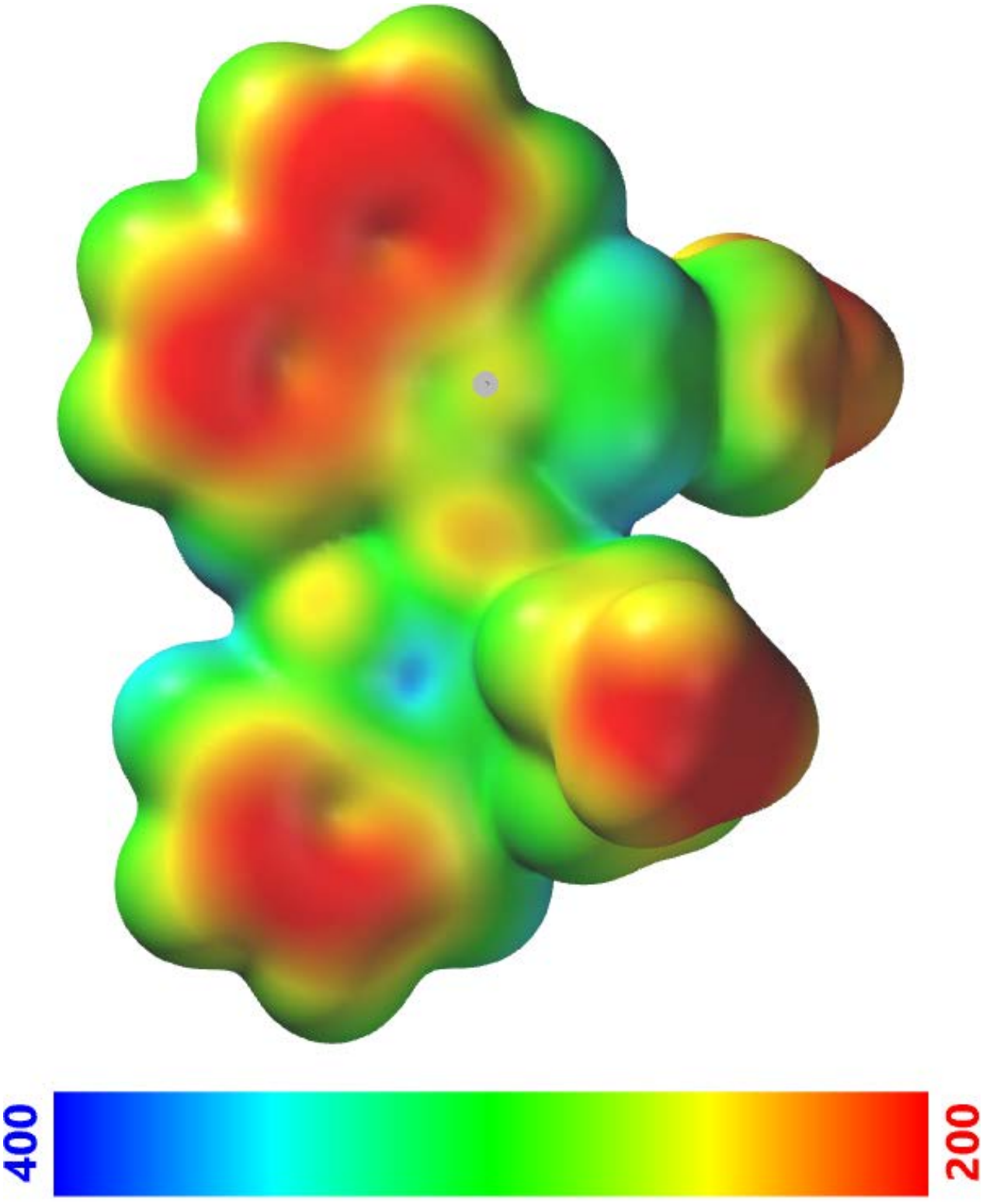

HOMO/LUMO

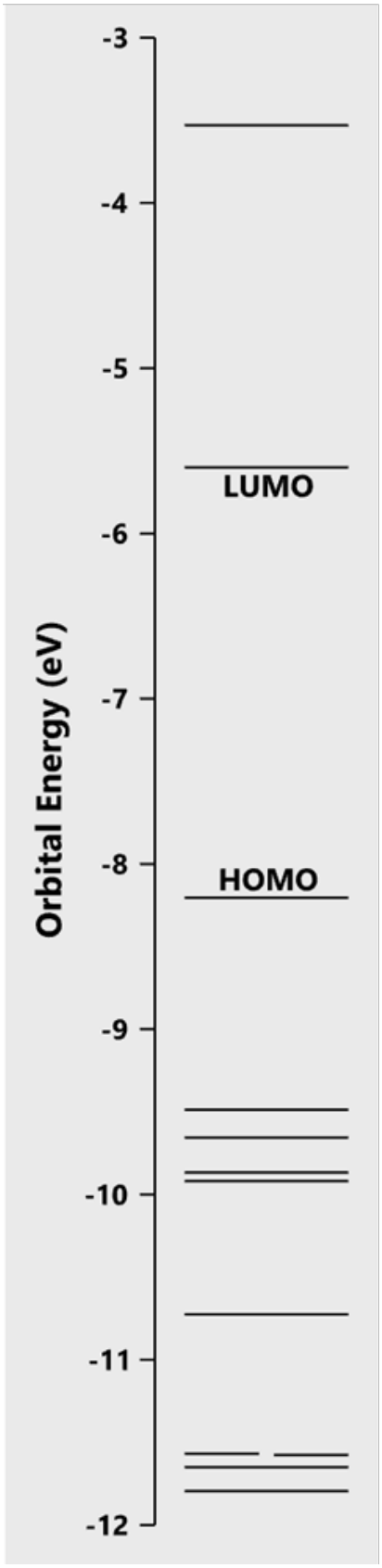

Gap = 2.64 eV

LUMO -5.56 eV

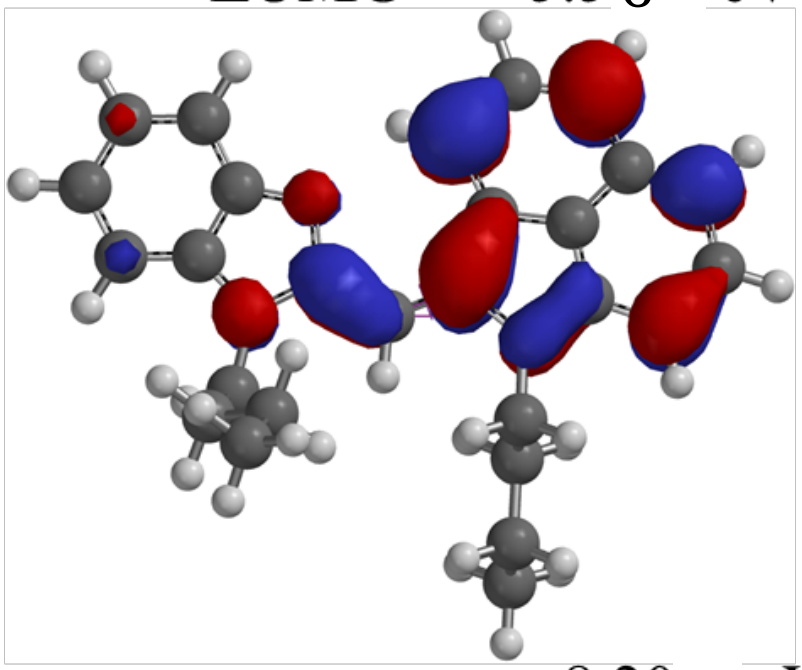

HOMO -8.20 eV

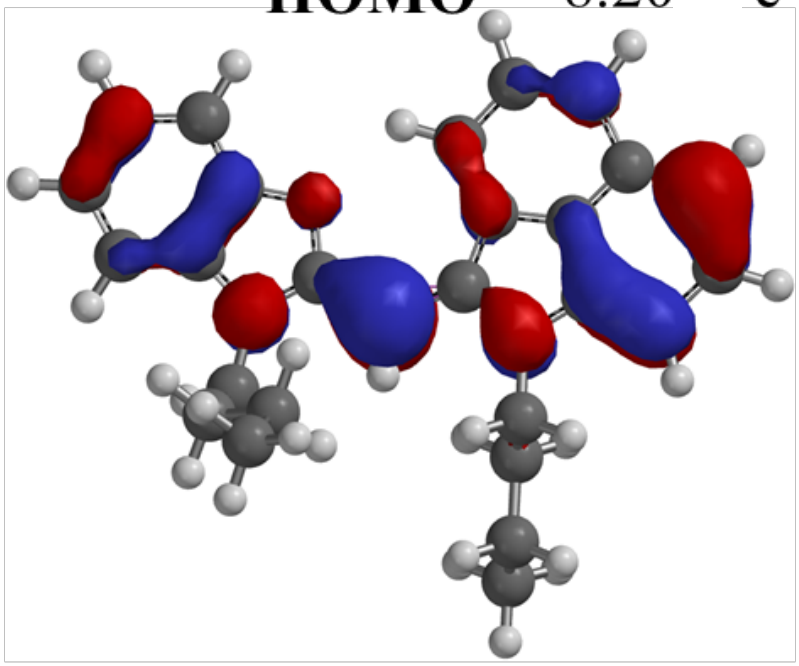

Appendix B.2. **Compound 6b**

^{1}H NMR (400 MHz, DMSO-d6) 25 °C

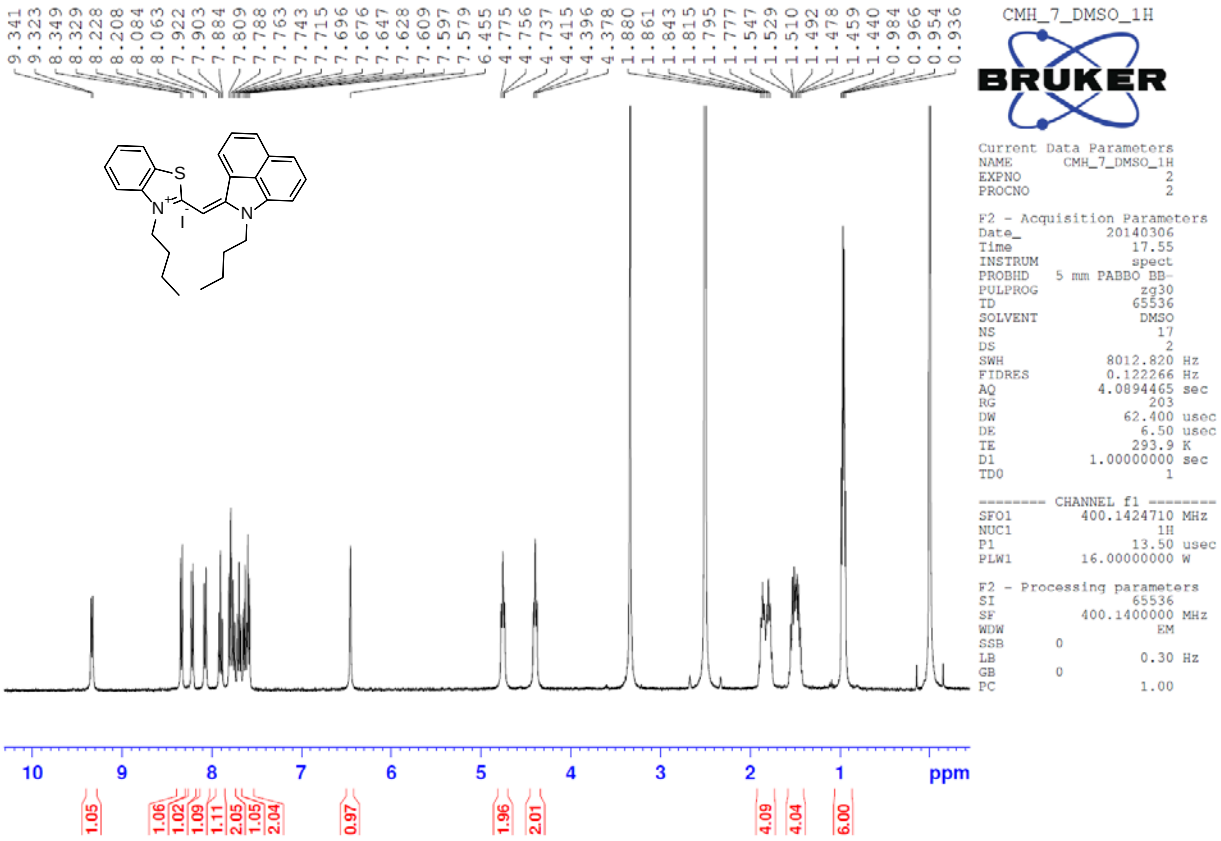

CMH_7_DMSO_1H

BRUKER

Current Data Parameters
NAME CMH_7_DMSO_1H
EXPNO 2
PROCNO 2

F2 - Acquisition Parameters
Date_ 20140306
Time 17.55
INSTRUM spect
PROBHD 5 mm PABBO BB-
PULPROG zg30
TD 65536
SOLVENT DMSO
NS 17
DS 2
SWH 8012.820 Hz
FIDRES 0.122266 Hz
AQ 4.0894465 sec
RG 203
DW 62.400 usec
DE 6.50 usec
TE 293.9 K
D1 1.00000000 sec
TD0 1

======== CHANNEL f1 ========
SFO1 400.1424710 MHz
NUC1 1H
P1 13.50 usec
PLW1 16.00000000 W

F2 - Processing parameters
SI 65536
SF 400.1400000 MHz
WDW EM
SSB 0
LB 0.30 Hz
GB 0
PC 1.00

^{13}C NMR (100 MHz, DMSO-d6) 25 °C

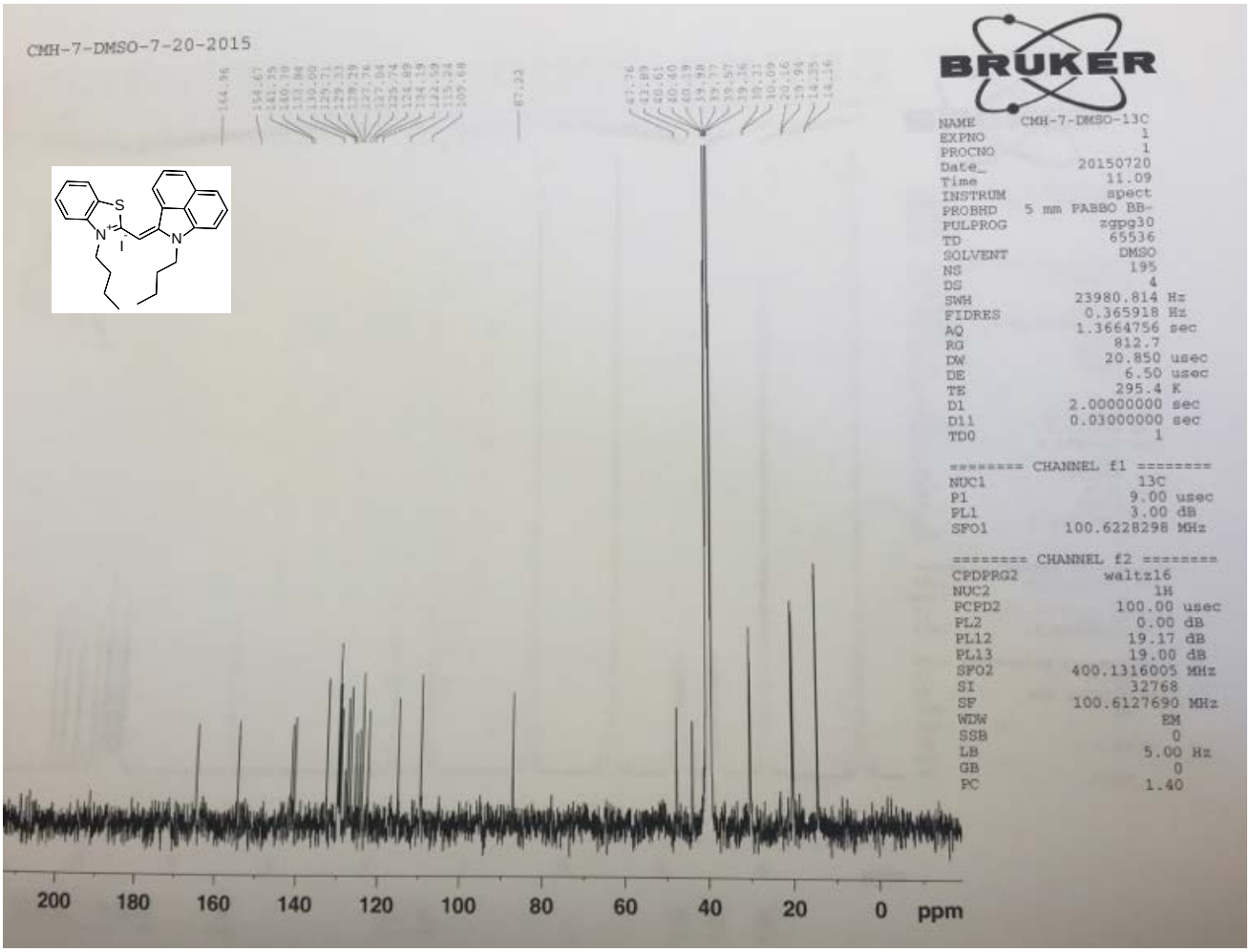

UV/Vis

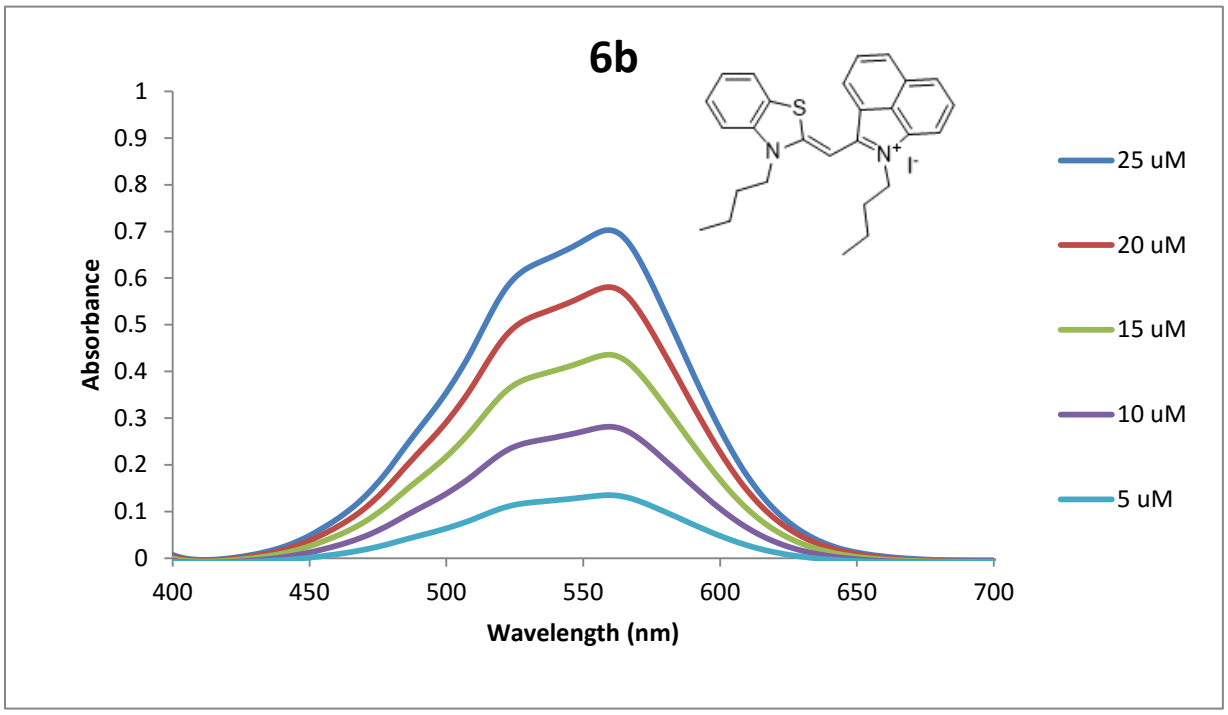
6b
Absorbance
Wavelength (nm)
25 uM
20 uM
15 uM
10 uM
5 uM

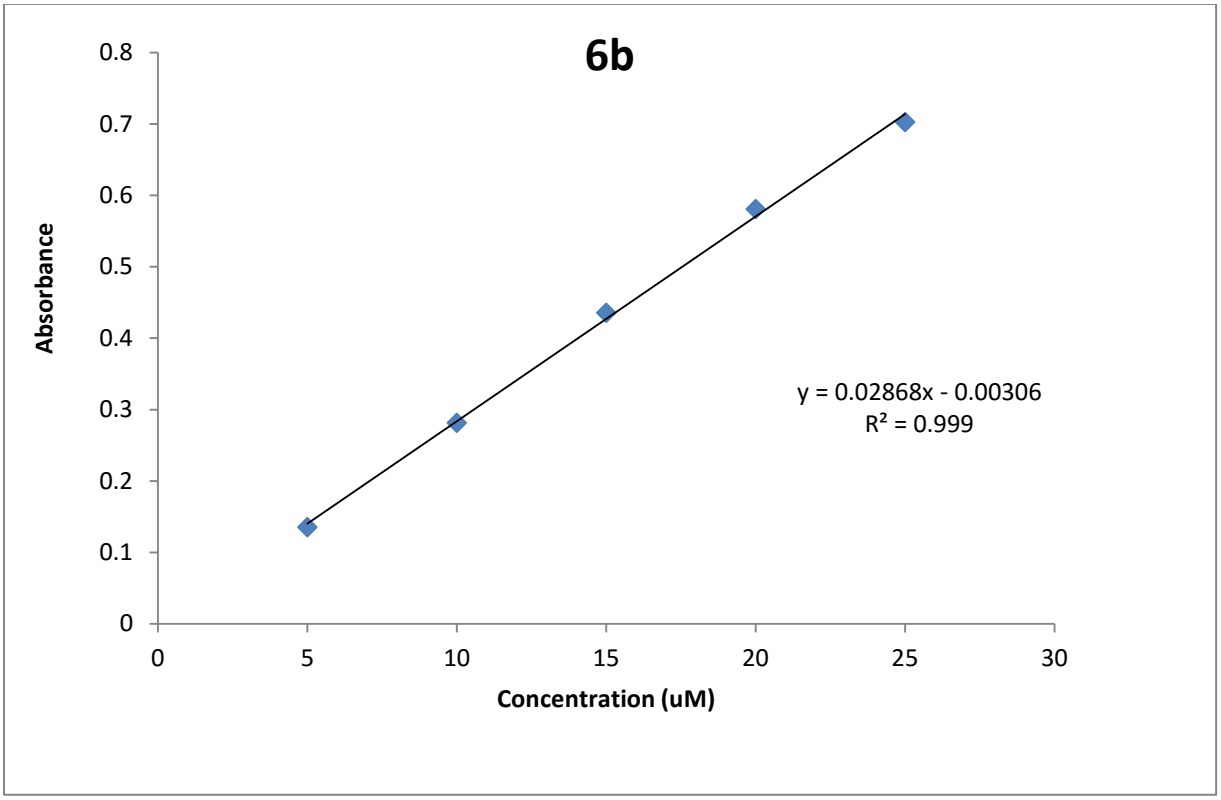
6b
Absorbance
Concentration (uM)
y = 0.02868x - 0.00306
R² = 0.999

DNA Binding

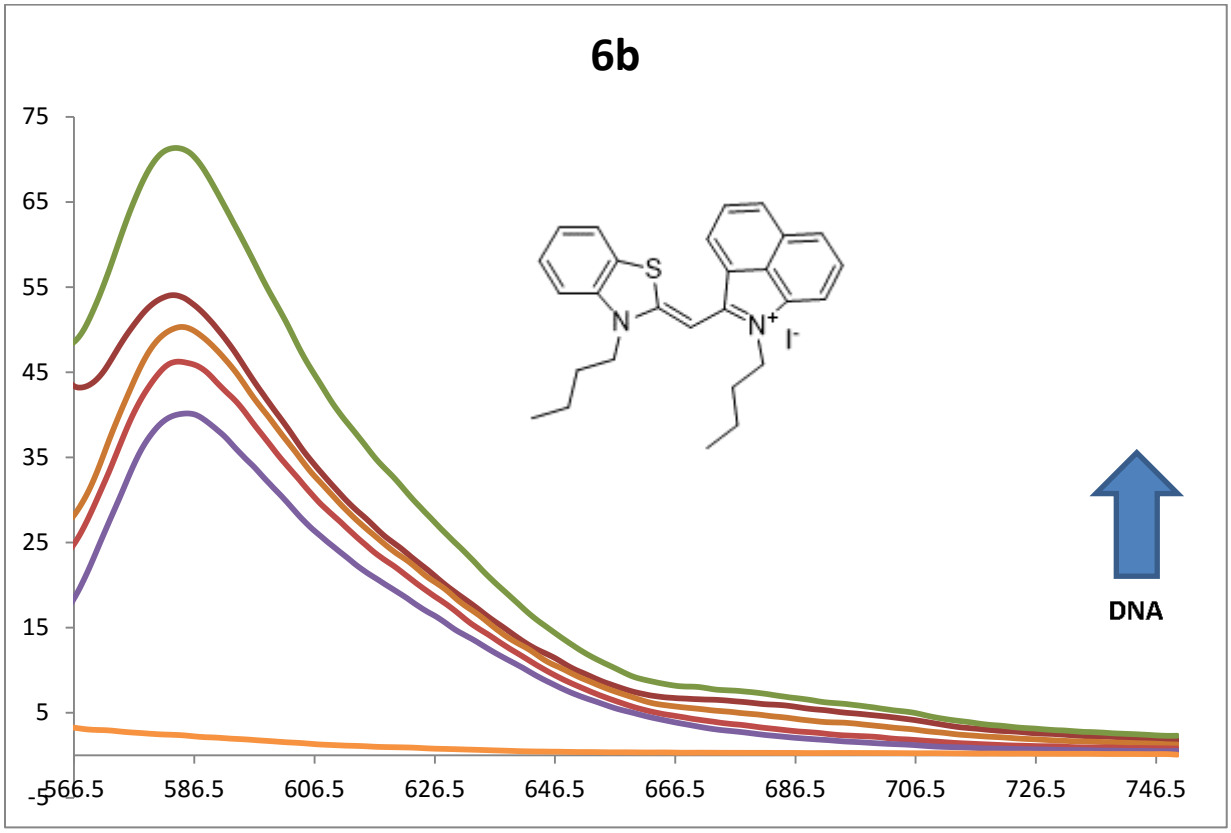

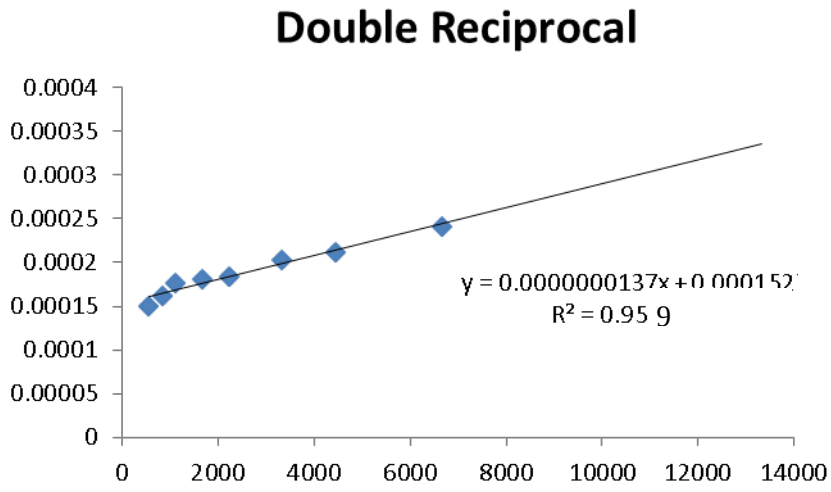

kb	1.11x10^4

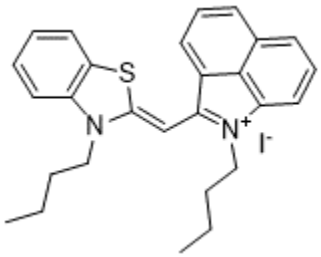

Electropotential Map [kJ/mol]

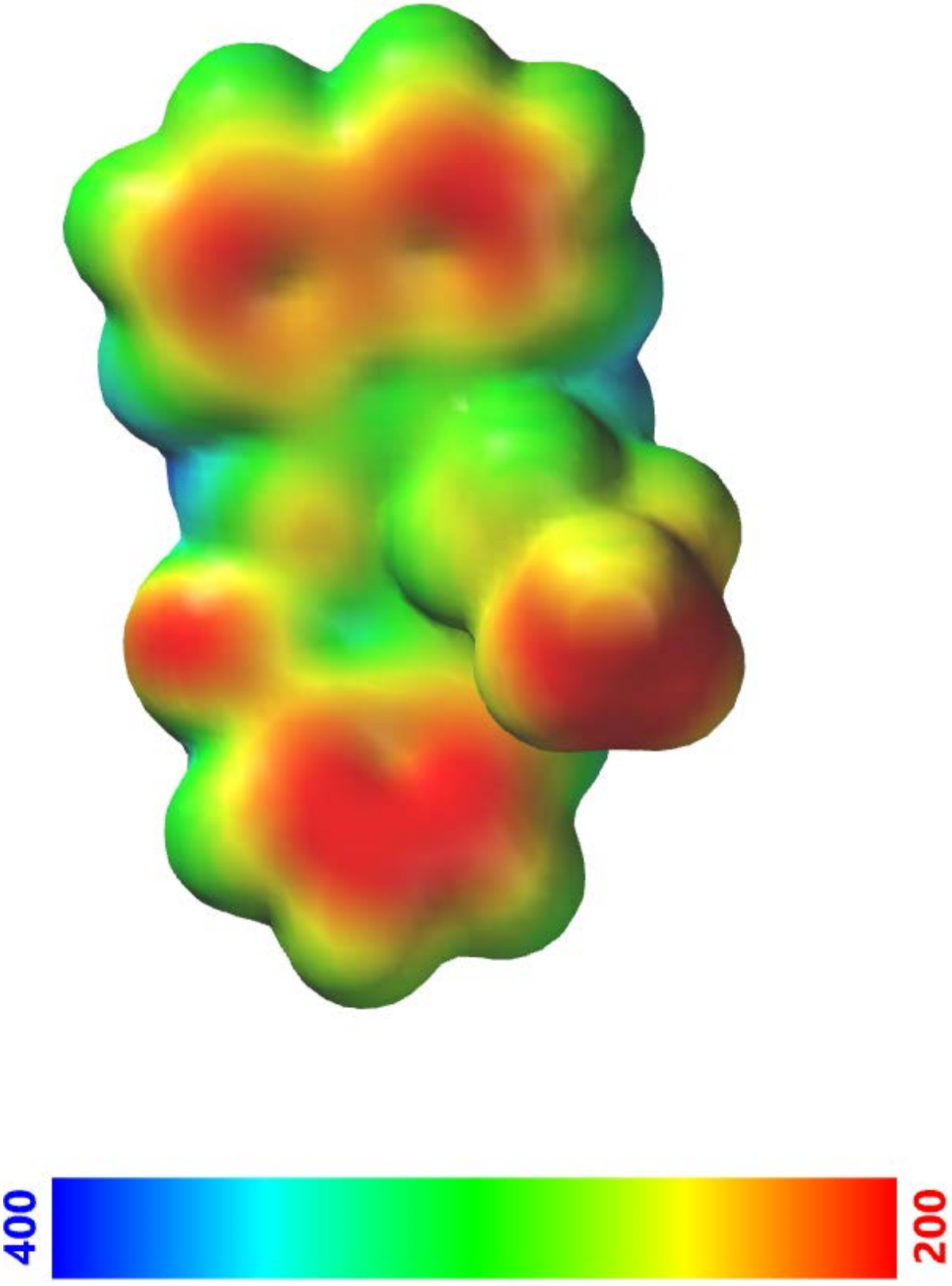

HOMO/LUMO

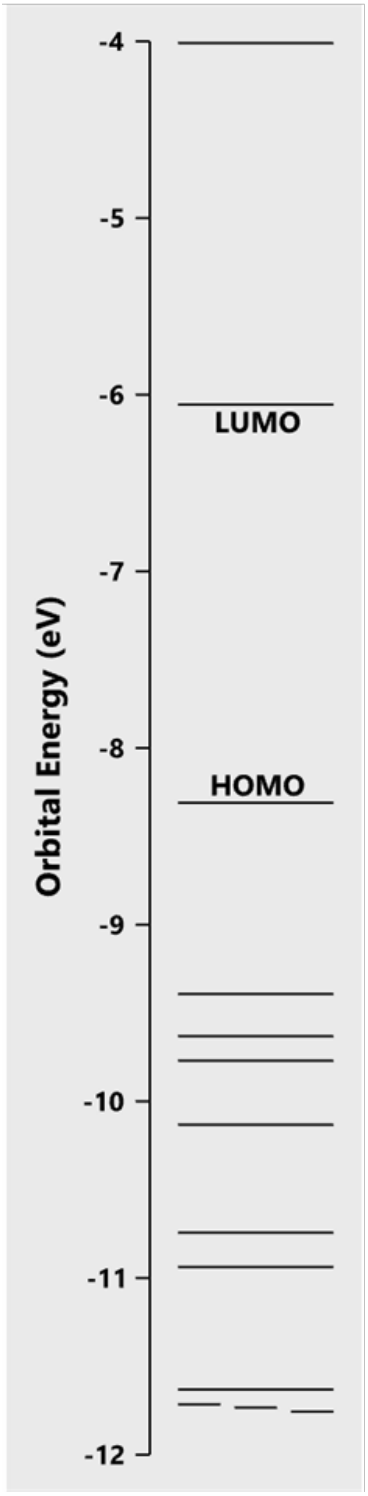

Gap = 2.25 eV

LUMO -6.05 eV

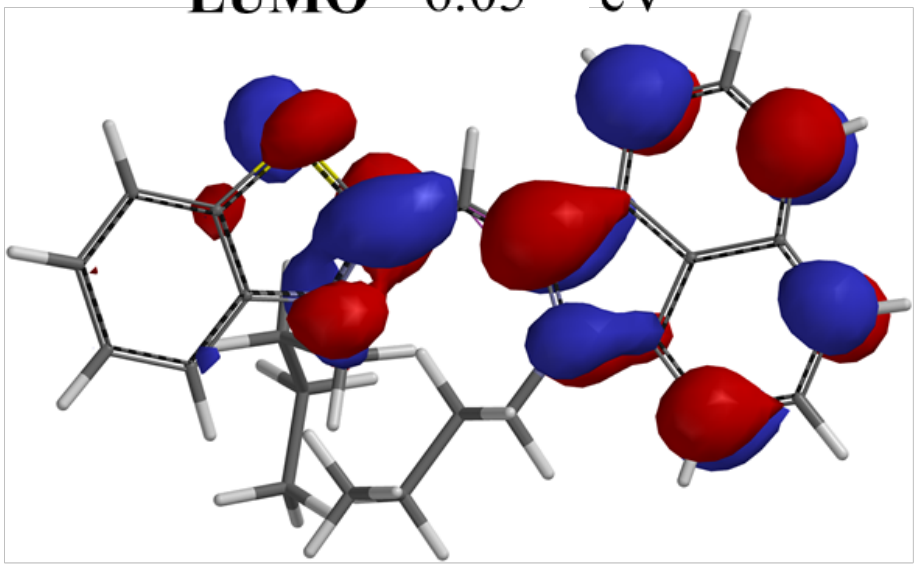

HOMO -8.30 eV

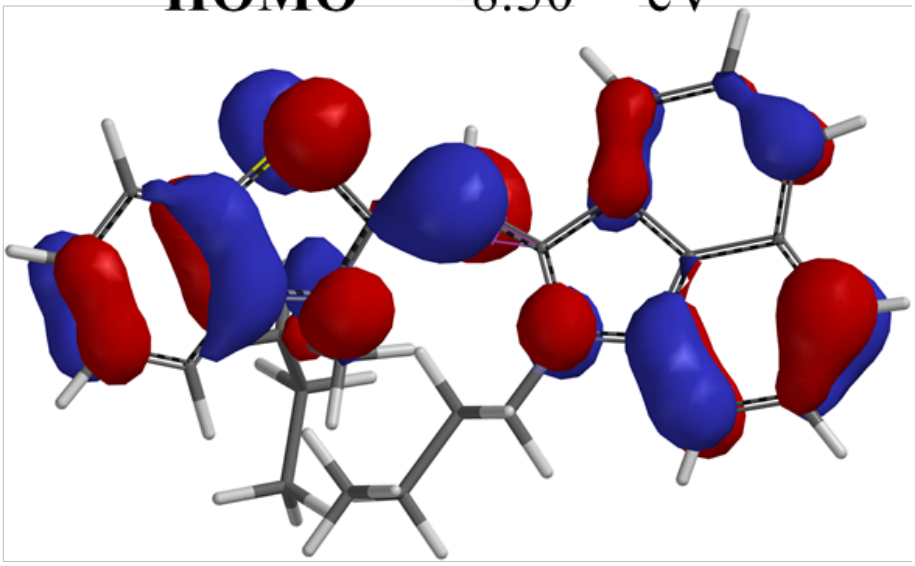

Appendix B.3. **Compound 6c**

^{1}H NMR (400 MHz, DMSO-d6) 25 °C

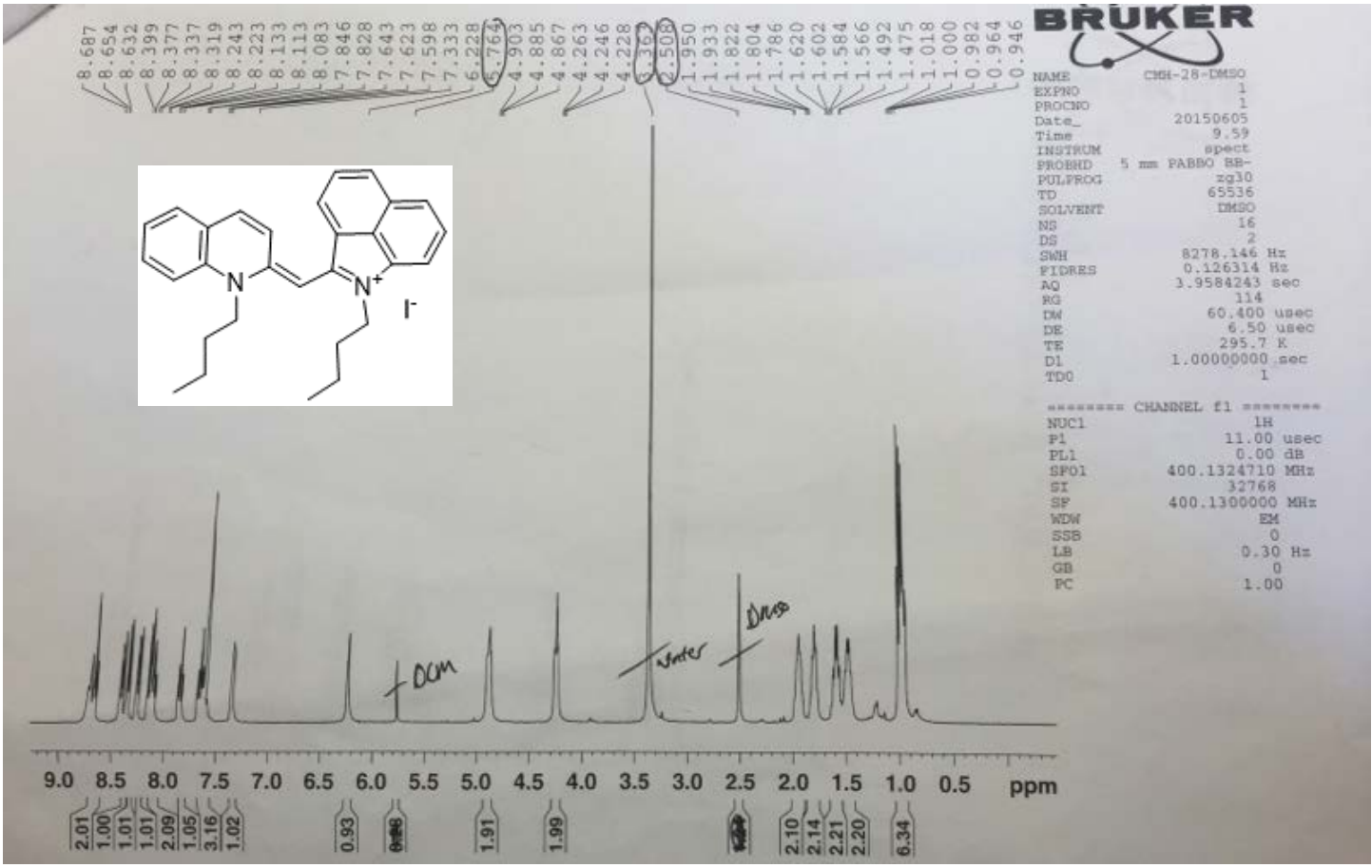

^{13}C NMR (100 MHz, DMSO-d6) 25 °C

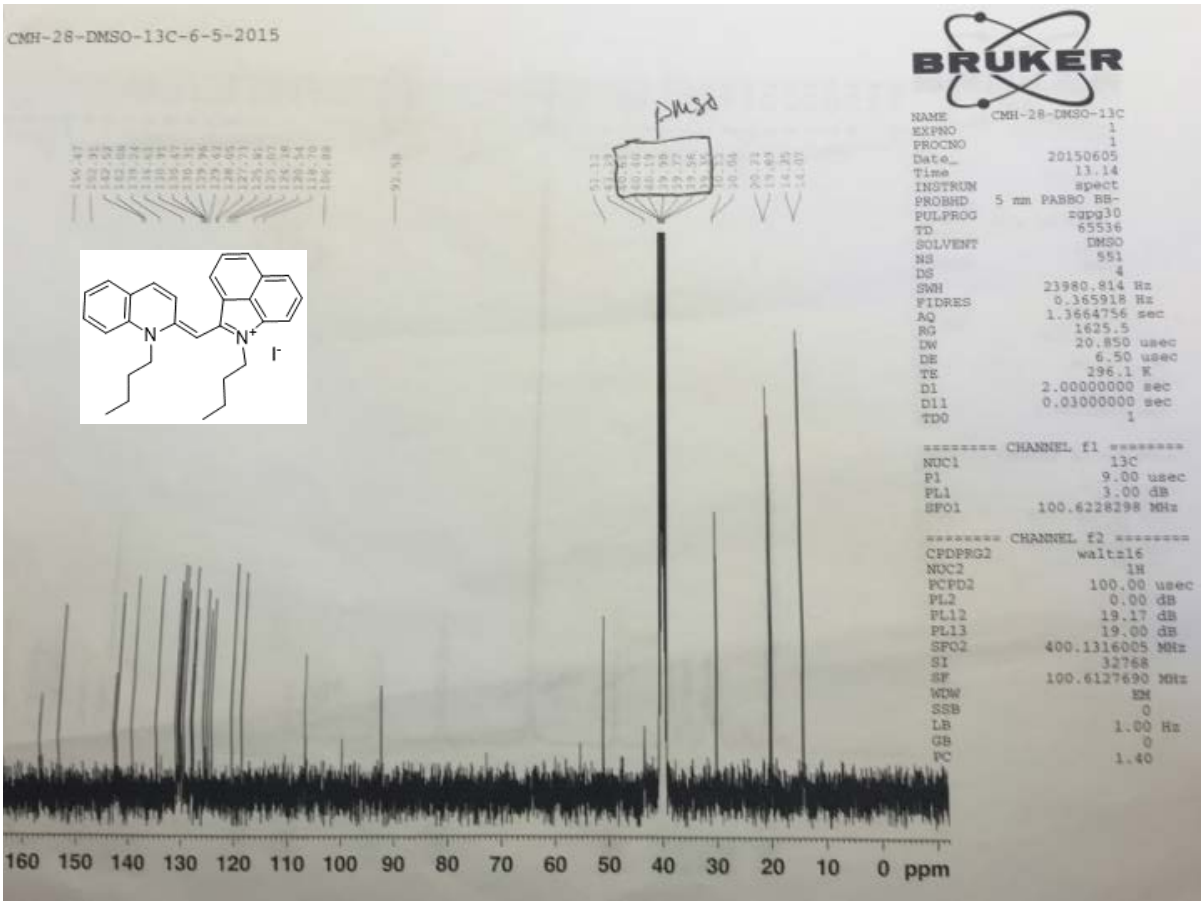

UV/Vis

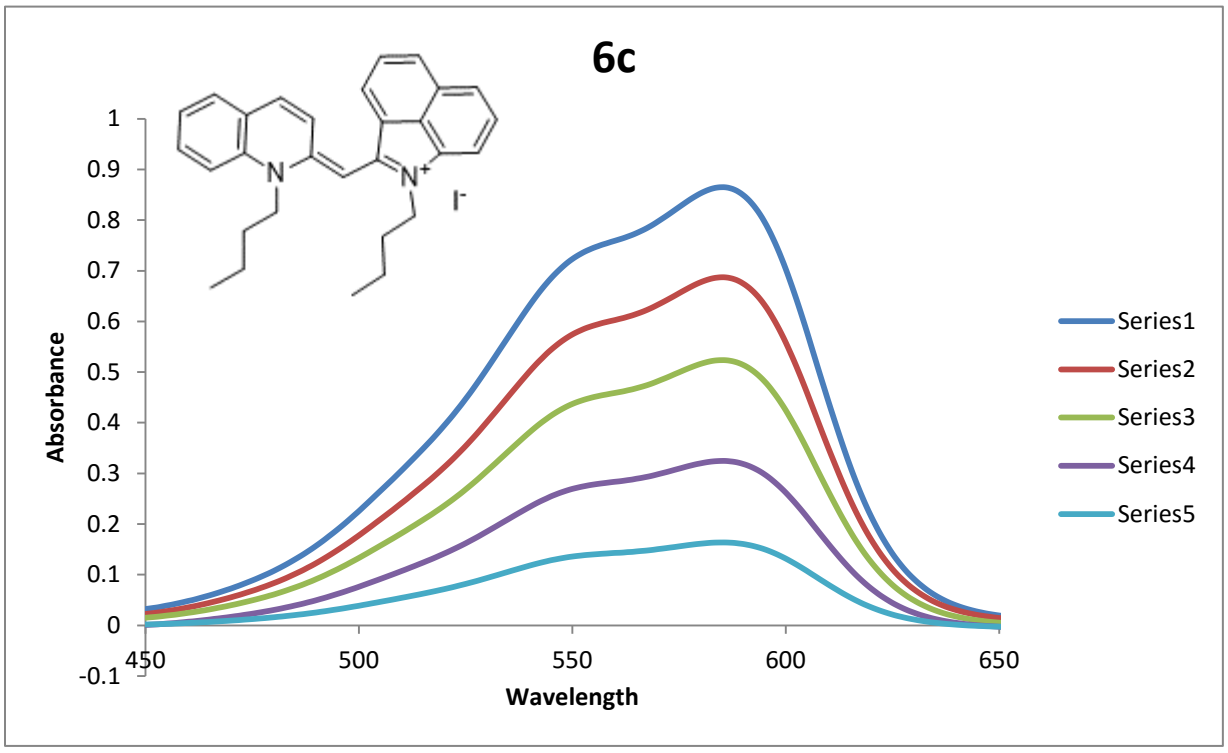
6c
N
N+
I-
Absorbance
Wavelength
1
0.9
0.8
0.7
0.6
0.5
0.4
0.3
0.2
0.1
0
-0.1
450
500
550
600
650
Series1
Series2
Series3
Series4
Series5

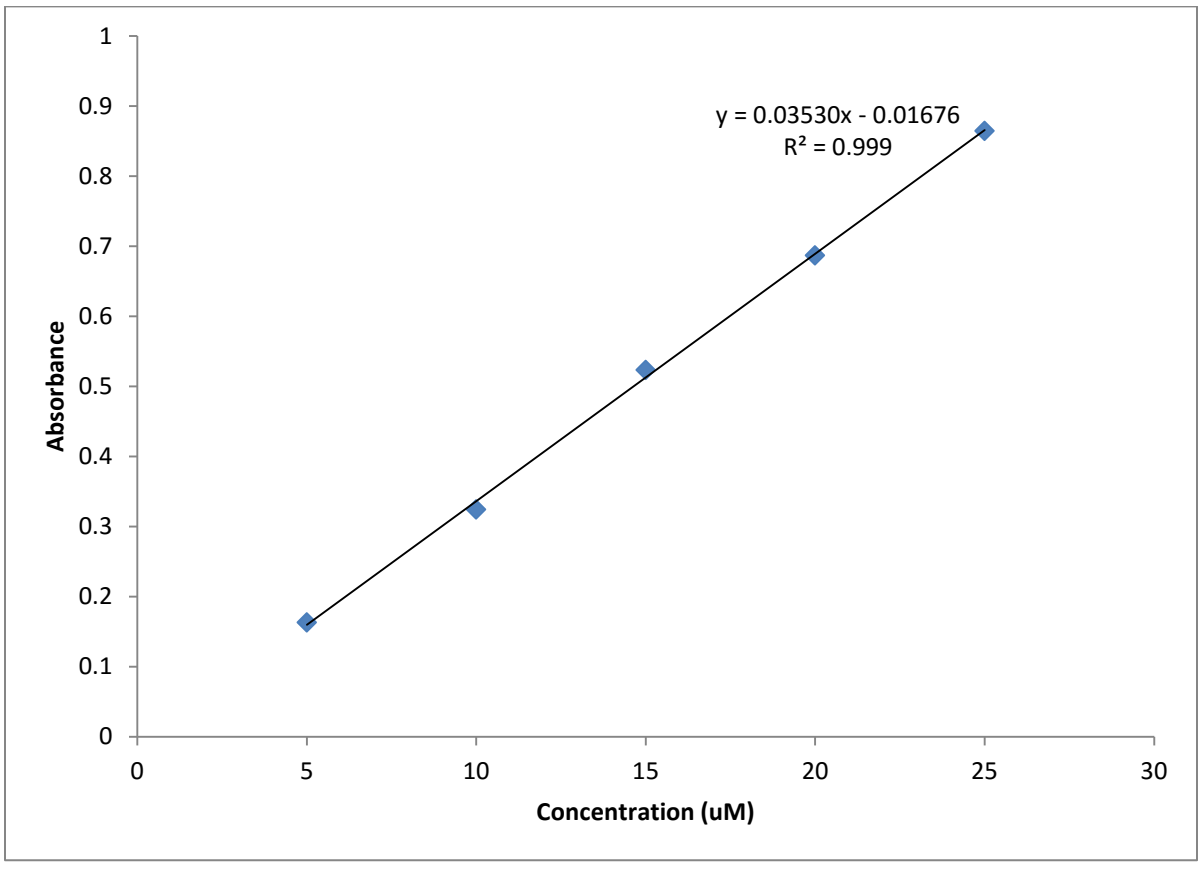
y = 0.03530x - 0.01676
R² = 0.999
Absorbance
Concentration (uM)
1
0.9
0.8
0.7
0.6
0.5
0.4
0.3
0.2
0.1
0
0
5
10
15
20
25
30

DNA Binding

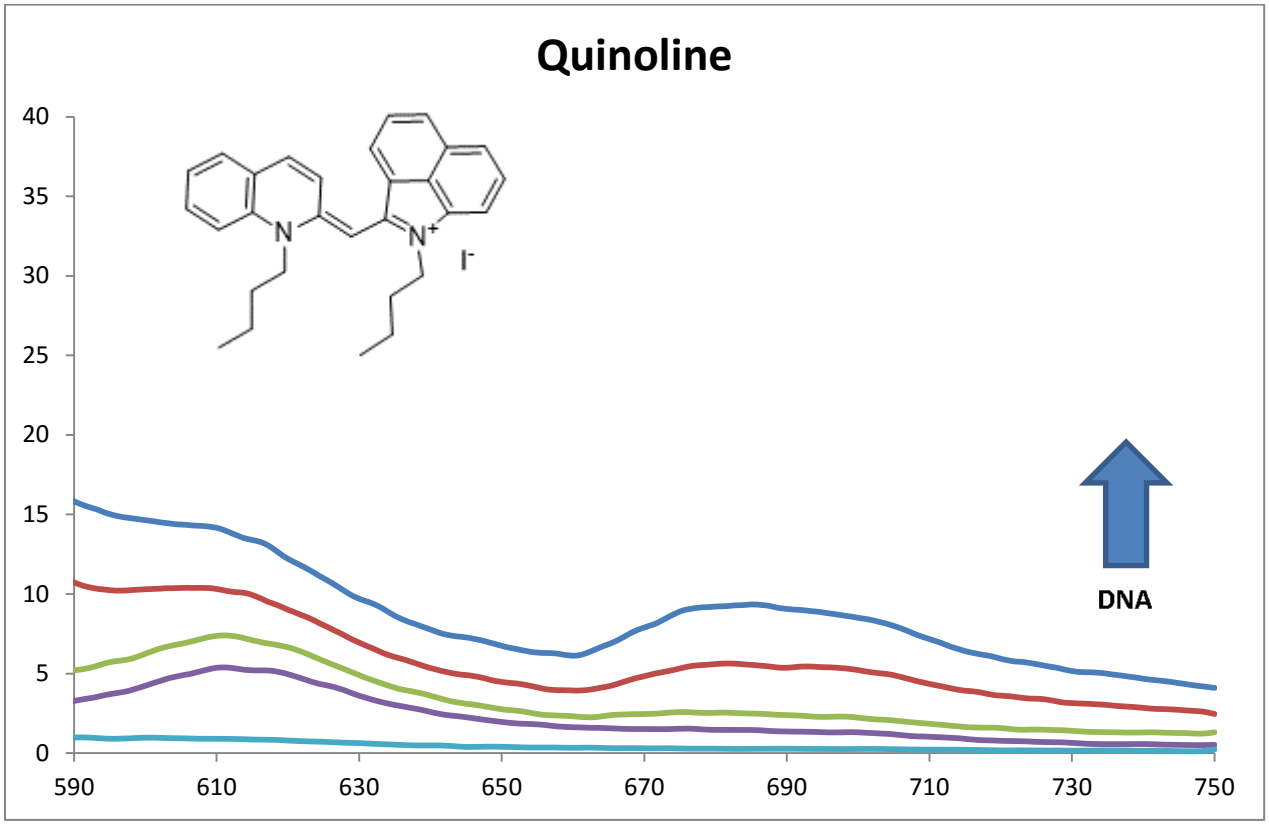
Quinoline
40
35
30
25
20
15
10
5
0
590
610
630
650
670
690
710
730
750
N
N+
I-
DNA

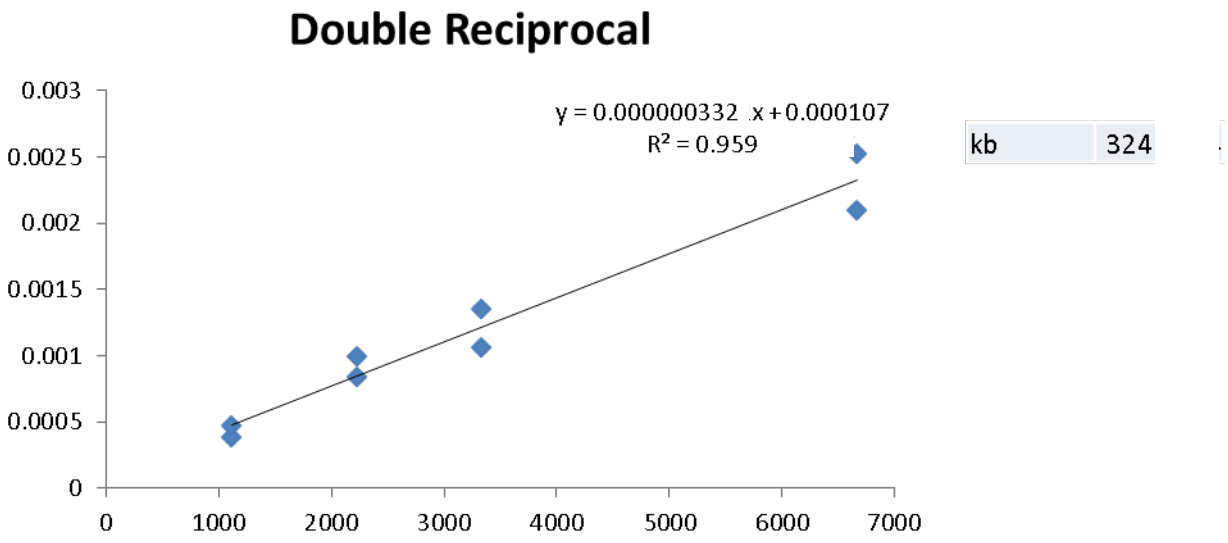
Double Reciprocal
y = 0.000000332 x + 0.000107
R² = 0.959
0.003
0.0025
0.002
0.0015
0.001
0.0005
0
0
1000
2000
3000
4000
5000
6000
7000
kb
324

Electropotential Map [kJ/mol]

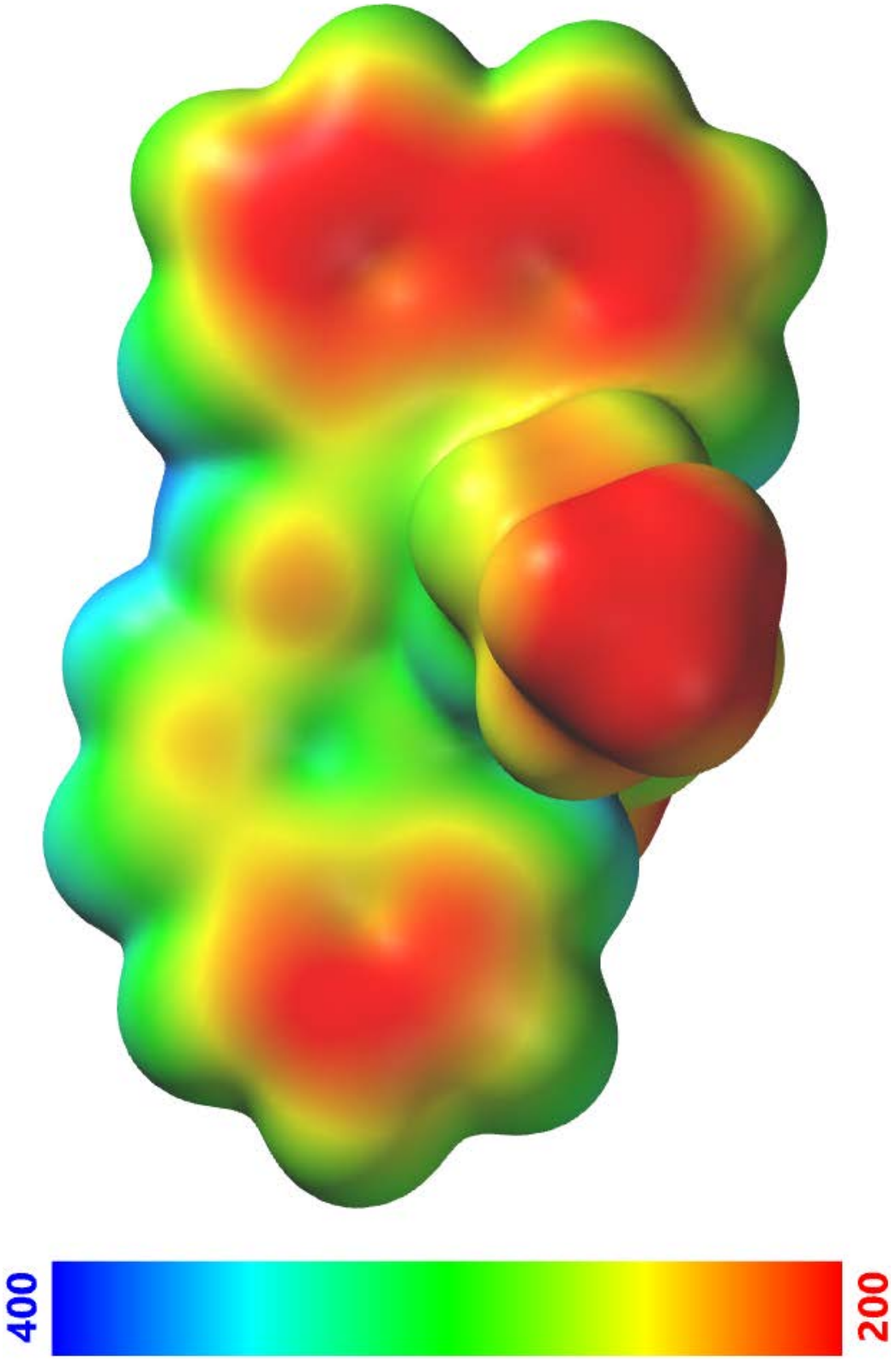

HOMO/LUMO

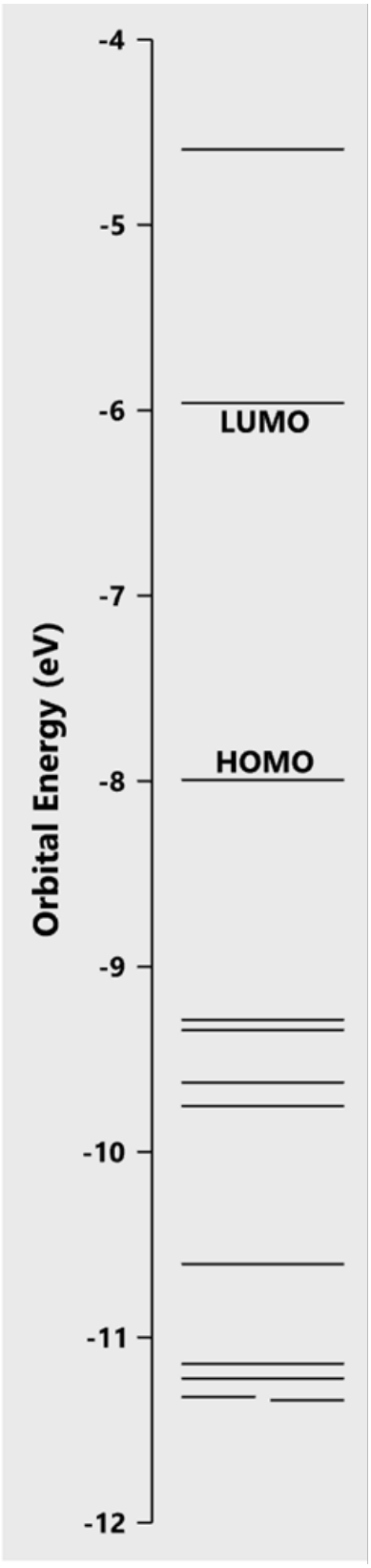

Gap = 2.03 eV

LUMO -5.96 eV

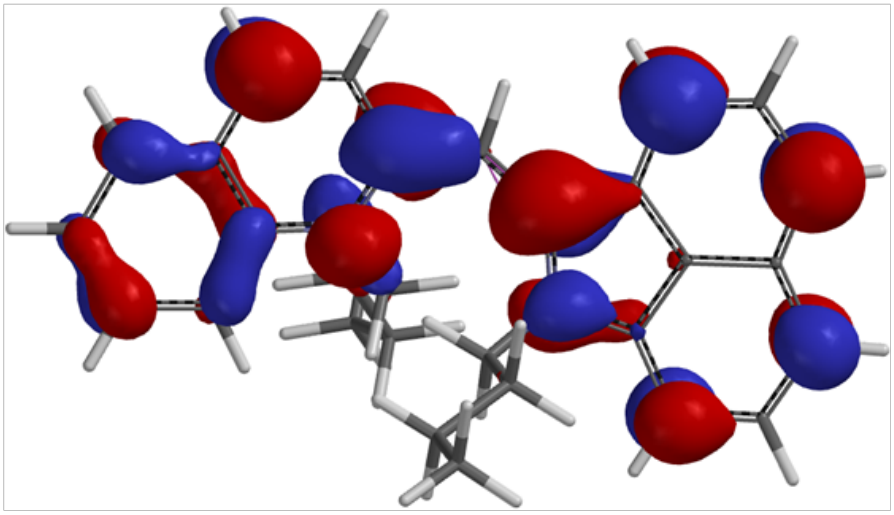

HOMO -7.99 eV

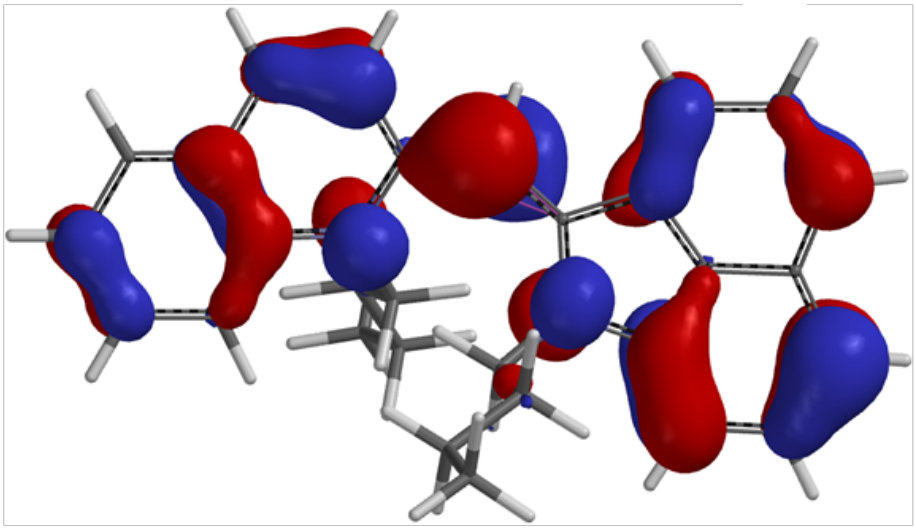

Appendix C Chapter 3

Appendix C.1. **Compound 4-methyl-Quinoline methyl**

^{1}H NMR (400 MHz, DMSO-d6) 25 °C

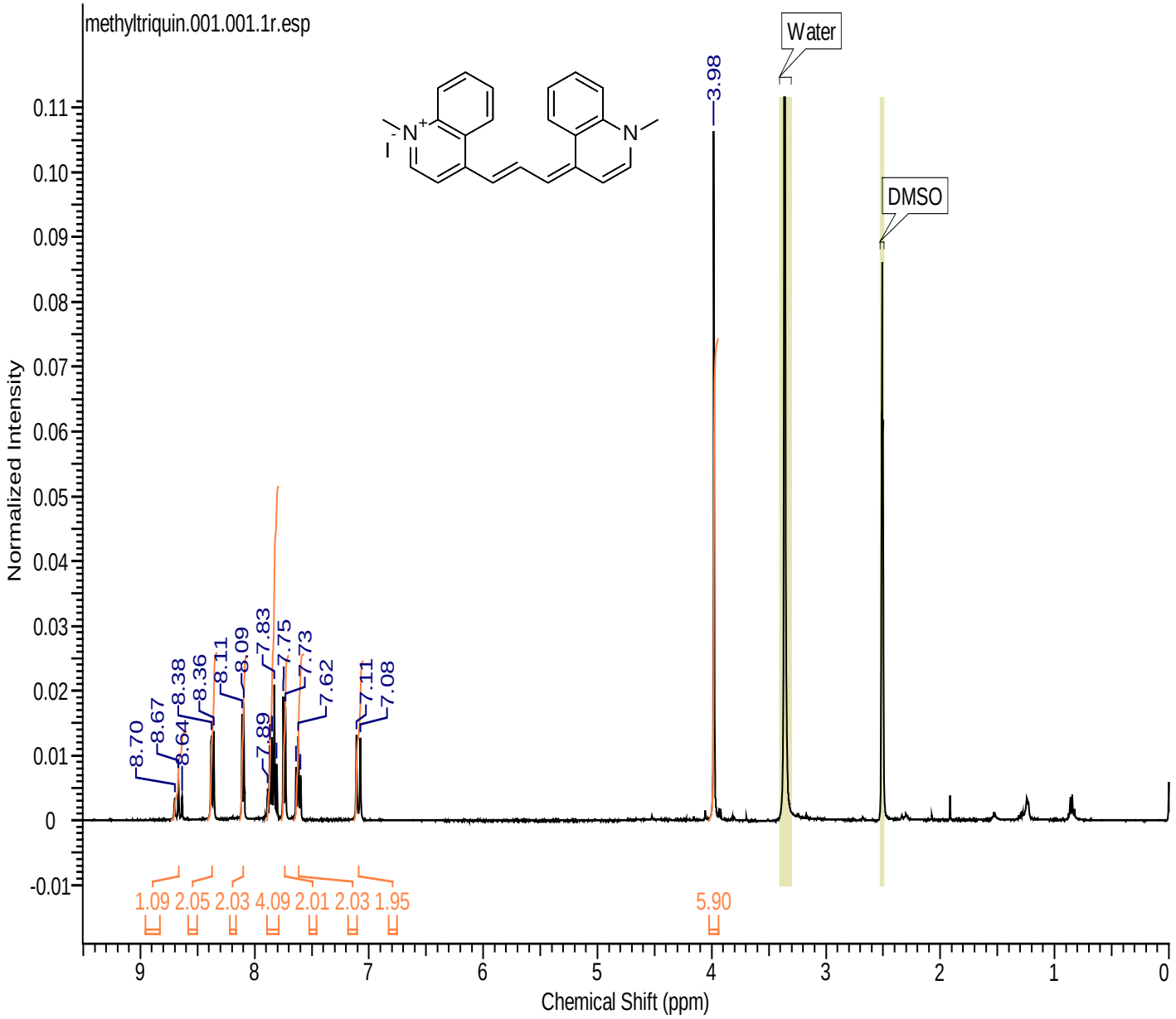

^{13}C NMR (100 MHz, DMSO-d6) 25 °C

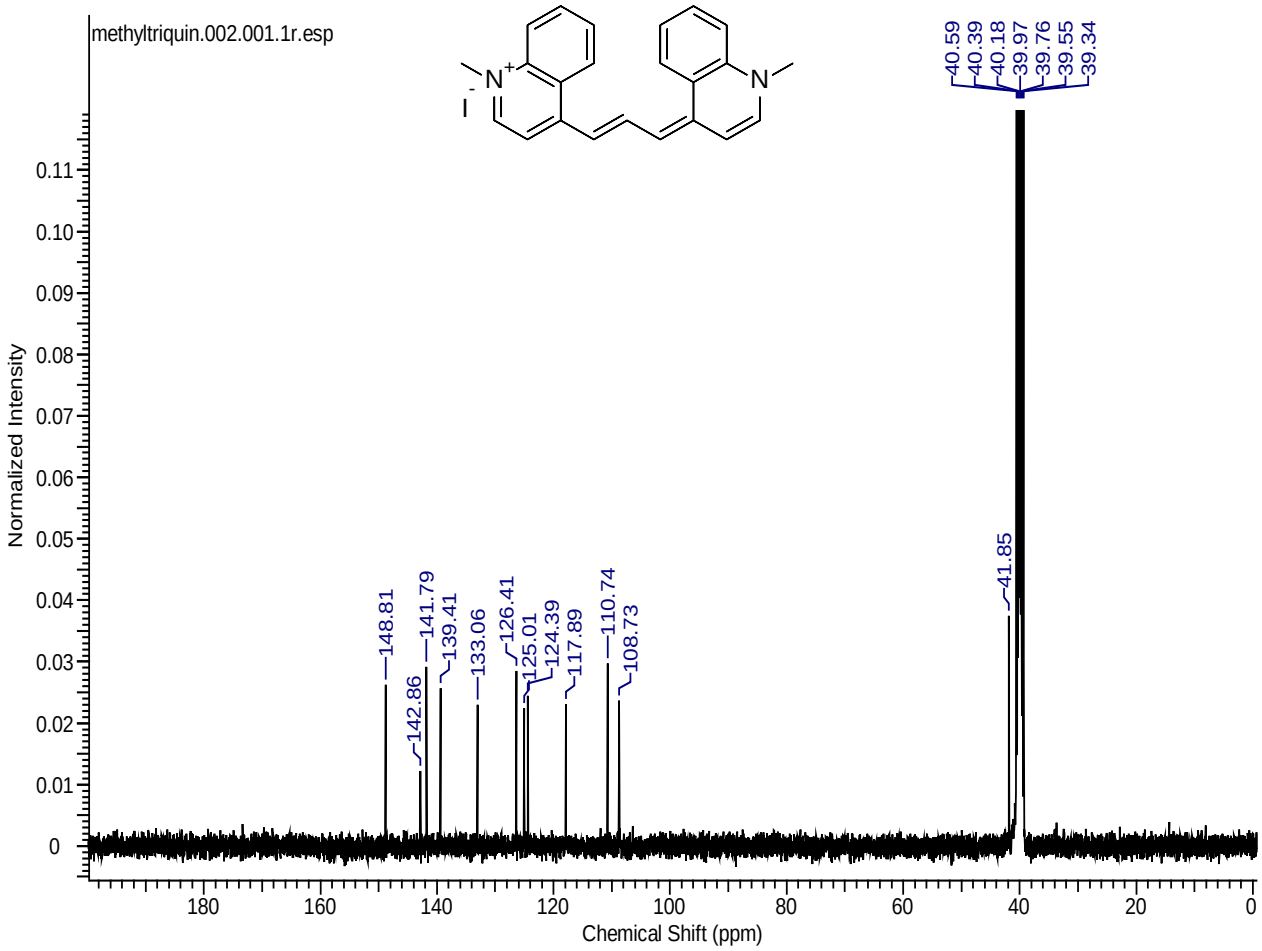

HOMO LUMO energy diagram

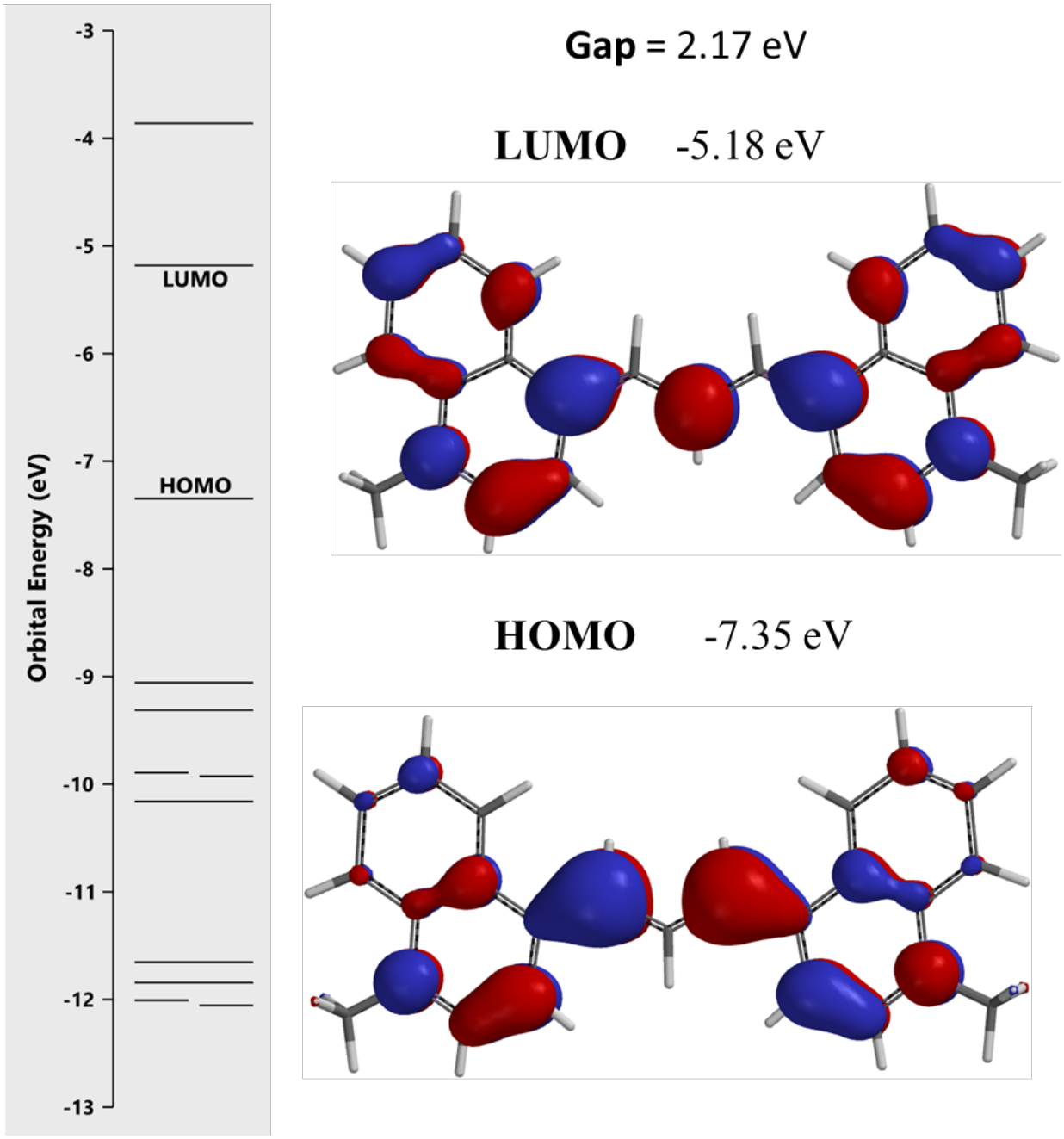

Optical properties

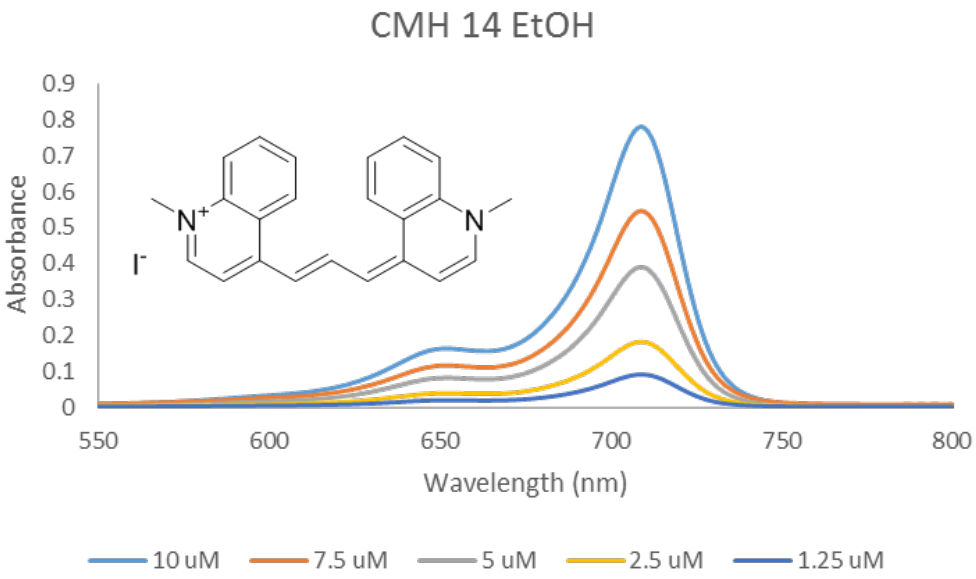

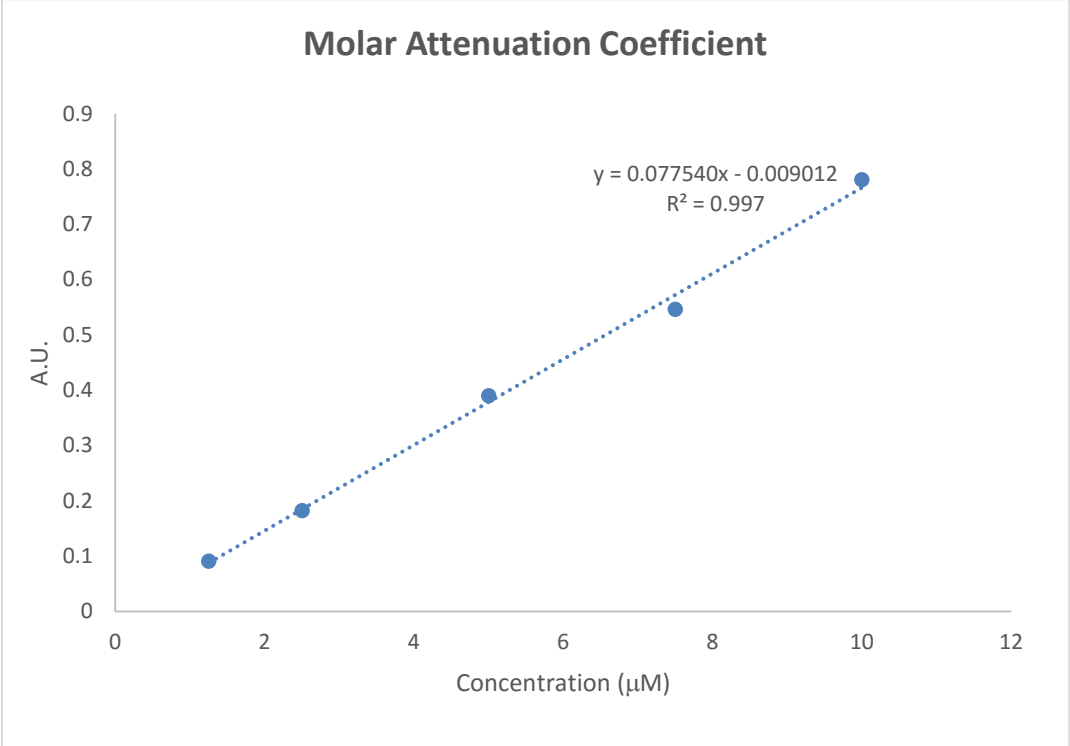

Appendix C.2. **Compound 4-methyl-Quinoline ethyl**

^{1}H NMR (400 MHz, DMSO-d6) 25 °C

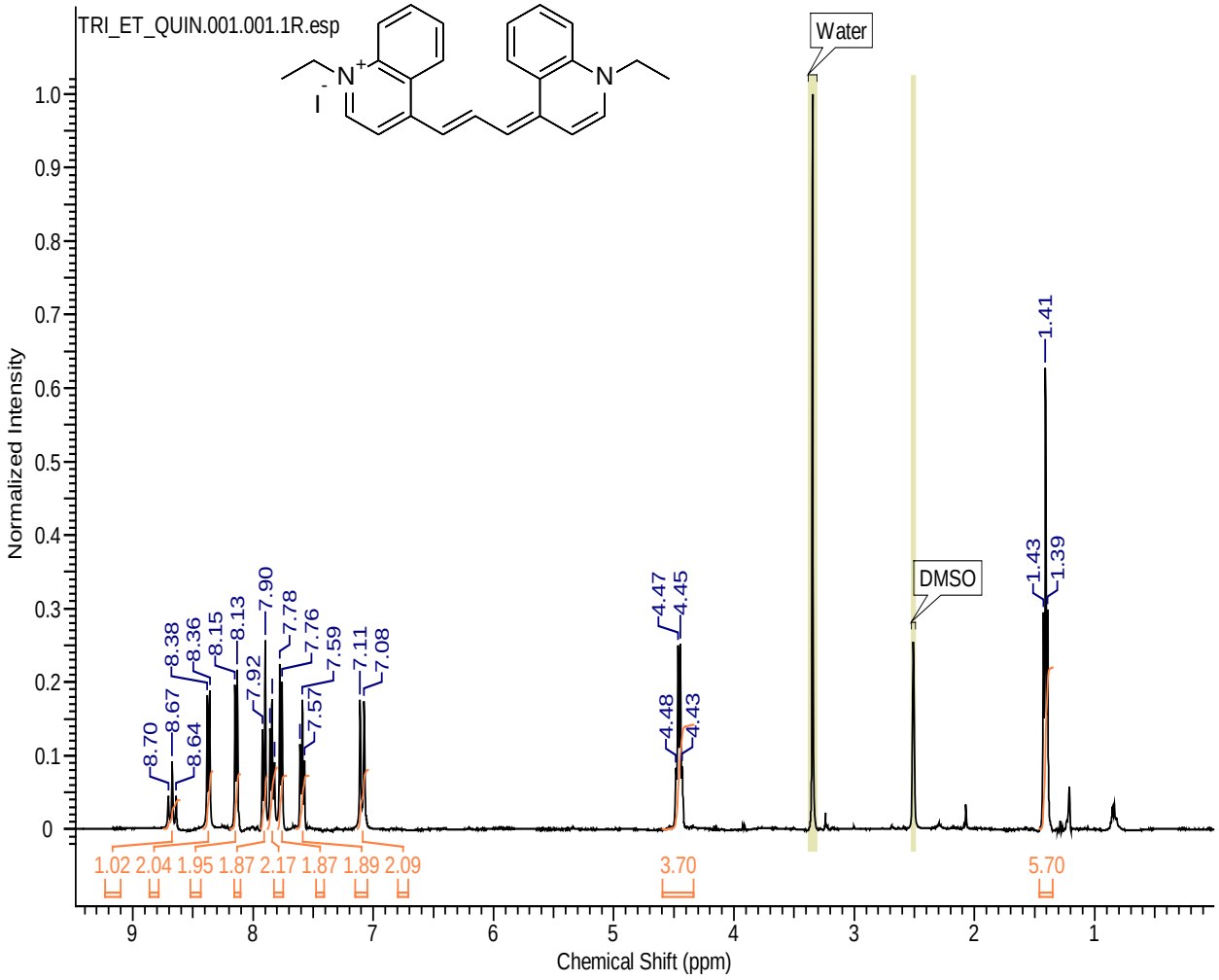

^{13}C NMR (100 MHz, DMSO-d6) 25 °C

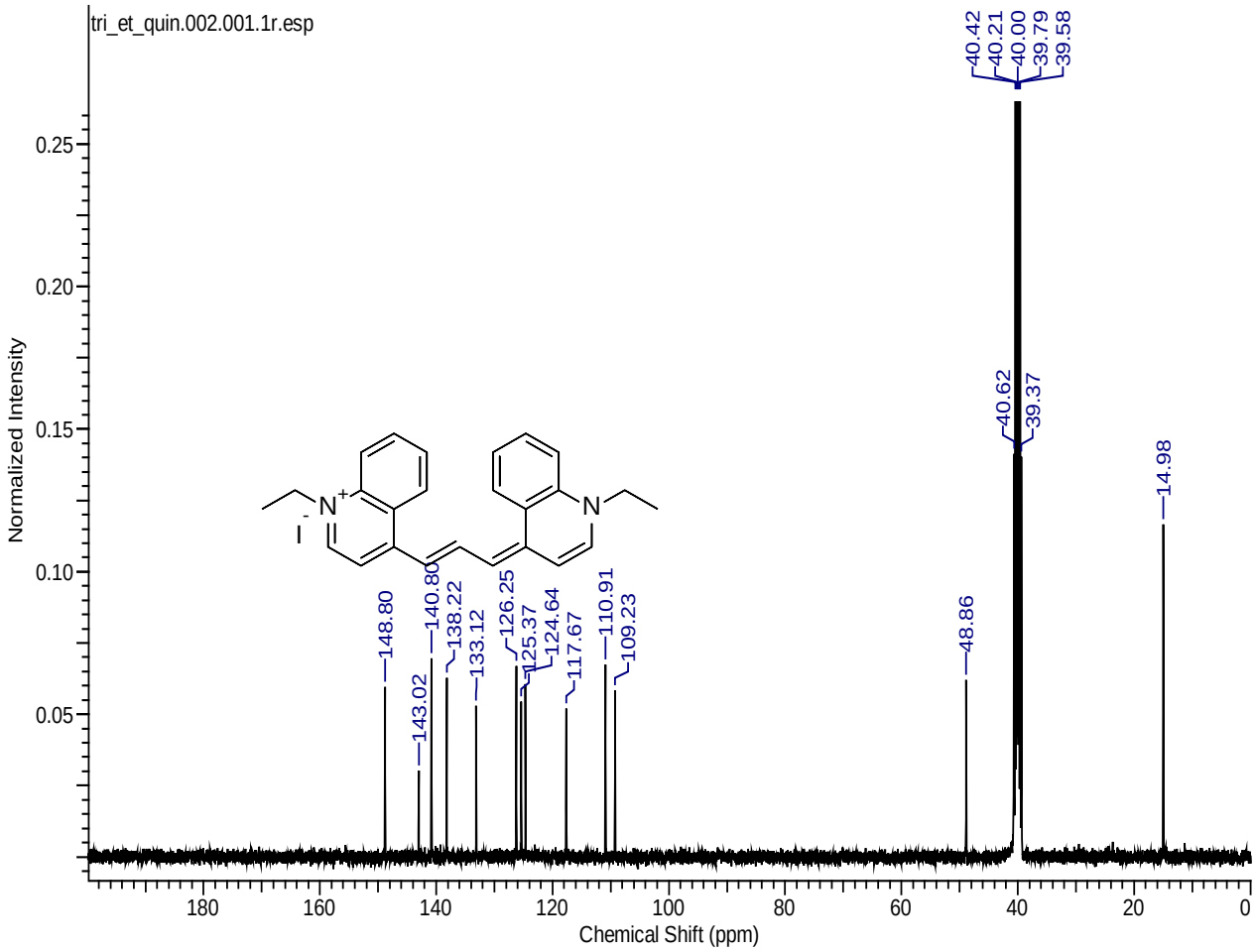

Appendix C.3. **Compound 4-methyl-Quinoline butyl**

^{1}H NMR (400 MHz, $CDCl_3$) 25 °C

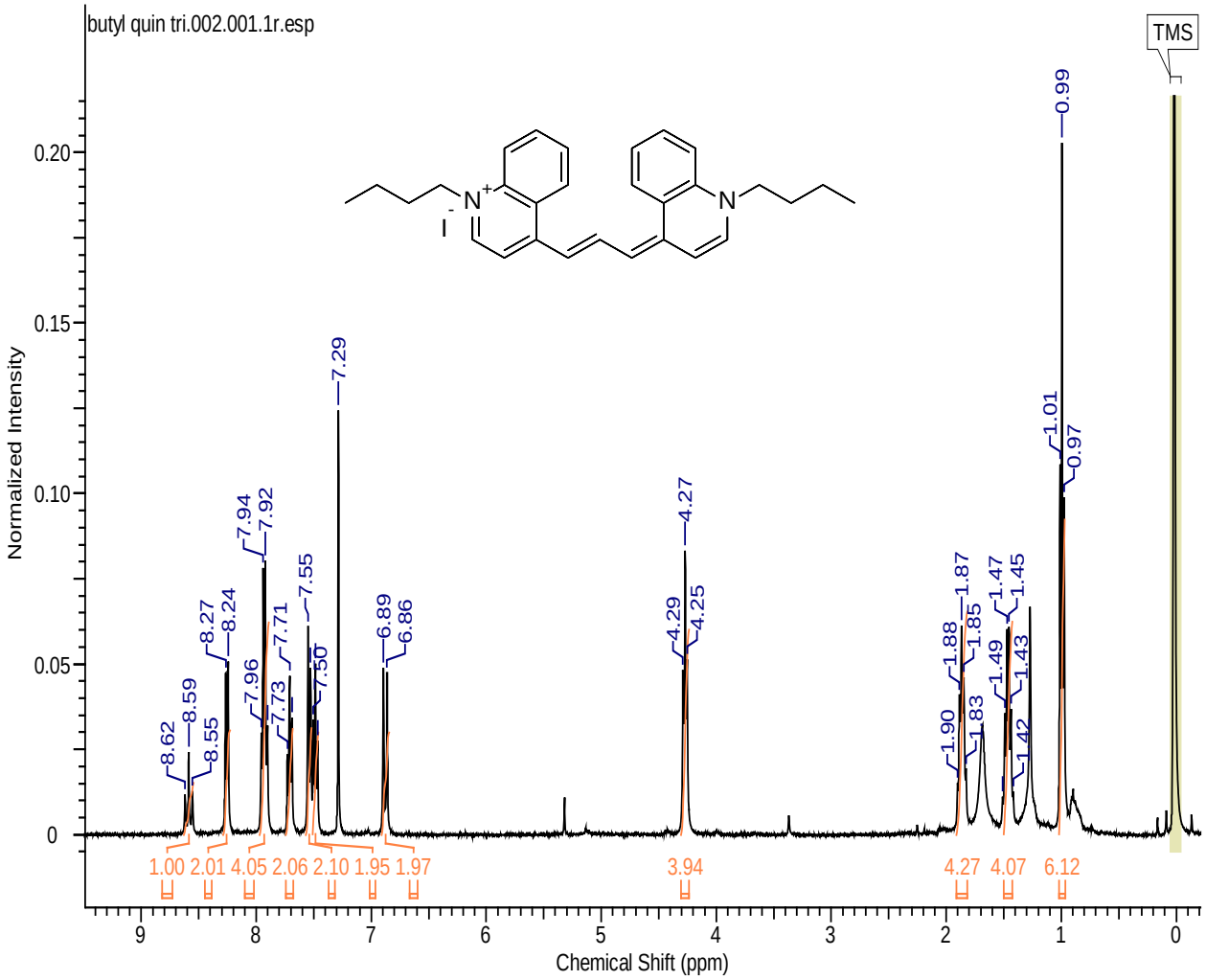

Appendix C.4. **Compound Phenanthridine methyl**

^{1}H NMR (400 MHz, DMSO-d6) 25 °C

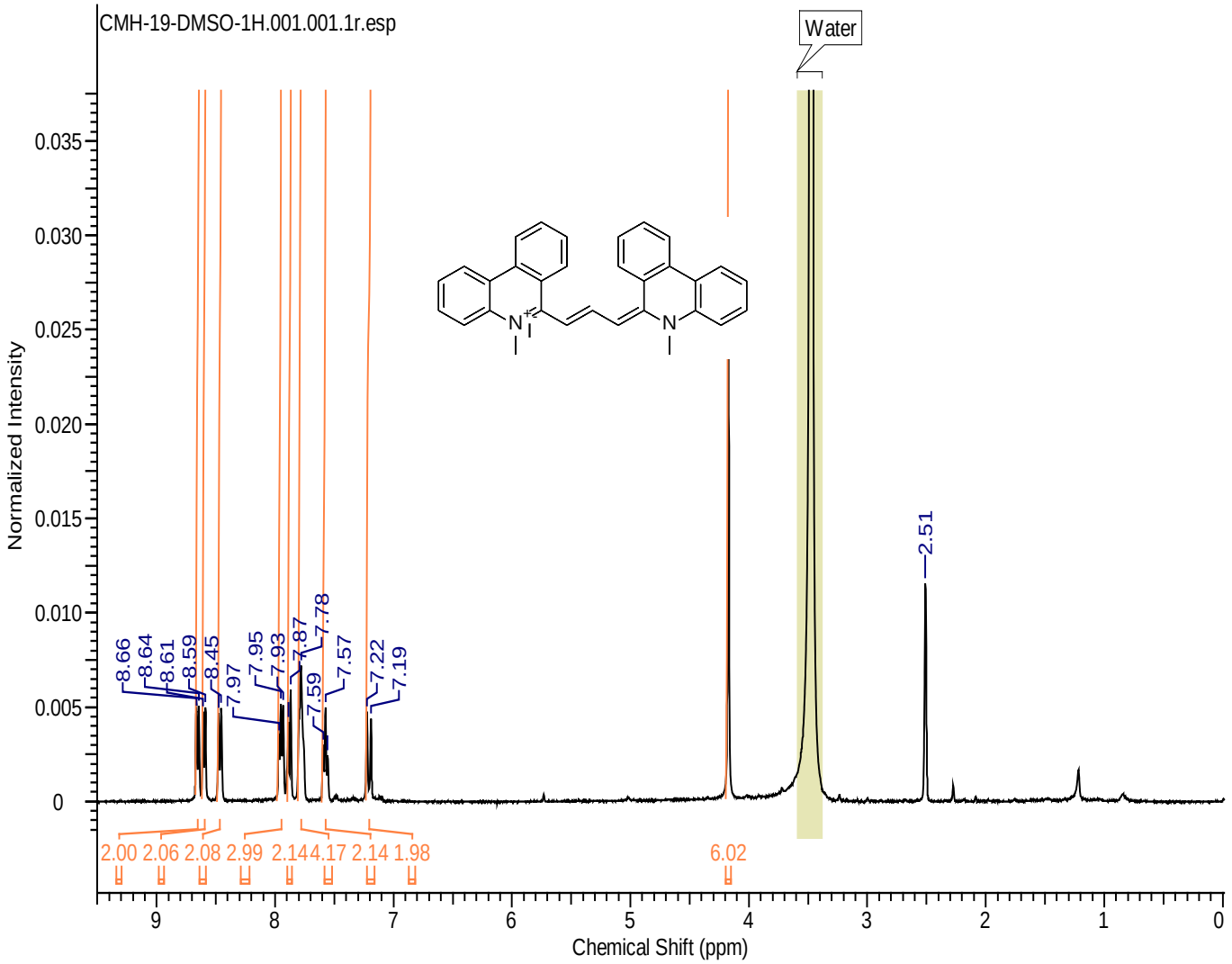

^{13}C NMR (100 MHz, DMSO-d6) 25 °C

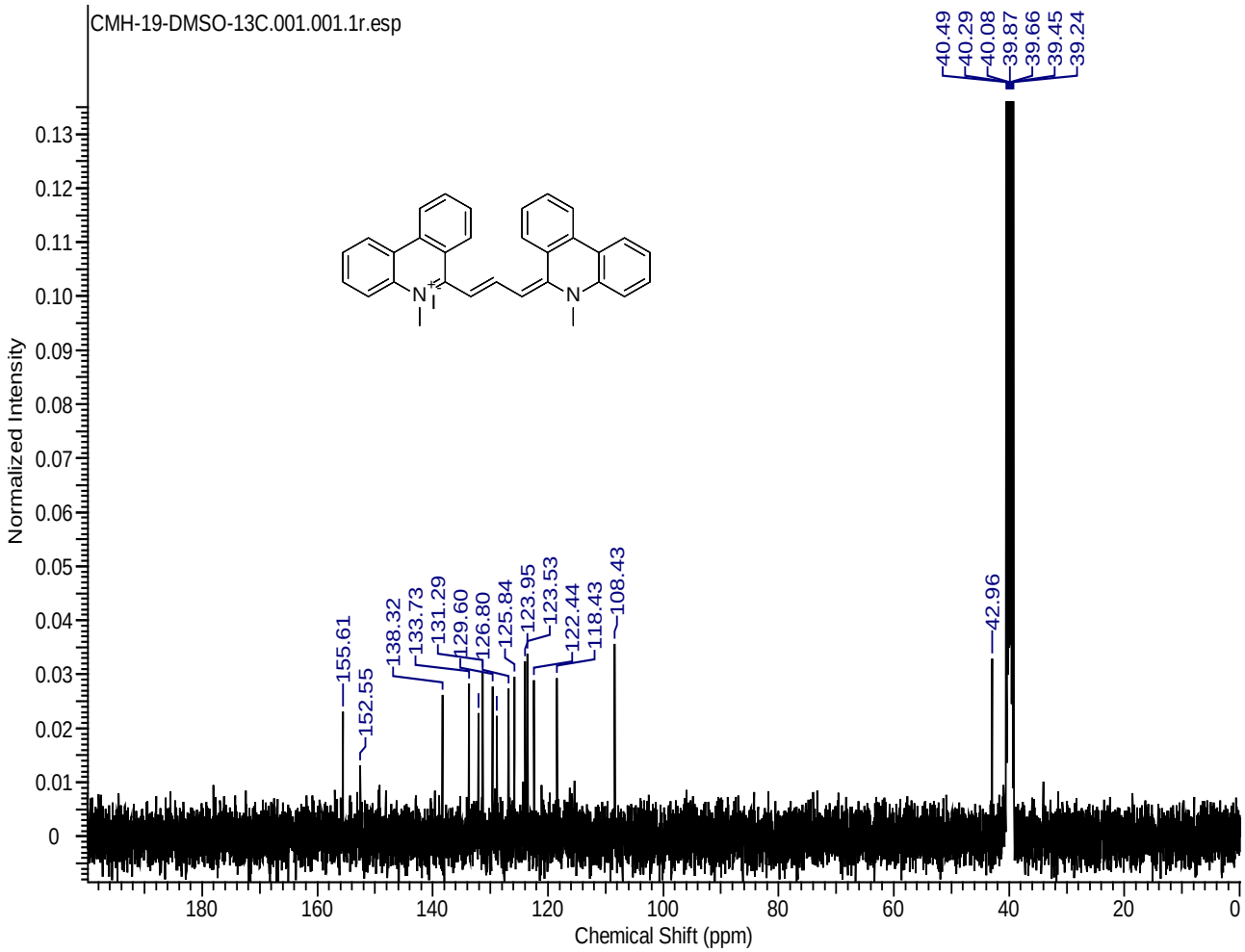

HOMO LUMO energy diagram

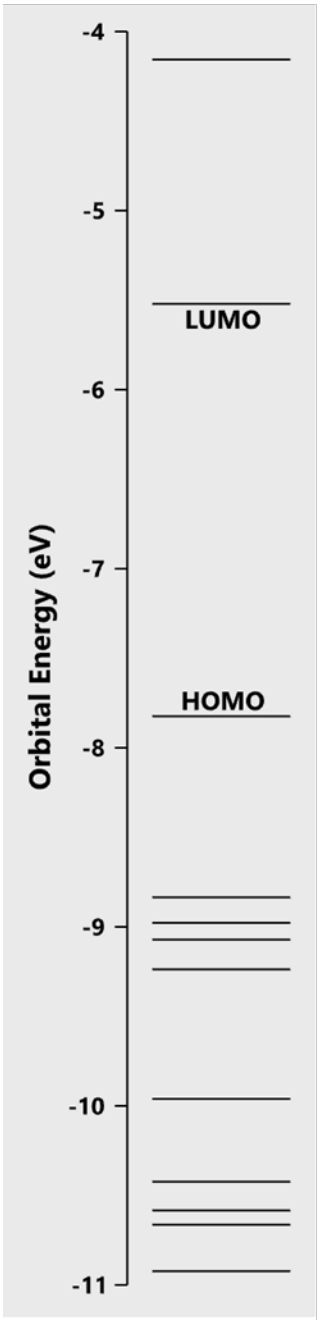

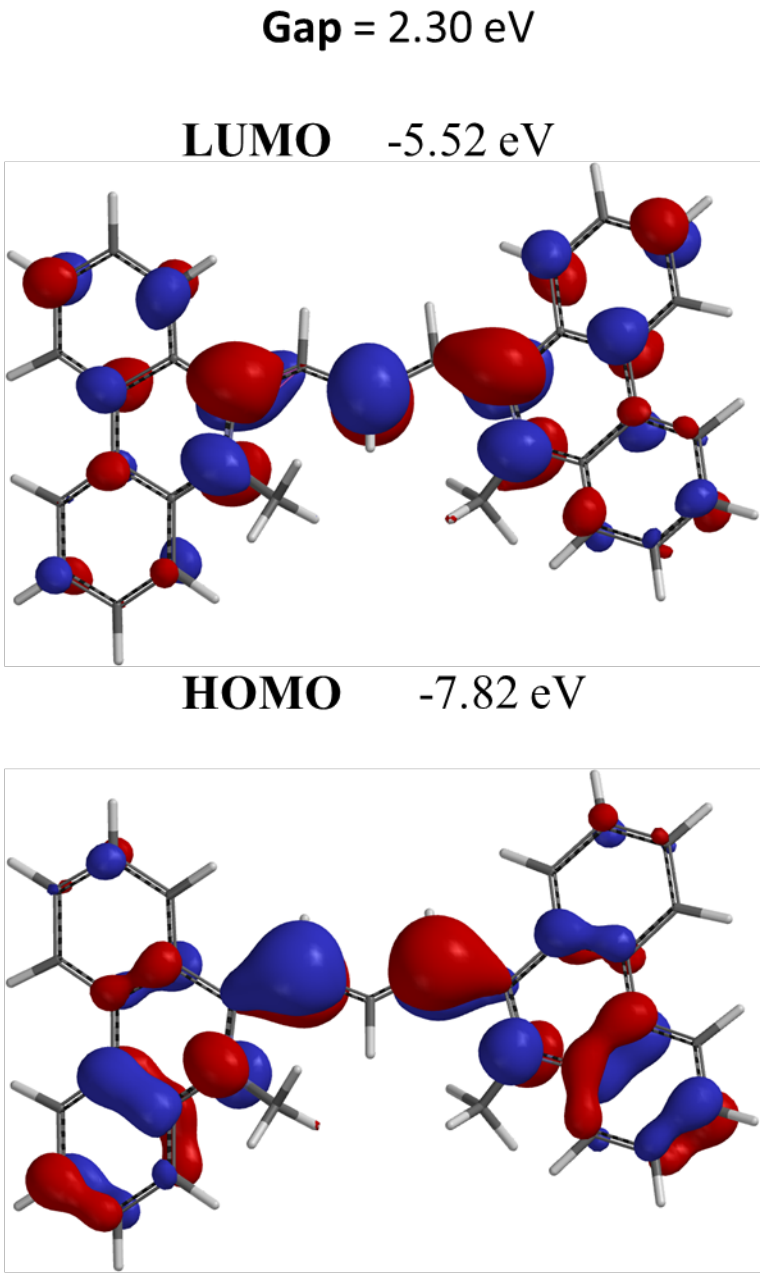

Optical Properties

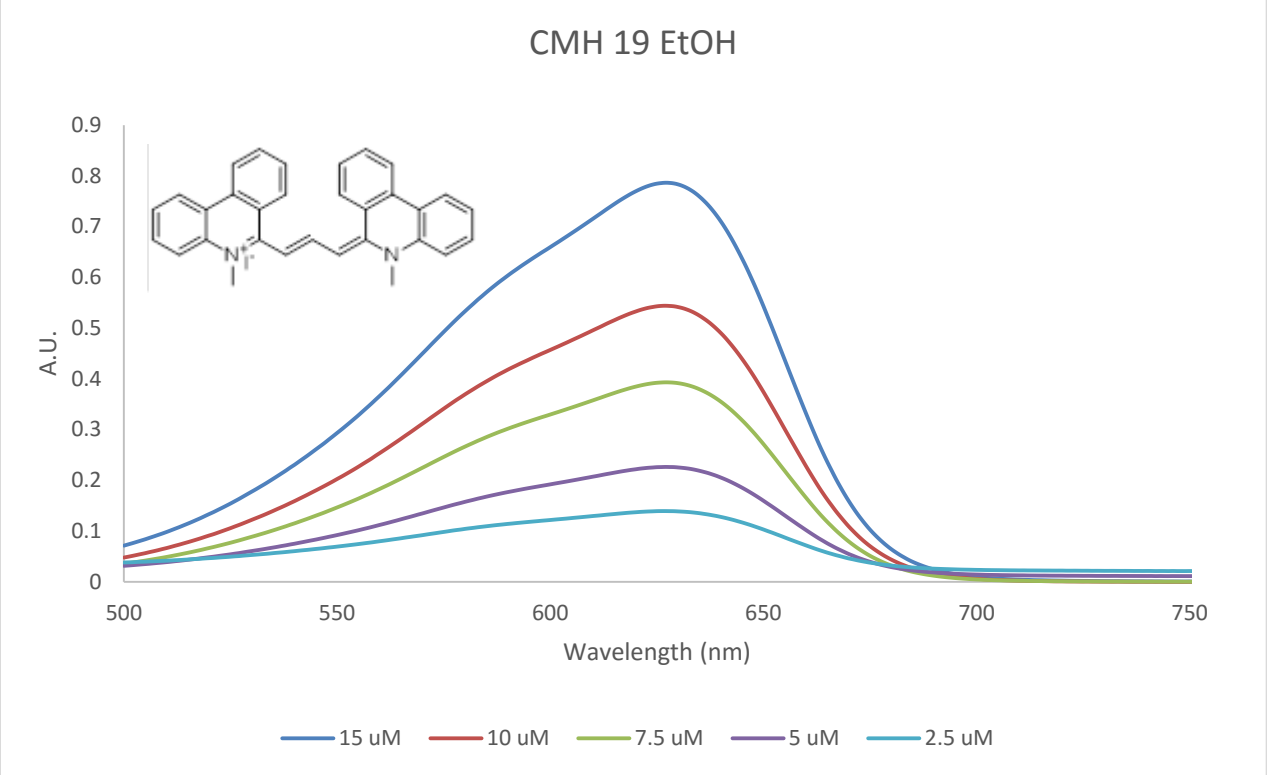

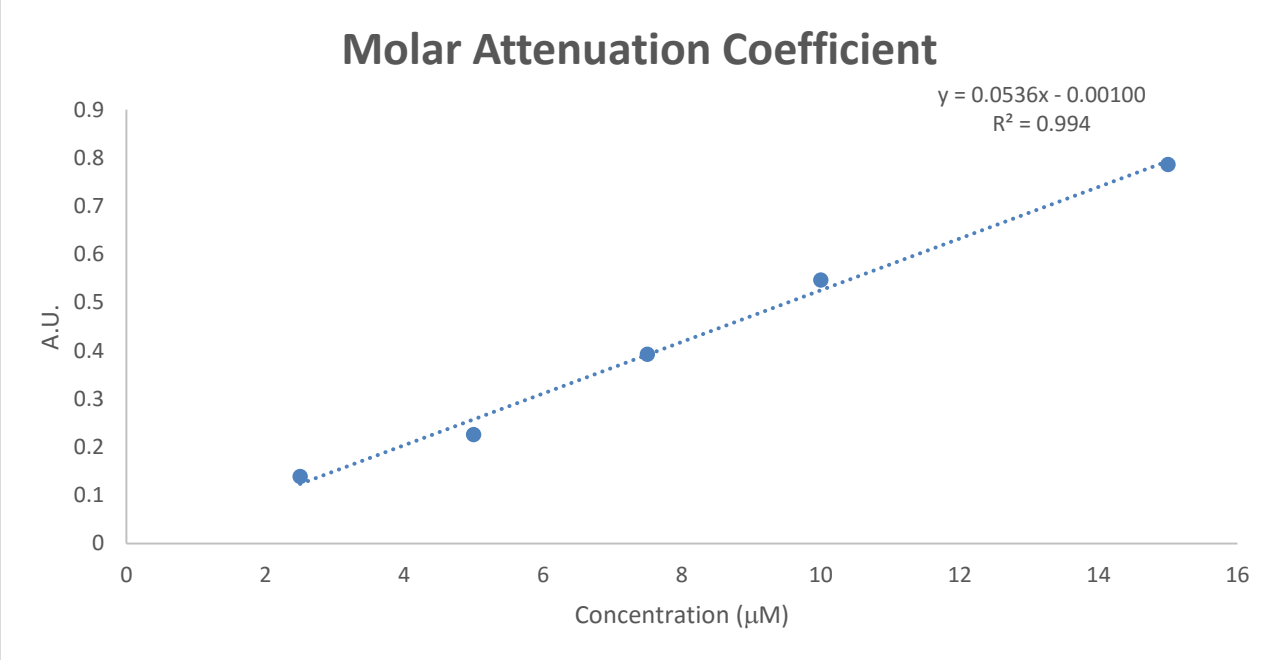

Appendix C.5. **Compound Phenanthridine ethyl**

^{1}H NMR (400 MHz, DMSO-d6) 25 °C

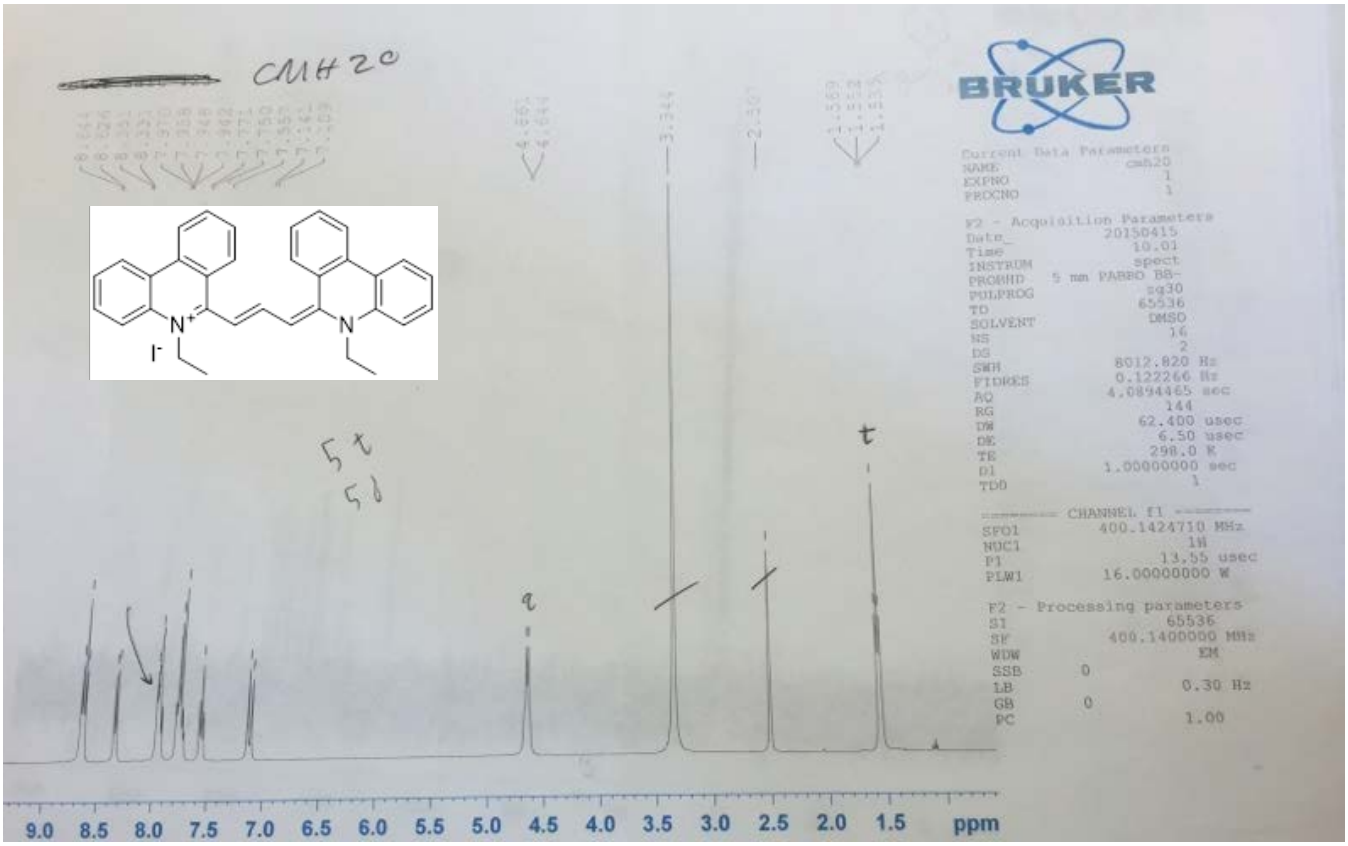

^{13}C NMR (100 MHz, DMSO-d6) 25 °C

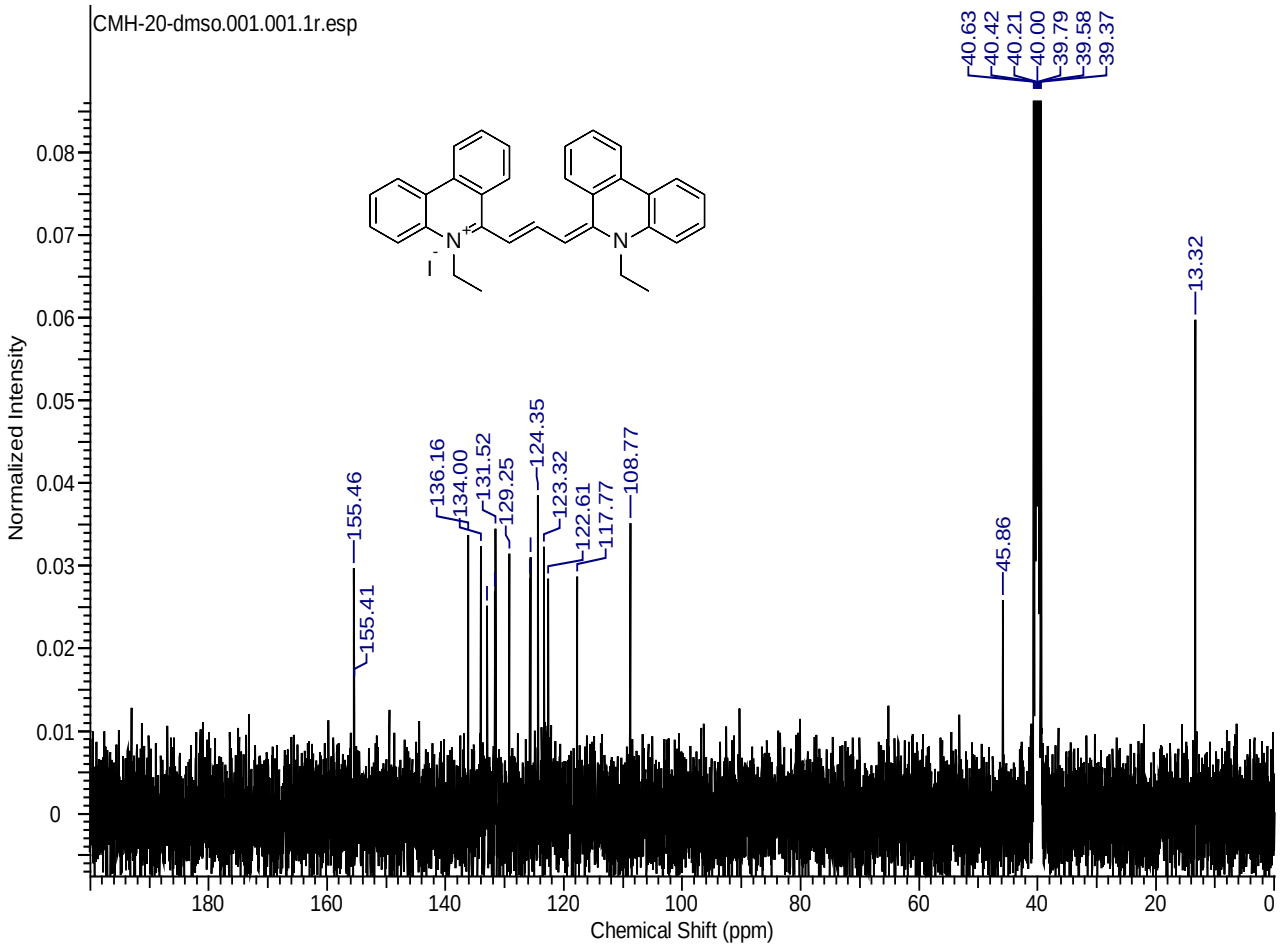

Appendix C.6. **Compound Bromo Phenanthridine methyl**

^{1}H NMR (400 MHz, DMSO-d6) 25 °C

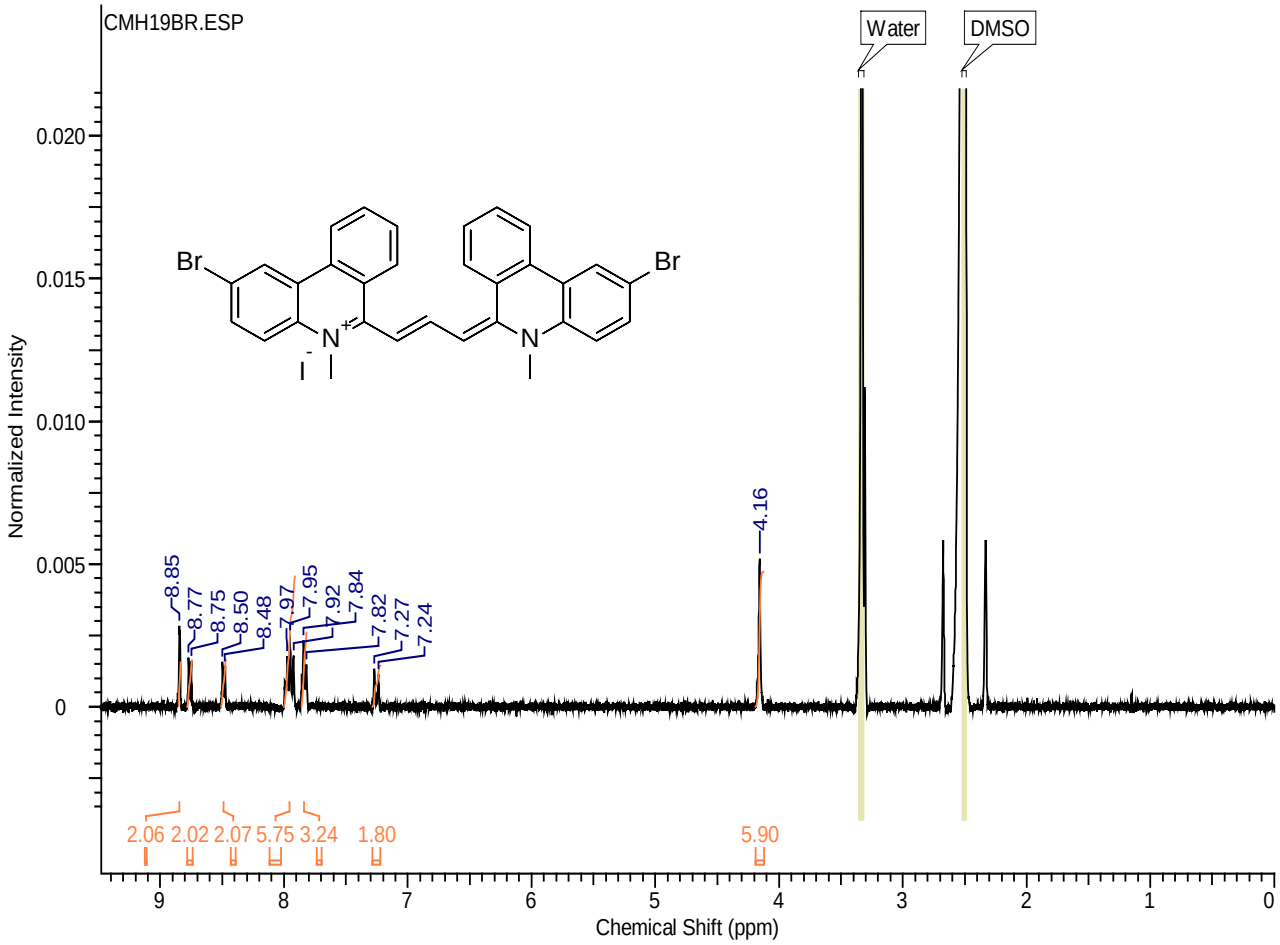

HOMO LUMO diagram

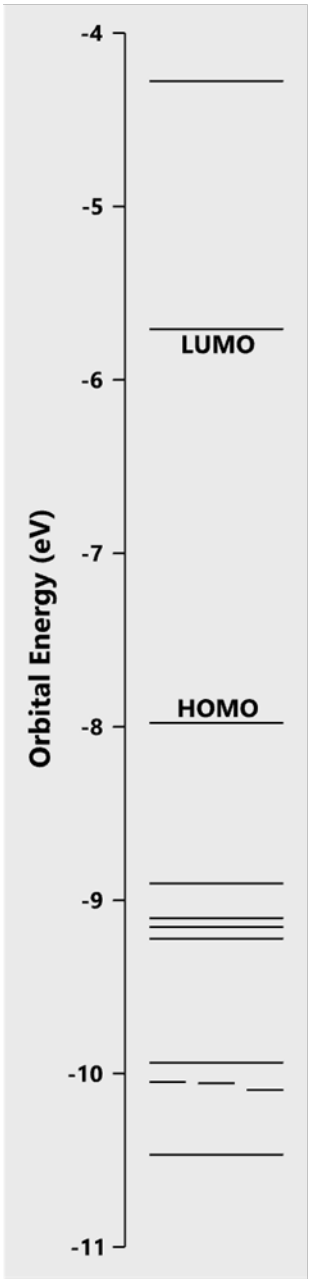

Gap = 2.27 eV

LUMO -5.71 eV

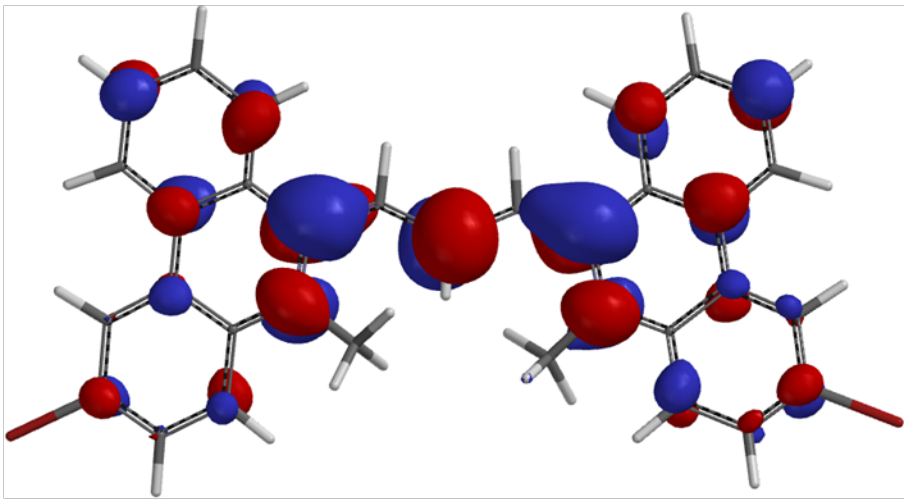

HOMO -7.98 eV

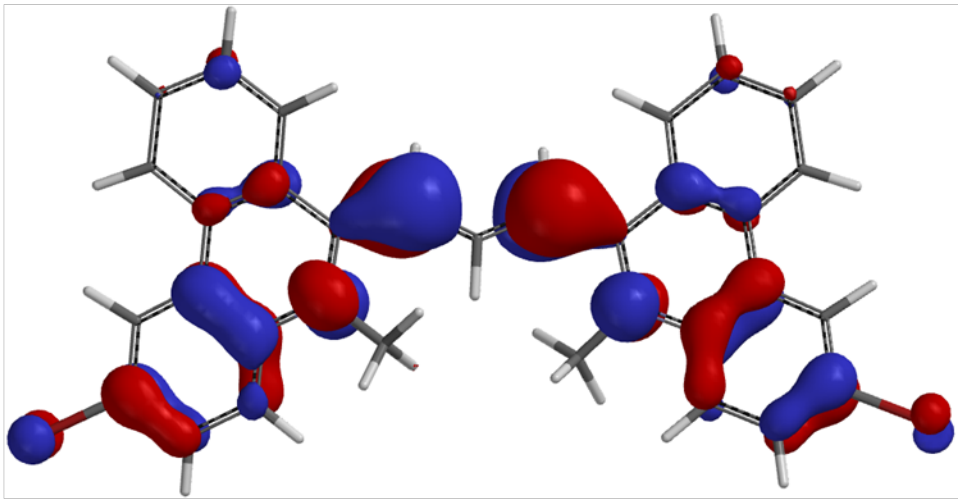

Optical properties

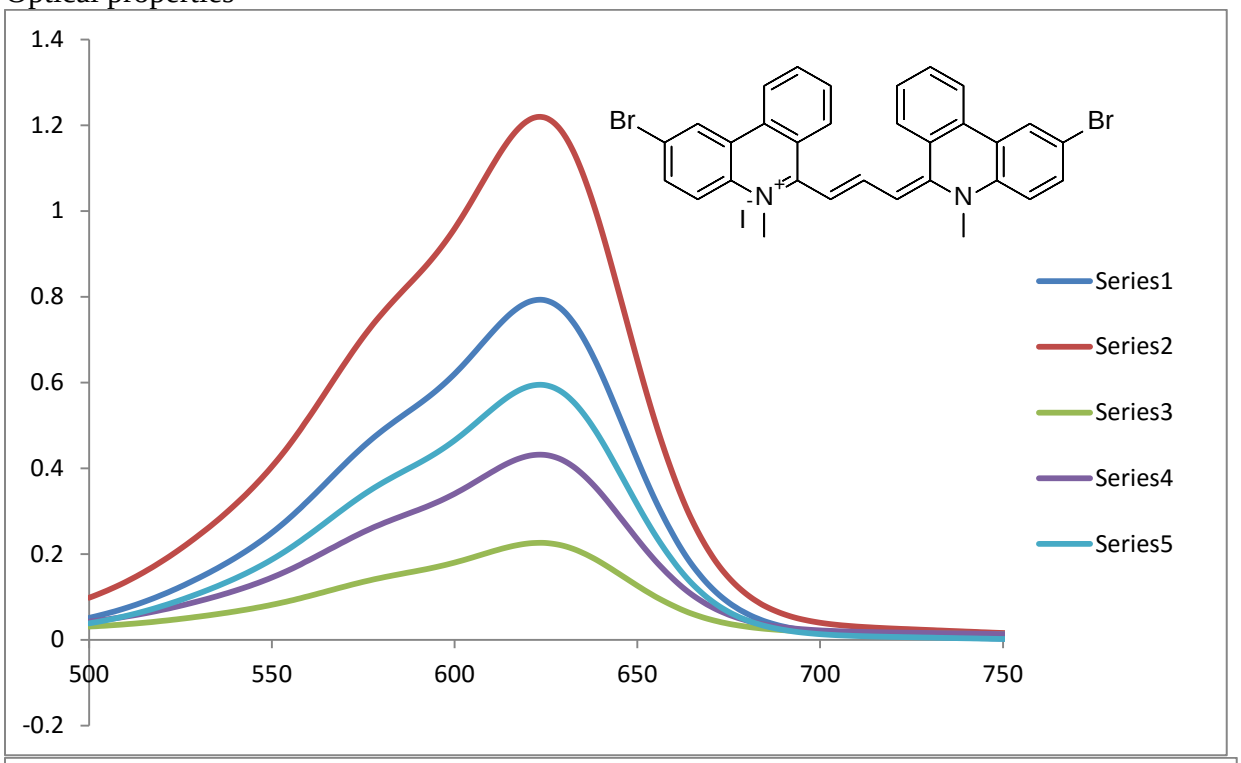

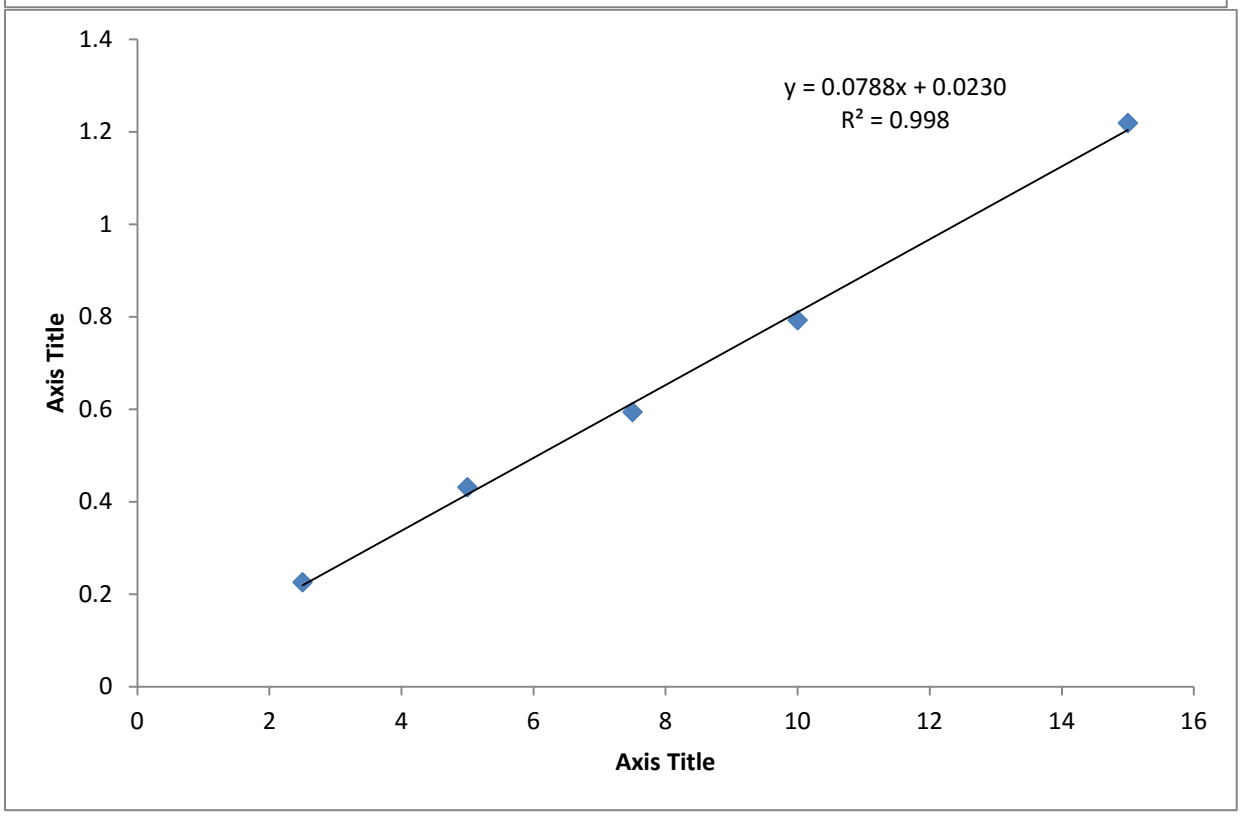

Appendix C.7. **Compound Bromo Phenanthridine ethyl**

^{1}H NMR (400 MHz, DMSO-d6) 25 °C

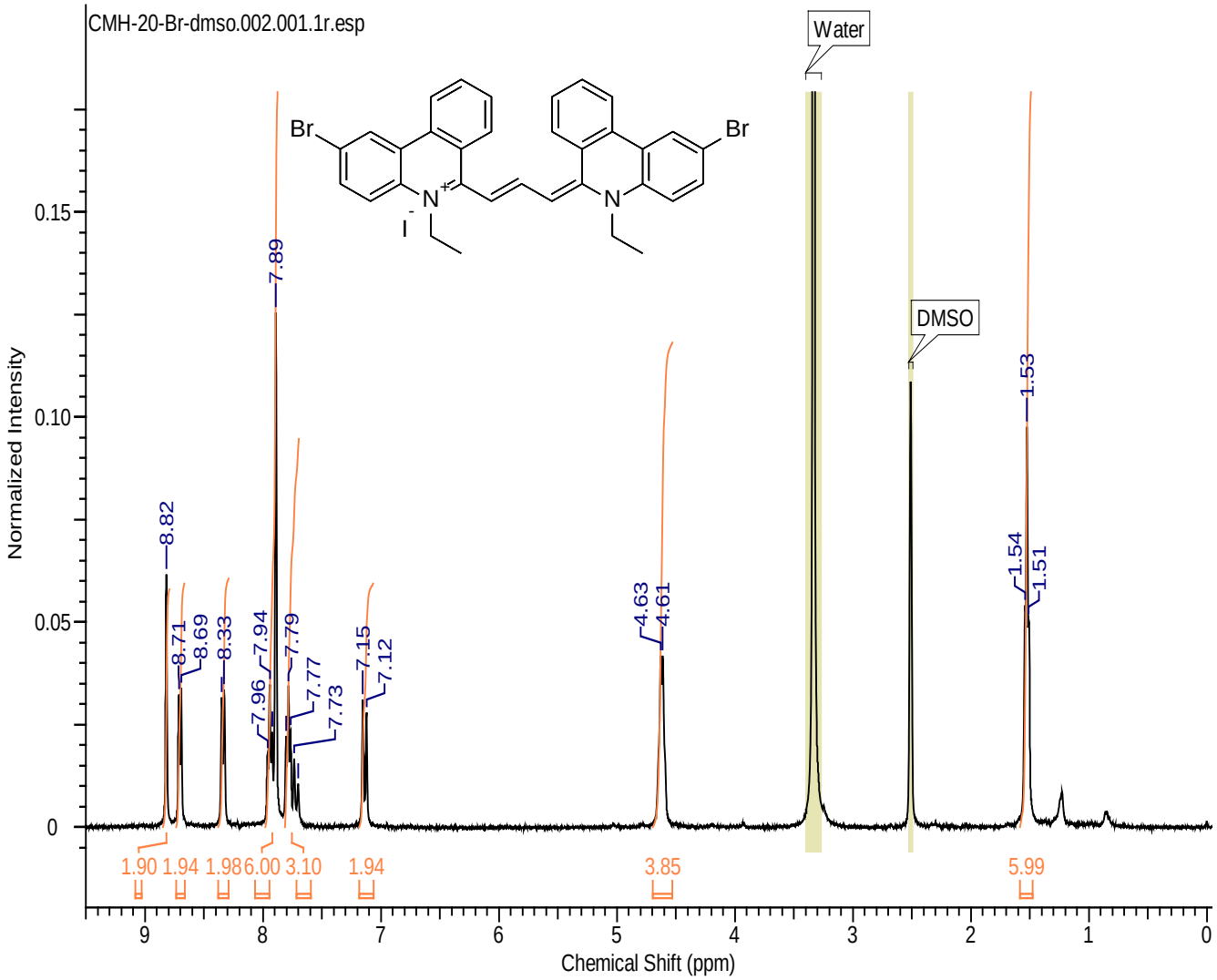

^{13}C NMR (100 MHz, DMSO-d6) 25 °C

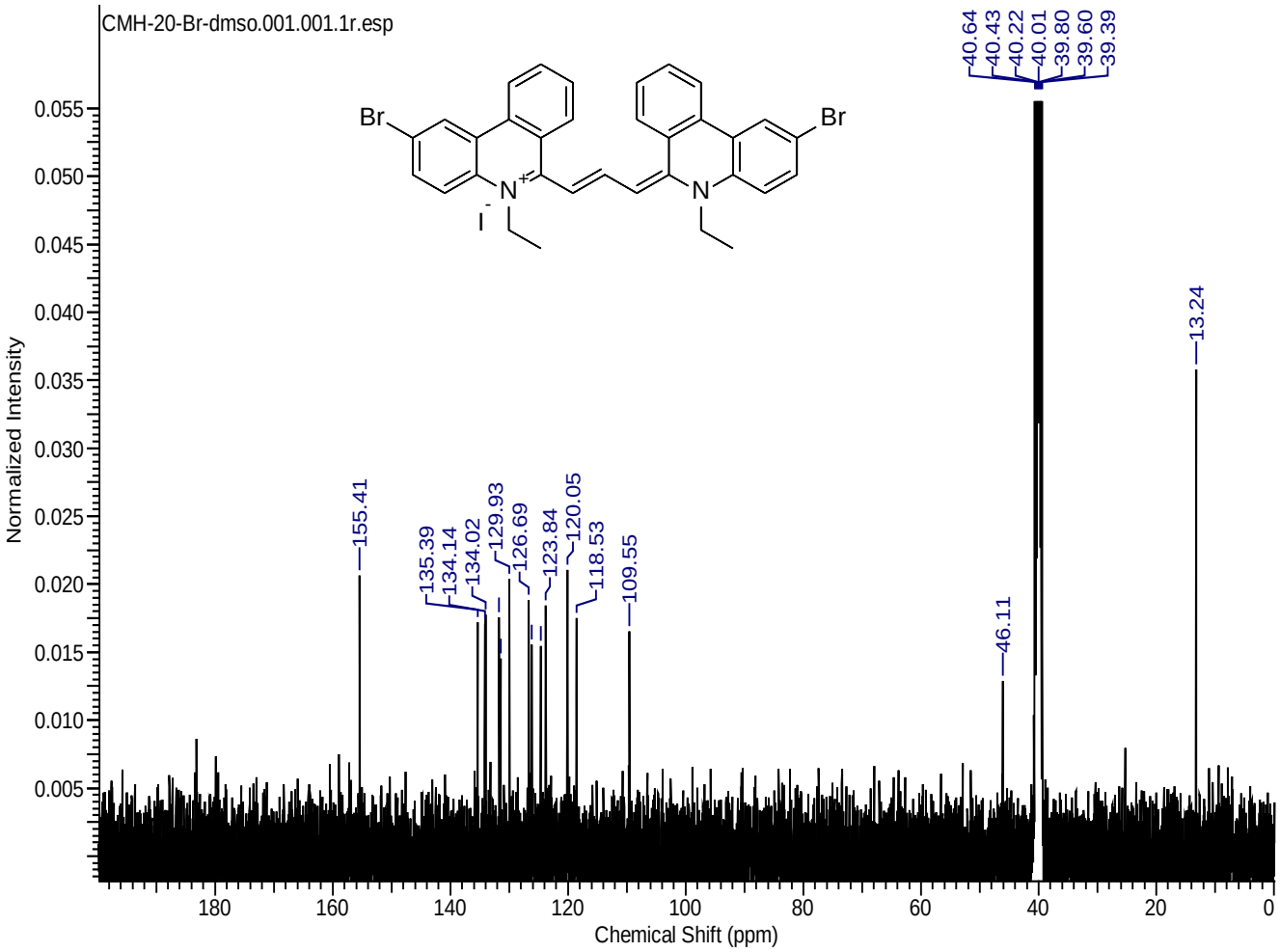

Appendix C.8. **Compound 2methyl quinoline methyl**

^{1}H NMR (400 MHz, DMSO-d6) 25 °C

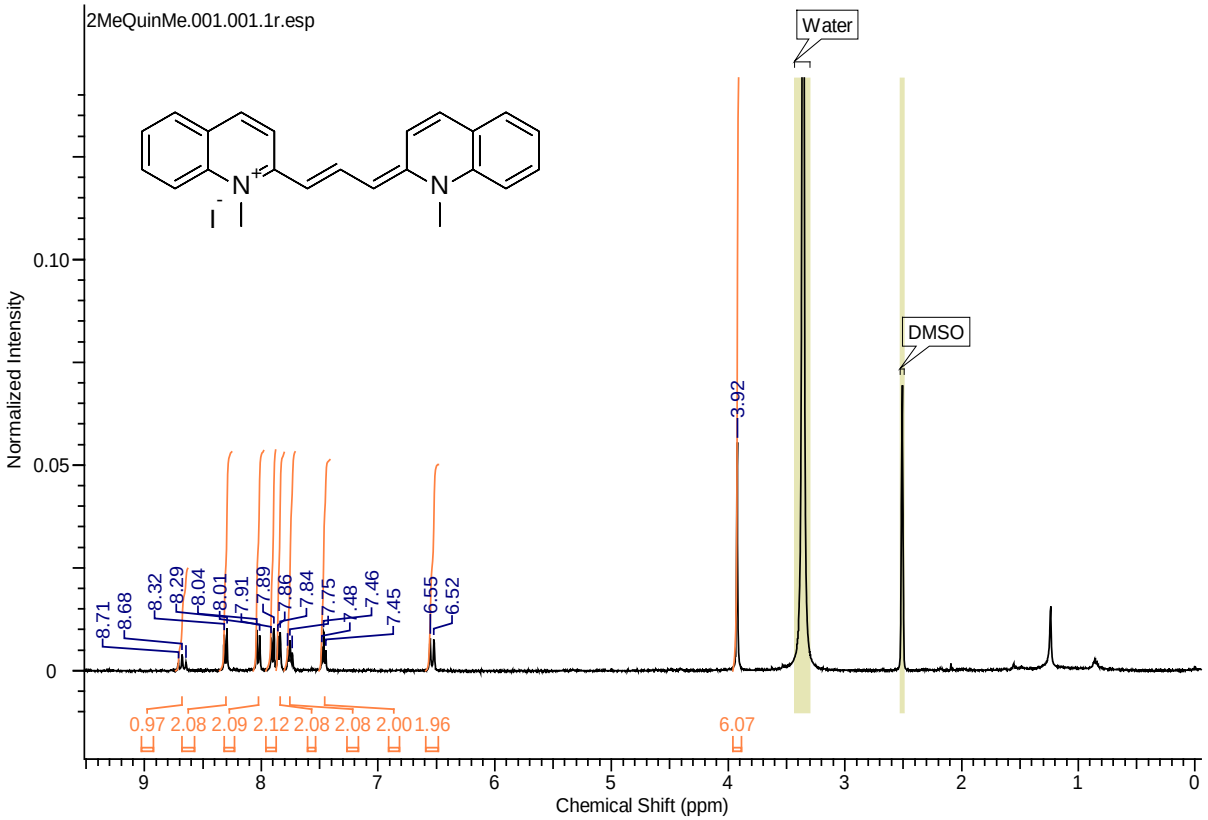

^{13}C NMR (100 MHz, DMSO-d6) 25 °C

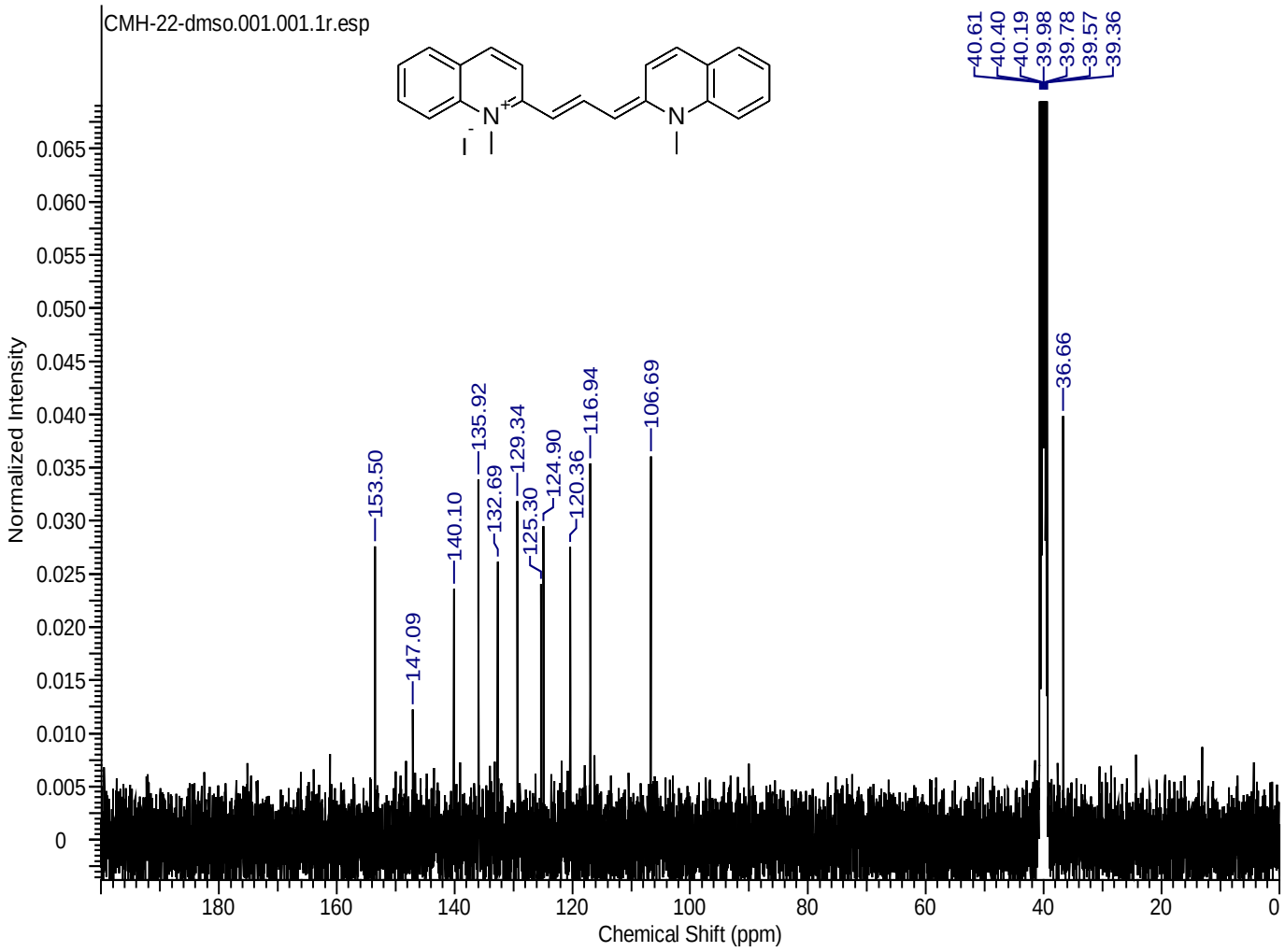
CMH-22-dmso.001.001.1r.esp
Normalized Intensity
Chemical Shift (ppm)
153.50
147.09
140.10
135.92
132.69
129.34
125.30
124.90
120.36
116.94
106.69
40.61
40.40
40.19
39.98
39.78
39.57
39.36
36.66

HOMO LUMO diagram

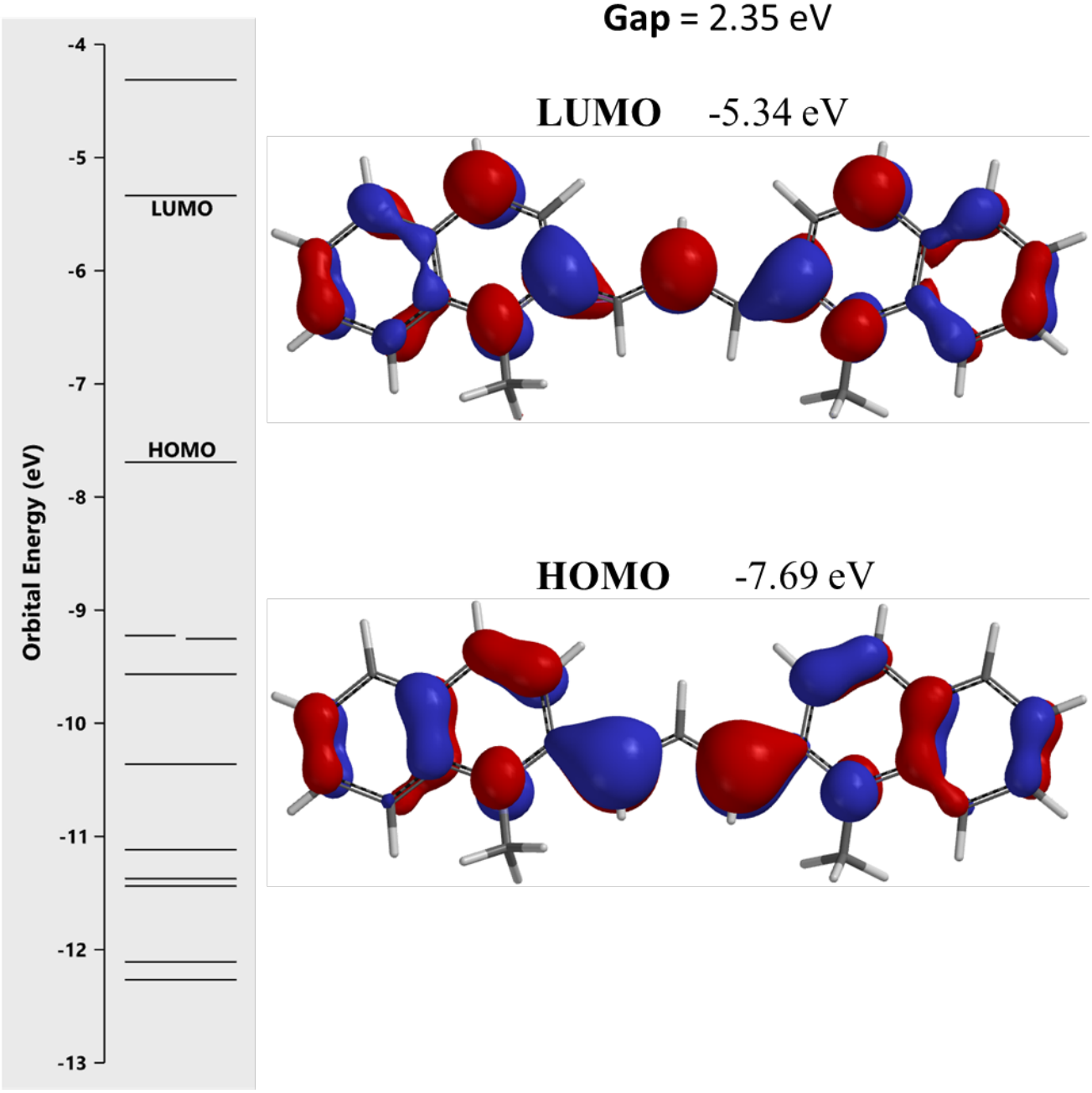

Optical properties

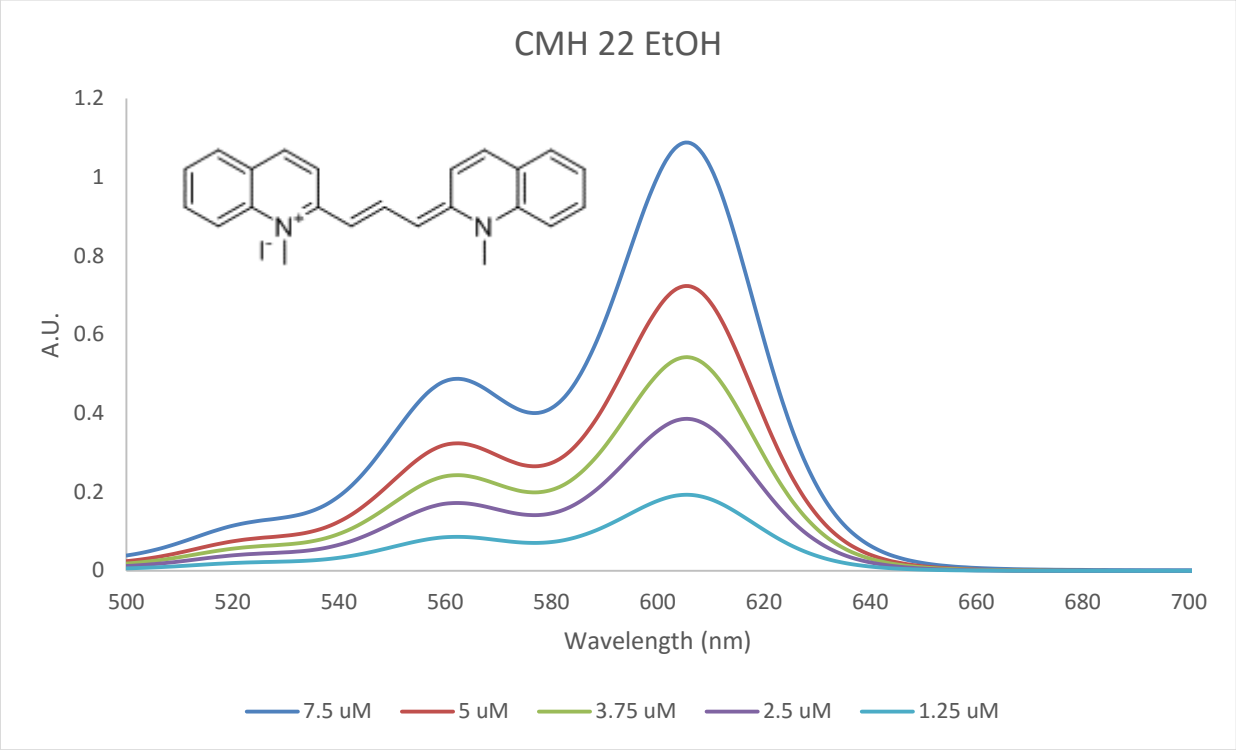

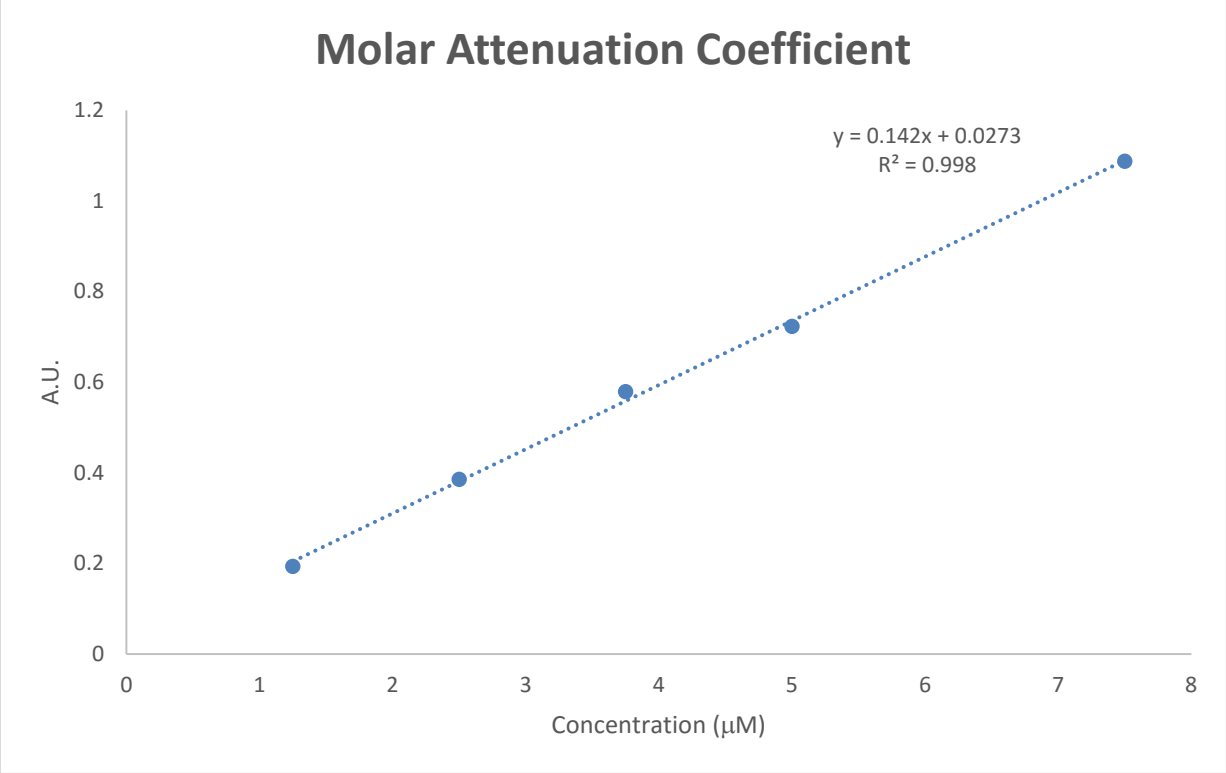

Appendix C.8. **Compound 2methyl quinoline ethyl**

^{1}H NMR (400 MHz, DMSO-d6) 25 °C

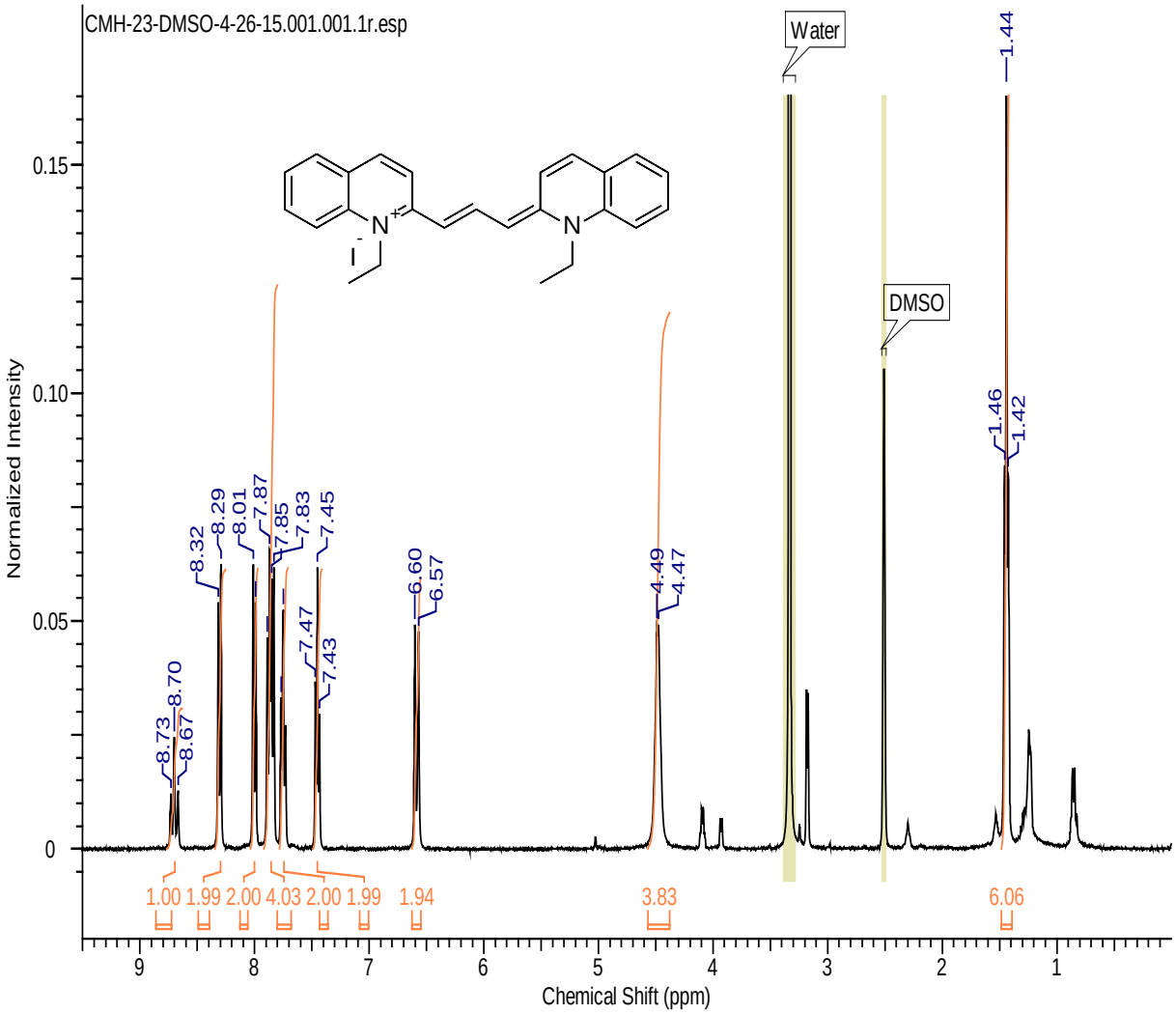

^{13}C NMR (100 MHz, DMSO-d6) 25 °C

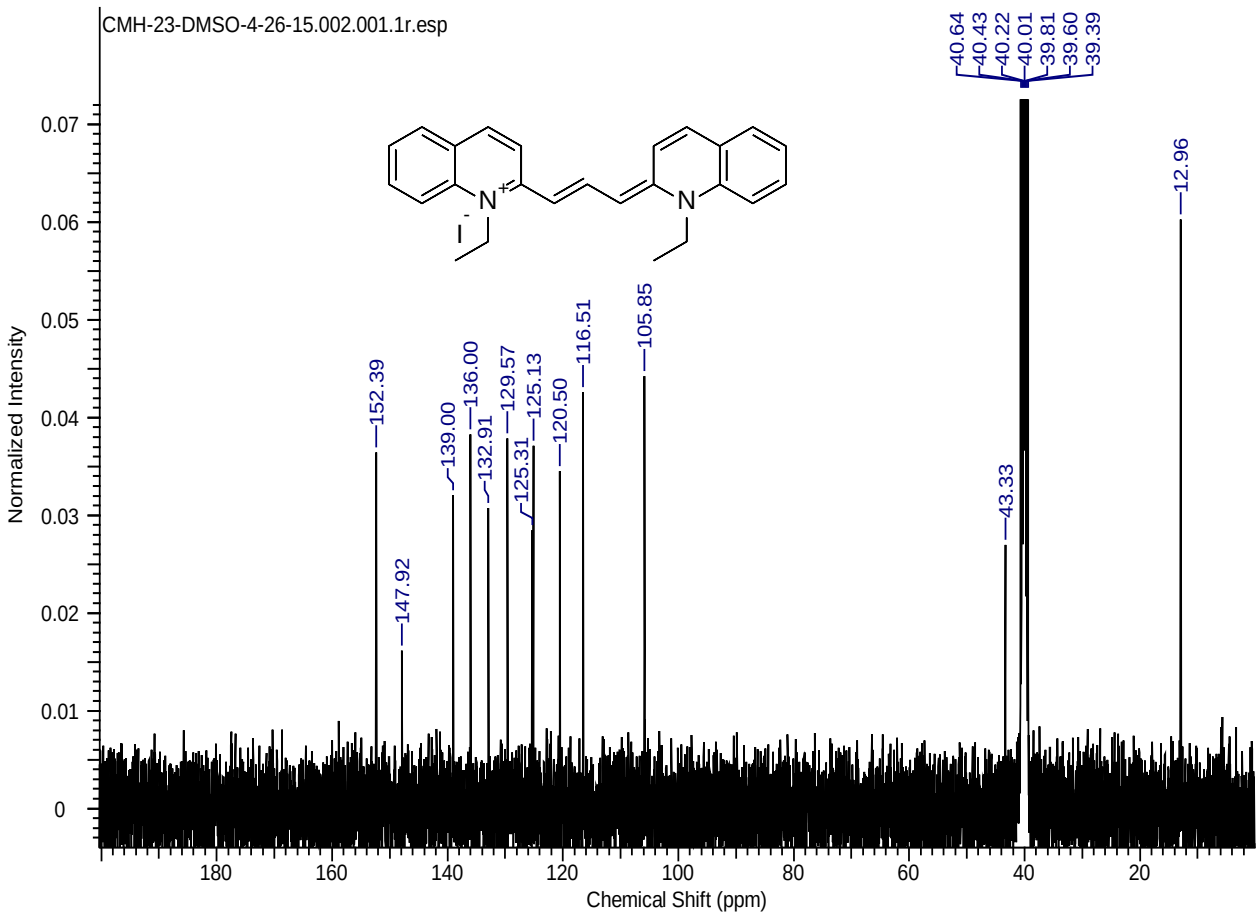

Appendix C.9. **Compound 2methyl quinoline butyl**

^{1}H NMR (400 MHz, DMSO-*d6*) 25 °C

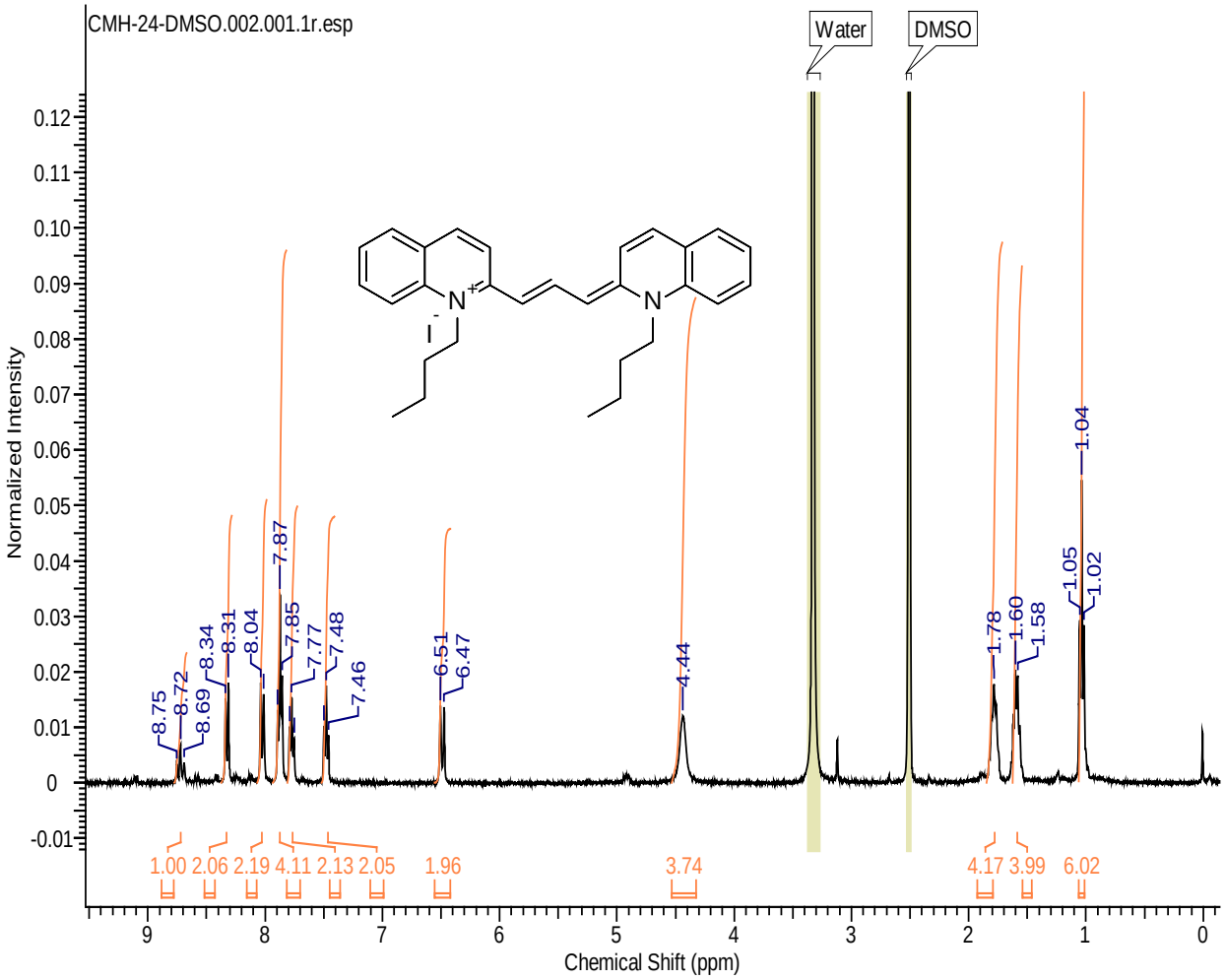

^{13}C NMR (100 MHz, DMSO-d6) 25 °C

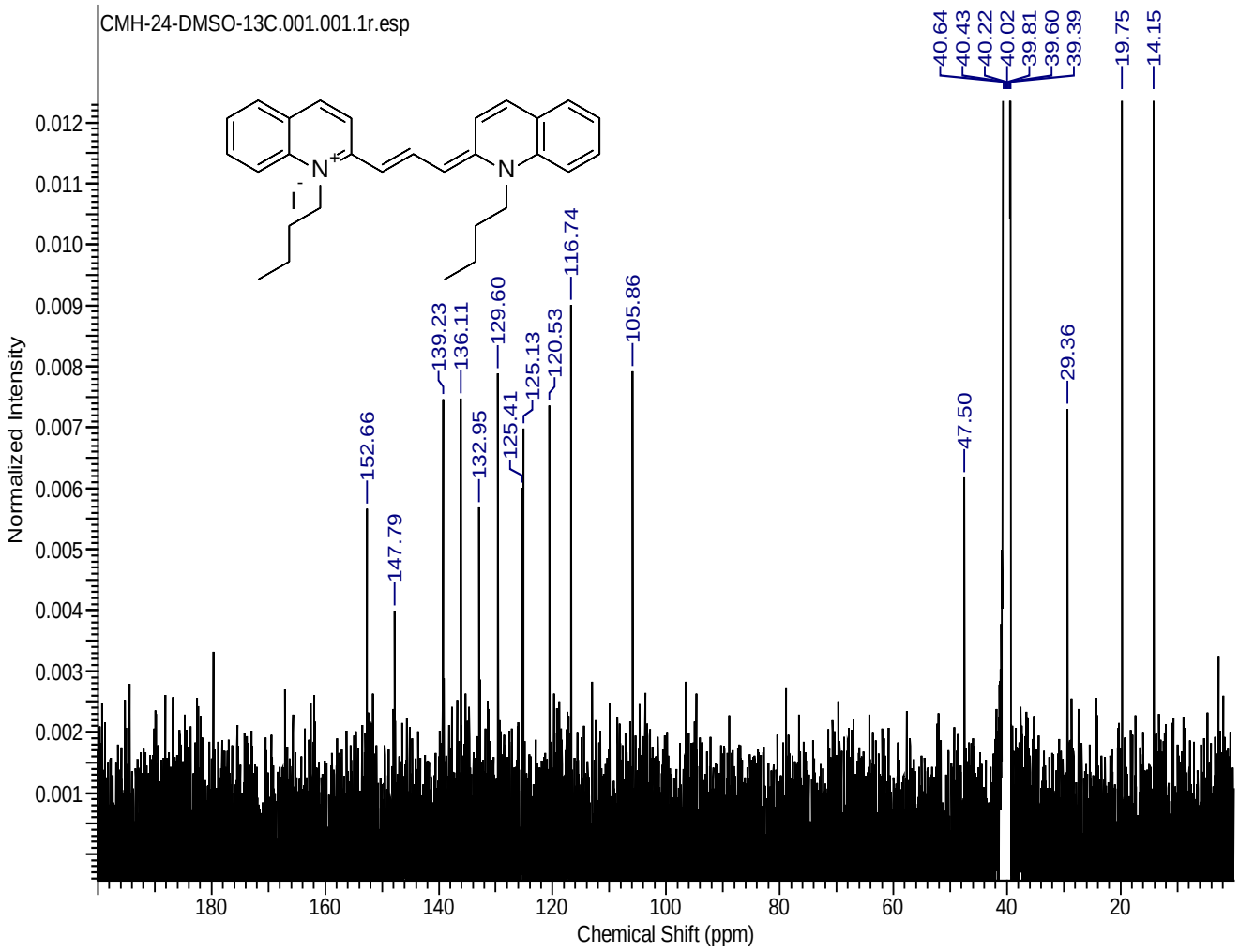

Appendix C.10. **Compound meso substituted 4 methyl quinoline methyl**

^{1}H NMR (400 MHz, DMSO-d6) 25 °C

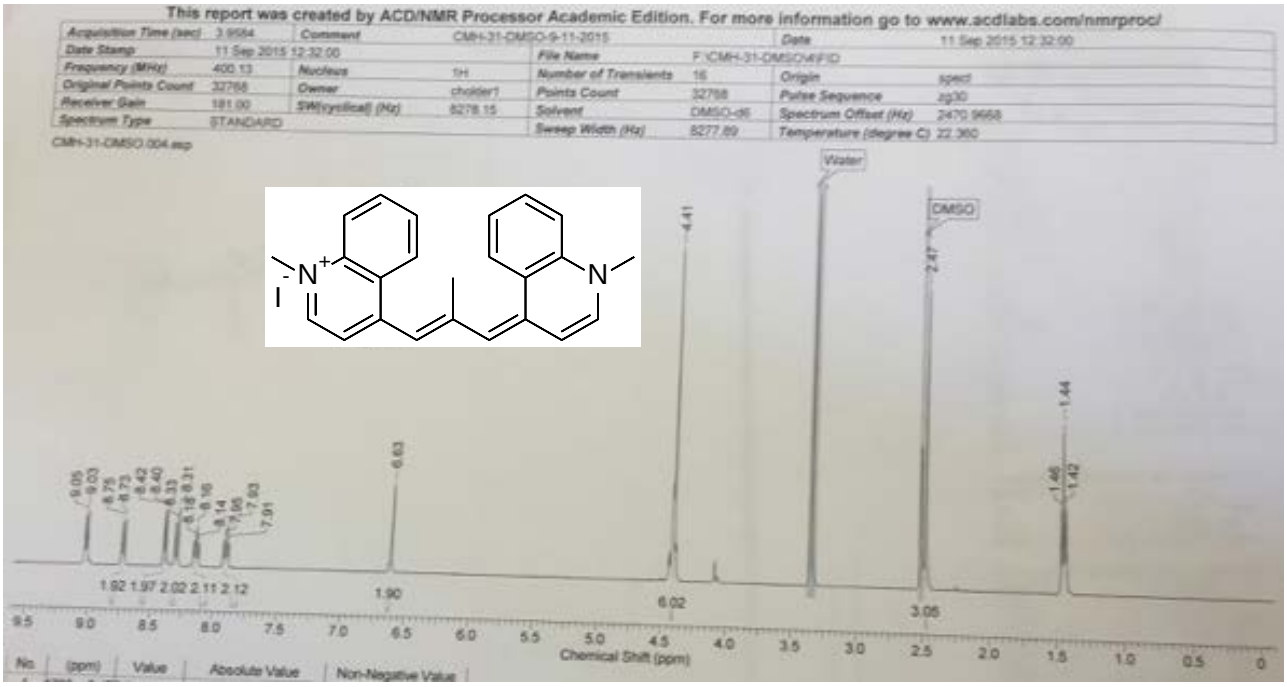

^{13}C NMR (100 MHz, DMSO-d6) 25 °C

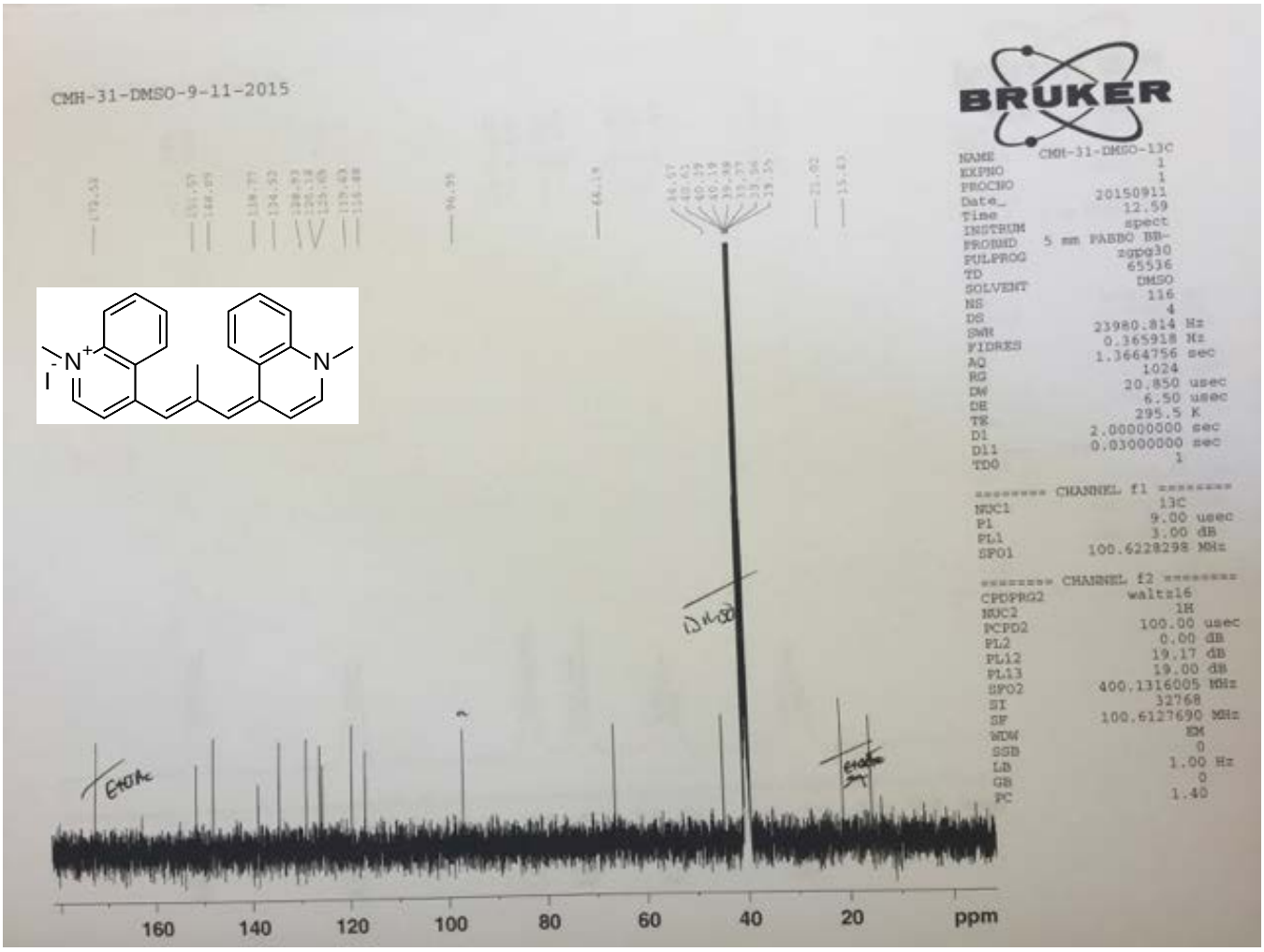

HOMO LUMO energy diagram